Climate Resilience and Vulnerability

of the Salt River Project Reservoir System,

Present and Future

by

Kevin W. Murphy

A Dissertation Presented in Partial Fulfillment
of the Requirements for the Degree
Doctor of Philosophy

Approved August 2016 by the
Graduate Supervisory Committee:

Randall S. Cerveny, Chair
Robert C. Balling, Jr.
Andrew W. Ellis
Jon A. Skindlov

ARIZONA STATE UNIVERSITY

December 2016

ABSTRACT

Water resource systems have provided vital support to transformative growth in the Southwest United States; and for more than a century the Salt River Project (SRP) has served as a model of success among multipurpose federal reclamation projects, currently delivering approximately 40% of water demand in the metropolitan Phoenix area. Drought concerns have sensitized water management to risks posed by natural variability and forthcoming climate change.

Full simulations originating in climate modeling have been the conventional approach to impacts assessment. But, once debatable climate projections are applied to hydrologic models challenged to accurately represent the region's arid hydrology, the range of possible scenarios enlarges as uncertainties propagate through sequential levels of modeling complexity. Numerous issues render future projections frustratingly uncertain, leading many researchers to conclude it will be some decades before hydroclimatic modeling can provide specific and useful information to water management.

Alternatively, this research investigation inverts the standard approach to vulnerability assessment and begins with characterization of the threatened system, proceeding backwards to the uncertain climate future. Thorough statistical analysis of historical watershed climate and runoff enabled development of (a) a stochastic simulation methodology for net basin supply (NBS) that renders the entire range of droughts, and (b) hydrologic sensitivities to temperature and precipitation changes. An operations simulation model was developed for assessing the SRP reservoir system's cumulative response to inflow variability and change. After analysis of the current

system's drought response, a set of climate change forecasts for the balance of this century were developed and translated through hydrologic sensitivities to drive alternative NBS time series assessed by reservoir operations modeling.

Statistically significant changes in key metrics were found for climate change forecasts, but the risk of reservoir depletion was found to remain zero. System outcomes fall within ranges to which water management is capable of responding. Actions taken to address natural variability are likely to be the same considered for climate change adaptation. This research approach provides specific risk assessments per unambiguous methods grounded in observational evidence in contrast to the uncertain projections thus far prepared for the region.

ACKNOWLEDGMENTS

Although the reservoir system at the center of this investigation is owned by the United States Bureau of Reclamation, the Salt River Project maintains exclusive water management control and operates the system for the benefit of their customers – primarily water managers at the municipal level. They have thereby been positioned to provide specific input to this study and feedback as to how the information from this work is useful to management planning processes and to interactions with the water providers they serve. Collaboration with SRP Water Resources Operations personnel has been instrumental in development of the reservoir simulation model and development of the stochastic runoff simulation methodology employed in this study, not to mention their numerous data contributions. SRP funding support was provided in summer-2011 for development of the stochastic simulation methodology. My sincerest thanks to Mark Hubbell, Yvonne Reinink, Tim Skarupa, Jon Skindlov, and James Walter who provided ongoing encouragement and assistance.

Drew Ellis, now at Virginia Tech, has patiently advised this investigator, probably for longer than he expected, providing key guidance along the way. Additionally, Drew authored the implementation of the ResSim model in FORTRAN and has been an ongoing resource in its utilization, for which I am very grateful. Many thanks to Randy Cerveny, whose enthusiasm and encouragement throughout this work was boundless. Many thanks to Robert Balling who provided the reminders this researcher needed to challenge the conventional and think differently. And, many thanks to my son, Ben Murphy, who eagerly applied his Python programming skills to kriging methods, without which hydrologic sensitivities might never have been revealed.

TABLE OF CONTENTS

Page

CHAPTER Page

CHAPTER Page

CHAPTER Page

LIST OF TABLES

Table Page

Table Page

LIST OF FIGURES

Figure Page

Figure Page

Figure Page

Figure Page

Figure Page

Figure Page

Figure Page

Figure Page

Figure Page

CHAPTER 1

INTRODUCTION

"Look deep into nature, and then you will understand everything better."
- Albert Einstein

The semi-arid Colorado River Basin (CRB) is a critical water resource spanning parts of seven western states of the United States and portions of northwestern Mexico. The highly dammed Colorado River and its tributaries provide municipal water supply to rapidly growing populations approaching 40 million people, irrigation water to more than 4 million acres of land, and hydroelectric power generation in excess of 4200 megawatts (U.S. Bureau of Reclamation 2012). Dammed rivers and large surface water reservoirs are important in the basin due to the semi-arid climate of the region, the high inter-annual variation in precipitation and runoff, the propensity for multi-year drought, and an increasing demand for water by a rapidly growing population. These factors combined with over-allocation of Colorado River water (Reisner 1986) and recent drought episodes have sensitized water management in the region to the threats that pose a challenge to water management strategies.

At the center of the Lower Basin of the CRB (LCRB) in central Arizona lie the Verde River, Tonto Creek, and Salt River sub-basins, encompassing approximately 33,000 square kilometers of watershed. Their surface water flows are managed by the Salt River Project (SRP) as they pass through a parallel series of reservoirs on the Salt and Verde Rivers and on to an extensive distribution system of canals and irrigation laterals in the Phoenix metropolitan area. Supplemented by groundwater wells, the SRP system provides water to a 248,200 acre service area within major portions of the

Phoenix area (Fig. 2.1.1) – satisfying approximately 40% of raw water demand for irrigation and municipal treatment purposes. SRP has been managing this water resource system for over a century through the utility cooperative 'Salt River Valley Water Users' Association', which operates alongside the public utility 'Salt River Project Agricultural Improvement and Power District' that provides electricity – a portion of which is hydroelectrically generated on the Salt River (SRP-c). SRP is the first and oldest multipurpose federal reclamation project in the United States, serving as a model of success for U.S. Reclamation Service projects in the arid West. The National Reclamation Act was passed in 1902 and implemented in the Progressive Era of United States history, originating in the conservation movement which stressed efficient development of America's natural resources while avoiding wasteful exploitation. The bill sought to make the desert bloom through wise management of precious water resources, turn the rivers of the West to useful purpose, and open the region for settlement. It inserted the federal government into the building of major engineering projects for water storage through financial assistance measures and provision of engineering expertise (Smith 1986). The SRP system has been one of the most formative physical influences on the geographic evolution of south-central Arizona, having supported the Phoenix metropolitan area's growth to the sixth (almost fifth) largest city in the United States over the last century.

1.1 Literature Review

(Note: In addition to the following discussion, literature reviews specific to each methodology employed in this study can be found in those sections of this document.)

As for many watersheds around the world, SRP management has been sensitized to the threats which climate issues pose to water resources in the future. Droughts within the past century of SRP system operation have had significant effects on water supply (Phillips et al. 2009). Paleo-climate records suggest that deeper and more prolonged droughts in the region are possible (Hirschboeck and Meko 2005, 2008). Climate projections indicate that a warmer and drier climate in many subtropical regions is forthcoming over the next several decades, exacerbating drought concerns (Kundzewicz et al. 2008; Ellis et al. 2008; Dominguez et al. 2010; Dominguez et al. 2012). Understanding the impacts of climate variability and change on a reservoir system is therefore essential to effective planning for the future. Thorough characterization of a water resource system to present and future climate stresses provides the insights necessary for short-term operational and long-term risk assessment and investment planning, ensuring water resource sustainability.

During the past several years climate change modeling studies have brought indications of an increasingly arid future for the western United States to the attention of the water community (Christensen et al. 2004; Seager et al. 2007; Christensen and Lettenmaier 2007; Hoerling and Eischeid 2007; Barnett et al. 2008). Two dozen general circulation models (GCMs) generally project increasing aridity driven by the pole-ward expansion of the subtropical dry zones, increasing lower atmosphere temperatures, and reductions in the all-important winter season precipitation (Intergovernmental Panel on Climate Change (IPCC) 2007, 2013; Seager and Vecchi 2010). The models indicate that drying should be underway (Milly et al. 2005; Seager et al. 2007; Hoerling and Eischeid 2007; Barnett and Pierce 2009; Hoerling et al. 2009). Research focused on reconciling

and narrowing the range of modeling projections (Hoerling et al. 2009) shows increasing surface air temperatures across the CRB of 2^{o}C or more by mid-century with some of this having already occurred. However, precipitation modeling has yielded a wide spread of projections from small gains up to a 15% reduction with substantial regional trend variations, poor representation of seasonal cycles, and findings that changes are more complex and less certain than those for temperature alone (IPCC 2007, 2013; Milly et al. 2005; Dominguez et al. 2010; Stephens et al. 2010). Gutzler et al. (2012) concluded that although temperature trends are evident in the Southwest United States and are reasonably well-represented in GCMs, any model-projected trends in precipitation are small relative to natural modes of variability, and therefore caution should be exercised in the attribution of drying to anything other than elevated temperature.

Once climate projections are applied to hydrologic models that are challenged to respond with accurate representations of an arid hydrology, the range of possible outcomes enlarges as uncertainties propagate through sequential levels of modeling complexity (Wilby and Dessai 2010; Vano et al. 2014). Salas et al. (2012) stated: "Although general circulation models have had success in the attribution of warming global temperatures to anthropogenic causes, their credibility and utility in reproducing variables that are relevant to hydrology and water resources applications is less clear." Such observations have lead Kundzewicz and Stakhiv (2010) to inquire whether the models are "ready for prime time" in direct application to water management issues. They point out that over the years climate modeling attention has shifted from concerns with climate effect mitigation options and policies for greenhouse gases (GHG) to a different set of users in search of information for developing adaptation strategies on the

local scale – the hydrologists and water managers. These users have raised pragmatic concerns about how useful downscaled GCMs can really be for specific decisions at their scale of interest. Kundzewicz and Stakhiv state: "Simply put, the current suite of climate models were not developed to provide the level of accuracy required for adaptation-type analysis. … To expect more from these models is simply unrealistic at this time."

While progress is made with each successive generation of models, Trenberth (2010) anticipated that the uncertainty in climate projections of the Fifth Assessment Report (AR5) of the IPCC would be greater than in previous modeling. This does appear to be the case for the CRB. While understanding of certain dynamics does increase, so does the realization that there are factors not previously accounted for which contribute cascading complexity. "Adding complexity to a modeled system when the real system is complex is no doubt essential for model development. It may, however, run the risk of turning a useful model into a research tool that is not yet skillful at making predictions." (Trenberth 2010). Meanwhile, and very importantly, as pointed out by Brown and Wilby (2012) there is a mistaken tendency for some stakeholders to perceive and treat model projections as forecasts. Pielke and Wilby (2012) remind us that "downscaling has practical value but with the very important caveat that it should be used for model sensitivity experiments and not as predictions." "It is inappropriate to present downscaled results to the impacts community as reflecting more than a subset of possible future climate risks."

Among a number of reasons that GCM-based modeling is unsatisfactory are: there are a variety of models and numerous scenario assumptions used, there are various downscaling methods used to translate coarse-scale model scenarios to a region of

interest with differing results, the coarse spatial resolutions do not adequately resolve hydrologic processes in key runoff regions, precipitation dynamics which are the main driver to runoff production are poorly represented, divergence between modeled and observed temperature changes at various levels of the atmosphere have emerged, sensitivities of surface hydrology to temperature and precipitation changes are often poorly understood, models do not represent important modes of natural variability (e.g. El Niño Southern Oscillation (ENSO), Atlantic Multi-decadal Oscillation (AMO), Pacific Decadal Oscillation (PDO)), and the number of sub-processes and their representations continue to expand. These result in climate model complexity struggling to replicate past climatology coupled to challenging hydrologic modeling of the semi-arid Southwest United States, yielding ranges of outcomes that do not reduce uncertainty of future projections. These problems render future risk projections for a water delivery system frustratingly uncertain (Gober et al. 2010; Galloway 2011; Gober 2013). A recent review by Vano et al. (2014) of the sources of uncertainty in future projections of Colorado River stream flow has reiterated many of these same modeling issues identified when the Water Utility Climate Alliance (2009) concluded, as did others (Seager and Vecchi 2010), that it will be some decades before models can provide accurate and detailed simulations of all the important regional dynamics correctly coupled into the global climate system and eventually provide useful projections to water management.

Beven (2011) notes that the path towards realistic models appears long and tortuous even with major coordinated international modeling efforts. While successive model generations will improve, in the meantime a lot of time, effort, and money are being invested in impact studies that can be questioned for whether they are fit for

adaptation management purposes. He echoes the concern that current generation projections are not entirely credible, but counsels water management against doing nothing and instead find alternative paths to adaptive solutions. Stakhiv (2011) considers adaptive management to be a superior and more practical alternative to the cascading uncertainties inherent in GCM-based assessments. He describes adaptation as a continuous process of vulnerability investigation which can and should deal explicitly with probabilistic threat assessments as part of operational management. Rogers (2008) argues that an adaptation path brings focus to policies and technologies that should be considered anyhow, regardless of hypotheses about the origins of forthcoming change. Those change arguments don't have to all be resolved to make progress; and regardless, decisions are likely to be the same.

1.2 Problem Statement and Alternative Investigative Approach

The conventional top-down, full-simulation approach to assessing climate change impacts on surface water supply involves three general steps for end-to-end modeling:

1) statistically or dynamically downscale air temperature and precipitation projections from a set of global climate models chosen to span the range of possible outcomes for the watersheds,
2) translate air temperature and precipitation projections yielded by the downscaled GCMs through land surface hydrology models (LSHMs) to establish runoff in the form of stream flow, and then
3) assess how surface water flows replenishing a managed reservoir system would be threatened by the projected runoff change under the climate change scenario.

Much of modeling research has centered on the first two steps with little attention yet given to step 3, due in part to the uncertainties generated by steps 1 & 2. Wilby and Dessai (2010) point out that there are few tangible examples of anticipatory adaptation decisions arising from this approach, as the envelope of uncertainty expands at each modeling step such that the resulting wide range of potential impacts and implied response are not practically useful. It can be noted from an analysis standpoint that a full simulation must be executed for each climate scenario. The rigor demanded in modeling a specific regional representation over multiple decades demands massive computational resources, potentially taking months to execute. Assumption modifications or assessments of alternative climate scenarios become a daunting challenge.

Given this state of the science, viable alternative approaches to risk assessment can make valuable contributions to water resource management while conventional modeling more fully develops in the years ahead. The research reported herein inverts the above sequence to a bottom-up approach for vulnerability analysis. Resource risk assessment can begin with the threatened system in question and proceed backwards to the uncertain climate future. It starts with diagnosis of the sensitivity of an impacted system to variability and change without confining the exercise to any specific climate change projection, the likelihood of which remains highly uncertain. Analysis is focused at the resource level and relies on sufficiently lengthy historical observations to assess the frequency and magnitude of threatening events and system response. And, since projections of the future are never really deterministic, the probabilistic nature of outcomes is addressed. This is consistent with practices in hydrologic engineering and quantifies the full range of future risks rather than dwelling on a limited set of scenarios.

Climate conditions relevant to decision sensitivity are then identified and linked to what is credible from available climate research and evidence. Impact models quantitatively analyze effects of change and, as indicated, motivate the search for more resilient options. Adaptation then involves coping with or reducing exposure to the identified threats through a set of feasible actions. This is where primary attention should be paid rather than dwelling on uncertain climate scenarios (Wilby and Dessai 2010; Brown and Wilby 2012; Brown et al. 2012; Pielke and Wilby 2012; Wilby et al. 2013). The products of this approach are more directly interpretable for risk characterization, system stress tests, evaluation of adaptation plan alternatives, planning strategies, and decision support. At the outset of this investigation limited examples from the implementation of this approach had been reported in the literature. As its utility has been recognized, some case studies have emerged such that at the 2015 American Geophysical Union Fall Meeting about a half dozen were reported, including this one. This investigation demonstrates the alternative investigative approach with a case study of the Salt River Project watersheds and reservoir system, thereby filling a void and demonstrating a path to applicable hydroclimate knowledge. Findings provide more specific meaning for the SRP system in contrast to the rather broad range of projections that have thus far been prepared for the region.

The various research components employed for this investigation have been developed in response to the contrasts that have emerged between the hydrological science perspective on implications of climate change (Koutsoyiannis et al. 2009) versus the climate change research outlook detailed in Chapter 3 from Working Group 2 in AR4 (and now AR5) from the IPCC (Kundzewicz et al. 2008; Kundzewicz et al. 2009).

Hydrologists challenge the idea that uncertainty is epistemic rather than structural; that is, whether it can be significantly reduced by increasing complexity in models. Rather, they suggest the structural character of uncertainty in climate and hydrologic behavior may have been under-rated and the magnitude of uncertainties is underestimated by the IPCC. The hydrology community views climate modeling as subscribing to a deterministic approach, while they instead approach natural processes with a pragmatic statistical description. These are different paradigms in modeling and understanding of natural processes. The hydrologist's stochastic representation does not seek to reduce a phenomenon to a series of cause-effect relationships coming to a single prediction; but instead accepts that complete end-to-end representations of all the involved dynamic processes may not be possible and instead seeks to quantify the uncertainties surrounding them through observational data. Stochastic representations may thereby provide an explanation for a natural variation in a time series which might otherwise appear as an exceptional non-stationarity (Koutsoyiannis et al. 2009).

Data are of primary importance within hydrology which embraces the premise that geosciences are by nature induction-based rather than deduction-based and therefore rely to a greater extent on historical data as the key to the future. Data play a crucial role in understanding past climatic and hydrological changes and provide primary guidance in tracing possible futures. Not that the future will mirror the past, but that the dynamic character of past climate needs to be fully explored to estimate future uncertainty. Data are indispensable to model building in the hydrological community. It guides model development, and data are employed for model validation using hold-out methods. It is established practice within the hydrology community (and in forecasting science) to test

model performance against observed data in an objective fashion. They note the lack of a validation process for IPCC models, which contributes to questioning their reliability. Independent efforts to do so (Koutsoyiannis et al. 2008; Anagnostopoulos et al. 2010; Fildes and Kourentzes 2011; Suckling and Smith 2013) indicate poor performance, resulting in strong reactions and tense exchanges between the communities (Galloway 2011). As an example, Koutsoyiannis et al. (2009) state that just using more un-validated models to produce ensembles of climate projections, as is IPCC climate modeling practice, does not provide a scientific basis for uncertainty estimation. If dispute over what constitutes "a scientific basis" can be set aside, useful points of advice for validation methods and rigorous uncertainty quantification should not be ignored. Entrenched adherence to a limited toolkit and refusal to embrace constructive criticism will not serve the stakeholders who await useful information. This study develops a methodology which employs tool sets from different disciplines and responds to justifiable critiques from differing perspectives to arrive at a vulnerability assessment for a key water resource system. As a transferable example built for the case of the Salt River Project, it can also serve the needs of other communities confronting similar, challenging adaptation planning.

In overview, this investigation consists of:

1. Establishment of a thorough baseline understanding of the envelope of natural climatic variability in net basin water supply (NBS) based on historical evidence. Use it to statistically generate long seasonal time series representative of the current dual-watershed system through stochastic simulation that yields the full range of possible drought and excess.

2. Quantification of the hydrologic sensitivity to climate of the Salt-Tonto and Verde watersheds and reservoirs in winter and summer, based upon empirical evidence from historical response. Specifically, development of algorithms for temperature sensitivity and precipitation elasticity as a function of NBS for each watershed-season and reservoir-season.
3. Development of a reservoir management simulation model that incorporates all aspects of the water delivery system and the web of operational guidelines used by SRP in its management, validated against the historical record and with SRP.
4. Assessment of baseline implications of the current NBS probability distribution to system vulnerability and resilience by exercising the reservoir operations simulation model with long stochastic simulation time series.
5. Development of a set of climate change projections across the 21st century for the SRP system which include (i) a most-likely forecast based in current understanding of forthcoming change and (ii) a higher stress-test of climate conditions based on the World Climate Research Program's Coupled Model Intercomparison Project (CMIP), a multi-model dataset developed to inform the IPCC.
6. Development of modified stochastic simulation time series by translation of a climate projection to modified NBS probability distributions according to the watersheds' and reservoirs' hydrologic sensitivity functions.
7. Assessment of the implications of the climate-modified simulation time series by processing them through the reservoir operations model.

8. Comparative statistical analyses of NBS and reservoir system outcomes between the baseline and climate change results.

Development of the most likely temperature forecast became a major sub-project of this investigation. It was motivated by the observation that CMIP projections are inconsistent with empirical evidence at the global and regional levels and by the absence of forecasting science best practices in IPCC methods.

1.3 Research Questions

The central research questions addressed by this investigation are:

> What are the probabilities of drought of various severities (duration and depth) in the SRP watersheds due to baseline natural climate variability, as evidenced by the historical record?
>
> How do the drought probability distributions change under a set of climate changes for a future timeframe?
>
> Under existing system operating guidelines, what are the differences in reservoir system response and vulnerability between current baseline climate variability and the change projections? What differences in adaptation responses might be indicated?

Impacts are measured by the primary statistical parameters of the output probability distributions for drought, water delivery reduction thresholds, and reservoir system depletion. Hypothesis testing is conducted for changes in probability distributions relative to the baseline case and in comparison to the 127 year historical record.

- The Null Hypothesis: there are no statistically significant differences in key impact parameters.
- The Alterative Hypothesis: statistically significant differences for key parameters can be demonstrated.

At the outset of the investigation it was anticipated that results would include:

- A probabilistic characterization of the range of drought duration and depth under which the SRP reservoir system has been operating, with an analysis of system vulnerability and resilience under current operating guidelines.
- A multi-decadal forecast of the Salt and Verde watersheds' net basin water supply, with anticipated performance metrics (i.e. error) and supported by climate change assumptions, including temperature and precipitation projections with consequent runoff response.
- A probabilistic characterization of long-term drought vulnerability with implications to sustainability and adaptive response of the SRP reservoir system over the next century, to both the forecasted and stress-test climates.
- A methodology which can be applied to various other issues of consequence to water management such as pluvial events, conditional reservoir depletion analysis, growth in water demand, or spillage to the main stem of the Colorado River.
- A discussion of considerations lying outside the methodology, together with the theoretical contributions of the work and how it could be applied to other watersheds.

And, of primary interest, do climate change outcomes fall within a range that management practices are capable of responding to? And, if not, what quantification of SRP system stress can be provided for considerations of threat response for this critical water resource?

CHAPTER 2

DATA SOURCES AND PREPARATION

2.1 Study Area and Time Horizon

Descriptions of the Salt River Project watersheds and reservoirs in central Arizona are available at http://www.srpnet.com/water/dams (SRP-a). The Tonto Creek watershed lies south of Payson between the Salt River and Verde River watersheds (Fig. 2.1.1; Appendix B). Tonto Creek enters the northwest side of Roosevelt Lake; and since its surface water supplements the Salt River at that reservoir, their data are combined for this study and generally referred to as the Salt side of the system. Throughout this document any reference to the 'Salt' also includes the Tonto watershed, unless specifically identified otherwise. The Salt and Verde basins adjoin one another, resulting in seasonal correlations in stream flow captured at two parallel series of downstream reservoirs. The C.C.Cragin reservoir, located just east of the Verde watershed is not included in this investigation due to its small size and uncertainties over how much of its water passes to the Verde River. Total storage capacity of the system's six reservoirs is 2.3 million acre-feet of water (Table 2.1.1), with most of it (88%) on the Salt side of the system, where Roosevelt Lake accounts for 71% of the total. Water releases from the Salt and Verde sides of the reservoir system to the Phoenix metropolitan area combine just upstream of the Granite Reef Dam. Water is diverted at the dam into a delivery system of canals bounding the north and south sides of SRP's service area. Total water delivery had been approximately 900,000 acre-feet/year for the several years preceding initiation of this study (Fig. F1), and that value is held fixed for the purposes of this investigation, following a representative seasonal cycle provided by SRP (Table F1).

While annual reservoir inflows are highly variable, long-term median flow from the watersheds has been close to delivery demand over the past several years. Reservoir inflows are typically proportioned between seasons and watersheds as given in Table 3.2.2.

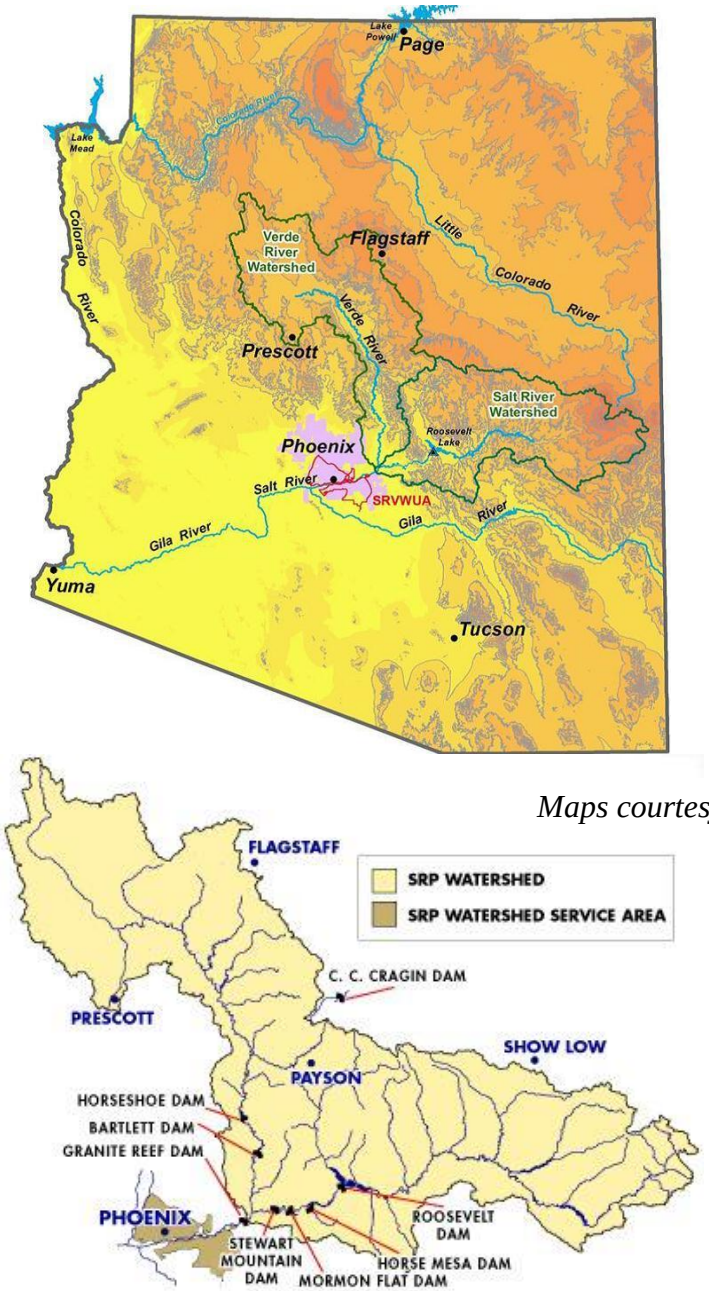

Maps courtesy of SRP

Figure 2.1.1. Salt River Project Watersheds, Reservoir System, and Service Area in Central Arizona (from SRP-a).

Table 2.1.1. The SRP Central Arizona Watersheds, USGS Gages and Reservoir System.

	Watershed	Median Elevation (m)	Drainage Area (km^2)
	Salt & Tonto	1,771	13,416
	Verde	1,649	15,265
	Gage #	Elevation (m)	Data Record
USGS Gage, above reservoirs (inflow)			
Salt River near Roosevelt	09498500	664	Oct-1913 to present
Tonto Creek near Roosevelt	09499500		Oct-1913 to Dec-1940
Tonto Creek above Gun Creek	09499000	769	Jan-1941 to present
Verde River at Bartlett Reservoir	09509000		Oct-1938 to Dec-1945
Verde River below Tangle Creek	09508500	618	Sep-1945 to present
USGS Gage, below reservoirs (discharge)			
Salt River below Stewart Mountain Dam	09502000	418	Oct-1934 to present
Verde River below Bartlett Dam	09510000	479	Oct-1913 to present

SRP Reservoirs' Capacity (acre-feet)	pre-1996	post-1996	
Roosevelt Lake	1,348,314	1,653,043	built 1905-1911, expanded 1996
Apache Lake, Horse Mesa Dam	245,138	245,138	built 1924-1927
Canyon Lake, Mormon Flat Dam	57,852	57,852	built 1923-1925
Saguaro Lake, Stewart Mountain Dam	69,765	69,765	built 1928-1930
Salt Sub-Total	1,721,069	2,025,798	
Bartlett Lake	178,186	178,186	built 1936-1939
Horseshoe Lake	109,217	109,217	built 1944-1946, spillway added 1949
Verde Sub-Total	287,403	287,403	
Total System	2,008,472	2,313,201	(1 acre-foot = 325,000 gallons)

No sedimentation of the reservoirs over time has been considered in this study.

Water management is concerned with two long-term planning horizons: a few decades ahead for operational issues, and a century into the future for major infrastructure investments and risk assessment. Many climate modeling exercises have reported change expectations at mid-century, now just a few decades away, as well as for the year 2100. The SRP system began operation over 100 years ago with the dedication of Roosevelt Dam, and a continuation of service through the rest of this century is expected. As discussed below, 118 years of climate data and 127 years of runoff history has been used

for this investigation, sufficient to capture about two cycles of major climate indices such as the AMO and PDO. As discussed below, drought risk statistics are typically expressed per a standardized time interval, such as per-century and the analyses within this investigation are performed on that basis. Applicability of findings is considered for the next few decades and the later part of this century.

2.2 Watershed and Reservoir Temperature and Precipitation

Fine-resolution gridded climate data sets suitable to matching the spatial boundaries of each watershed are available from the Parameter-elevation Regressions on Independent Slopes Model (PRISM) (Daly et al. 1994; 2002). The resolution of PRISM grid cells is 0.0416 degrees of latitude and longitude (approximately 4 km). PRISM generates monthly estimates of temperature and precipitation for each grid cell using station data, spatial data sets, and expert guidance. A set of rules, decisions, and calculations are used to weigh station data for use in linear regression analyses to create the temperature and precipitation grids. Factors in the weighting method include distance from a station, elevation, clustering of stations, topographic characteristics (to account for local inversions and rain shadow effects), and proximity to coastlines (Daly et al. 2002). The grid cells of each sub-basin draining unregulated flow to the United States Geological Survey (USGS) gages at reservoir input were identified by Ellis et al. (2008) using hydrologic unit code (HUC) boundaries and the PRISM digital elevation model (DEM). In cases where the HUC boundary extended beyond the drainage area of a particular gage, the PRISM DEM was used to delineate a revised drainage divide. The PRISM data periods of record are from 1895 to the present, with no missing records.

Data for 1895-2013 was used for most of this investigation's analyses, with 2014-2015 later appended for ancillary statistics.

Using PRISM air temperature values, mean monthly temperature was calculated by the average of the mean monthly maximum and minimum for each grid cell, and then a total sub-basin monthly value was calculated by weighting per the area of each constituent grid cell. The PRISM database provides a monthly precipitation depth for each grid cell. The total precipitation depth for each sub-basin was calculated by weighting the precipitation values per the area of each constituent grid cell. The area of each grid cell was multiplied by its monthly precipitation value to produce a volume of precipitation, which was then summed for total monthly volume of precipitation falling onto a watershed converted to acre-feet, the familiar unit of measurement for U.S. water management professionals.

Additionally, the PRISM grid cell nearest each of the six dams in the Salt and Verde reservoir system was identified and their historical series of mean monthly air temperature and monthly precipitation were extracted for each dam location. The data were weighted per reservoir capacities to arrive at monthly temperature and precipitation data series for each side of the dam complex.

2.3 Global Temperature

Global monthly temperature anomalies, HadCRUT.4.4.0.0, were obtained from the Met Office Hadley Centre (Morice et al. 2012), available for 1850-2015, which are expressed relative to a 1961-1990 reference period. For this analysis the time series was uniformly reset to a zero pre-industrial (19^{th} century) baseline by the cumulative average

level of the time series before its rise (0.339^{o}C). In mid-2015 the T.4.3.0.0 data set was superseded by the T.4.4.0.0 data set. The differences between them are minor and have no influence on analysis conducted for this investigation.

2.4 Atmospheric CO_2

Monthly mean atmospheric CO_2 data were obtained from the NOAA Earth System Research Laboratory Global Monitoring Division (Dlugokencky and Tans). The globally averaged marine surface monthly mean data were utilized for 1980 to present, appended to Mauna Loa data for 1958 to 1979, and supplemented with South Pole station data for the 1958 water year (Keeling et al. 1976).

2.5 Runoff

Runoff volume data were sourced from the archive of the USGS daily stream flow data (USGS-NWIS). These gages (Table 2.1.1) are located just above the first point of interception in each river as input at a reservoir, capturing the flow originating in upstream grid cells. Data acquisition began in 1913 for the Salt and Verde Rivers and for Tonto Creek (USGS-NWIS; SRP-b). Flow rates reported by the USGS were converted to acre-feet of water within monthly time intervals. For the purpose of this study the Salt River and Tonto Creek inflows to Roosevelt Lake are combined to one data series for the Salt side of the system. Tonto Creek contributes approximately 15% supplemental inflow, and other small creeks are of no consequence. The Salt and Tonto watersheds' climate data are also combined and thereafter titled as the Salt. Some missing monthly

data for the Verde gage were completed by interpolation with partial gage information and by input-output balance calculations from reservoir storage data.

Additionally, SRP produced a reconstruction of monthly stream flow data at the position of the USGS reservoir inflow gages back to 1889 (Phillips et al. 2009; provided in personal communication). The extended record includes the severe drought of 1898-1904 on the Salt and Verde basins and therefore has been included for the fullest characterization of the range of hydrologic conditions on the basins.

Reconstruction of pre-historic stream flows for the Salt and Verde rivers using tree-ring analysis was completed in 2005 by paleoclimate scientists at the University of Arizona (Hirschboeck and Meko 2005). Their monthly runoff estimates date from 1361 to 2005. Those data broaden the range of evidentiary hydrological conditions on the basins by revealing extended periods of drought larger than occurred during the instrumental record. Comparative statistical analyses were performed for the period of data overlap with USGS stream gages. While runoff patterns generally aligned, markedly different behavior was found on a year-by-year basis, casting doubt whether tree-ring data could accurately inform runoff probability distributions, which is a central objective of this investigation. The comparisons were shared with D. Meko who acknowledged statistical biases and constrained minimum and maximum flows, indicating they are attributable to data transformation methods used for the tree-ring study. Therefore, the tree-ring data set was set aside for the analyses conducted during this investigation. It was noted that similar periods of drought indicated by the tree-ring analysis were also revealed by the stochastic simulation conducted for this study.

2.6 Reservoir Releases

USGS daily stream flow data are available for positions below Bartlett Dam and Stewart Mountain Dam (USGS-NWIS; SRP-b) from the dates at which the reservoirs went into service by which reservoir discharge can be measured for the Verde and Salt sides of the reservoir system, respectively. The data begin from the dates at which the reservoirs went into service (Table 2.1.1).

2.7 Reservoir Storage

SRP maintains the historical series of daily water volume stored in each of the six reservoirs beginning in 1931 on the Salt system and 1946 on the Verde system (SRP-a; supplemented in personal communication). The data series extends through the present day with no gaps.

2.8 Miscellaneous Loss (and Gain)

Exploratory data analysis revealed that there are important miscellaneous losses and gains of water at the reservoirs which affect water balances driving reservoir system operation and affecting water supplies for fulfillment of contractual water delivery requirements. Losses may be due to evapotranspiration and interactions between surface and sub-surface water in the proximity of the reservoirs. As well, during some periods of high precipitation and runoff the reservoirs experience gains larger than the loss mechanisms, possibly due to combinations of direct precipitation on reservoirs, overland flow bypassing a stream gage, streambed modifications, or gage calibration performance. The net loss or gain is quantified by the difference between reservoir inflows and releases

compared to storage changes over a time period. The imbalance is termed 'miscellaneous loss' because it is expected to be 'missing' and is entered as a positive value in system balancing. A negative miscellaneous loss term denotes a gain in reservoir storage that is not supported by the difference between inflow and discharge. Net basin supply of available surface water is equivalent to runoff measured at the reservoir input gages less the miscellaneous loss (NBS=RO-ML).

The climatic dependencies of miscellaneous loss for each watershed-season were examined using PRISM data-derived air temperature and precipitation data at the reservoir locations over the period 1946 through 2010 (Verde reservoir system period of record). The relationships were applied to PRISM data to estimate miscellaneous loss from 1895 through 1945, and analogous-year sequences were used to estimate values for the period 1889-1894. The earlier-year estimates were appended to post-1945 actuals to obtain a data series of miscellaneous loss for the Salt and the Verde reservoirs for each winter and summer season, 1889 to the present. Full series were used in most analyses of this investigation. But, when precise miscellaneous loss values were important, only direct-calculation values were used. For example, NBS probability distribution estimates utilized all data since 1889 while portions of the hydroclimatic sensitivity analyses employed post-1935 (Salt) and post-1945 (Verde) data.

2.9 Deseasonalization of Data

Analyses in this study have been performed on an annual basis and per two climatically and hydrologically distinct runoff seasons. A winter runoff season containing the wetter and cooler period of fall through winter into spring is driven by

large-scale synoptic systems which are crucial to replenishment of surface water storage not only due to the large precipitation event volumes, but also much lower evapotranspiration (ET), allowing flows to reach the reservoirs with modest runoff efficiency. The warmer, drier summer runoff season involves the spatially diverse convective dynamics of the North American monsoon and high ET such that runoff efficiencies are small. Water managers of the western United States utilize a 'water year' calendar which is defined as beginning October 1st, the point at which summer and heavy customer demand has passed but winter precipitation has usually not yet begun, thereby defining the end of the summer season and start of the winter season. May 1st is a key management date in SRP's transition from winter to summer operations and for water delivery planning, although some winter snow melt in the Salt watershed occasionally extends into May. Although operational management of the SRP reservoir system occurs on a daily basis, the key guiding decisions are well-represented on a seasonal basis. Analyses were therefore performed for the two seasons and on a water year basis by aggregation of monthly data to the winter season of October 1 through April 30 and summer season of May 1 through September 30, as well as for the full water year. As an example, the 1914 water year encompasses the 1914 winter (1-Oct-1913 to 30-Apr-1914) and the 1914 summer (1-May-1914 to 30-Sep-1914).

2.10 Validity Considerations

As discussed above regarding miscellaneous loss and gain, high runoff events were identified when USGS stream gage measurements might not have accurately reported total flow. It is therefore possible that high runoff data values could be under-

reported. These events have been reconciled by examining reservoir storage history for seasonal input-output flow balance to assess any understatements. This method also quantifies all water losses which occur at the reservoirs so that net basin supply of surface water for the system is represented as accurately as possible.

The primary variable of interest for this investigation is the difference of runoff and net miscellaneous loss, or net basin supply (NBS=RO-ML). The distinction between runoff and net basin supply is important because their probability distributions are different. NBS extends to a lower bound at the minimum side due to net losses and extends farther to the high side due to net gains. Droughts are therefore exacerbated when multiple years occur from the low side while reservoir refresh rate is enhanced by net gains.

The 127 years of NBS data available for this study are one of the longest such series for a watershed in the western United States. To the extent that sufficient characterization data dictate feasibility of the proposed investigative approach, study of the Salt and Verde is a good test case. To ensure a valid analysis, characterization data should capture as much natural variability as possible for the best assessment of all parts of probability distributions. It can be noted that the Salt & Verde data encompass approximately two cycles of the AMO-PDO and a large variety of ENSO events, so a range of climate influences are embodied in the data used in this investigation.

Much of the methodology to be employed in this investigation was preliminarily tested and its validity established. The models and characterization methods have been found to constitute a feasible approach for the motivating research question. However, validity concerns arise when results fall outside the bounds of expected outcomes.

Therefore, comparisons to the observational record were periodically employed to confirm that simulation results provide time series sequences consistent with historical evidence.

The deterministic reservoir operations simulation model, ResSim, was built based upon an understanding of SRP operating guidelines as of 2011. It provides outcomes based on what should transpire when the specific rules built into the model are followed. Of course, it is always possible that in specific future situations alternate decisions might be taken. The model cannot deal with those digressions; nor can it anticipate whether decades from now the guidelines will have been superseded. But, ResSim can adequately serve as the basis to identify most-likely outcomes for key variables under the currently defined set of operating rules and to generate comparative results.

Validity of forecasts of the future can be assessed through examination of the assumptions used in their construction until there is a future outcome against which to measure forecast accuracy, which is the ultimate validity test. To achieve this, best practices of forecasting science require an assessment of how the forecast methodology would have performed against the historical record using only data available at the time the forecast was made. This analysis is performed in the climate change forecast section (Sec.3.6). That, together with all detailed assumptions, is the current basis for forecast validity assessment.

In considering internal validity, it should be noted that explorations of all causal relationships affecting quantitative outcomes lies beyond the scope of this research. But, this study explores those that are most important to establishing the analytical

assumptions employed; and a number of avenues for follow-on research can be identified from this investigation.

CHAPTER 3

METHODOLOGY

The successful completion of this research depends on the development of five methodological components, that their underlying assumptions are internally consistent and supportive, data interfaces are effective, and findings are interpretable and useful to water management and the hydroclimate scientific community. The major components are:

(i) an assessment of the stationarity of climate and stream flow which supports a manageable set of assumptions for the following components,

(ii) a stochastic simulation methodology for generating multi-year, representative flows from joint watershed-season probability distributions,

(iii) a diagnosis of hydrologic sensitivity to climate with two heuristics: temperature sensitivity (S_T) and precipitation elasticity (ε_p) of runoff,

(iv) climate forecasts that can be translated to modifications of the probability distributions for generating time series of alternative flows.

(v) and, a reservoir operations model through which impacts can be assessed.

The methods development for these research components are described below, preceded by the introduction of smoothing methods applied in analyses and some system characterizations.

An evaluation of the feasibility of this investigative approach was sequentially explored in parts. The reservoir simulation model was developed and tested in cooperation with SRP. Stationarity assessment methods were developed and findings published in the Journal of Hydrology (Murphy and Ellis 2014). The stochastic simulation methodology was developed and demonstrated with generation of a 10,000-year NBS time series, and some modifications were identified and implemented (Ellis and Murphy 2012). Challenging parts of this investigation were the development of climate sensitivity algorithms (presented at the AGU 2014 and AMS 2015 conferences) and forecasts of future temperature and precipitation (presented at the ISF 2015, ISF 2016, and AMS 2016 conferences). All the above are grounded in empirical evidence. These components draw from a breadth of climate research findings and are new, alternative outlooks necessitated by shortcomings of climate-hydrologic modeling which motivated this alternative investigative approach.

3.1 Low-Pass Filter Smoothing of Time Series

The most useful analytic tool for understanding the behavior of a time series is a graphical portrayal of its trend-cycle, particularly in situations of high natural variability that can disguise the evolution of underlying behavior. A variety of smoothing methods can be employed to achieve a graphical portrayal of the underlying trend-cycle behavior of a time series (Burt and Barber 1996). These range from simple moving averages to decomposition by autoregressive integrated moving average algorithms to complex filters with specific weighting functions used to suppress specific constituent frequencies while passing those which provide insight to underlying periodicities of the time series. For

this study a low-pass Lanczos filter design was adopted (Burt and Barber 1996, 531), with the objective of revealing decadal and longer patterns in the temperature, precipitation, and runoff data series. A decadal cutoff filter will have an amplitude response that drops to 50% at a cutoff frequency, f_{cut}, of one cycle in 10 years, or 0.1 cycles per observation. The Lanczos filter's preliminary coefficients were calculated from:

$c_0 = 2\, f_{cut}$, the central coefficient (3.1)

$$c_k = \frac{\sin(2\pi\, f_{cut} k)}{\pi k} \cdot \frac{\sin(\pi k/(m+1))}{\pi k/(m+1)} \qquad (3.2)$$

for k = 1, 2, 3, …, m ; and $c_{-k} = c_k$

where:

f_{cut} is the chosen cutoff frequency, in cycles per observation and the filter length, L = 2m +1

The filter coefficients are symmetric around a center point and should sum to 1.0. If preliminary coefficients do not sum to 1.0, they are simply normalized to arrive at the final coefficients:

$$C_k = c_k / \sum_{k=-m}^{m} c_k \qquad (3.3)$$

The suitability of this low pass filter design was evaluated using highly variable time series, which are the precipitation and runoff data. Through examination of the response to various combinations of filter length, L, and cutoff frequency, f_{cut}, the design parameters in Table 3.1.1 were identified which provided good smoothing for all data. All calculations in this study are displayed at the center of the data interval evaluated, so a 15-year filtered value contains ±7 years from the center point. As the end of a series is

approached the shorter filter lengths can be sequentially applied to continue the smoothed curve to within a few years of the end of a series, although with some sub-decadal response. As future data become available, application of longer filters may adjust the trend-cycle's tail position. The smoothing filters (Table 3.1.2) have been consistently applied for all variables, seasons, and watersheds graphically reported in this study.

Table 3.1.1. Lanczos Smoothing Filter Design Parameters.

filter length, L (years)	cutoff frequency, f_{cut} (cycles/observation)
15	0.1
13	0.1
11	0.1
9	1/L
7	1/L

Table 3.1.2. Lanczos Smoothing Filter Coefficients.

		Center Point														
L	f_{cut}	**-7**	**-6**	**-5**	**-4**	**-3**	**-2**	**-1**	**0**	**1**	**2**	**3**	**4**	**5**	**6**	**7**
15	0.100	-5.88E-03	-9.14E-03	3.58E-18	2.91E-02	7.73E-02	1.33E-01	1.78E-01	1.95E-01	1.78E-01	1.33E-01	7.73E-02	2.91E-02	3.58E-18	-9.14E-03	-5.88E-03
13	0.100		-4.96E-03	2.68E-18	2.51E-02	7.22E-02	1.30E-01	1.79E-01	1.98E-01	1.79E-01	1.30E-01	7.22E-02	2.51E-02	2.68E-18	-4.96E-03	
11	0.100			1.53E-18	1.98E-02	6.59E-02	1.28E-01	1.83E-01	2.05E-01	1.83E-01	1.28E-01	6.59E-02	1.98E-02	1.53E-18		
9	0.111				6.72E-03	4.89E-02	1.25E-01	2.02E-01	2.34E-01	2.02E-01	1.25E-01	4.89E-02	6.72E-03			
7	0.143					1.44E-02	1.03E-01	2.34E-01	2.98E-01	2.34E-01	1.03E-01	1.44E-02				

3.2 System Characterization

The semi-arid Salt & Verde River watersheds occupy a geographically, geologically, and climatologically diverse region of central Arizona with a hydrology unlike those of other water resource systems that have been studied, even within the CRB. It would be a mistake to apply specific research conclusions from the Upper Basin of the CRB (UCRB) to these LCRB watersheds, although the general methods described herein can be applied elsewhere. Simplifying assumptions of normality in various variables do not apply to the Salt and Verde. Seasonal climate shifts are extreme, natural

variability is prevalent, and hydroclimate distributions are highly skewed. These characteristics were apparently known and incorporated to the SRP system design over a century ago at a time when the instrumental record was in its infancy. Now, at more than 120 years of data, the Salt-Verde system has one of the longest data records for a water resource system in the western United States. A thorough characterization of many variables is therefore feasible, with many ways in which they can be reported. Much of this is provided in the methodology development sections of this document, since the algorithms needed to link methods are grounded in the empirical evidence. What follows are some characterizations not provided in subsequent document sections.

3.2.1 Monthly to Seasonal Characterization

Typical monthly precipitation and runoff on the Salt-Tonto and Verde watersheds are shown in Figures 3.2.1 & 3.2.2. It is readily apparent that monthly precipitation is dual-moded, with maximums in January and August. However, runoff from winter precipitation is generally delayed to late-winter-early-spring through snowpack accumulation and melting. Despite cool winter-spring temperatures, the runoff efficiency is typically only 15% on the Salt and 11% on the Verde. In part this is due to intermittency of precipitation events necessitating soil re-saturation before the next runoff-yielding event occurs. The large monsoonal summer rains yield very low runoff (7% Salt, 4% Verde) due to high summer evapotranspiration on the watersheds. It quickly becomes apparent that replenishment of the reservoirs is primarily dependent on large winter precipitation events and/or their continuity, as summer precipitation yield cannot make up for large winter deficiencies.

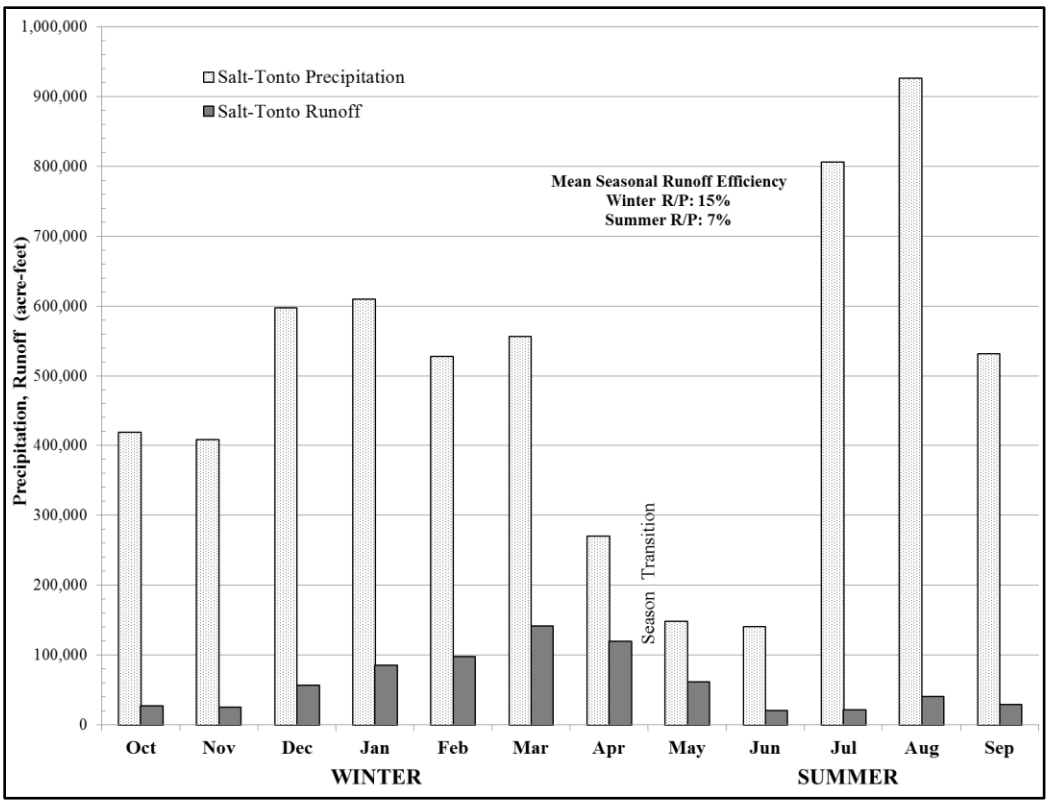

Figure 3.2.1. Typical Monthly Precipitation and Runoff Cycle of the Salt Watershed.

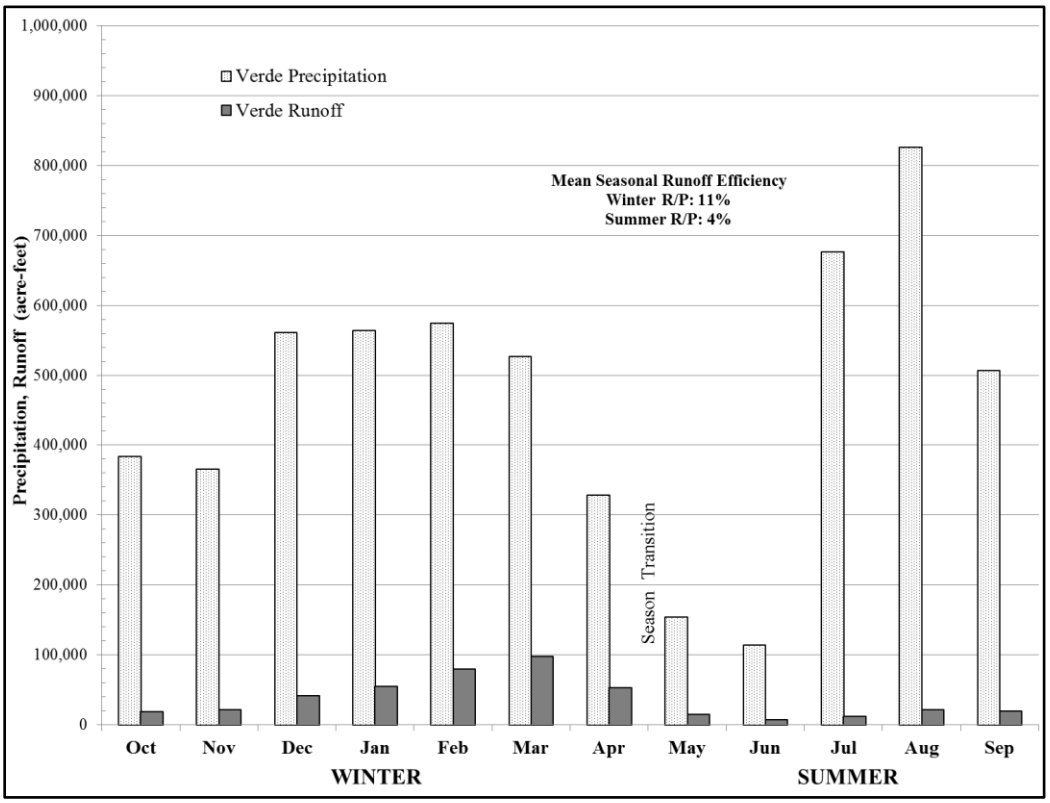

Figure 3.2.2. Typical Monthly Precipitation and Runoff Cycle of the Verde Watershed.

The cumulative runoff from the watersheds as a proportion of a typical water year's total is shown in Figure 3.2.3. Runoff in the fall months is below an equal monthly average. Then, as most runoff follows winter precipitation, about 80% of the year's yield is complete by the end of April on the Verde and the end of May on the Salt. The inflection points at those times indicate when winter runoff is largely complete and the natural hydroclimate transition into summer is occurring. Salt runoff is delayed relative to the Verde due its higher elevation terrain and cooler climate where more precipitation falls as snow with a later melt. The watershed and reservoir conditions are known to SRP water management by late-winter, and corresponding decisions are taken by May 1st. That date was therefore taken as the demarcation point for the seasonally-

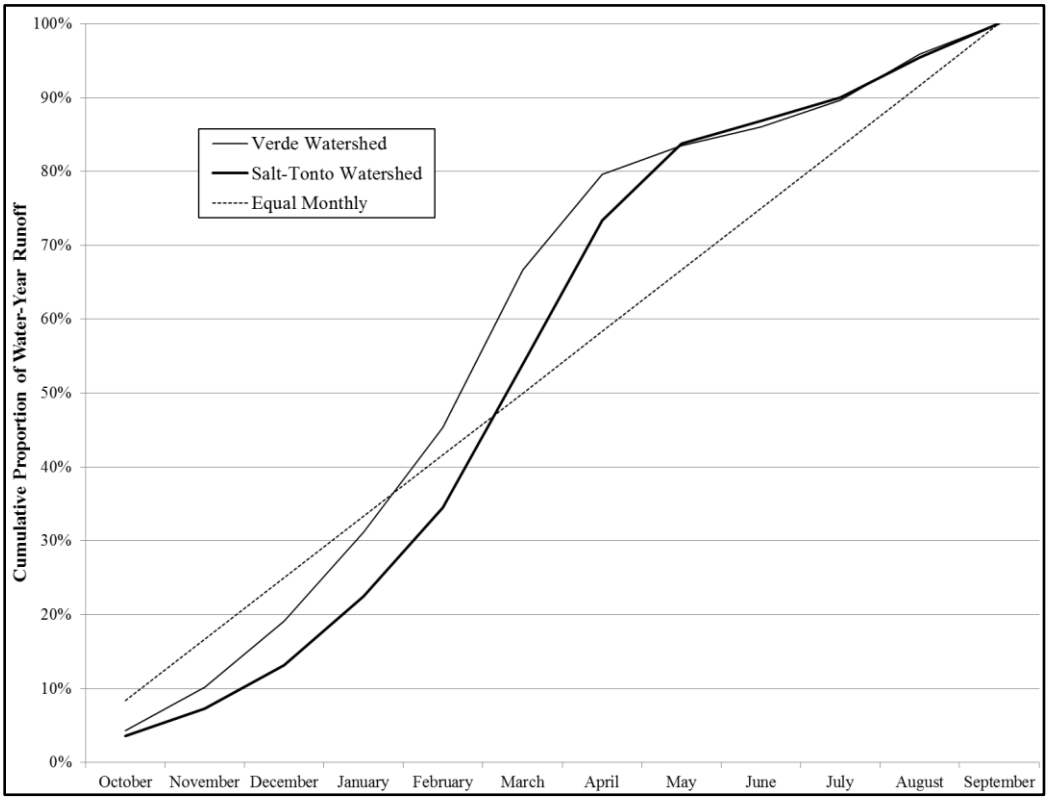

Figure 3.2.3. Typical Cumulative Monthly Proportion of Runoff Through the Water Year.

based analyses of this investigation even though not all Salt runoff will have occurred during a wet year. As discussed in the stochastic simulation section of this document (Sec.3.4), Salt runoff carryover into May increases winter-to-summer correlation which is exploited in that methodology.

Typical monthly runoff to the reservoirs is shown in Figure 3.2.4 to occur earlier than water deliveries to customers are required. About 60% of annual deliveries occur over the 5 months of summer, with 40% taking place over the 7 winter months. The purpose of the reservoirs is thereby fulfilled, retaining the resource until it is needed in mid-summer, as well as buffering against high year-to-year variability.

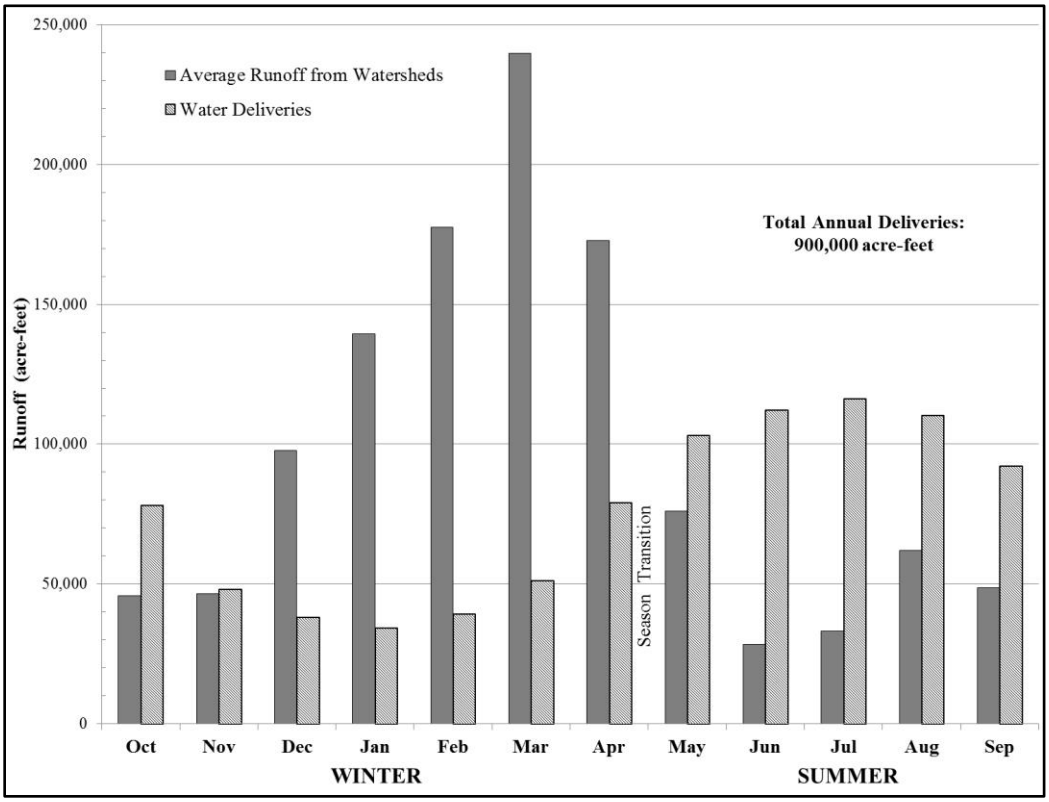

Figure 3.2.4. Typical Monthly Runoff to Reservoirs and Monthly Water Delivery Schedule.

3.2.2 30-Year Climate Normals

Climate-normal temperature and precipitation are often used as reference values for various comparison purposes. They are calculated from the trailing 30 years of data at a decadal time-step (1901-1930, 1911-1940, …, 1981-2010) and used for comparative purposes until again updated. If persistent climate variability or trends are present comparisons with climate normals may have questionable informative validity. For example, only climate-normal temperature values from 1960 to 1990 remained approximately consistent within the historical record (Figs. 3.2.5 & 3.2.6). Adjacent calculations were strongly influenced by warming trends that should instead be compared to other, earlier reference periods. That approach is taken in the climate change forecast section (Sec. 3.6) of this document.

Similarly, 30-year trailing average precipitation values for each watershed-season are given in Figures 3.2.7 & 3.2.8 where extended periods of natural variability are evident, particularly in winter. Figure 3.2.9 combines the watersheds for a calculation of each season's variability in proportion to the long-term average. The historical periods of drought and excess are evident, and 30-year trailing averages vary by about ±5% in summer and -10% to +15% in winter. As will be shown in the results chapter (Chap. 4) of this document, such variability may be sufficient to offset anticipated warming impacts on runoff such that future elevated temperature effects may not be resolvable amidst precipitation variability.

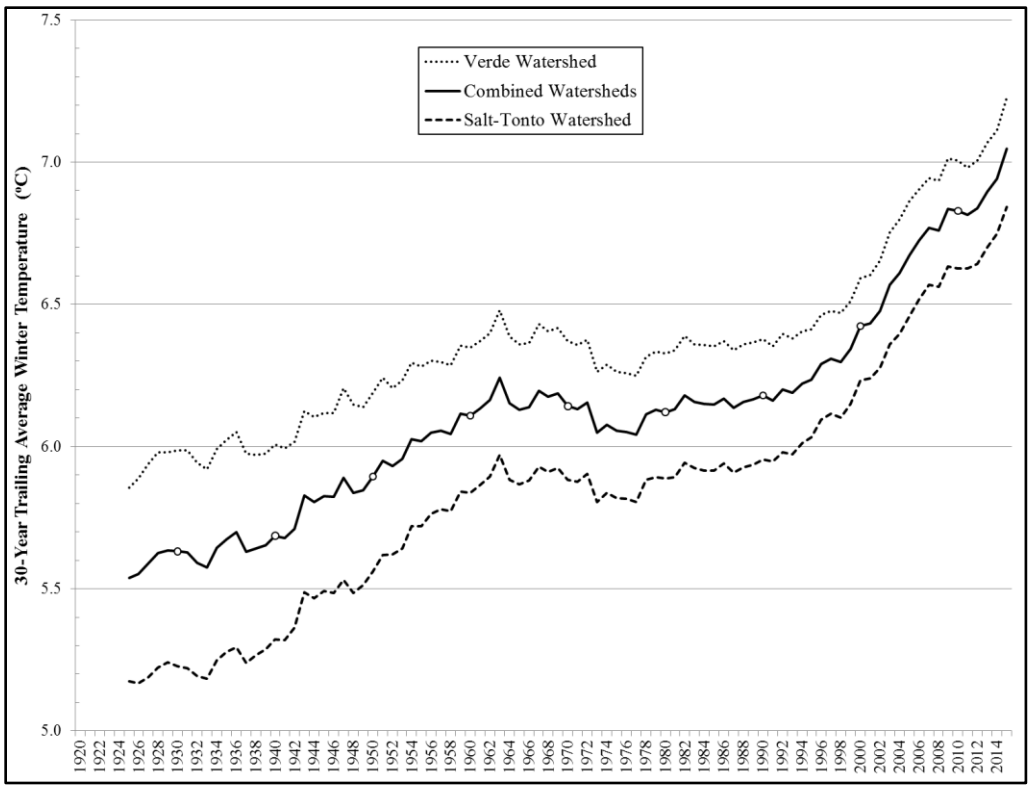

Figure 3.2.5. 30-Year Climate-Normal Winter Temperatures.

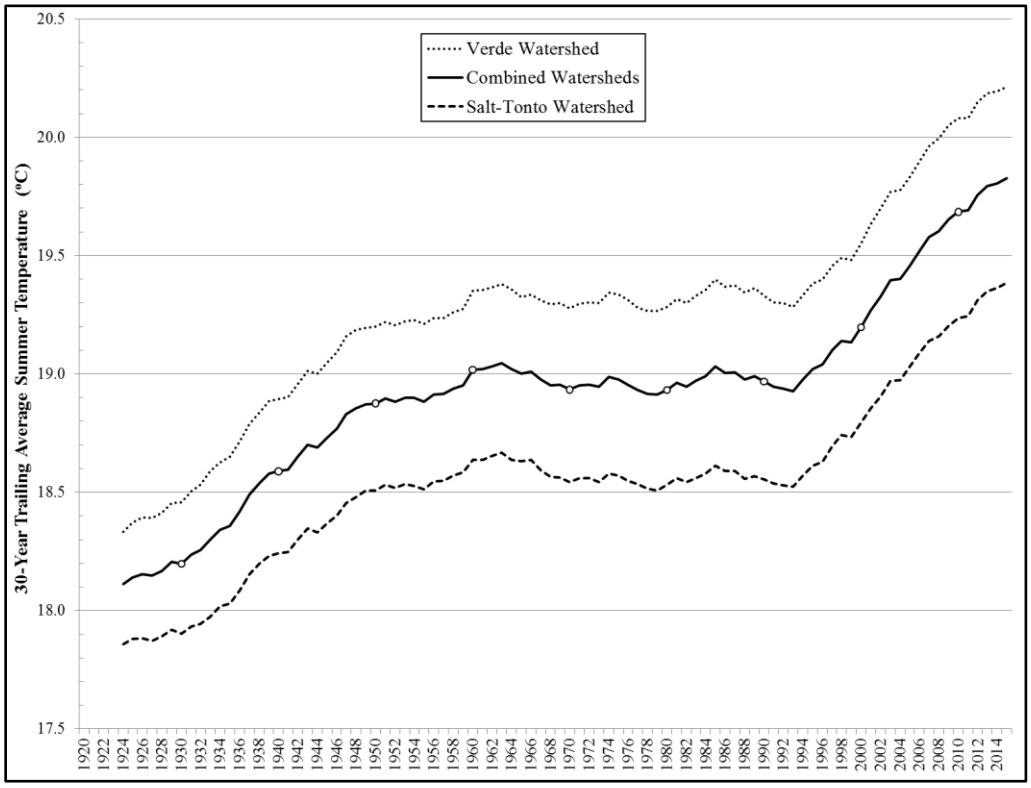

Figure 3.2.6. 30-Year Climate-Normal Summer Temperatures.

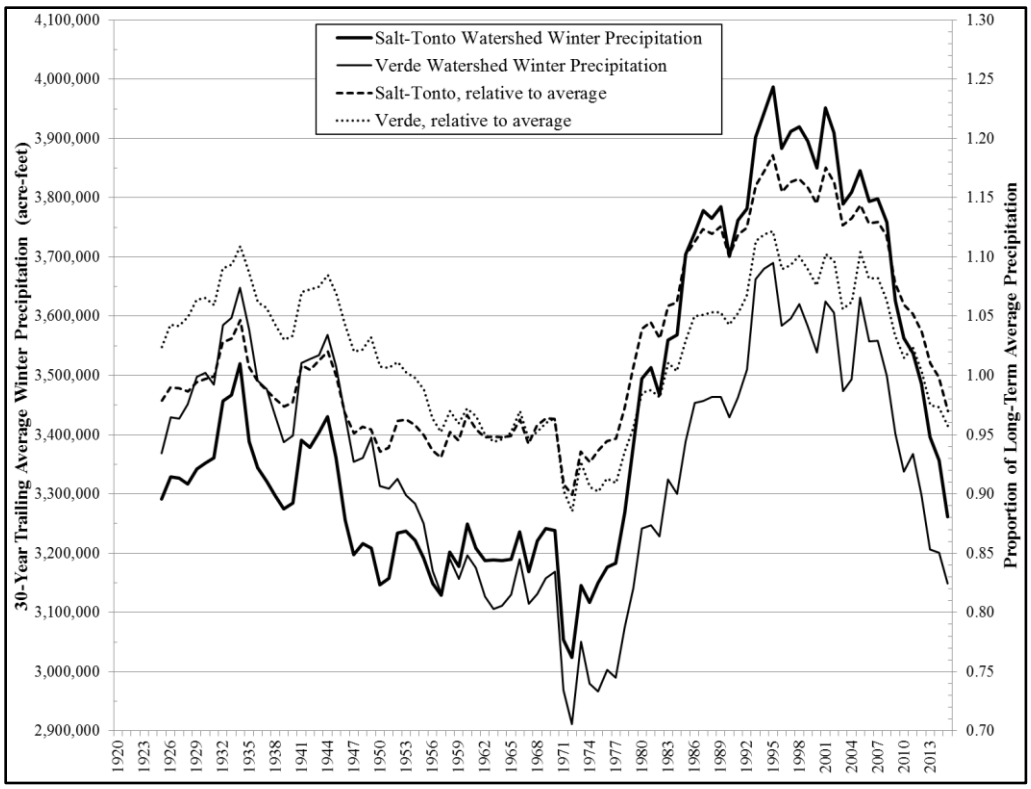

Figure 3.2.7. 30-Year Climate-Normal Winter Precipitation.

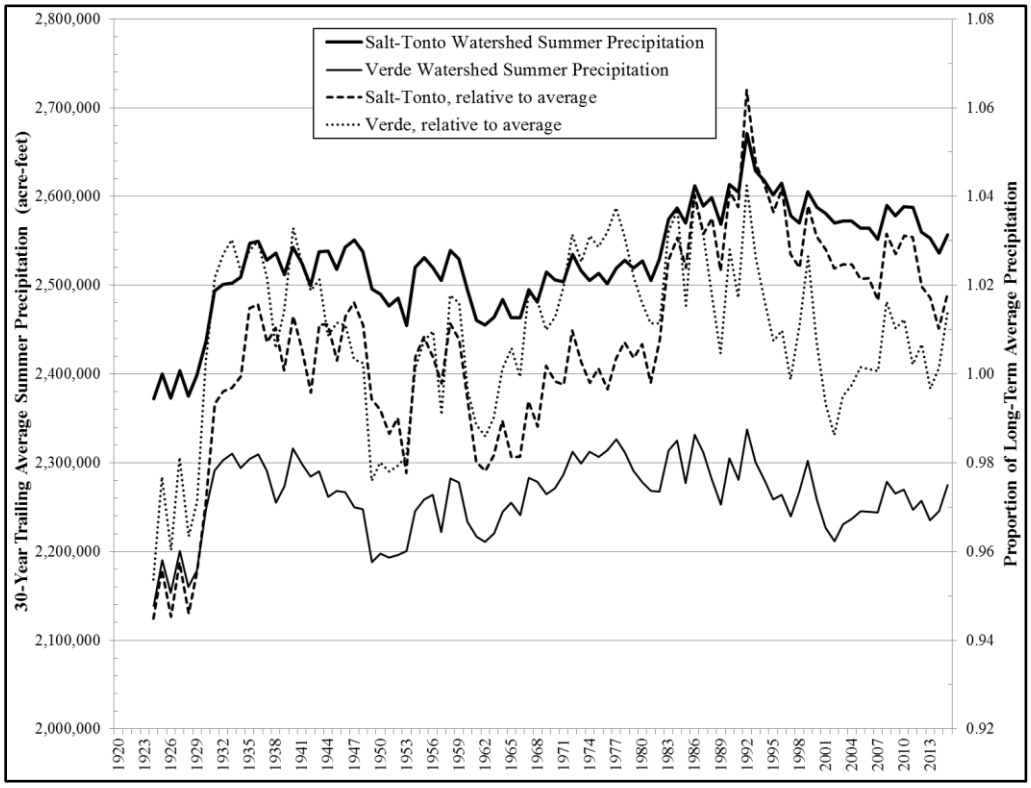

Figure 3.2.8. 30-Year Climate-Normal Summer Precipitation.

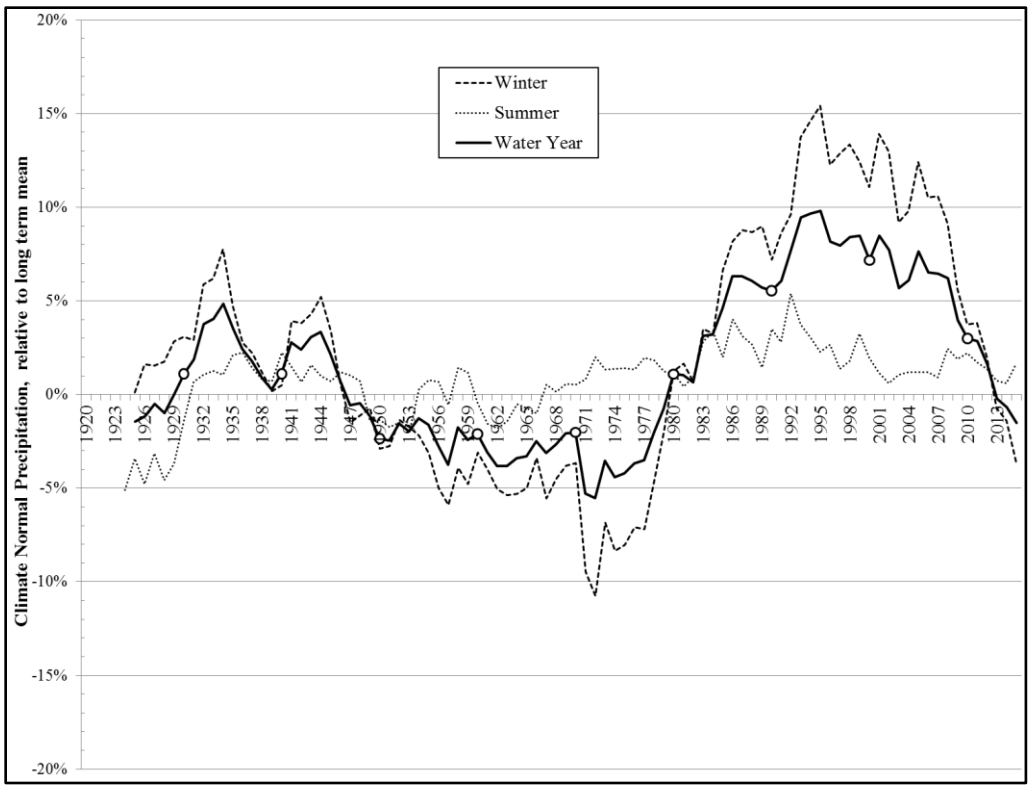

Figure 3.2.9. Variation in Climate-Normal Precipitation Relative to the Long-Term Average.

3.2.3 Importance of Winter Precipitation

The information above is indicative of the importance of winter precipitation as the primary governing influence on reservoir system sustainability. Tables 3.2.1 & 3.2.2 compare the proportions of precipitation and runoff among each watershed-season. While summer precipitation is 43% of what falls in a water year, it only accounts for 25% of reservoir system inflows due to low runoff efficiency amidst high evapotranspiration. Summer effects are most pronounced on the Verde basin where warming has been highest and streamflows reduced for a variety of reasons, as reviewed in subsequent chapters of this document.

Table 3.2.1. Proportions of Typical Annual Precipitation on Watersheds.

	Winter	Summer	Annual
Salt-Tonto	29%	23%	52%
Verde	28%	20%	48%
Total	57%	43%	

Table 3.2.2. Proportions of Typical Annual Reservoir System Inflows.

	Winter	Summer	Annual
Salt-Tonto	43%	17%	60%
Verde	32%	8%	40%
Total	75%	25%	

The winter precipitation time series in Figure 3.2.10 will be tested and found to be stationary over the instrumental record. Nevertheless, as can be seen, that does not preclude the series from having periods both above and below the long-term mean. Pluvial periods are notable following the 1890s drought and again from the mid-1970s to mid-1990s with intervening drought-prone periods. Such natural variability becomes accentuated by low runoff efficiencies so that precipitation coefficients of variation of 0.40 are amplified to 0.87 for runoff (Table 3.3.5, Fig. 3.2.18). It is noted that the Salt and Verde precipitation series are highly correlated (Fig. 3.2.11), and that Verde precipitation tended to be slightly higher than the Salt before 1950, but lower thereafter. This is a small but interesting observation whose investigation was outside the scope of this research.

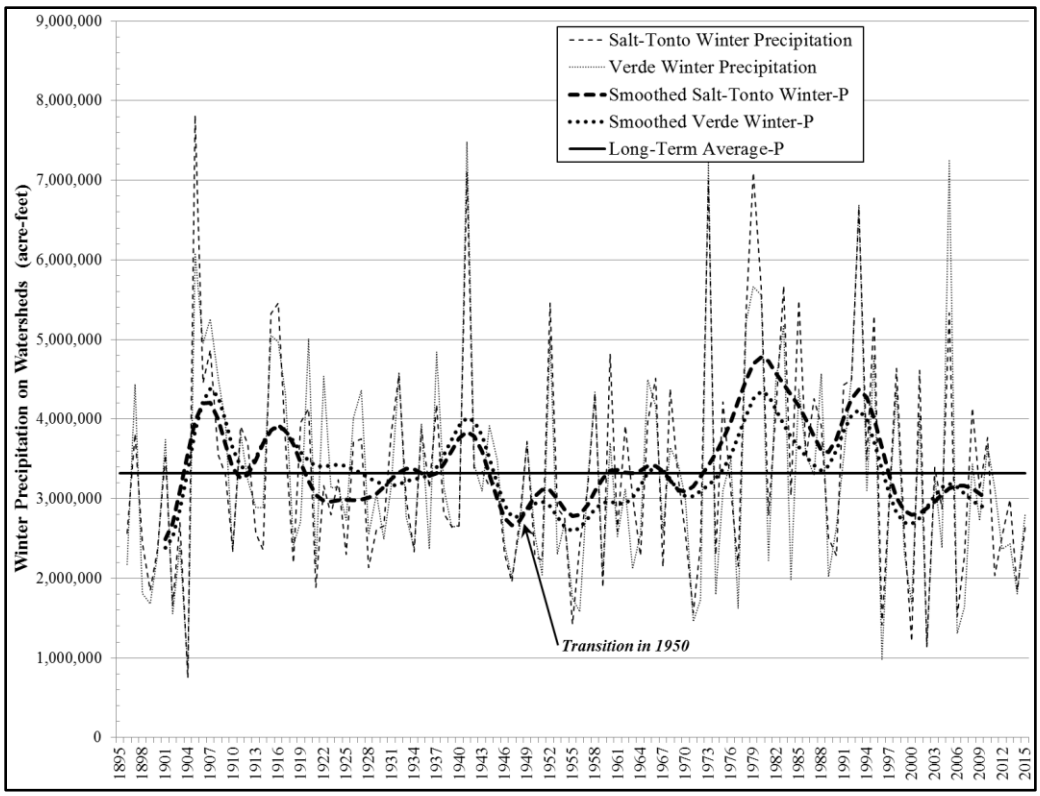

Figure 3.2.10. Time Series of Winter Precipitation on the Watersheds.

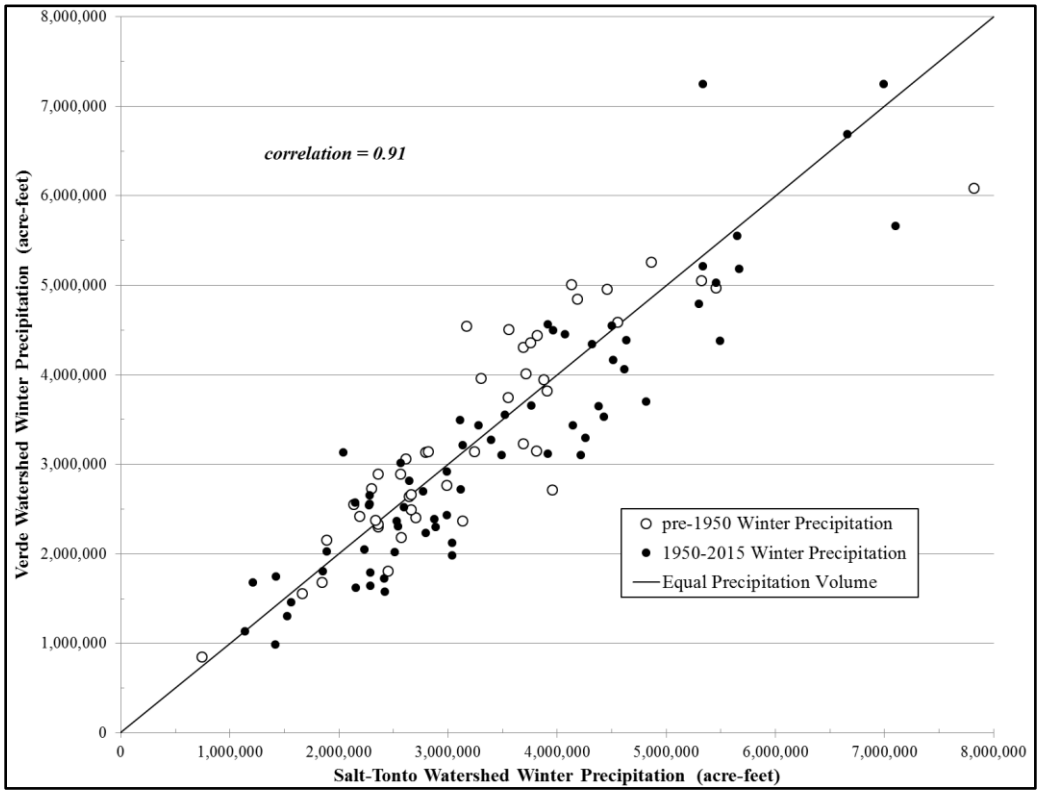

Figure 3.2.11. High Correlation of Salt and Verde Precipitation Time Series.

3.2.4 Runoff Efficiency of Precipitation

Comparative time series of precipitation and runoff are shown in Figures 3.2.12 to 3.2.15, along with runoff efficiency observations. Wet years tend to have higher efficiency while dry ones are lower, again highlighting the importance of wet winters. Verde summer R/P has remained very low since 1928 when a step-change in the runoff series occurred. This is explored further in the stationarity section (Sec.3.3) of this document. The important dependency of runoff efficiency on precipitation level will be explored in the hydroclimate sensitivity section (Sec. 3.5) of this document.

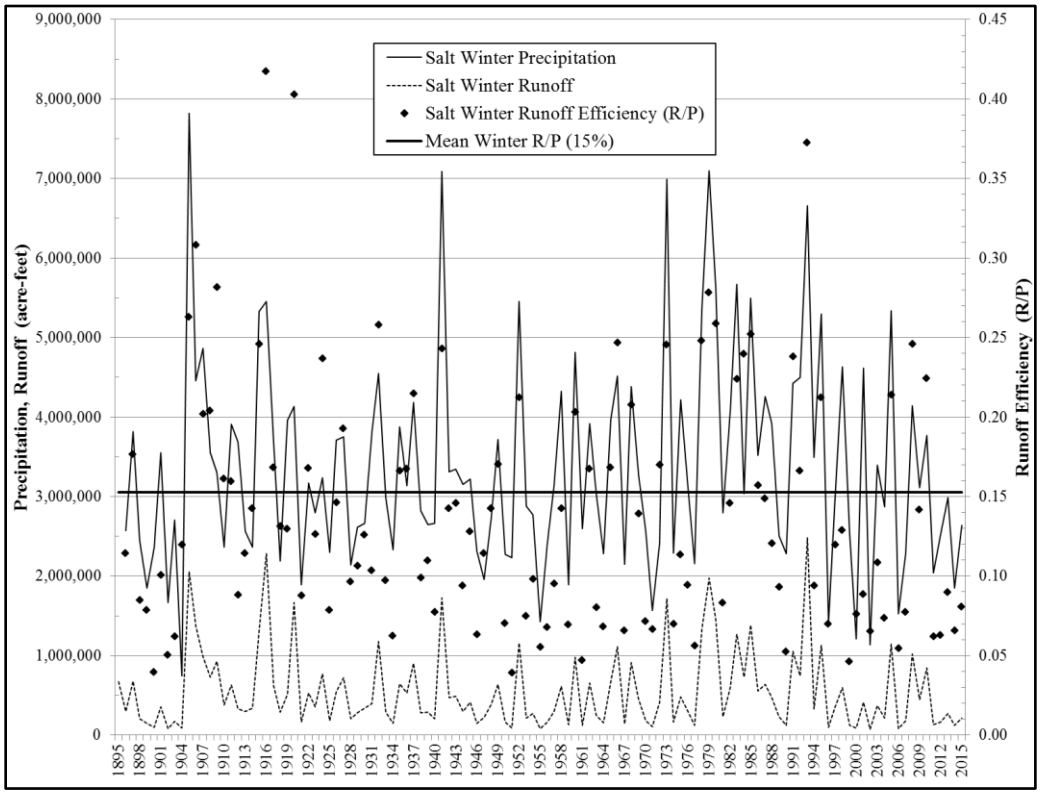

Figure 3.2.12. Time Series of Salt Winter Precipitation, Runoff, and Runoff Efficiency.

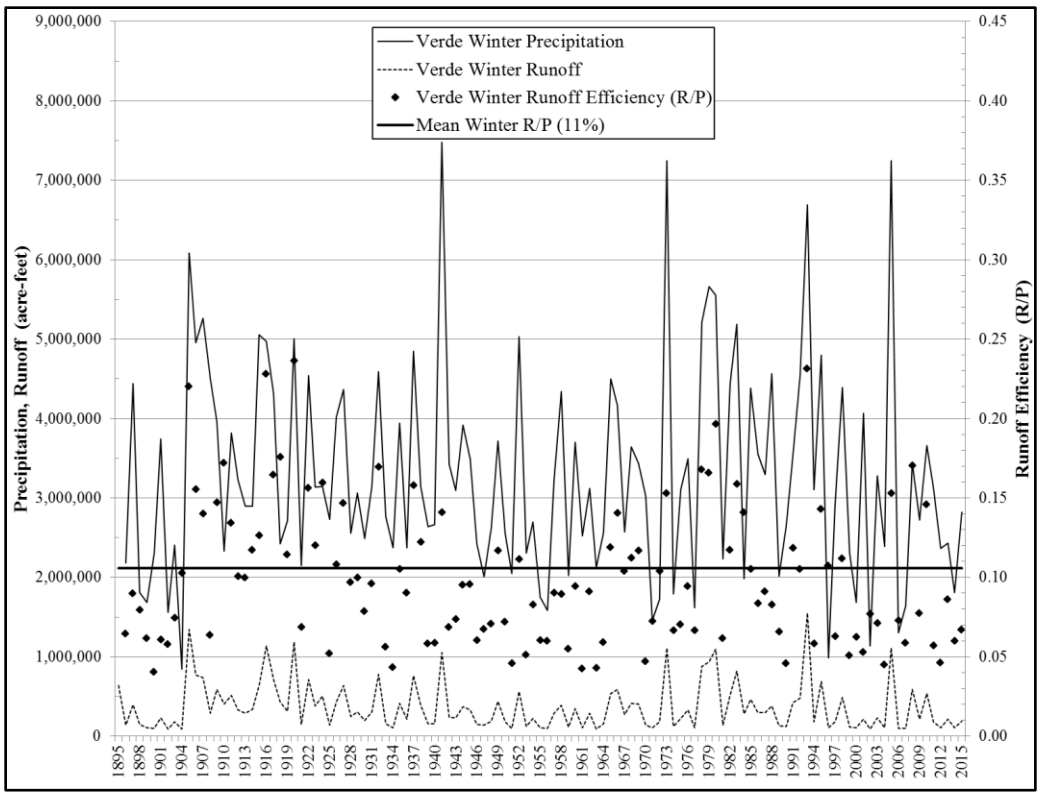

Figure 3.2.13. Time Series of Verde Winter Precipitation, Runoff, and Runoff Efficiency.

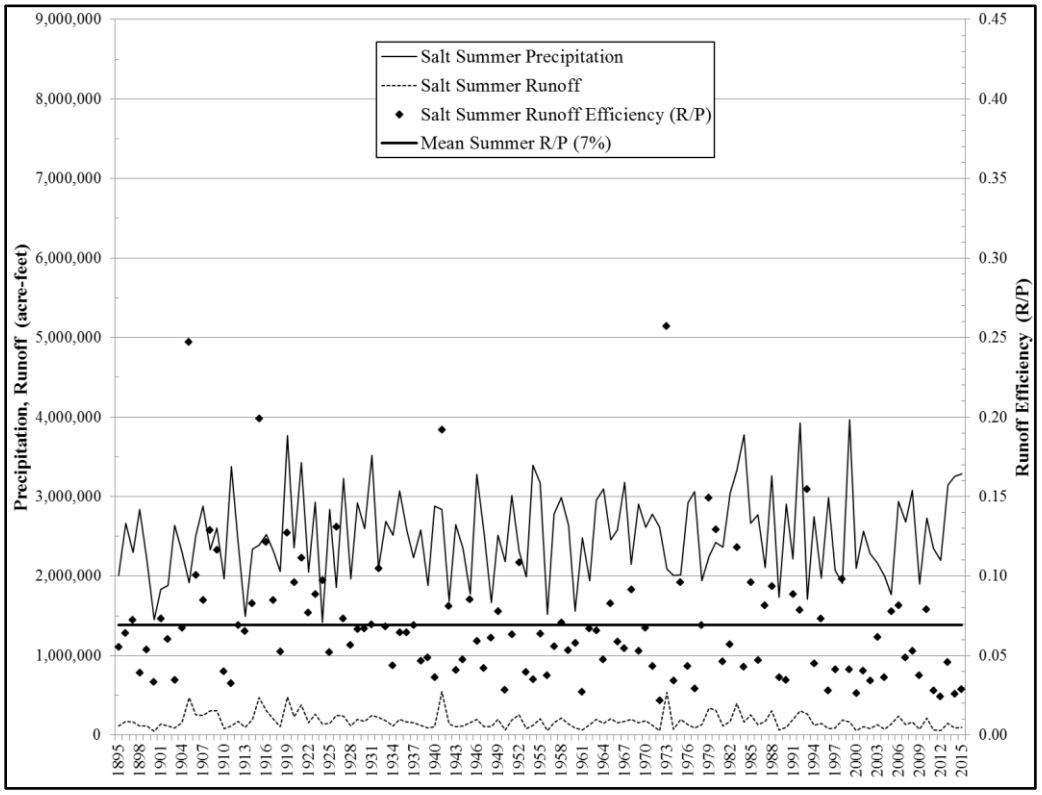

Figure 3.2.14. Time Series of Salt Summer Precipitation, Runoff, and Runoff Efficiency.

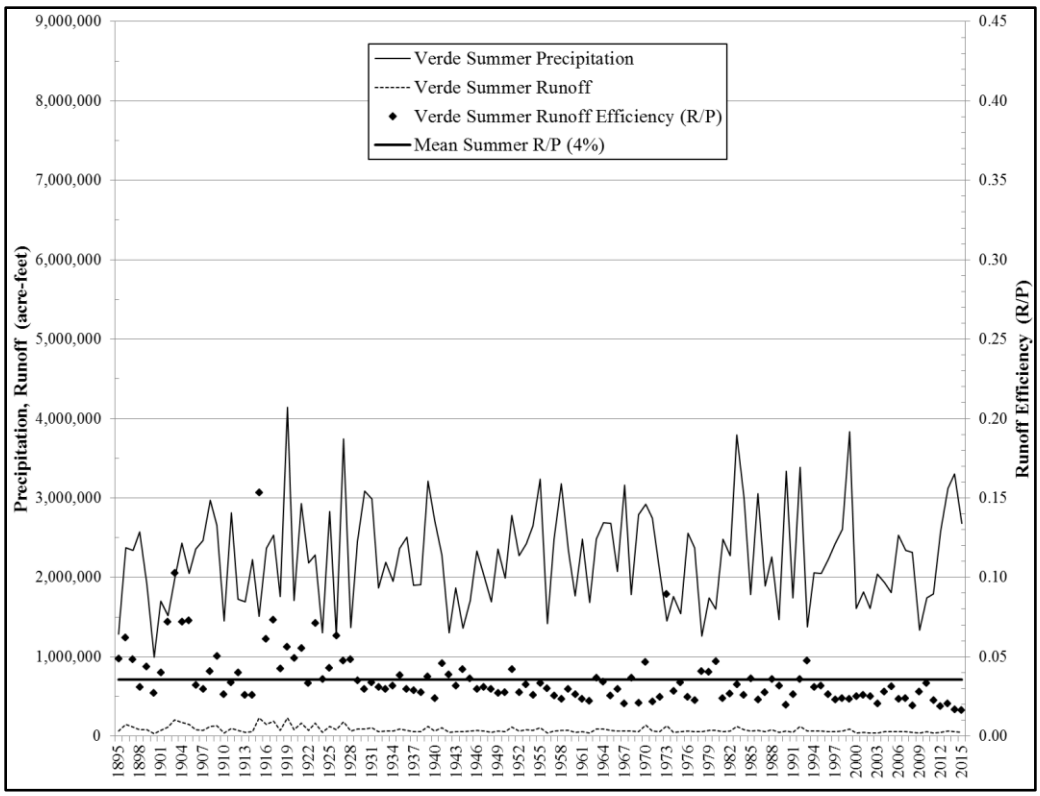

Figure 3.2.15. Time Series of Verde Summer Precipitation, Runoff, and Runoff Efficiency.

3.2.5 Net Basin Supply

Net basin supply of water is defined as runoff less any miscellaneous losses which result in reservoir storage different from what would be expected per the gaged inflows and outflows. Figures 3.2.16 & 3.2.17 provide some insight to the influence of miscellaneous loss factors as a function of runoff level. If there were no losses NBS should equal runoff along the equivalence line. At low runoff levels during dry years, during both winter and summer, there are small losses. These are most notable on the Salt side of the system where the largest reservoirs are located, and NBS tends to be lower than runoff. However, at levels in the upper tail of the runoff distribution NBS

tends to be higher than runoff where there are net storage gains not captured by the stream gages. These are important water supplements during wet winters. The time series of NBS, which is the central variable of interest for this investigation, is shown in Figure 3.2.18. Drought-free periods correspond to the pluvial precipitation eras, and droughts of the past 127 years are noted (drought is defined in Sec. 4.2.1). These will be compared to simulation results later in this document. It can also be noted that the recent 2011-2015 drought may not yet be ended, as 2016 data is incomplete at the time of this writing.

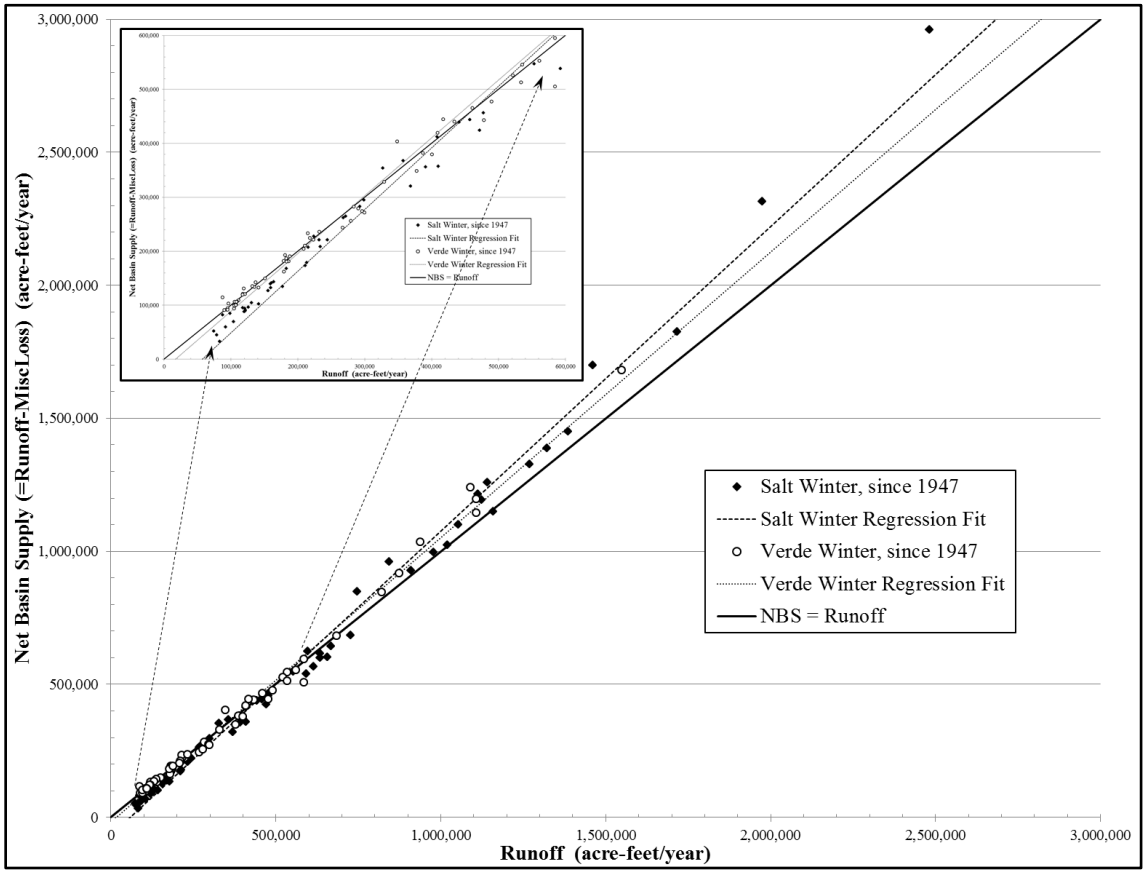

Figure 3.2.16. Net Basin Supply Compared to Watersheds' Runoff in Winter.

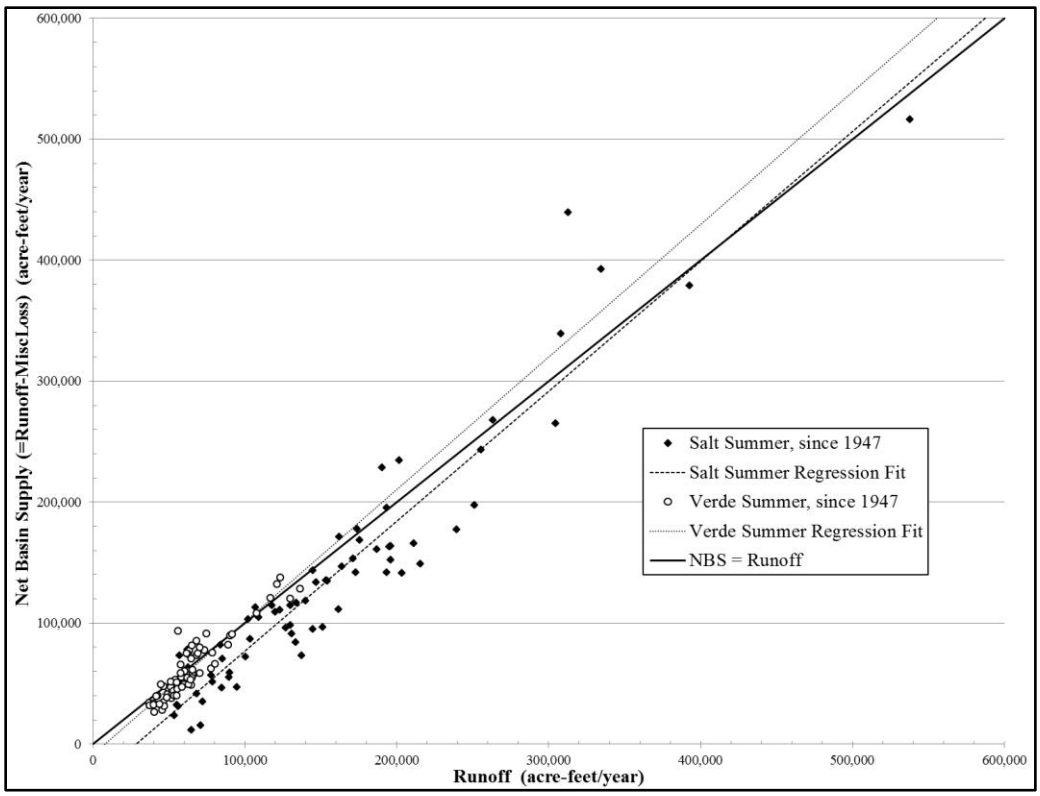

Figure 3.2.17. Net Basin Supply Compared to Watersheds' Runoff in Summer.

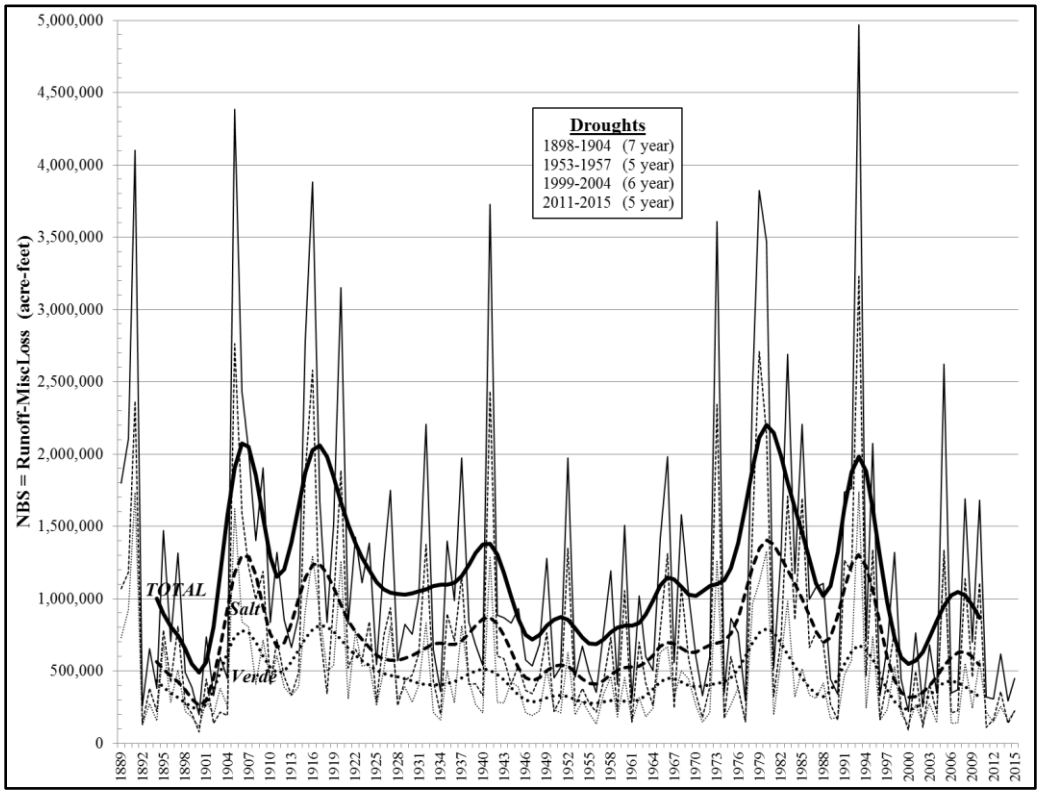

Figure 3.2.18. Time Series of Water-Year Net Basin Supply.

3.2.6 Time Series Analyses

A historical perspective on how the important variables addressed in this investigation have evolved over time helps to inform the analyses. A number of time series are reported in various sections of this document, so a summary table is provided here to assist the reader in referencing them.

Table 3.2.3. Reference Table, Hydroclimate Variable Time Series.

	Temperature	Precipitation	Runoff	NBS
Salt watershed, Winter	Fig. 3.3.1	Fig. 3.3.3	Fig. 3.3.2	
	Fig. E2	Fig. 3.2.10		
		Fig. 3.2.12	Fig. 3.2.12	
Salt watershed, Summer	Fig. E4		Fig. 3.3.6	
		Fig. 3.2.14	Fig. 3.2.14	
Salt watershed, Water Year				Fig. 3.2.18
Verde watershed, Winter	Fig. E1	Fig. 3.2.10		
		Fig. 3.2.13	Fig. 3.2.13	
Verde watershed, Summer	Fig. E3	Fig. 3.3.4	Fig. 3.3.5	
		Fig. 3.2.15	Fig. 3.2.15	
Verde watershed, Water Year				Fig. 3.2.18
Water Year, both watersheds	Fig. 3.6.17			Fig. 3.2.18
	Fig. E9			
Salt reservoirs, Winter	Fig. E6			
Salt reservoirs, Summer	Fig. E8			
Verde reservoirs, Winter	Fig. E5			
Verde reservoirs, Summer	Fig. E7			
Water Year, all reservoirs	Fig. E10			

3.3 Stationarity of Climate and Streamflow

3.3.1 Abstract

Several studies drawing upon general circulation models have investigated the potential impacts of future climate change on precipitation and runoff to stream flow in the Southwest United States, suggesting reduced runoff in response to increasing temperatures and less precipitation. With the hydroclimatic changes considered to be underway, water management professionals have been (erroneously) counseled to abandon historical assumptions of stationarity in the natural systems governing surface water replenishments. Stationarity is predicated upon an assumption that the generating process is in equilibrium around an underlying mean and that variance remains constant over time. Stationarity assumptions for each hydroclimate variable are central to the stochastic methodology and multi-decadal forecasts developed for this investigation.

To examine the evidence of forthcoming change, the long-term records of surface temperature and precipitation in the Salt and Verde watersheds along with corresponding gage records were evaluated with time series analysis methods and testing criteria established per statistical definitions of stationarity. Statistically significant temperature increases were found, with persistently non-stationary time series in the recent record relative to the earlier historical record. However, tests of precipitation and runoff did not reveal persistent reductions, indicating that they have remained stationary processes. They display transitions through periods of drought and excess, with recent precipitation and stream flows found to be close to the long-term averages. The analysis has been extended with the Hurst-Kolmogorov methodology, and there are emerging indications of summer runoff and miscellaneous loss effects from elevated temperature. Those are

further explored in the hydrologic sensitivities to climate section (Sec. 3.5) of this document.

The central Arizona hydroclimate does not appear to have exited the envelope of natural variability which would threaten the effective range of the SRP infrastructure. As has been noted by Stakhiv (2011), there have been very few failures of the nation's water management infrastructure within its design capacity. Abandonment of stationarity assumptions for precipitation and runoff is not necessarily supported by the evidence, making it premature to discard its historical records as an instrument by which to assess sustainability of the water resource system. A supportable case can still be made for stationarity-based analysis, and it would be more appropriate to conduct adaptation analyses with application of evidence-based stationary or non-stationary assumptions as warranted, followed by an assessment of decision risk sensitivity to hydroclimate scenarios consistent with understandings of the region under study, as suggested by Wilby and Dessai (2010), Lins and Cohn (2011), Stakhiv (2011), Matalas (2012), Salas et al. (2012), and Brown and Wilby (2012).

3.3.2 Questioning Stationarity

Amidst the complexities and the challenge of incorporating uncertain hydroclimatic trends into water resource forecasts, the attention of the water management community was heightened by the assertions made by Milly et al. (2008) who stated that the concept of stationarity, "the idea that natural systems fluctuate within an unchanging envelope of variability – a foundational concept in water-resource engineering", should be abandoned; and that, since "it cannot be revived", only non-stationary models should henceforth be used in water resource planning. As they explained,

> "For a time, hydroclimate had not demonstrably exited the envelope of natural variability and/or the effective range of optimally operated infrastructure." But, that "In view of the magnitude and ubiquity of the hydroclimatic change apparently now underway, we assert that stationarity is dead" … "because substantial anthropogenic change of Earth's climate is altering the means and extremes of precipitation, evapotranspiration, and rates of discharge of rivers." "The global pattern of observed annual streamflow trends is unlikely to have arisen from unforced variability and is consistent with modeled response to climate forcing."

The stationarity question is not only important because of hypothesized climate change impact to stream flow, but also because it raised the question whether important statistical analysis tools employed by hydrologists will remain valid in the coming decades. As will become evident through this investigation, the stationarity behavior of hydrologic processes has a direct bearing on how the system can be modeled, understood, and forecast for future water management purposes. Considerable debate over stationarity has ensued and it remains an ongoing question (Galloway 2011). The hydrologist's perspective remains distinctly different from the climatologist's for reasons originating in definitions and analytic methodology, which has contributed to the hesitancy by water management to embrace climate modeling outcomes. Confirming the role of stationarity as a foundational concept in system analysis, Nelson (1995) pointed out that, "… the concept of stationarity underlies much of stochastic modeling." Knowledge of whether or not a process generating sequential outcomes is stationary is particularly important to probabilistic representations of the process because non-

stationary modeling is significantly more complex. That is not to say that what might be identified by a climatologist or a statistician as nonstationary behavior cannot be adequately represented in hydrologic modeling. Employment of the stationarity concept within hydrology distinguishes between whether or not changing time series can be modeled with a substantiated set of probabilistic assumptions historically and going forward. If it can, then the series is considered stationary. So, what might at first appear nonstationary can instead conceptually be stationary to the hydrologist. On the other hand, the hydrologist must guard against unsubstantiated stationarity assumptions that can expose model outcomes to understatements of the real risks in the system (Koutsoyiannis et al. 2009). This investigation employs exhaustive stationarity assessments and explicitly defines stationarity assumptions made for the future, grounding them in empirical evidence and current research findings.

An analysis was conducted and published in the Journal of Hydrology (Murphy and Ellis 2014) to confirm whether or not hydrologic variables in the CRB have become non-stationary in their time series per statisticians' definition. Following are extracts from that paper.

3.3.3 Definitions

Some clarification and specificity in the definition of "stationarity" is instructive for an objective and quantifiable assessment. Nelson (1995, 38,185) provides a statistical definition:

> "When the distribution of a process that evolves over time does not depend on time, the process is *time stationary*." "The time-stationarity property in continuous time is: $\Pr\{Y_{t+\Delta t} = j \mid Y_t = i\}$ is the same for all $t \geq 0$ "

So, for any time lag, Δt, between observation intervals the probability distribution for any observation given the (same) probability distribution for another observation elsewhere in the series will be the same for all points in the time series – making a stationary probability distribution equivalent across time, t.

Characterization of stationarity is also of fundamental importance in the application of various forecasting methods, as noted by Makridakis et al. (1998, 136):

> "… *stationary*, meaning that the process generating the data is in equilibrium around a constant value (the underlying mean) and that the variance around the mean remains constant over time."

This is supported in a number of statistics texts, including Burt and Barber (1996, 505): "A stochastic process is stationary if its statistical moments are invariant over time." Additionally, they state:

> "Note that varying degrees, or order, of stationarity are possible. For example, a process might be stationary in the mean, but not in the variance. ….. stationarity at a given order requires stationarity at all lower orders.'

Shumway and Stoffer (2010) also distinguish between orders of stationarity, clarifying with a distinction between strictly stationary and weakly stationary time series. They define a time series as strictly stationary if all moments of its probability function are identical across time, while a weakly stationary time series is constant in just its mean and covariance functions. In general, researchers have acknowledged that in practice it is typically feasible to test just the first and second moments (mean and variance) of a series, and that this is considered sufficient in practice to evaluate whether or not a time series is stationary for most purposes. Therefore, while multiple methods are employed

for the study reported below, the most rigorous assessments through hypothesis testing are focused on the mean and variance of the time series across the historical record.

3.3.4 Autocorrelation and Graphical Analysis

Makridakis et al. (1998) provide some useful guidance about methods to ascertain whether or not a time series is stationary:

> "The visual plot of a time series is often enough to convince a forecaster that the data are stationary or non-stationary. The autocorrelation plot can also readily expose non-stationarity in the mean. The autocorrelations of stationary data drop to zero relatively quickly, while for a non-stationary series they are significantly different from zero for several time lags."

Autocorrelation functions (ACFs) were examined in the preliminary screening for stationarity of each time series of this study. All statistically significant ACFs are reported in the results below, and thorough graphical analyses provide insight to the behavior indicated by ACFs.

3.3.5 Statistical Testing of the First Moment: Mean

The primary approach employed in the stationarity testing study involves a comparison of intervals in the time series against earlier parts of the historical record to ascertain whether the probability distribution within the sampled window is different from the distribution of earlier observations. Among the methods available for statistical significance testing, nonparametric methods are often applied when the nature of the underlying population distribution is unknown or the requirements of a parametric test cannot be met. However, a nonparametric alternative is almost always less powerful than a comparable parametric procedure, provided the parametric test's assumptions are not violated (Burt and Barber 1996; DeGroot and Schervish 2012). Sufficient data exist for

this study from which the distribution of the analyzed variables can be reasonably assessed. This study therefore utilizes parametric testing methods, validly applied in conformance with their requirements considering the characteristic nature of the variable under consideration.

The most common test utilized for parametric statistical inference is the t-test. The methodology for its use in classical hypothesis testing is well-documented (Burt and Barber 1996). Standard two-sample difference-of-means testing between distinct intervals in the time series has been utilized to test for stationarity in the first moment of the probability distributions. The central limit theorem states that, regardless of the nature of the distribution of observations, with a sufficiently large sample size the sample mean is approximately normally distributed. So, even with skewed distributions, t-testing of the mean can remain robust. A sample containing at least thirty observations is commonly considered to be sufficient for valid testing (Burt and Barber 1996, 268-271), and this is the minimum used for this analysis.

There are two formulations of the t-test under assumptions of either equal or non-equal sample population variances. Since it was not a-priori known whether the variances from different intervals in the time series would be equivalent, both testing formulations were applied. Subsequently, testing for equality of variances provided the information needed to adopt one or the other computation for each specific point of hypothesis testing in the time series. Variances were usually found to be consistent across a series.

3.3.6 Statistical Testing of the Second Moment: Variance

The F-test is the common parametric test for equality of variance between two populations, whose test statistic is the ratio of sample variances (Burt and Barber 1996; DeGroot and Schervish 2012). However, the test is sensitive to departures from normality in population distributions. A case can be made for normality of deseasonalized temperature, but the test will not be reliable when applied to the skewed distributions of Salt and Verde runoff and precipitation. Therefore this study employed the Levene test for equality of variances as an alternative that has been shown to have both good robustness and power with heavily tailed and skewed variables (NIST 2012). It can be applied using the mean, the median, or a trimmed mean of subgroups for statistical significance testing using F-statistic tables. The formulation based on the median was used for all variables, while the F-test was also performed for temperature.

3.3.7 Hypothesis Testing, Confidence Levels

Knowledge of whether a generating process is stationary is particularly important because modeling of non-stationary processes involves more sophisticated models. This is readily apparent by the observation that, if persistently non-stationary, each time step in a series is dependent upon the history of all preceding time steps. The probability functions generating sequential time steps must therefore incorporate more variables and establish complicated time-dependent parameterizations of how they will evolve (e.g., trend and cyclicality), while it may not even be exactly clear how they have changed in the historical series. Such complexity will not serve to reduce uncertainty of findings, but rather are likely to complicate and obscure them. So, while the suggestion that water managers should embrace non-stationary modeling may be appropriate if non-stationary

behavior of the time series can be proven, the complexities and expense in doing so are clearly sufficient to force the planner to examine his assumptions with great scrutiny. Furthermore, water infrastructure investments are expensive, involve very long lead-time planning, and entail decision-making processes that scrutinize every assumption, which will include questions of stationarity. For these reasons the hypothesis testing formulations employed in this assessment are constructed such that the null hypothesis of stationarity must be rejected to a reasonable level of statistical confidence before accepting the alternative hypothesis that the time series is non-stationary. So, the research question and the hypotheses for this assessment are:

> Are temperature, precipitation, and runoff stationary in the Salt and Verde watersheds – with particular attention to the recent record relative to the earlier record where less anthropogenic influences were at work? And, more specifically as regards the first moment, have there been persistent temperature increases and decreases in precipitation and runoff?
>
> Null Hypothesis, H_o: No statistically significant difference in sample mean or variance versus the historical record can be established.
>
> Alternative Hypothesis, H_A: The difference in sample mean or variance versus the historical record is statistically significant.

A standard α-value of 5% was used for all statistical hypotheses testing. It is readily apparent from graphical analyses whether a sampled interval is above or below a reference mean, therefore making a test in one direction of change as the research question requires. Testing of the sample mean is thereby conducted to a 95% confidence level. Testing for a change of variance was also conducted to a 95% confidence level.

3.3.8 Reference Sample Population for Hypothesis Testing

To address the research question, interest lies in hypothesis testing of recent data against the earlier historical record to ascertain whether the probability distribution of observations within the recent sample window is different from the distribution of prior observations. The test sample and earlier reference period should each be composed of a contiguous data interval with the minimum thirty year sample size. A test sample of 31 years was used so that its position is recorded as the center year of the time interval. For example, a test sample centered on 1997 spans the years 1982 to 2012, inclusive. This could be tested against the earlier record extending from the first year of record through 1981.

Two approaches for a reference time segment were used in this study: the first thirty years of the historical record, and all cumulative years preceding the test sample interval. The first thirty years is farther back in time and therefore less affected by the evolution of anthropogenic forcings. If the first thirty years of record happened to fall at a period of generally high or low values in the early record, then tests must be evaluated with that taken into consideration. The use of more years subsequent to the first thirty increases the degrees of freedom for statistical significance testing, thereby increasing the power of the test to resolve changes in mean and variance. With hypothesis testing conducted against those two reference time periods, many hundreds of hypothesis tests were performed in the assessment of the three hydroclimate variables for each watershed-season at every possible test year for mean and variance. While there were some slight differences between the first-30-years reference method and the cumulative-years method, findings were found to be essentially the same. Better parameter estimations

from a larger sample size along with avoiding some vagaries of the first-30-years era lead to the cumulative-years method being the preferred approach. Those are the results reported below to simplify the summaries.

3.3.9 Results, Temperature

Statistically significant ACF values are tabulated in Table 3.3.1, and some useful indications of non-stationarity in temperature are apparent. Positive autocorrelations with coefficients in the range of 0.3-0.6 persist in most of the temperature time series out to a lag of several years, indicating non-stationary means. All the time series were graphically analyzed in the manner shown in Figure 3.3.1. The historical data series is shown along with the filter-smoothed series. The cumulative mean is plotted along with the mean of the entire population of observations which, of course, are equivalent at the end of the series. The first complete water year of data is 1896, so 30-year reference statistics are first available in 1925, after which 31-year test samples can be evaluated. The sliding 31-year test sample mean is shown as the bold-dashed curve, beginning with 1941 (spanning 1926-1956 data) and extending to 1997 (spanning 1982-2012 data). Hypothesis testing is performed by comparison of the statistics of each test sample interval to the cumulative statistics of all data through the point 16 years prior. In Figure 3.3.1 the difference-of-means is statistically significant across all years.

Table 3.3.1. Autocorrelations of Hydroclimate Variables for Each Watershed, by Water Year.

	Lag:	1	2	3	4	5	6	7	8	9	10	11	12
Temperature													
	Salt	0.47	0.50	0.57	0.58	0.42	0.49	0.47	0.41				
	Verde	0.40	0.43	0.53	0.53	0.37	0.40	0.40	0.38				
Precipitation													
	Salt	no statistically significant ACF											
	Verde	no statistically significant ACF											
Runoff													
	Salt	no statistically significant ACF											
	Verde	no statistically significant ACF											

only statistically significant values are shown

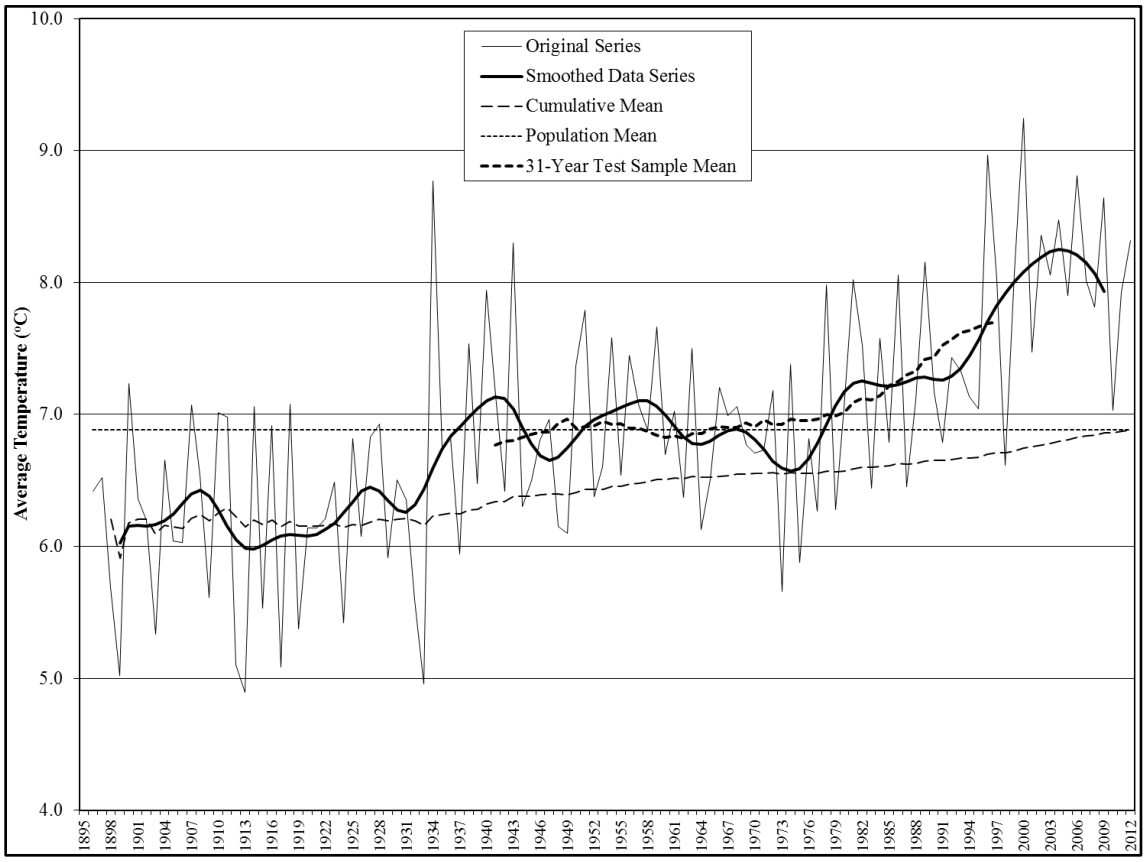

Figure 3.3.1. Average Temperature of the Salt Watershed in the Winter Season.

Each temperature trend-cycle was found to have its own unique pattern, but they all display some similar characteristics which reveal when non-stationary behavior emerged. Average temperature increased during two periods: the 1930s, and from about 1980 to the 2000s. The 1930s increase was generally sufficient to reject the null hypothesis for tests of the mean for all watershed-seasons (Table 3.3.2). Rising temperatures raise the cumulative mean over time, which is another method by which to detect non-stationarity. Average temperature ceased to rise or declined slightly after the 1930s before rising again in recent decades. For the Verde watershed in winter this resulted in a narrowing in the difference-of-means sufficient for the null hypothesis to not be rejected in some intermediate years; but the recent rise caused it to be rejected again. As well, there were some periods of changing variability which resulted in rejection of the null hypothesis for variance tests. But, those are of less consequence than assessments of the mean for overall conclusions of non-stationary average temperature.

Table 3.3.2. Stationarity of Temperature, Hypothesis Test Results.

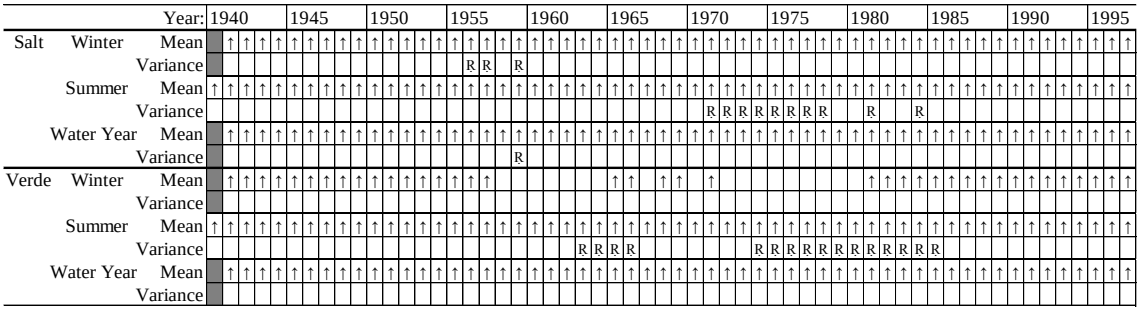

A symbol indicates when the null hypothesis was rejected: ↑ = test-sample mean was higher than reference population mean, ↓ = test-sample mean was lower than reference population mean, R = unequal variances.

3.3.10 Results, Precipitation and Runoff

The autocorrelations for Salt and Verde precipitation and runoff essentially indicate stationarity in their means (Table 3.3.1). Runoff hypothesis tests for difference-of-means briefly reject the null hypothesis during the 1950s drought for the Salt (Fig. 3.3.2) watershed, but across more years for the Verde (Table 3.3.4). There are notably fewer rejections of the null hypothesis for precipitation (Table 3.3.3, Fig. 3.3.3), attributable to the different coefficient of variation of the variables as well as the scaling of runoff elasticity with precipitation level. The wet winters of the 1980s-1990s result in rejection of the null hypothesis across those years to the high side, which ended as the LCRB transitioned into the 2000s drought from which there is recovery to the mean in recent years.

Table 3.3.3. Stationarity of Precipitation, Hypothesis Test Results.

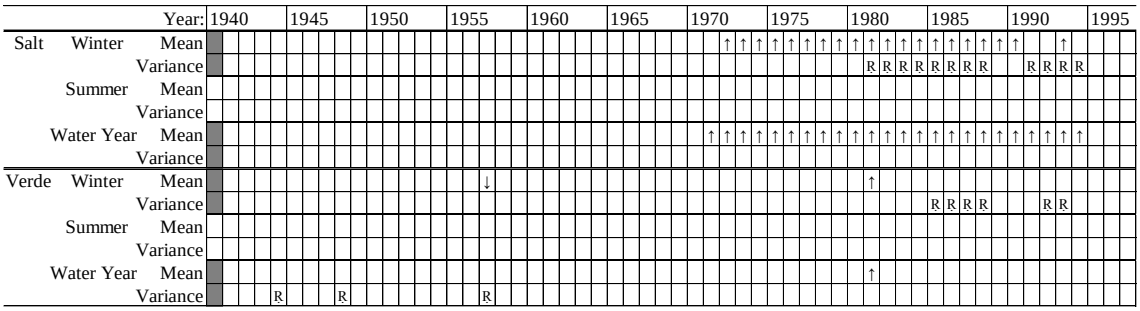

A symbol indicates when the null hypothesis was rejected: ↑ = test-sample mean was higher than reference population mean, ↓ = test-sample mean was lower than reference population mean, R = unequal variances.

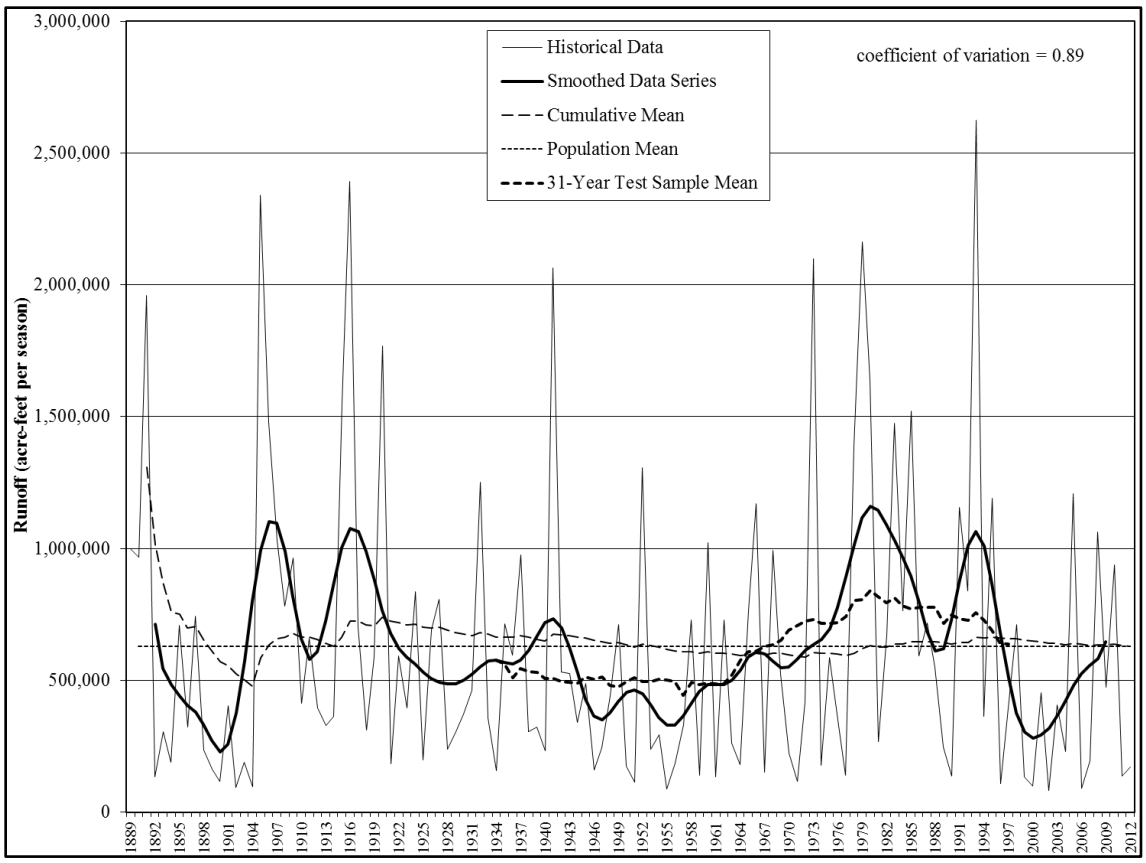

Figure 3.3.2. Runoff from the Salt Watershed in the Winter Season.

Table 3.3.4. Stationarity of Runoff, Hypothesis Test Results.

			Year:	1930	1935	1940	1945	1950	1955	1960	1965	1970	1975	1980	1985	1990	1995
Salt	Winter	Mean			↓				↓					↑	↑	↑	↑		
		Variance			R														
	Summer	Mean				↓	↓	↓	↓	↓	↓	↓	↓				↓		
		Variance				R	R			R	R								
	Water Year	Mean			↓		↓	↓	↓	↓		↓	↓		↑	↑			
		Variance			R	R													
Verde	Winter	Mean			↓		↓	↓	↓	↓	↓	↓	↓	↓	↓	↓	↓	↓	↓
		Variance			R		R	R	R	R	R	R	R	R	R	R	R	R	
	Summer	Mean			↓	↓	↓	↓	↓	↓	↓	↓	↓	↓	↓	↓	↓	↓	↓
		Variance			R	R	R	R	R	R	R	R	R	R	R	R	R	R	R
	Water Year	Mean			↓	↓	↓	↓	↓	↓	↓	↓	↓	↓	↓	↓	↓	↓	↓
		Variance			R	R	R	R	R	R	R	R	R	R	R	R	R	R	R

A symbol indicates when the null hypothesis was rejected: ↑ = test-sample mean was higher than reference population mean, ↓ = test-sample mean was lower than reference population mean, R = unequal variances.

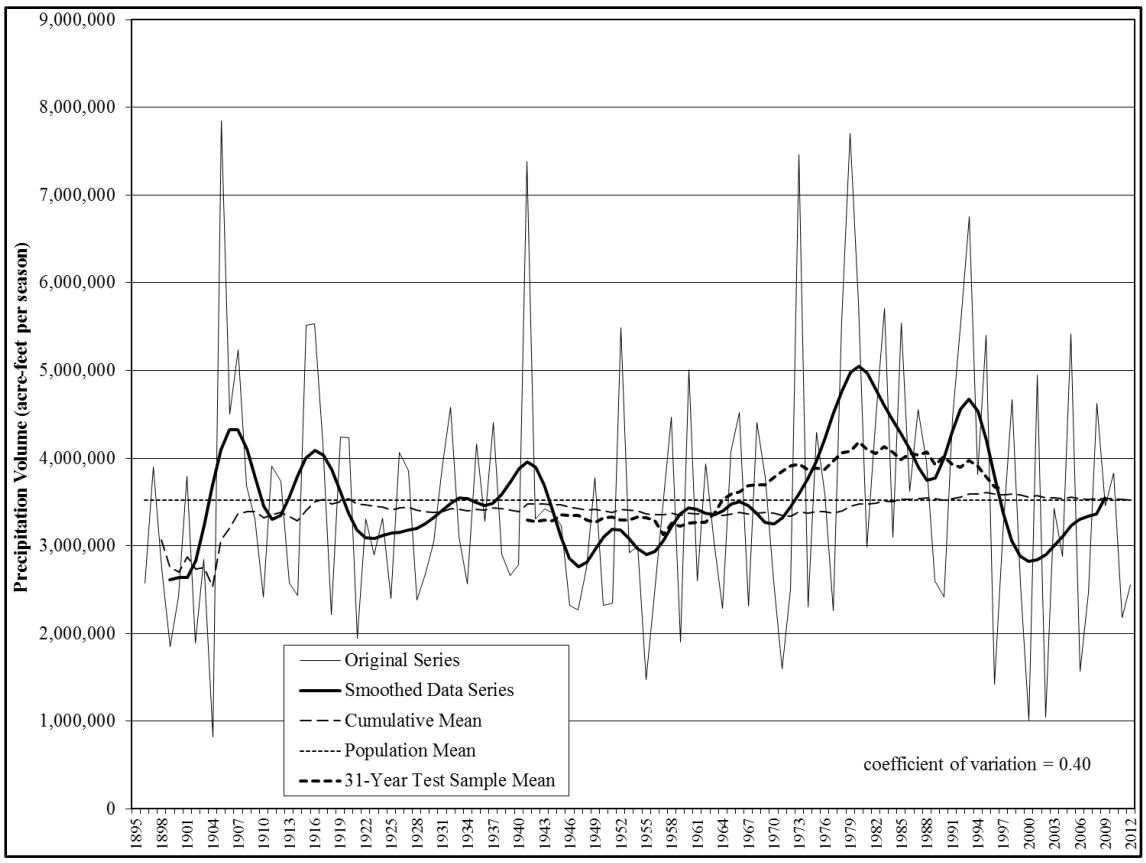

Figure 3.3.3. Precipitation on the Salt Watershed in the Winter Season.

So, a distillation of hundreds of hypothesis tests reveals that the watersheds exhibit periods of winter precipitation and hence runoff both above and below the long-term mean. These temporal transitions over periods of a couple decades invariably return to the long-term average. The cumulative mean curves remain relatively consistent over time, indicating stationarity of the aggregate mean of the underlying generating processes. One might question whether such transitory trend-cycle variations can originate from a stationary probability distribution. To answer this, best-fit probability distributions to the history of the Salt and Verde flows were derived as described in the stochastic simulation section (Sec. 3.4) of this document. The distributions were used to

generate long time series of random outcomes from stationary representations of the watersheds' fixed means, variances and skewness. A 500-year generated sequence of total flow by water year is shown in Figure 3.4.17 compared to the historical series to reveal similarities in trend-cycle behavior (e.g., amplitude and temporality). It therefore appears feasible that excursions around the long-term historical mean are transitory presentations of the underlying generating process, supporting conclusions of stationarity for precipitation and runoff.

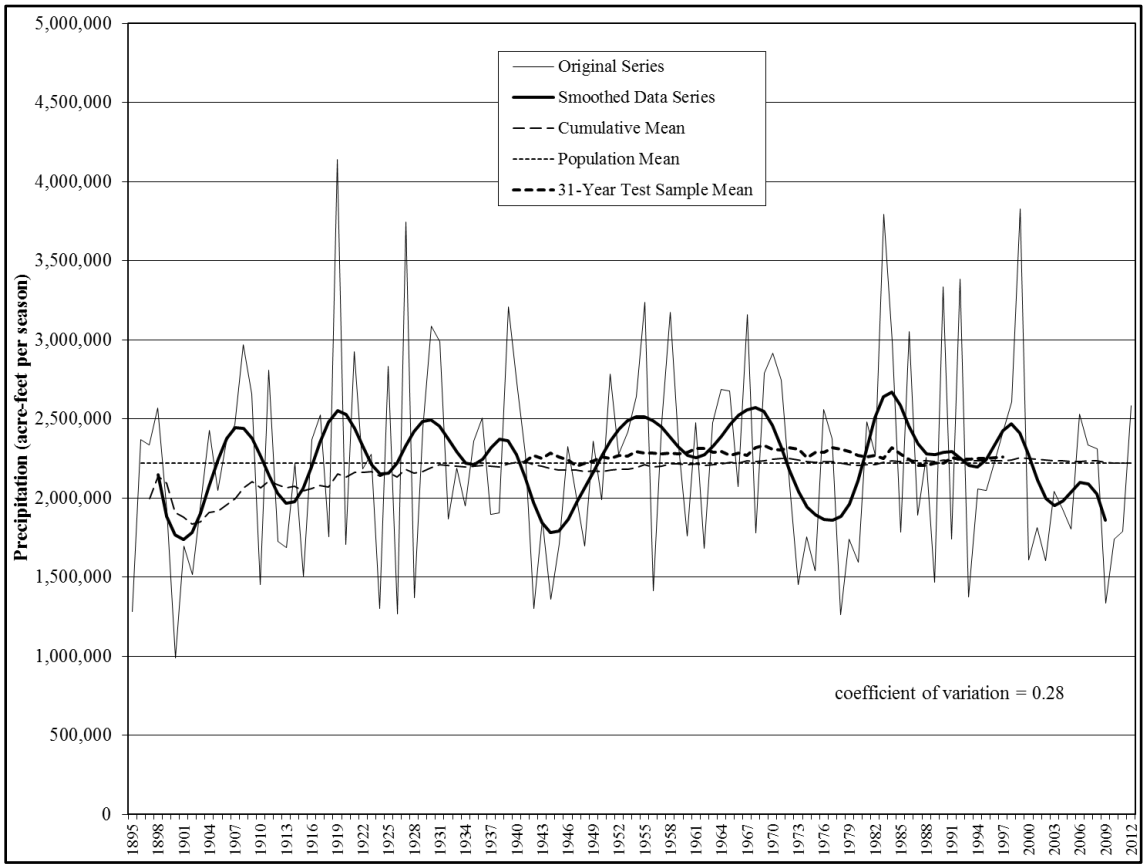

Figure 3.3.4. Precipitation on the Verde Watershed in the Summer Season.

Summer results are distinctly different from the winter season in the LCRB. The Verde basin's precipitation example of this is shown in Figure 3.3.4. The null hypothesis

was not rejected for any mean or variance hypothesis tests conducted on this series (Table 3.3.3). It would be expected that a similarly consistent history would be reflected in the runoff time series; but this was not entirely the case. Rather, a change in the watershed's runoff data series is evident in the late 1920s (Fig. 3.3.5). At that time the running rate of approximately 100,000 acre-feet/summer descended to around 70,000 acre-feet/summer. As can be seen in the figure, test samples are thereafter sufficiently low relative to the reference time period that the null hypothesis is rejected in testing of the mean. Variability of the series is also much reduced, so that variance tests also reject the null hypothesis. Differences are large enough that this test result persists through the ensuing

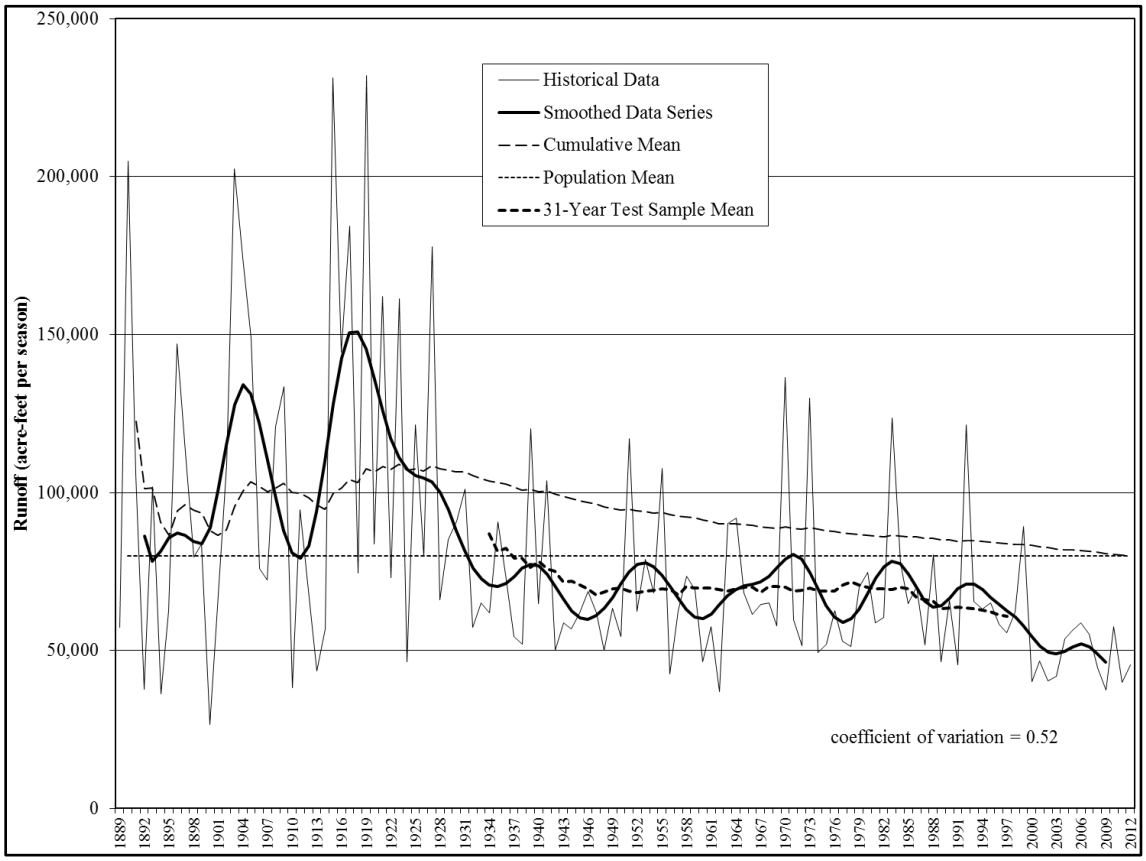

Figure 3.3.5. Runoff from the Verde Watershed in the Summer Season.

several decades of data. The Salt watershed also had a summer runoff transition in the late 1920s; but unlike the Verde, it returned to its earlier level (Fig. 3.3.6). For the Salt, rejection of the null hypothesis only persisted until a near-equilibration of the cumulative mean in the mid-1960s. The average levels of Salt and Verde summer runoff data series have remained relatively constant since the 1920s, although it appears the Verde's may have commenced a further decline since the 1990s.

The Verde summer runoff time series was also tested without pre-1928 data, so that a reference mean is established from the 1928-57 average. Test samples from 1958 to present are not statistically different from that reference timeframe, confirming

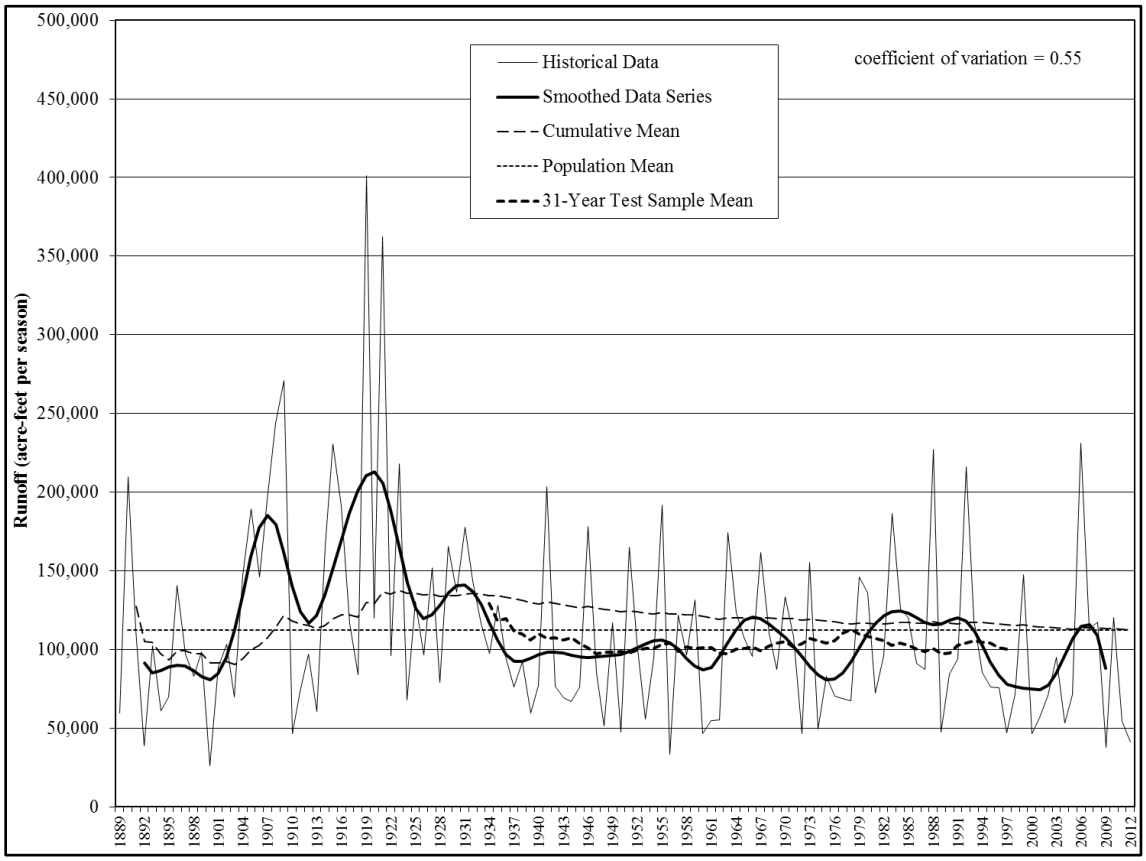

Figure 3.3.6. Runoff from the Salt Watershed in the Summer Season.

stationarity across recent decades. So, what led to the change in Verde summer runoff levels in the 1920s? The lack of transition features in the coincident precipitation and temperature series indicate it is not driven by climate. The history of population growth and consequent water consumption along this Arizona river pose the hypothesis that introduction of water diversions and groundwater pumping have impaired flows, particularly to serve high water demand in summer. Winter consumption is significantly less at a much lower proportion of flow and therefore its impact is not evident in the winter runoff series. Ongoing studies and controversies over water usage and rights in reaches of the Verde River basin lend credence to this hypothesis (Alam 1997; Garner and Bills 2012). This example serves as a counter-argument to the suggestion that once changed, stationarity is lost forever. In this case it was re-established at a level around which hydrologic planning has been conducted for decades. This changed time series is instructive to detection of an anthropogenic influence, albeit not the one anticipated.

3.3.11 Discussion

The decadal variations revealed in this analysis illustrate why the application of trend calculations to intermediate historical intervals is limited in the challenge of identifying whether a change is something other than a temporal effect arising from natural variability. Random selections of numbers from a stationary distribution can readily generate periods in a time series which falsely portray a trend several times more often than expected (Percival and Rothrock 2005). Trend identification results have been found to depend on the methodology used (Baillie and Chung 2002; Mills 2010), with the primary challenge being a low signal-to-noise ratio of emerging trends in a climate time series. The temporary rejection rates of the null hypothesis in this assessment are

consistent with those warnings which motivate the use of the longest available records for comparisons (WMO 1966).

There are multiple possible origins of non-stationarity that can arise in the time series of a hydroclimate variable: landscape interventions changing the precipitation-runoff relationships, various natural events (e.g., fire, floods) that change surface behavior, variations in ocean-atmosphere couplings, and anthropogenic global warming affecting the hydrologic cycle (Salas et al. 2012). The effect of landscape interventions is seen in the Verde summer runoff data, resulting in a shift to lower volumes and resetting at a new, stationary level for several subsequent decades. The pluvial periods of heavy precipitation and the historical drought intervals are often attributed to sea surface temperature (SST) variations affecting ocean-atmosphere coupling, although they provide only a partial explanation of variability and remain a difficult basis from which to make predictions of precipitation and runoff (Balling and Goodrich 2007; Thomas 2007; McCabe and Wolock 2012; Nowak et al. 2012). While the observed temperature increases may be attributable, at least in part, to anthropogenic global warming, manifestations of its effects on the hydrologic cycle remain elusive. No persistent impairment of precipitation and runoff has been found through this method of analysis, and it is difficult to identify any emerging trends in those variables. Statistically, they remain stationary while temperature is persistently non-stationary.

The absence of change in the precipitation and runoff time series when an expectation of nonstationarity has been promulgated through modeling research raises questions about causal mechanisms and detectability of changes should they occur. Expectations of enhanced precipitation yield are often predicated upon the increasing

moisture carrying capacity of warmer air. The expression of this relationship in terms of saturation vapor pressure (the Clausius-Clapeyron equation) quantifies the maximum holding capacity of air as an exponential function of temperature. One degree's change of capacity at low temperatures is therefore much smaller than at high temperatures and is approximately 7%/^{o}K at average temperature (10^{o}C). This relationship only quantifies the maximum carrying capacity, but not the actual water vapor which is taken up by an air mass – which is a function of the evaporative dynamics where the air mass originated. Actual water vapor content in the Southwest United States is typically much less than capacity as evidenced in higher lifting condensation levels than are found in other regions of North America. Climate modeling is often conducted under an assumption that relative humidity remains constant with temperature over large spatial scales; and so proportionally more water vapor is assumed to be present, which would enhance precipitation and change its spatial distribution. However, at regional scales of interest, such assumptions must be examined carefully. Moisture recycling within the CRB is estimated to only contribute a few percent of total atmospheric water vapor, with most of it originating in maritime climates that is advected into the western United States. The dominant maritime-polar air masses originate in the northern Pacific Ocean. During summer lower portions of the CRB are affected by maritime-tropical monsoon air masses originating in the Gulf of California and Gulf of Mexico. The near-surface temperature changes reviewed earlier in this paper do not apply to those maritime regions, and their long-term relative humidity changes have not been closely analyzed, in large part due to the absence of an observation network in those regions.

Runoff is obviously linked to seasonal precipitation dynamics, as the primary contributor to the hydrologic process. Once on the ground, the energy budget as reflected in temperature along with surface dynamics determine the yield to runoff measured as stream flow. Surface water resource systems are most dependent upon runoff during the winter season. Evapotranspiration is at a minimum during that time of year due to dormant vegetation and low temperatures. Potential evapotranspiration (PE) has an exponential temperature dependence often represented by the Hamon equation, going as $e^{0.062T}$ (Ellis et al. 2008). As such, PE is small at low temperatures, increasing at 6.4%/ ^{o}K. This allows for soil moisture recharge and the subsequent overland flow of surplus water. Maintenance of cool near-surface temperature maximizes yield during the runoff season. Maritime-polar air masses arrive in the CRB accompanied by colder transient temperatures during and shortly after precipitation events, whether occurring as rain or snow. Assuming soil moisture recharge has occurred, short overland transit times minimize surface water exposure to evapotranspiration. The stream gages examined in this study are typically within a couple days of the points of precipitation while depressed temperatures are still present. Even in the warm watersheds of the LCRB summer temperatures can readily drop several degrees during a monsoon precipitation event that results in a flash flood once near-surface soil moisture recharge has occurred. However, summer soil moisture deficits and PE are often so high that little surplus is available and summer runoff efficiencies are much lower than in winter. The temperature changes noted in this stationarity assessment are an order of magnitude smaller than the temperature depression occurring on meteorological time scales, whether winter or summer.

Table 3.3.5. Coefficients of Variation (standard deviation divided by mean).

	Temperature		Precipitation		Runoff	
	Winter	Summer	Winter	Summer	Winter	Summer
Salt & Tonto	0.91	0.72	0.40	0.24	0.89	0.55
Verde	0.90	0.90	0.41	0.28	0.84	0.52

A review of the time series analyzed in this assessment reveals that detectability of a persistent change in the mean of a hydroclimate variable depends upon the series' inherent variability. As has been seen, temperature changes of 1.0^{o} to 1.5^{o}C are resolvable when standard deviations are in the range of 0.7^{o} to $1.0\,^{o}$C. However, ability to resolve changes in precipitation and runoff in the watersheds are more challenging, depending on their coefficients of variation (Table 3.3.5). Empirical validation of a single-digit runoff change is unlikely amidst coefficients of variation an order of magnitude larger. Resolving changes must therefore await more years' data for larger sample sizes to reduce uncertainty of the estimated mean. Detection of any changed level of the series must also then be questioned for whether it is a persistent change or another of the transients generated by an underlying stationary process. Multiple decades of evidence will therefore be required before change validation is feasible by the methods employed above.

While hypothesis testing of a time series may conclude it has remained stationary, that finding does not preclude the possibility that very small changes lie within the evidence but have not yet emerged enough to reject the null hypothesis. It is noted that limited data over recent years is available at the elevated post-2000 temperature level; and yet the recent hydroclimatic condition is what has been speculated to impair runoff. Temperature dependence of evapotranspiration is well-known from other research (Ellis

et al. 2008, Vano et al. 2012) and would be expected to affect watershed runoff and miscellaneous losses at the reservoirs. Therefore further analysis using Hurst-Kolmogorov methods was conducted subsequent to publication of the Murphy and Ellis (2014) paper to investigate whether some persistent change may be emerging but is not yet fully revealed.

3.3.12 Hurst-Kolmogorov Behavior

Hurst-Kolmogorov (HK) behavior can be viewed as the clustering in time of similar natural outcomes different than would occur with purely random events. The influence upon stochastic outcomes was investigated by English hydrologist H.E. Hurst who studied persistence in natural processes (particularly long-term Nile River flows) and Russian mathematician A.N. Kolmogorov who devised its stochastic representation as a mathematical tool for turbulence research. Important characteristics of HK behavior include long and potentially large excursions from an average level (Koutsoyiannis et al. 2008), with important implications to stationarity considerations (Koutsoyiannis 2011).

The temporal persistence is quantified through the HK statistic, H. If a process is purely random around a consistent mean with fixed variance, then it is known that the sample variance of the sample mean, S_{ave}^2, is inversely proportional to sample size, n –

$$S_{ave}^2 = S_x^2 / n \quad \text{or} \quad S_{ave} = S_x / n^{1/2} \tag{3.4}$$

where S_x^2 is the population variance

If the mean or variance of the generating process is changing in time the exponent does not hold, but can be characterized using the HK statistic, H –

$$S_{ave} = S_x / n^{1-H} \tag{3.5}$$

where H = 0.5 for a stable, purely random process

A series persistently changing in time has an exaggerated S_{ave} in a manner proportional to H ranging upwards to 1.0 where the sample variance of the mean is indistinguishable from the population variance. Therefore a solution for H based upon historical data to date provides insight to whether a persistent change might be emerging. The calculation is derived as follows:

$$S_{ave} = S_x / n^{1-H} \tag{3.6}$$

$$n^{1-H} = S_x / S_{ave} \tag{3.7}$$

taking log of both sides and reducing …

$$(1-H)\ \ln(n) = \ln(S_x / S_{ave}) \tag{3.8}$$

$$H = 1- [\ln(S_x / S_{ave}) / \ln(n)] \tag{3.9}$$

which can be rewritten for the purpose of graphical analysis as …

$$(1-H)\ \ln(n) = \ln(S_x) - \ln(S_{ave}) \tag{3.10}$$

$$\ln(S_{ave}) = (H-1)\ \ln(n) + \ln(S_x) \tag{3.11}$$

which is now in a form to be linearly plotted as $y = mx + b$.

The population standard deviation, S_x, is taken for the entire series and its natural log is the intercept value of the plot. Multiple sample mean calculations can be made for every possible value of n and the standard deviation of each of those is S_{ave} (as a function of n). Its natural log is plotted per log of sample size, n, and the resulting slope of the curve is 1-H as shown in Figures 3.3.7 to 3.3.12. When sample size becomes large in proportion to population size the curve becomes less representative of the temporal evolution of the series, and local slope becomes less informative, and H values fall below 0.5 as seen at the right side of the plots. Short interval estimates of H are made leading

up to that point in the graphic analysis and those cumulative assessments are given in Table 3.3.6 for the hydroclimate variables by watershed-season.

Table 3.3.6. H-Value Estimates from Hurst-Kolmogorov Analyses.

	Salt	Verde
Temperature		
Winter	0.79	0.72
Summer	0.84	0.85
Precipitation		
Winter	0.55	0.46
Summer	0.39	0.45-0.49
Runoff		
Winter	0.54	0.56
Summer	0.59	
Summer, post-1928		0.53
NBS = RO-ML		
Winter	0.53	0.55
Summer	0.60	
Summer, post-1928		0.59

Values larger than ~0.55 may indicate persistent nonstationarity.

H-values for temperature data are in the range of 0.72 to 0.85 and are distinctly different than 0.5, confirming the persistent nonstationarity of those time series. Precipitation H-values are around 0.5, confirming the stationarity findings above by other methods for those series. H-values for winter runoff and winter RO-ML are in the range of 0.5 to 0.56, and stationarity can still be assumed. However, slightly higher values are found for the summer season. For our key variable, NBS=RO-ML, Salt summer H=0.60 and Verde summer H=0.59. These values are slightly higher than those for runoff alone.

Two observations, though not conclusive, can be drawn from the HK analysis: (1) there may be some summer runoff impairment emerging with recent elevated temperatures which cannot yet be identified by hypothesis testing between time intervals, and (2) a further contribution to summer miscellaneous loss may also be emerging in the time series. As will be reported in the hydrologic sensitivities section (Sec. 3.5) of this document, these are where important hydroclimate dependencies were found.

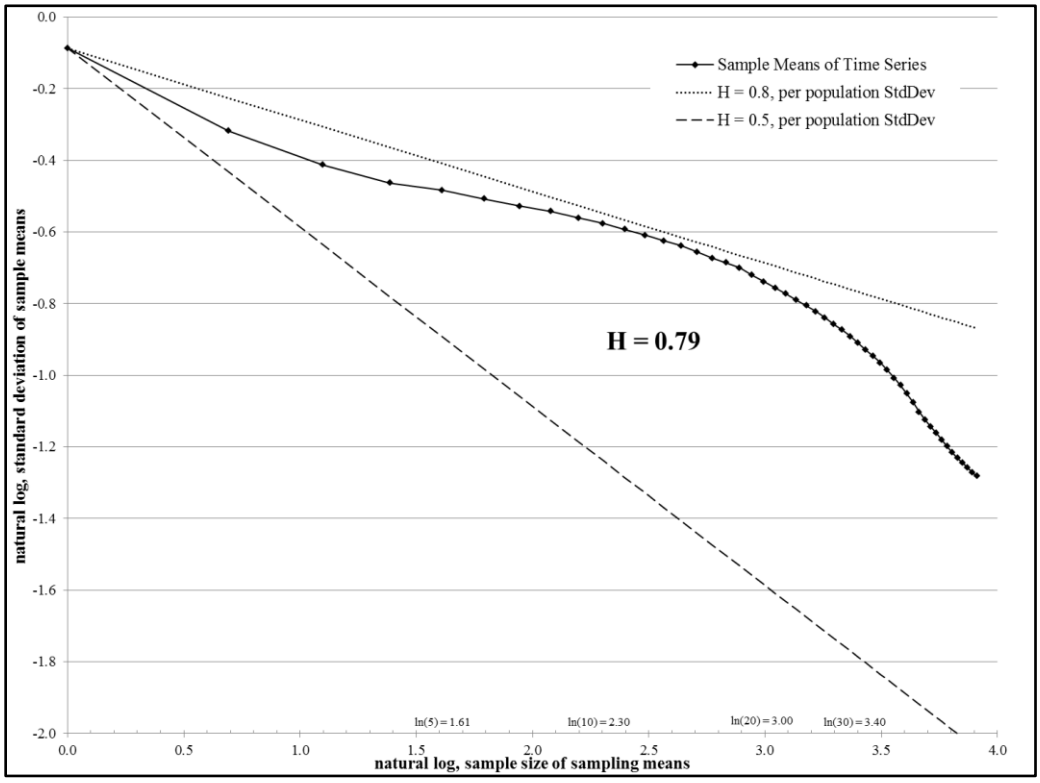

Figure 3.3.7. Hurst-Kolmogorov Analysis, Salt Watershed Winter Temperature.

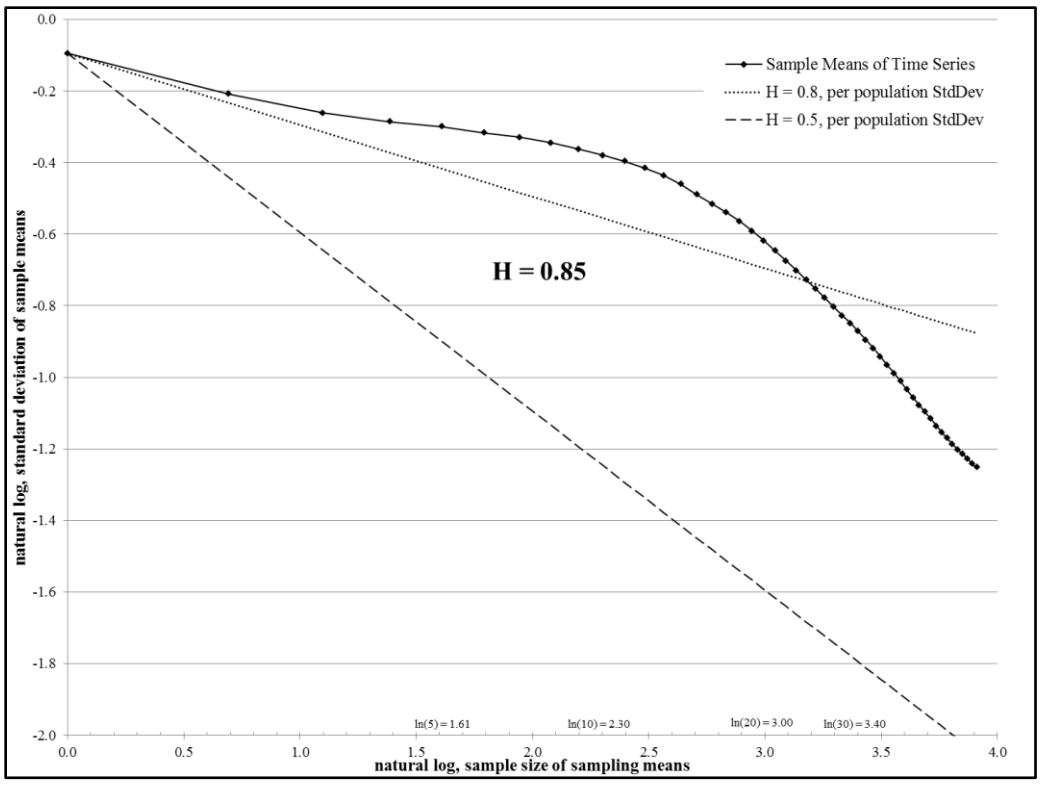

Figure 3.3.8. Hurst-Kolmogorov Analysis, Verde Watershed Summer Temperature.

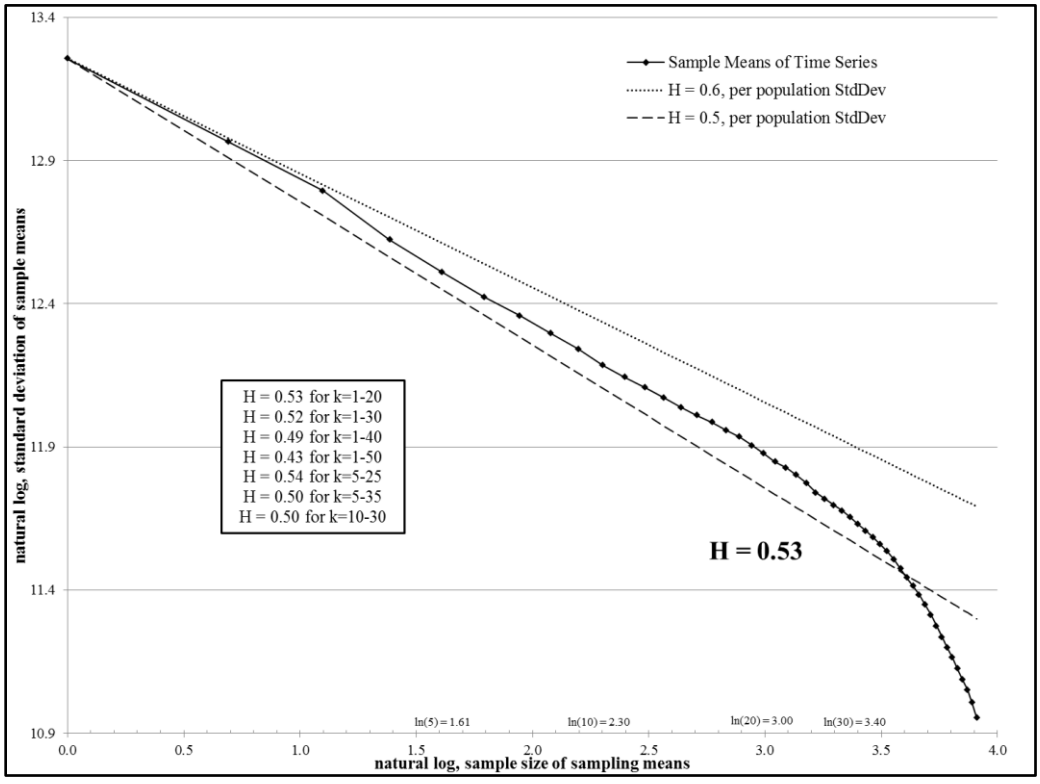

Figure 3.3.9. Hurst-Kolmogorov Analysis, Salt Watershed Winter NBS.

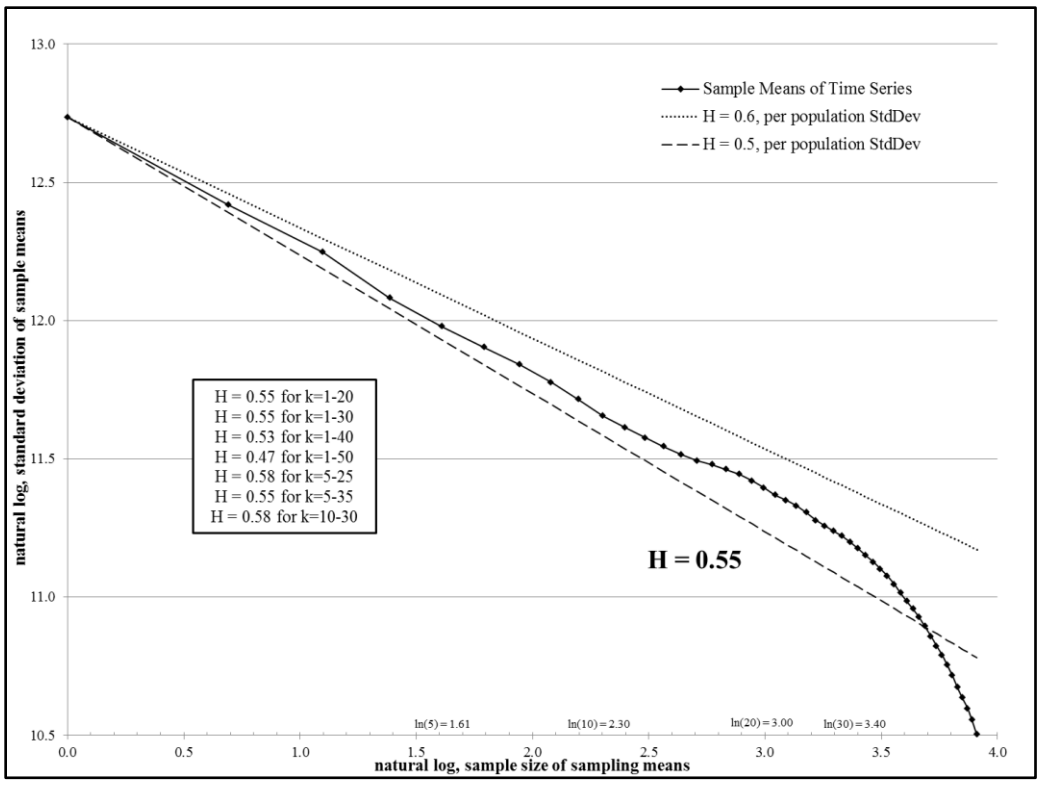

Figure 3.3.10. Hurst-Kolmogorov Analysis, Verde Watershed Winter NBS.

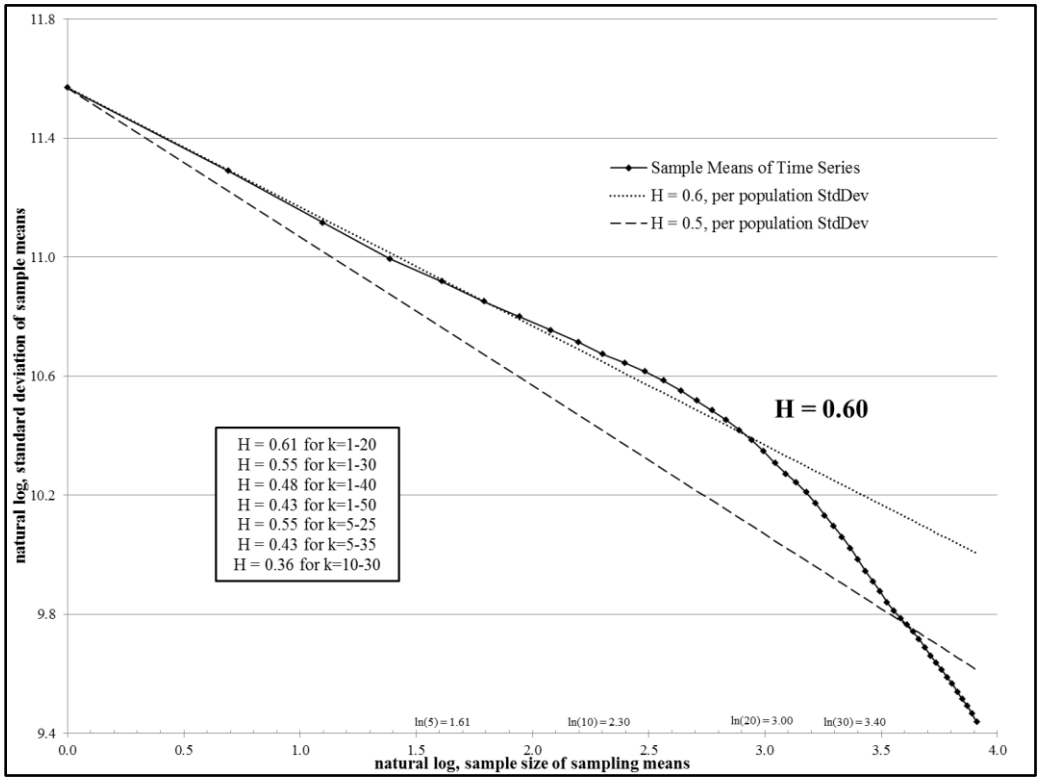

Figure 3.3.11. Hurst-Kolmogorov Analysis, Salt Watershed Summer NBS.

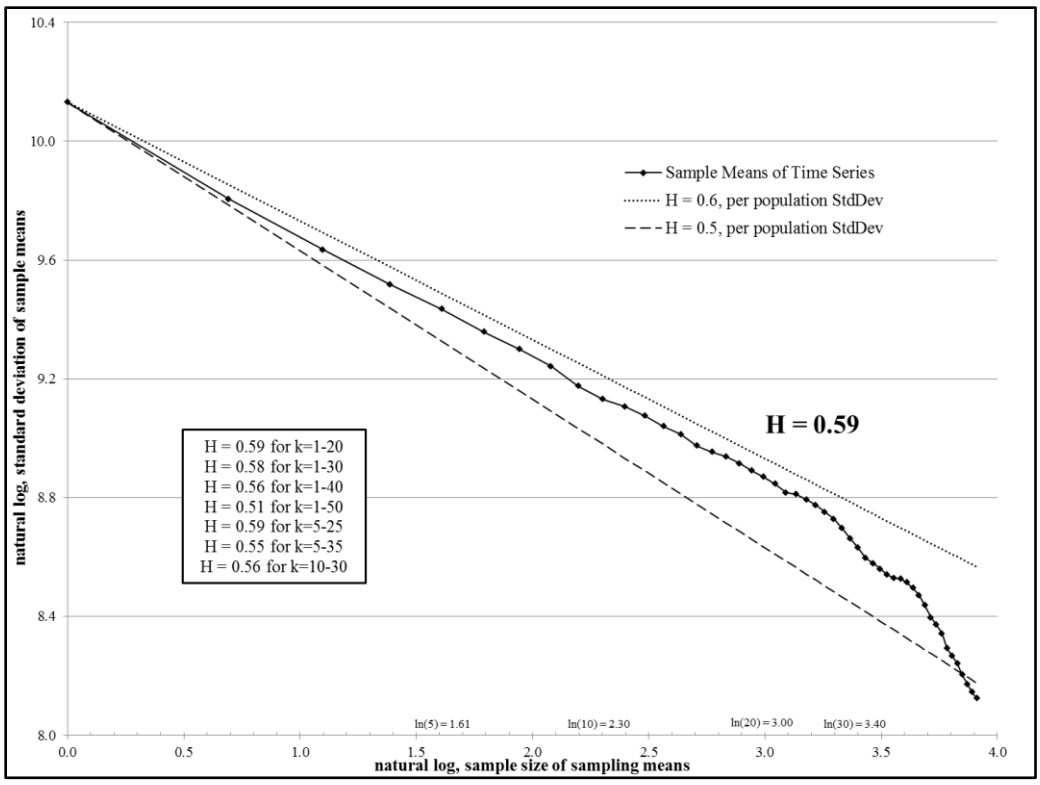

Figure 3.3.12. Hurst-Kolmogorov Analysis, Verde Watershed Summer NBS.

3.4 Stochastic Simulation of Net Basin Supply

3.4.1 Abstract

Risk assessment of the SRP system, as currently configured and managed, must thoroughly address the naturally high hydroclimate variability before considerations of climate change can be addressed. The short, historical streamflow record was but one of many possible outcome sequences that could have occurred, and a fuller exploration of the possible range beyond those evident in the instrumental record can facilitate sustainability planning and adaptation to climate change scenarios. Methods were developed in this study to generate long seasonal time series of net basin water supply by Monte Carlo simulations of the Salt and Verde watersheds that can be analyzed for probabilistic insights. Other efforts to generate stochastic flow representations have been limited by normality distribution assumptions, inability to represent the covariance of flow contributions from multiple watersheds, complexities of different seasonal origins of precipitation and runoff dependencies, and constraints from spectral properties of the observational record. Those were overcome in this study through stationarity assessments and development of joint probability distributions with highly skewed discrete density functions characteristic of the different watershed-season behaviors derived from a 127 year record. As well, methods of introducing season-to-season correlations owing to antecedent precipitation-runoff efficiency enhancements have been incorporated.

Representative 10,000-year time series have been stochastically generated which reflect a full range of temporal variability in flow volume distributions. Extreme value statistical analysis methods can then be employed to characterize periods of flow deficit

per specific definitions of a drought. Of concern for water resources are periods of net flows lower than those necessary to maintain reservoirs without sequential depletions. The analysis has yielded risk representations of the full range of drought in both duration and severity, providing useful quantitative guidance to management. Similarly, the risks of extremely high flows can be quantified.

Future climate change can then be translated to adjustments of the stochastic simulation probability functions to generate alternative 10,000-year sequences. Hypothesis testing between the baseline and changed cases serves as the basis upon which research questions are answered. This methodology demonstrates that the instrumented historical record, once fully characterized and probabilistically represented, can yield many more insights to threatening periods of both hydrologic deficit and excess than is often assumed.

Funding support was provided by the Salt River Project for development of this stochastic simulation methodology (Ellis and Murphy 2012).

3.4.2 Introduction

A shortcoming of various other hydrologic analyses of surface water systems conducted to date is that existing datasets, whether instrumental or paleoclimate, are a limited temporal representation of natural climate variability. We cannot expect the historical runoff record to exactly repeat itself again in the future. Other approaches dwelling solely on history therefore may not necessarily incorporate the full range of possible temporal evolution with the high year-to-year variability that characterizes precipitation and runoff in the Southwest United States. While the Salt-Verde system has one of the longest instrumented records in the western United States at 127 years, it

nevertheless contains only a very limited sample of the full range of drought and excess which are possible in the region. Analysis of tree-ring records indicates that longer and deeper drought have occurred in the past (Hirschboeck and Meko 2005, 2008). But, while providing more insight, those data cover only a handful of centuries and are still a limited representation of possible outcomes. What has occurred in the past is but one rendition from a broad probability distribution which must be thoroughly characterized for alternative outcomes that could have occurred. Consideration should be given not just to the historical record but to all possible alternative sequences expressed in a rigorous probabilistic manner. To establish current system vulnerabilities the objective therefore becomes identifying a probability distribution function (pdf) of NBS derived from the empirical evidence which represents the baseline characteristics of the SRP system. Then, to assess a future climate change scenario, that pdf (or a time series rendered from the pdf) can be modified according to the hypothesized projections translated through hydrologic sensitivity algorithms derived in the next section of this document (Sec. 3.5). Hypothesis testing between the baseline and change case then serves as the basis upon which the research questions with regard to climate change are answered. There is high value in diagnosing system sensitivity to variability and change without confining the exercise to one specific climate change projection, since each is afflicted with uncertainty. A quickly executable methodology is therefore desired which can translate alternative projections to a modified pdf and NBS time series.

A solution lies in employing a simulation model for study purposes to generate very long synthetic runoff time series of feasible although artificial representations which capture all possible outcome sequences, especially those with low probability. To ensure

that event sequences within a generated series are indeed feasible and occur with an accurate probabilistic representation, the model must embody the complex statistical relationships that represent the watersheds' behavior, including cross-watershed seasonal correlations and between-season runoff dependencies. Any year-to-year autocorrelations should be incorporated in the methodology, but stationarity analysis of the Salt and Verde has shown those to be zero (Sec. 3.3.4). Annual runoff has been determined to be independent and identically distributed (i.i.d.), although season-to-season dependencies have been identified in the watersheds. As described below, year-to-year independence readily facilitates employment of Monte Carlo simulation methods using probability distributions derived from empirical evidence. Season-to-season and cross-watershed dependencies can be represented through dual-watershed joint-seasonal probability distributions derived per the historical record. The 127 year documented history of the Salt and Verde was thoroughly assessed to conclude that it provides sufficient data from which to establish the baseline behavior of the watersheds and develop a frequentist methodology, while it was not clear how to employ a Bayesian approach. (Frequentist = standard interpretation of probability used for scientific modeling experiments wherein underlying probabilities are fixed and observational variations are due to the sampling process; Bayesian = probabilities are uncertain and change as data are acquired, updating prior assumptions.)

During a pilot project study conducted for development and proof-of-method (Ellis and Murphy 2012), a thorough analysis was conducted, and probability functions were developed and built into a complete stochastic modeling process that generates flows for each watershed in the two seasons. An initial 10,000-year runoff sequence was

generated having characteristics comparing favorably to the historical runoff record. The simulation model results convinced investigators that the full range of possible drought can be generated that is representative of the behavior of the watersheds in both seasons. A few improvements were identified from that work and have been incorporated in the methodology described below such that it renders the current characteristics of the watersheds.

3.4.3 Simulation Sample Size

Very long time series for the four watershed-seasons can be stochastically generated by the simulation model. Since analysis of results will be considered on a per-century basis, at least 100 centuries are desired to enable assessment of small probability (~1%) outcomes. Therefore time series with a simulation length of 10,000 years have been employed, which are manageable within a spreadsheet analysis toolkit. It was noted during the 2012 study (Ellis and Murphy 2012) that there might be variability in resultant 10,000-year summary statistics that should be assessed to address the research questions. Hypothesis test confidence levels are dependent on sample size, so assessments will statistically benefit from analysis of multiple 10,000-year series. The 2012 study also revealed a few long-duration droughts that require more sampling for better small-probability statistics. About 11 such series was estimated to be required. This investigation proceeded to develop a library of twelve time series, a biblical number representing completeness. A total of 120,000 years of simulation data was thereby generated which are sufficient to assess the statistics of interest. This much data provide a robust, baseline assessment against which hypothesized future changes may be analyzed with confidence through comparative statistics.

3.4.4 Probability Distribution Development

Findings of stationarity for precipitation and runoff in the Salt and Verde watersheds demonstrate that, in general, the entire historical record can be used for the probabilistic characterizations required for stochastic simulation model development. The one exception is Verde runoff in summer. As explained in Murphy and Ellis (2014) and in the stationarity section of this document (Sec. 3.3.10), it is believed that water diversions on the Verde River subsequent to the mid-1920s resulted in a step-change in the time series to a re-established level which has tested stationary since that time, although the recent 15-20 year pattern should be questioned. Therefore only observational data since 1928 have been used to characterize the Verde summer season and develop its probability distributions. Since that time Verde summer inflows account for a single digit percentage of annual NBS for the reservoir system (Table 3.2.2), so it is not a major influence on overall reservoir system sustainability. The highest Verde runoff values in summer are notably lower since the 1920s, so the maximum level of its probability distribution (150,000 acre-feet) was limited below what occurred in the early record. The HK analysis provided further indication of recent warming effects on summer runoff. There are limited years yet available by which to quantify a runoff distribution shift, but the hydrologic sensitivities to climate analysis (Sec. 3.5) was used for guidance in distribution modification owing to the 1990s warming period. The Salt summer runoff distribution was similarly scrutinized.

The finding that all historical NBS time series have negligible and statistically non-significant autocorrelations supports an assumption that their outcomes are i.i.d., which is a fortuitous result since it simplifies algorithm development for the stochastic

numerical generating methodology. And, as discussed further below for the drought characterization and impact analysis methodologies, i.i.d. findings at the annual level enable an i.i.d. assumption over multi-year intervals, so that Poisson and exponential probability distribution descriptions can be employed for drought events.

Each sample distribution of a watershed-season was first examined to ascertain whether it can be represented by a parametric function – in particular whether it could be fit by an exponential probability distribution. Exploratory data analysis quickly revealed that the distributions are bounded on the low side and highly asymmetric with a long tail to the high side, which is characteristic of the exponential function. But because of a non-zero low-end limit due to base flow from the watersheds and some structure in inflection points it could not be concluded that an exponential fit was appropriate; so it was instead decided to derive discrete pdfs. The process for doing so utilized the following constraints and guidelines:

- Examine the full sample to determine reasonable minimum and maximum bounds based upon the evidence and expected watershed behavior.
- Partition the distribution into small enough interval spacing for a near-continuous distribution. It was found that approximately 300 cells between the minimum and maximum bounds would be sufficient.
- Calculate the cumulative probability curve (CumProb) of the sample distributions. The pdf is the slope function of the cumulative probability. The CumProb provides a good visual representation of the distribution to reveal structure and assess fit.

- Examine the histogram of the sample at a variety of bin intervals to note the position of modes and any characteristic shape of the distribution which can be identified.
- Develop step-wise best-fit approximations to the CumProb curve.
- Approximately match key probability levels in the sample distribution at the mode, median, inflection points, and any extreme events.
- The pdf should monotonically increase approaching the mode and monotonically decrease away from the mode.
- Apply careful attention to the low and high ends of the distribution. The low side represents probabilities of drought and the small probabilities in the high-end tail are instrumental to periodic fast reservoir replenishments that also provide a key cumulative reservoir impact.
- The pdf and CumProb curves should be smooth, continuous, and make sense.

The Salt watershed in winter provides the largest inflow to the reservoirs, and its discrete CumProb and pdf functions are shown in Figure 3.4.1. The discrete CumProb and pdf functions developed for the Salt watershed in summer are shown in Figure 3.4.2. The structure of the summer function differs from winter due to the different origins of precipitation and dramatically different evapotranspiration. The discrete CumProb and pdf functions derived for the Verde watershed are shown in Figure 3.4.3 (winter) and in Figure 3.4.4 (summer). Comparison of the four pdfs in Figure 3.4.5 shows the importance of periodic high winter flows for system replenishment.

It can be noted that the general shape of the winter Salt and Verde pdfs are similar and nearly exponential. The summer pdfs for the two basins are similar to each other; but there are distinguishable differences between winter and summer. During the pilot project study (Ellis and Murphy 2012) some potential structure in the shape of the summer pdfs above the modes was noted. This was analyzed to find no explanatory influence of any monsoon dynamic or seasonal timing. Instead, it was due to fitting uncertainty with the small sample of high events and periodic winter runoff carryover on the Salt beyond the May 1st delineation of seasons. Hence, the summer pdfs now exhibit the continuity as shown in Figures 3.4.2 and 3.4.4 and have larger relative breadth in comparison to winter.

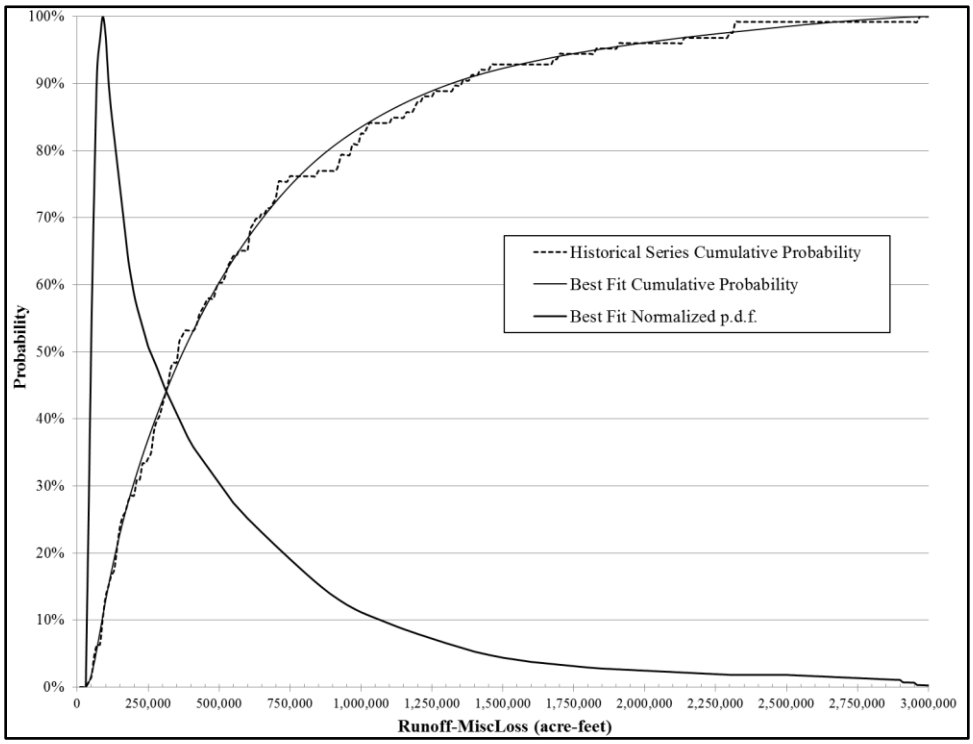

Figure 3.4.1. Salt Winter NBS Probability Distribution Function and Cumulative Probability.

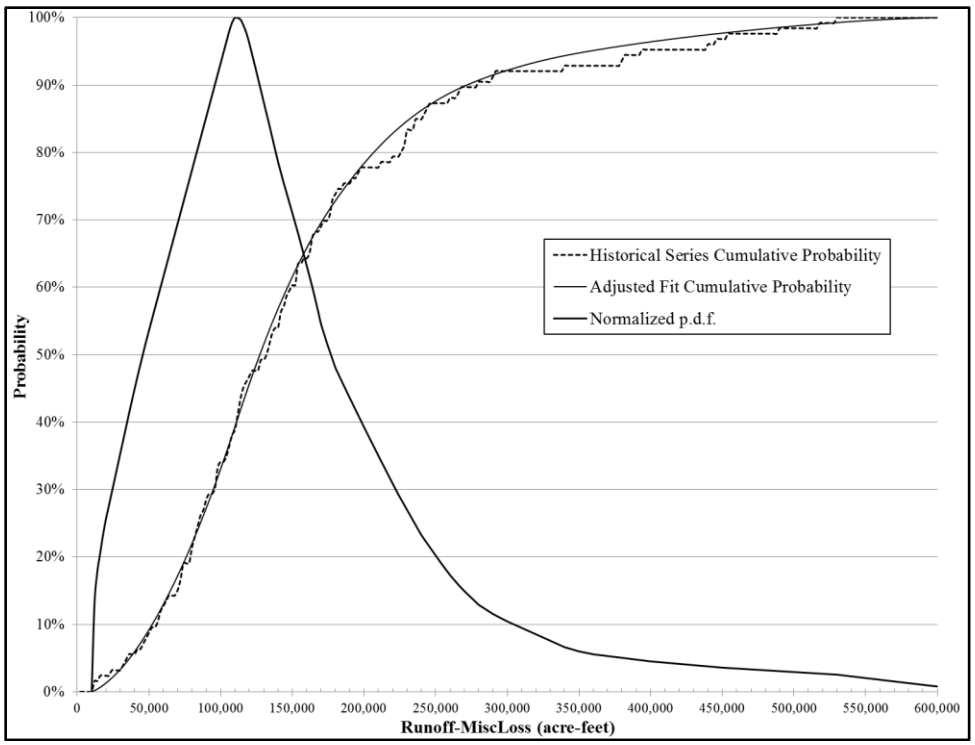

Figure 3.4.2. Salt Summer NBS Probability Distribution Function and Cumulative Probability. The fit has been slightly adjusted for an estimate of the current, post-1990s distribution.

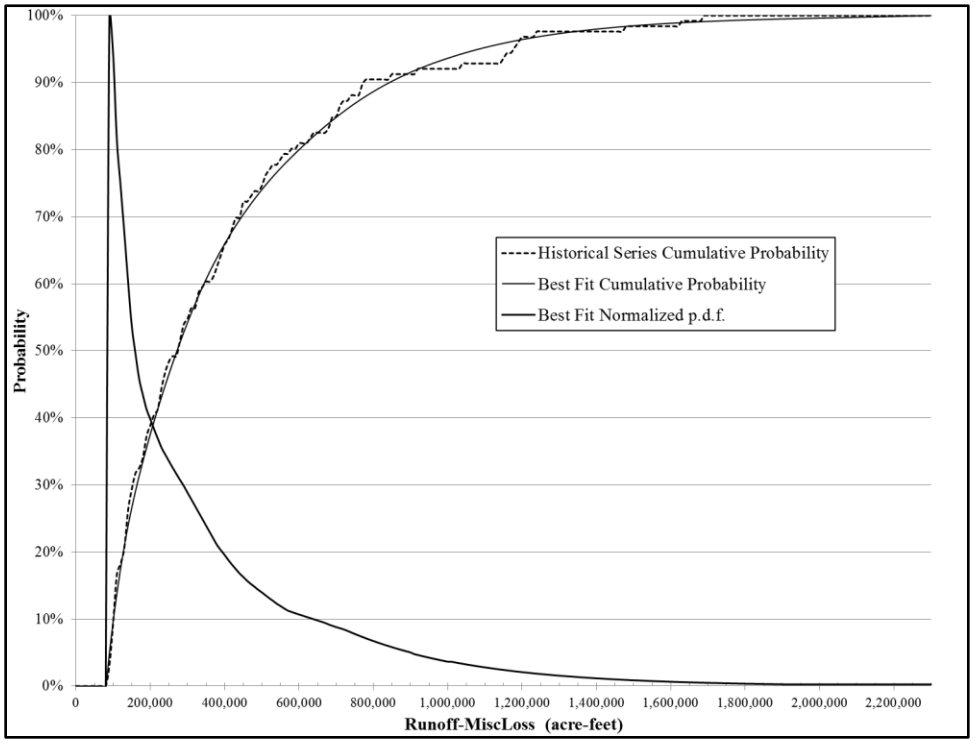

Figure 3.4.3. Verde Winter NBS Probability Distribution Function and Cumulative Probability.

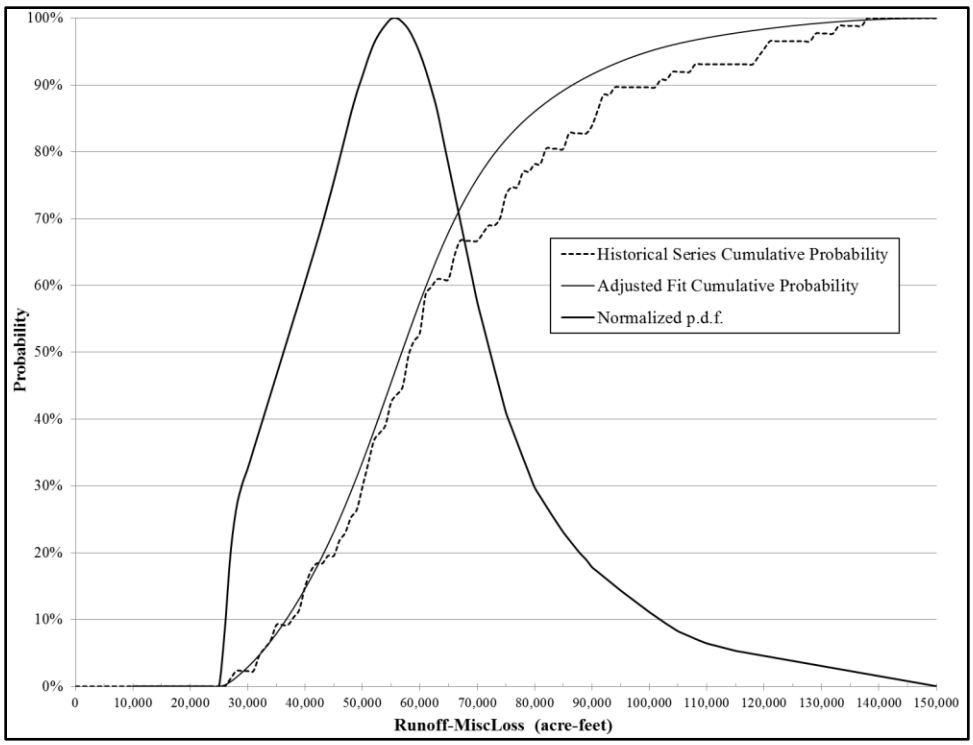

Figure 3.4.4. Verde Summer NBS Probability Distribution Function and Cumulative Probability. The fit has been downward-adjusted for an estimate of the current, post-1990s distribution.

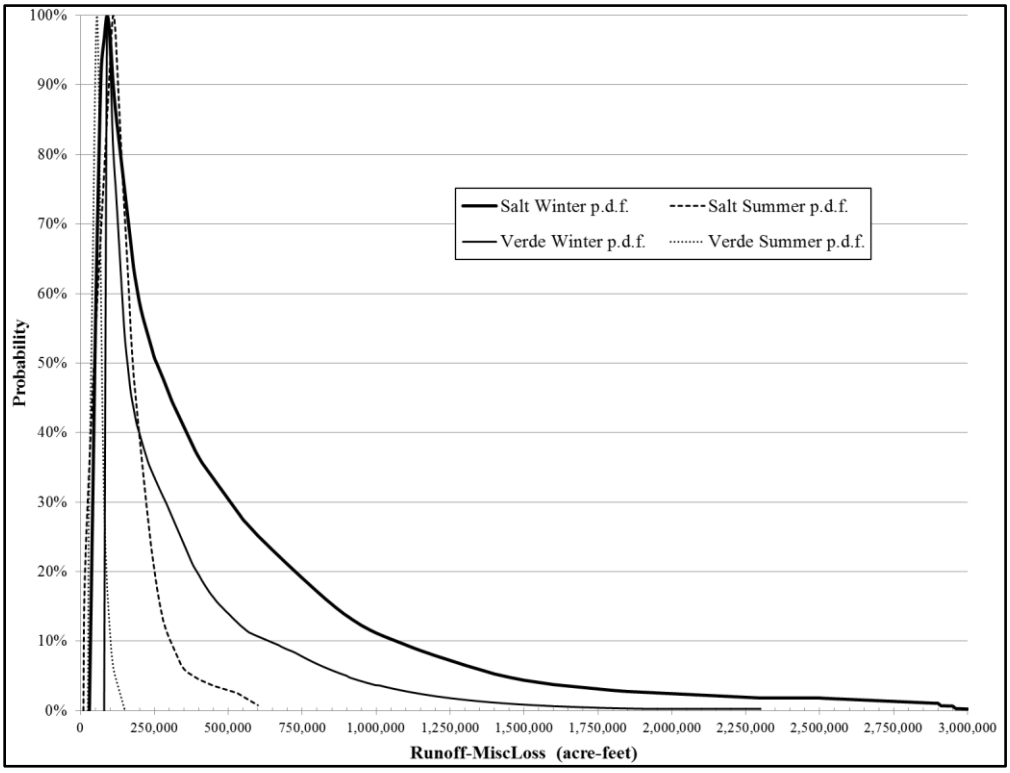

Figure 3.4.5. Comparison of Watershed-Season NBS pdfs.

3.4.5 Correlation Between Watersheds

A comparison among the watershed gage records reveals seasonal covariance between the Salt and Verde watersheds. This is expected considering their spatial proximity to one another. Large, organized synoptic-scale storms drive winter precipitation which can overspread both watersheds. Summer precipitation originates in more irregular patterns of monsoon outbreaks. Hence runoff correlation between watersheds is expected to be stronger in winter, and this was found to be the case. Winter correlation among the 127-year observations is 0.934 and summer correlation across the past 85 years is 0.647, and both are statistically significant (Table 3.4.1).

Scatterplots reveal the interrelationship between the watersheds that must be incorporated in the methodology for generating a random sequence of water-years (see Figs. 3.4.6 and 3.4.7). The methodology to generate an outcome from this joint probability relationship must account for the slope as well as the distribution of residuals around the trend between the watersheds. The process used to arrive at statistical relationships describing the joint probability distributions was:

- With a linear correlation (transformed as necessary), calculate the slope and intercept of the relationship.
- De-trend the sample data by the linear fit and calculate the residuals.
- Examine the distribution of residuals for a probability function which can be applied to it (as further described below). If possible, parameterize the function and use it to describe the joint probability distribution.
- Asymmetries were often found so that positive residuals were distributed differently than negative ones. In such cases identify the median of the residual's

population, apply a median-adjustment, and repartition the median-adjusted residuals into positive and negative sample sets.

- Analyze the positive median-adjusted residuals separately from the negative group. Assess whether their distribution varies with scale of the abscissa variable. If it does, partition the samples accordingly (but beware of reducing sample size to such an extent that parameter estimations will be prone to uncertainty).
- Symmetrize the residual population (clones of the opposite sign) and perform normality tests. If it is normal, calculate the sample standard deviation and conclude that the distribution is described by N(0, standard deviation) with mean=0. In some cases the sample standard deviation may scale with the abscissa variable.
- If not normal, assess whether the residuals can be described by an exponential distribution, Exp(lambda), where lambda is the inverse of both the mean and the standard deviation. Near-equivalence of the sample mean and standard deviation make it readily apparent whether the residuals are exponentially-distributed.
- If the residuals cannot be described as either normal or exponential, consider alternative functions or develop a discrete pdf as previously described for pdf development.

Descriptions of the joint probability distributions that were derived for Verde vs Salt in winter and in summer are shown in Figures 3.4.6 and 3.4.7. Further details of the algorithms are provided in Appendix C. To generate a random outcome, a residual value is generated according to the parameterization shown. The choice of whether a positive

or negative residual will be used is made by random number generation per the binomial distribution B(1,p), where p=0.5. Once the residual is median-adjusted and the trend component added, the result is checked to assure it does not fall below the minimum pdf bound. If it does, it is simply regenerated.

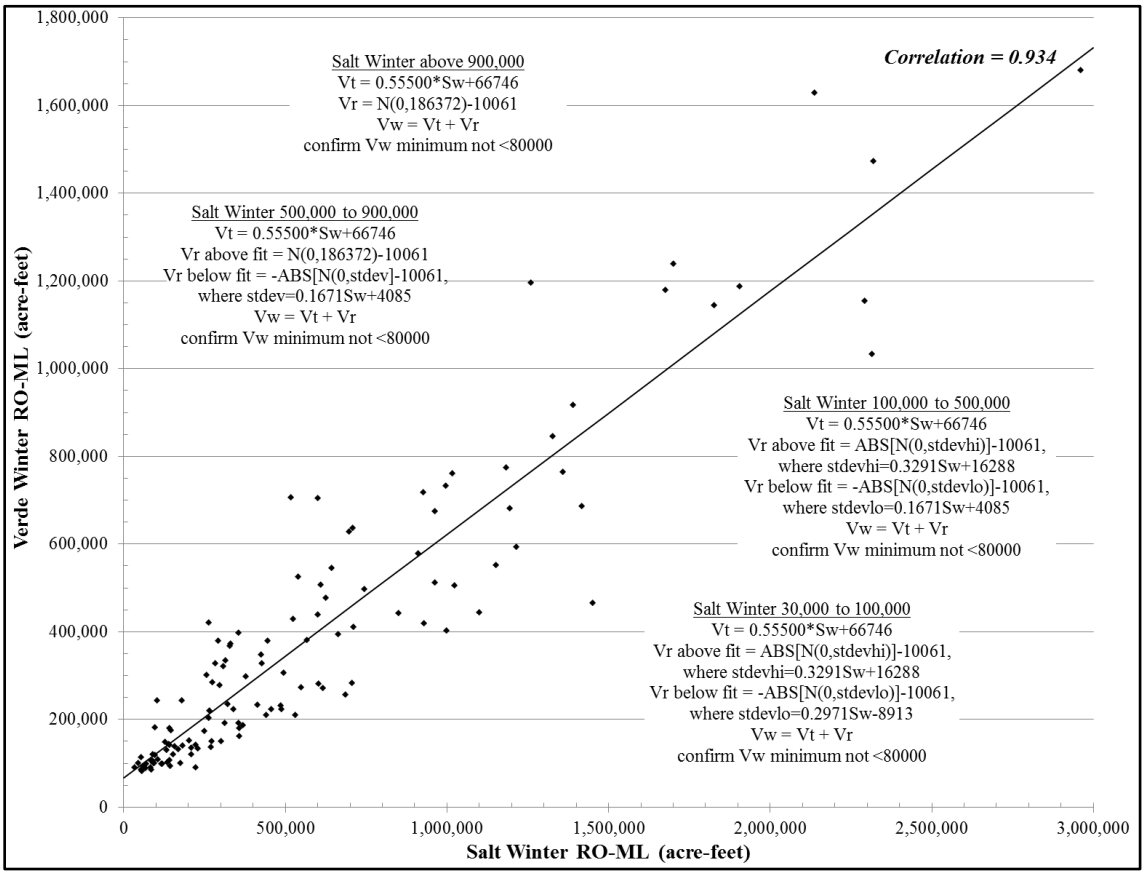

Figure 3.4.6. The Correlation of Verde and Salt Winter NBS and Their Joint Probability Algorithms.

The algorithms describing the joint probability distribution shown in Figure 3.4.6 are used to generate correlated outcomes for the Verde in winter from a Salt-winter NBS series that has been generated from the Salt-winter pdf. Similarly, the joint probability distribution described in Figure 3.4.7 is used to generate correlated outcomes for the

Verde in summer from a Salt-summer NBS series. It is important to note that the Salt-summer series must be generated as described in the next section to reflect the winter-to-summer correlation on the Salt (0.613, statistically significant), that arises in part due to incomplete winter flows by May 1st carrying over into the beginning of summer.

The Verde-winter, Salt-summer, and Verde-summer correlated series that are generated must be compared to and reconciled against their characteristic pdf. This process is discussed in the section below describing the method for generating a complete random sequence.

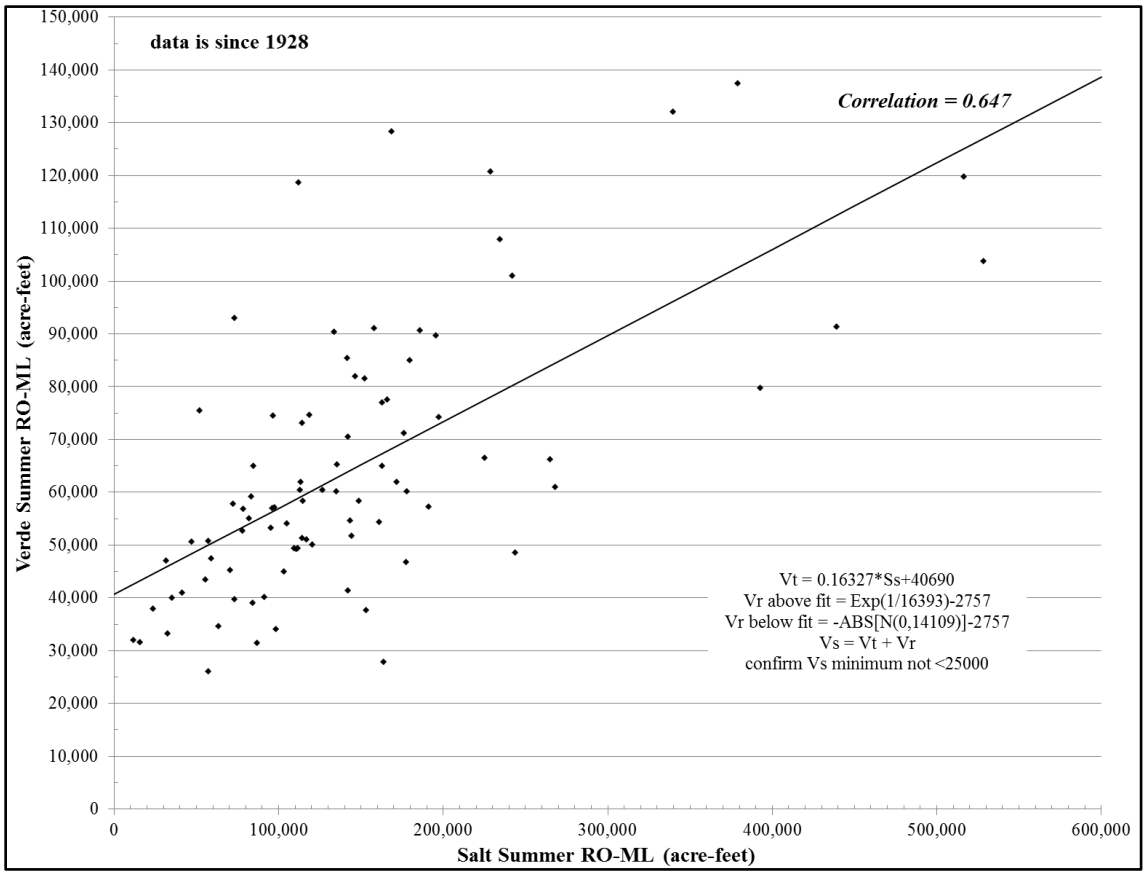

Figure 3.4.7. The Correlation of Verde and Salt Summer NBS and Their Joint Probability Algorithms.

3.4.6 Season-to-Season Effects

Small antecedent seasonal effects have been noted during investigations of watershed behavior in the Colorado River Basin. Residual soil moisture, or lack thereof, can affect runoff behavior in the next season. This can contribute a season-to-season correlation in the range of 0.2 to 0.3, a modest although sometimes statistically significant value. The weak dependency might tempt one to ignore this effect for some analyses, but considering the uncertain importance they might lend to cumulative drought or reservoir effects, this study incorporated them where necessary.

A large Salt winter-to-summer correlation of 0.613 (Table 3.4.1, Fig. 3.4.8), due in part to the May 1st season transition, necessitates it being explicitly incorporated in the random series generation process. The correlation is fortuitous, as it introduces desirable strength in the joint probability functions. The algorithms describing the joint probability distribution for Salt winter-summer were developed per the same procedure outlined above for between-watershed distributions and is given in Figure 3.4.8.

Table 3.4.1. Watershed-to-Watershed and Season-to-Season Correlation Coefficients (r) of the Historical NBS Data Series for the Salt and Verde Watersheds.

	r (1889-2014)	p-value	r (1928-2014)	p-value
Winter, Salt-Verde	**0.934**	0.000	0.935	0.000
Summer, Salt-Verde	0.620	0.000	**0.647**	0.000
Salt winter-to-summer	**0.613**	0.000	0.640	0.000
Salt summer-to-winter	0.271	0.002	**0.099**	0.364
Verde winter-to-summer	0.256	0.004	**0.296**	0.005
Verde summer-to-winter	0.340	0.000	**0.067**	0.539

bolded values are the correlations targeted for simulation algorithm development

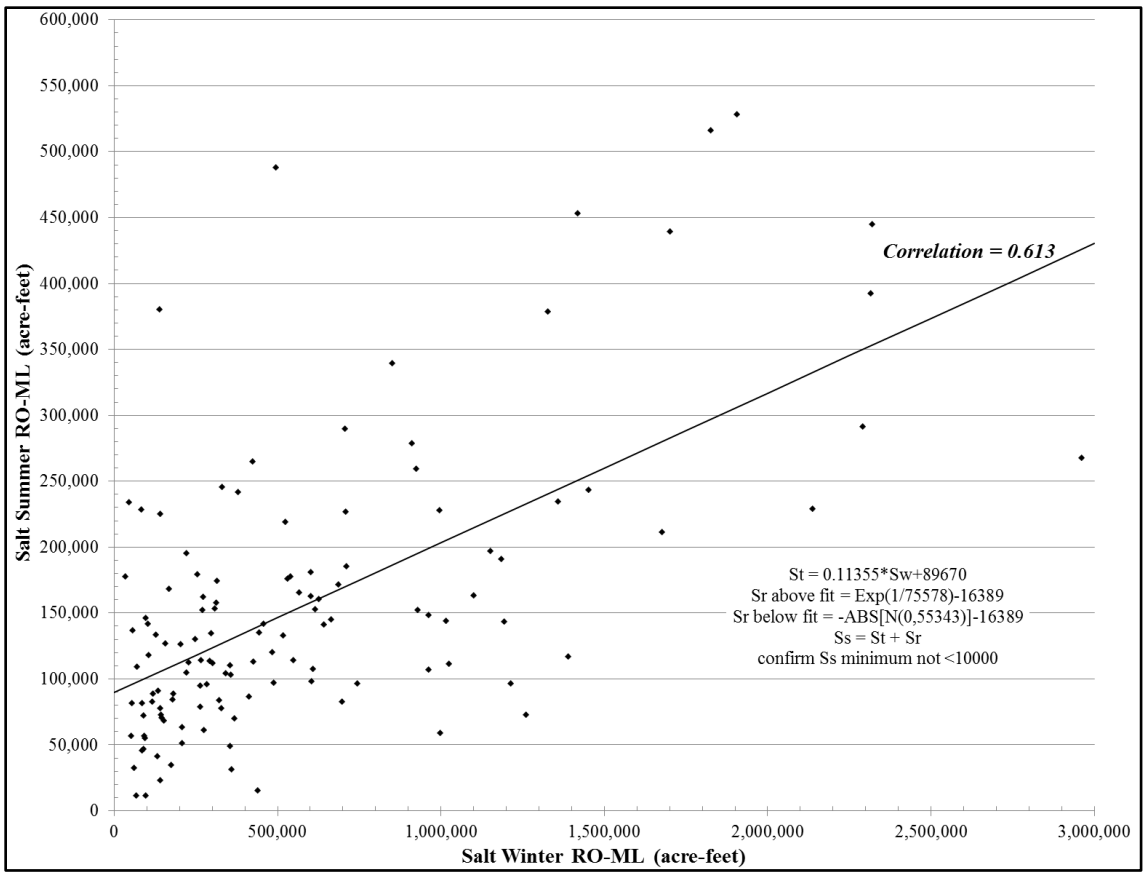

Figure 3.4.8. The Correlation of Salt Summer NBS with Prior Winter Salt NBS and the Joint Probability Algorithms.

A similar analysis was conducted for the Verde winter-to-summer joint distribution. However, it was found unnecessary to explicitly incorporate it in the random sequence generation process outlined below because linkages among the other joint distributions were sufficient to introduce a Verde correlation between winter and summer in generated sequences.

The methodology development described thus far has been within a single water-year, with each water-year a separately generated record having no relationship to adjacent years. Now, however, it should be noted that summer-to-winter correlations are a linkage from the summer of one water-year to the winter of the following water-year.

Creating linkage between adjacent water-years was a challenging part of the pilot study (Ellis and Murphy 2012) that involved resequencing of similar years. However, after further analysis of the correlation's evolution over time, it was noted that the pre-instrumental data reconstruction (1889-1912) was contributing to a correlation while the instrumental record was not. Summer-to-winter correlations are small (<0.1) and not statistically significant when calculated over just the instrumental period (Table 3.4.1). Without knowledge of how the data reconstruction might have adopted this characteristic, it was decided to assume no statistically significant summer-to-winter relationship as the more recent data indicate.

3.4.7 Generation of 10,000-Year Sequences

The first step towards construction of a 10,000-year series is the generation of 10,000 outcomes from each of the four discrete pdfs depicted in Figures 3.4.1 to 3.4.4. Many statistical software programs can accomplish this and the random number generator functions in Excel2010 were used to generate a dozen such series for each pdf. Distributions of the 120,000 generated years are shown compared to their target pdf in Figures 3.4.9 to 3.4.12. As can be seen, generated series have small variations converging to the pdf curve.

The series in Figures 3.4.9 to 3.4.12 will be completely independent of each other as-generated and not have the required correlations between watersheds or seasons. The first step towards introducing those applies the algorithms given in Figure 3.4.6 to each 10,000-year series generated from the Salt winter pdf to generate an accompanying, correlated Verde winter series. Those Verde outcomes could be used as-is; but it was found that while they were close to the desired distribution, an improvement could be

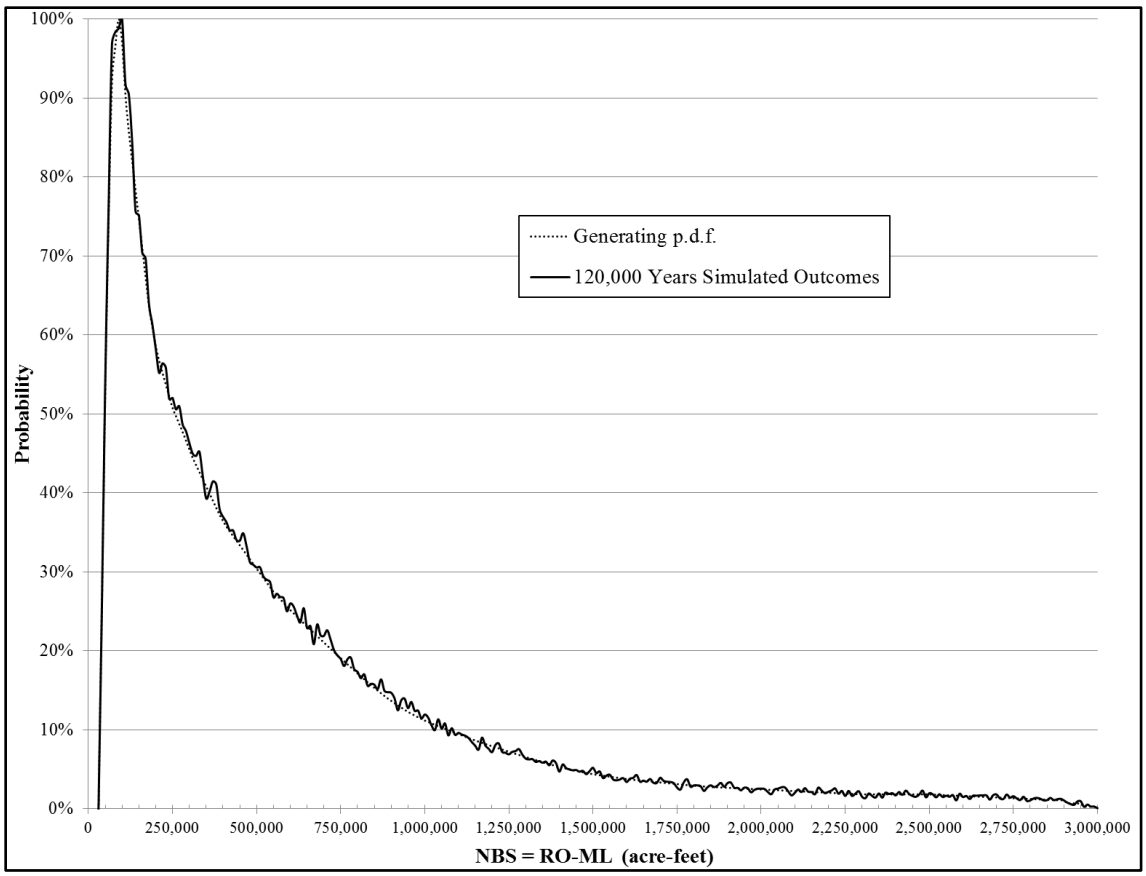

Figure 3.4.9. The Salt Watershed Winter NBS p.d.f. and Distribution of 120,000 Generated Outcomes.

made by reconciling them with the Verde winter series independently generated for Figure 3.4.11. The reconciliation procedure sorts each of the Verde winter series in ascending order and then substitutes the pdf-generated values for the correlation-generated values. The substitution is therefore essentially occurring on a nearest-outcome basis between the two Verde series. The year and Salt winter values accompany the sort-and-substitute process so that the joint series can be returned to the original year sequence by sorting on it. The result was Salt-Verde winter correlations shown in Table 3.4.2 versus the target of 0.934.

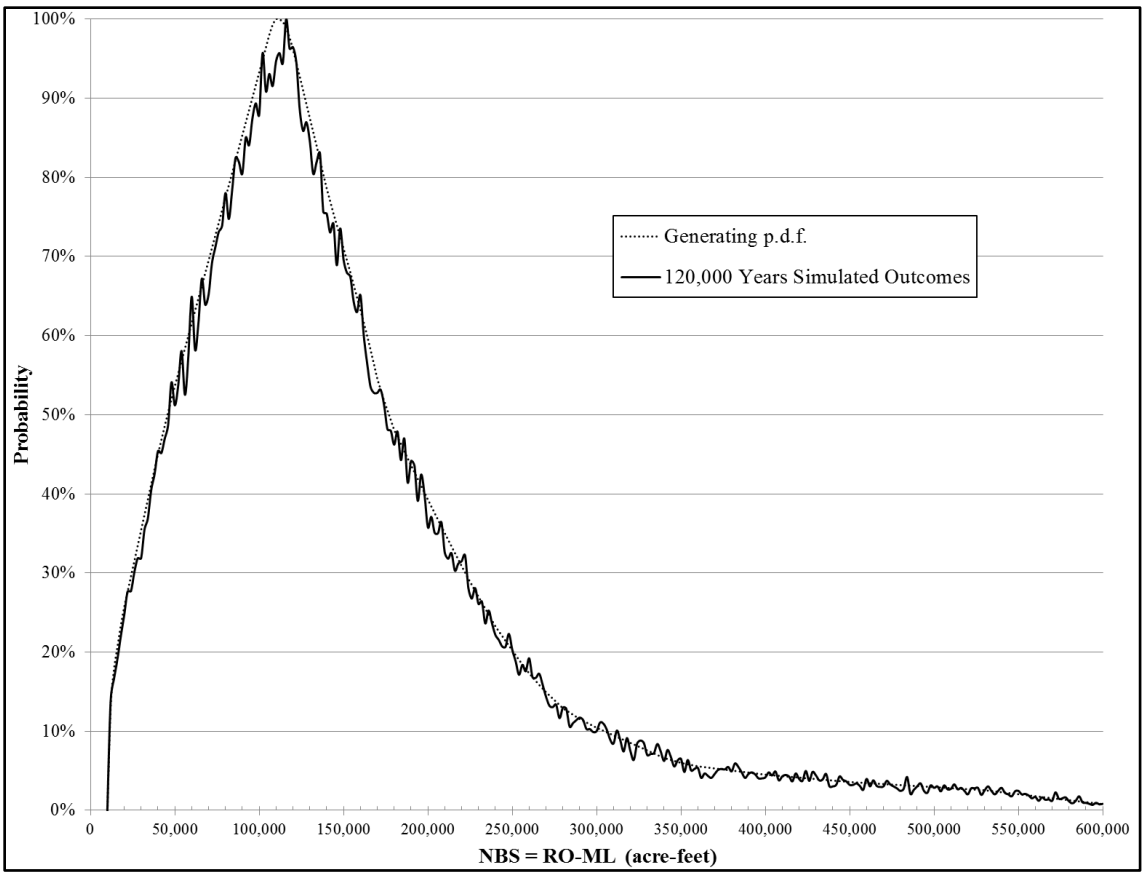

Figure 3.4.10. The Salt Watershed Summer NBS p.d.f. and Distribution of 120,000 Generated Outcomes.

The next step introduces a Salt winter-to-summer correlation by applying the algorithms given in Figure 3.4.8 for Salt summer to each 10,000-year series generated from the Salt winter pdf. The process is conducted in a similar manner to what was described above for the Verde winter. A reconciliation procedure sorts the correlation-generated and the pdf-generated Salt summer values and substitutes the later for the former. The dual winter series and year have accompanied the sort so that all are returned to the original year sequence. The result was the Salt winter-to-summer correlations shown in Table 3.4.2 versus the target of 0.613.

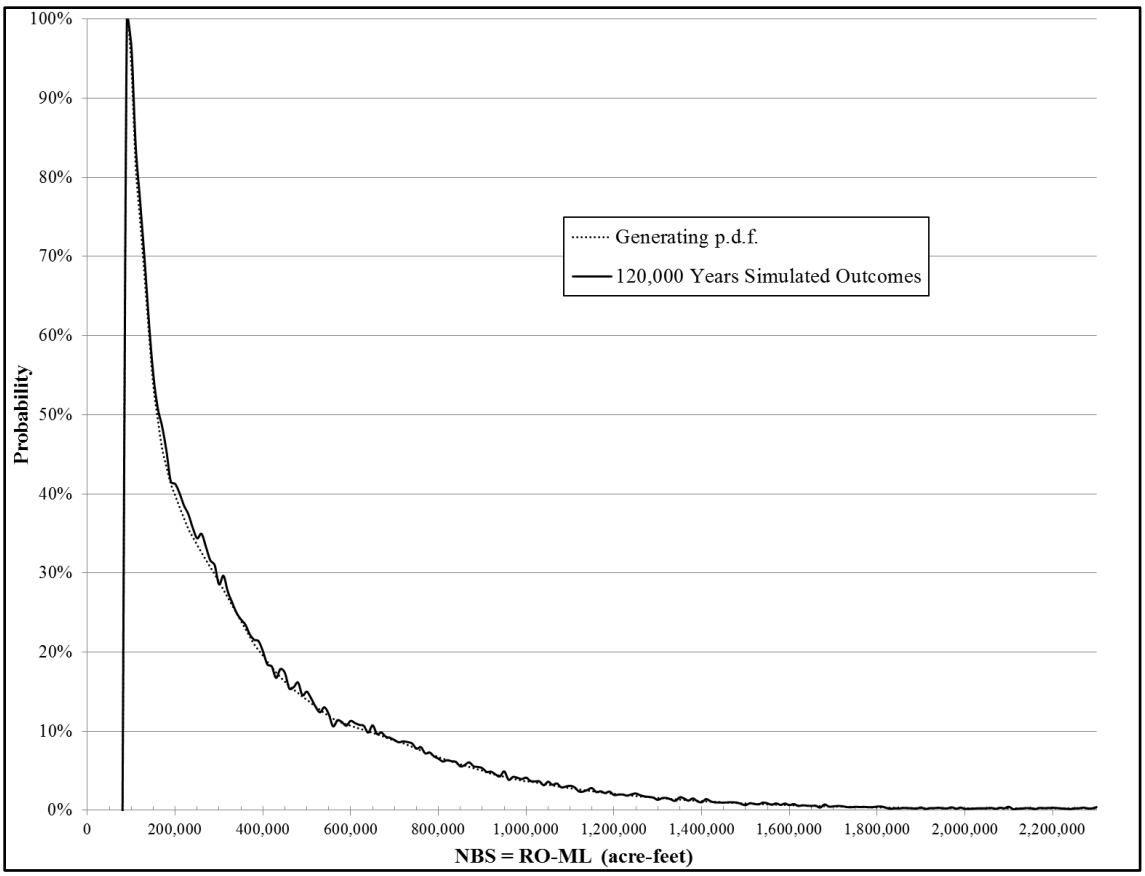

Figure 3.4.11. The Verde Watershed Winter NBS p.d.f. and Distribution of 120,000 Generated Outcomes.

Similarly, a correlated series for Verde in summer is introduced from the Salt in summer with the correlation algorithms described in Figure 3.4.7. Following the reconciliation procedure with the pdf-generated series and a re-sorting, the summer correlations between watersheds are as given in Table 3.4.2. While correlations are close, results could be modified by slope-tuning the linear relationship depicted in the figures. However, this method was not employed in any of the algorithms for creation of correlated random sequences used in this study.

The remaining correlation of interest within a water-year is the Verde winter-to-summer. As previously mentioned, it was found that the correlation algorithms already

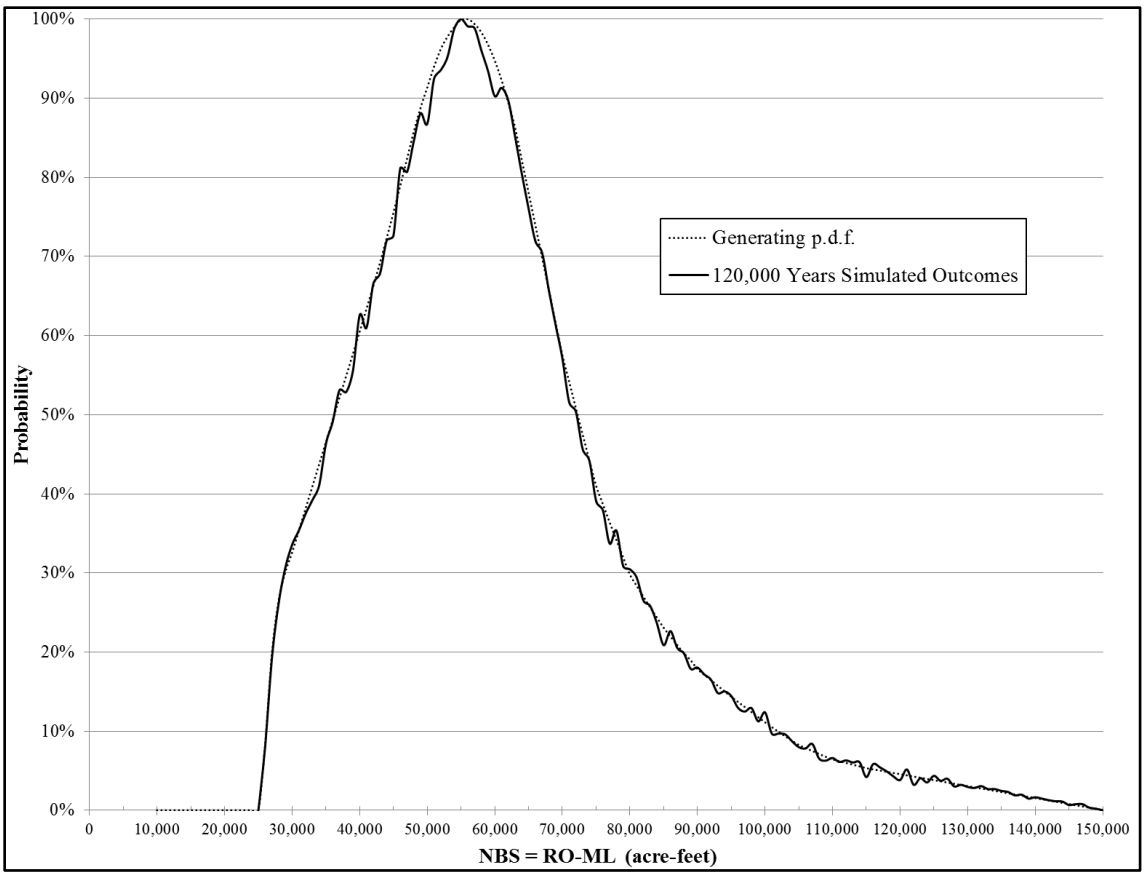

Figure 3.4.12. The Verde Watershed Summer NBS p.d.f. and Distribution of 120,000 Generated Outcomes.

applied generated a linkage between these seasons on the Verde. The correlation results are documented in Table 3.4.2 where it can be seen that the Verde winter-to-summer correlation has been more than achieved and all others are close to the target values.

The scatterplot positions of a 10,000 year sequence of values generated for the winter season between the Salt and Verde watersheds is shown in Figure 3.4.13 along with the historical observations. As can be seen, the generated values overlay the field of observations reasonably well. The watersheds' scatterplot in summer is shown in Figure 3.4.14. It was found that the correlation algorithm to the high-side of the trend follows an

exponential distribution. This high-side exponential behavior was found for both the Salt and Verde in summer, and results in a long high-side tail of generated values.

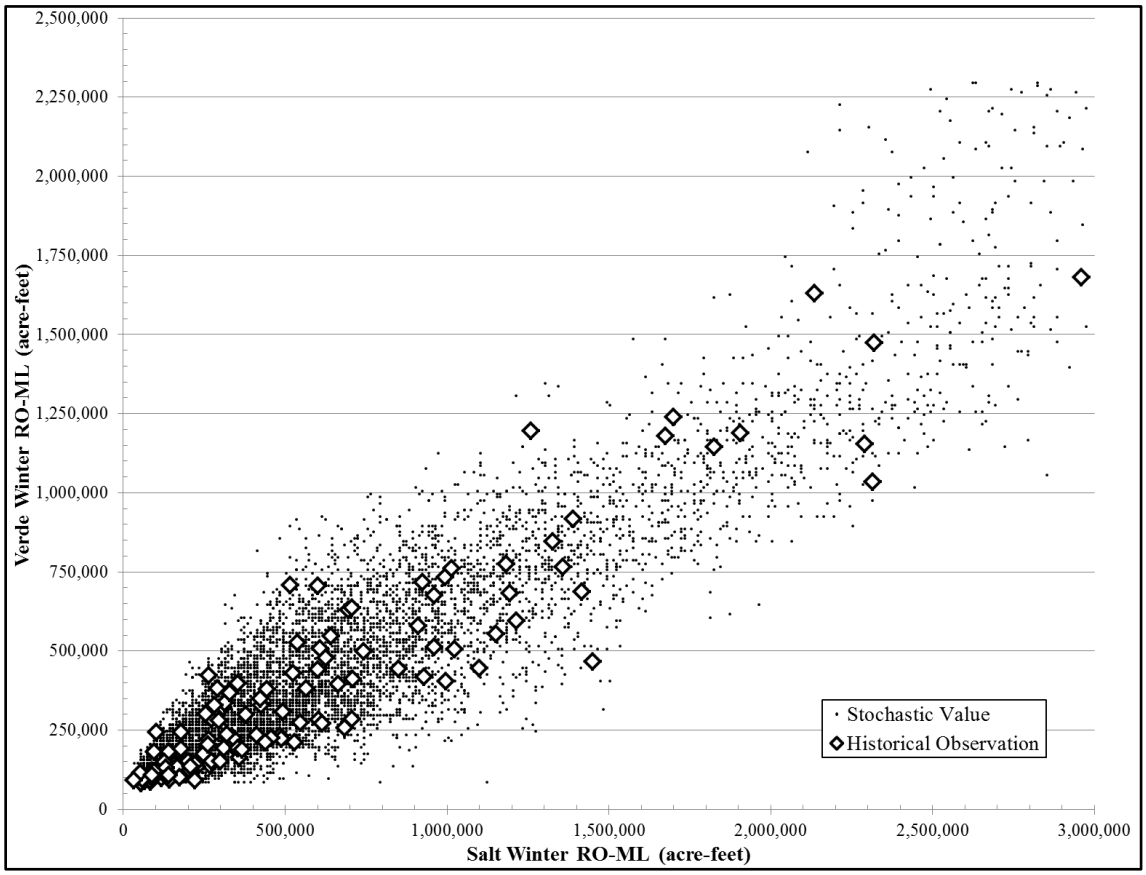

Figure 3.4.13. Salt and Verde in Winter; 10,000-Years of Stochastically Generated NBS Values in Comparison to Historical Observations.

Table 3.4.2. Salt-to-Verde and Season-to-Season NBS Correlation Coefficients for the Dozen 10,000-Year Stochastic Series Compared to the Historical Data Series.

	ANNUAL NBS (acre-feet/year)		CORRELATIONS					
			Salt-to-Verde		Winter-to-Summer		Summer-to-Winter *	
	Median	Mean	Winter	Summer	Salt	Verde	Salt *	Verde *
Historical Record	835,681	1,184,014	0.93	0.65	0.61	0.30	0.10	0.07
10,000-Year Stochastic								
Sequence A	850,500	1,159,526	0.92	0.67	0.61	0.38	-0.03	-0.02
Sequence B	830,500	1,159,741	0.92	0.67	0.63	0.39	0.01	0.02
Sequence C	851,500	1,170,977	0.93	0.68	0.62	0.38	0.00	0.01
Sequence D	848,500	1,155,608	0.92	0.67	0.61	0.38	-0.01	-0.02
Sequence E	850,500	1,166,511	0.93	0.68	0.62	0.39	0.01	0.00
Sequence F	866,500	1,168,955	0.92	0.67	0.62	0.38	-0.01	0.00
Sequence G	845,000	1,157,149	0.93	0.66	0.63	0.39	0.01	0.00
Sequence H	848,500	1,161,951	0.92	0.67	0.61	0.38	-0.02	-0.01
Sequence I	857,000	1,171,184	0.93	0.67	0.62	0.39	0.01	-0.01
Sequence J	846,000	1,168,140	0.92	0.67	0.61	0.38	0.00	0.00
Sequence K	856,500	1,169,523	0.92	0.67	0.61	0.39	0.01	0.00
Sequence L	848,500	1,158,858	0.93	0.66	0.61	0.37	0.00	0.01
All 120,000 years	849,500	1,164,010	0.92	0.67	0.62	0.38	0.00	0.00

* = not statistically significant

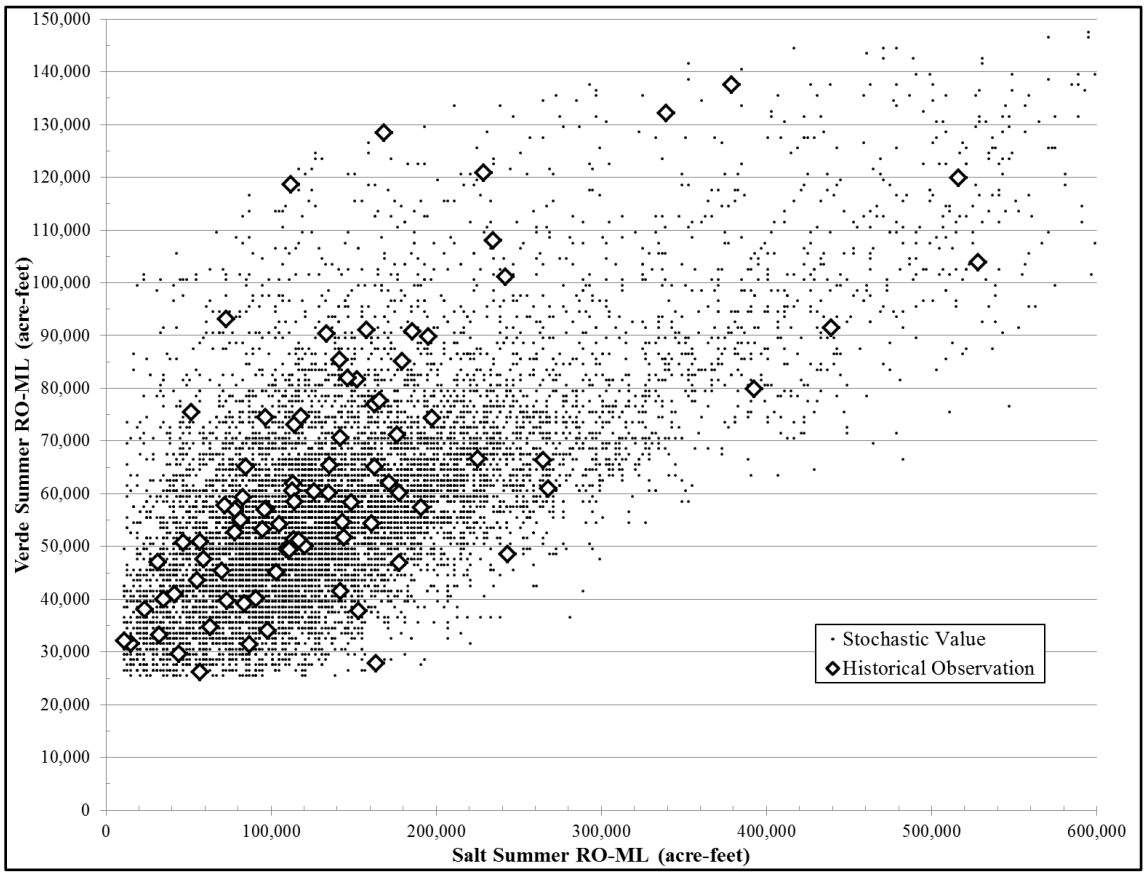

Figure 3.4.14. Salt and Verde in Summer; 10,000-Years of Stochastically Generated NBS Values in Comparison to Historical Observations.

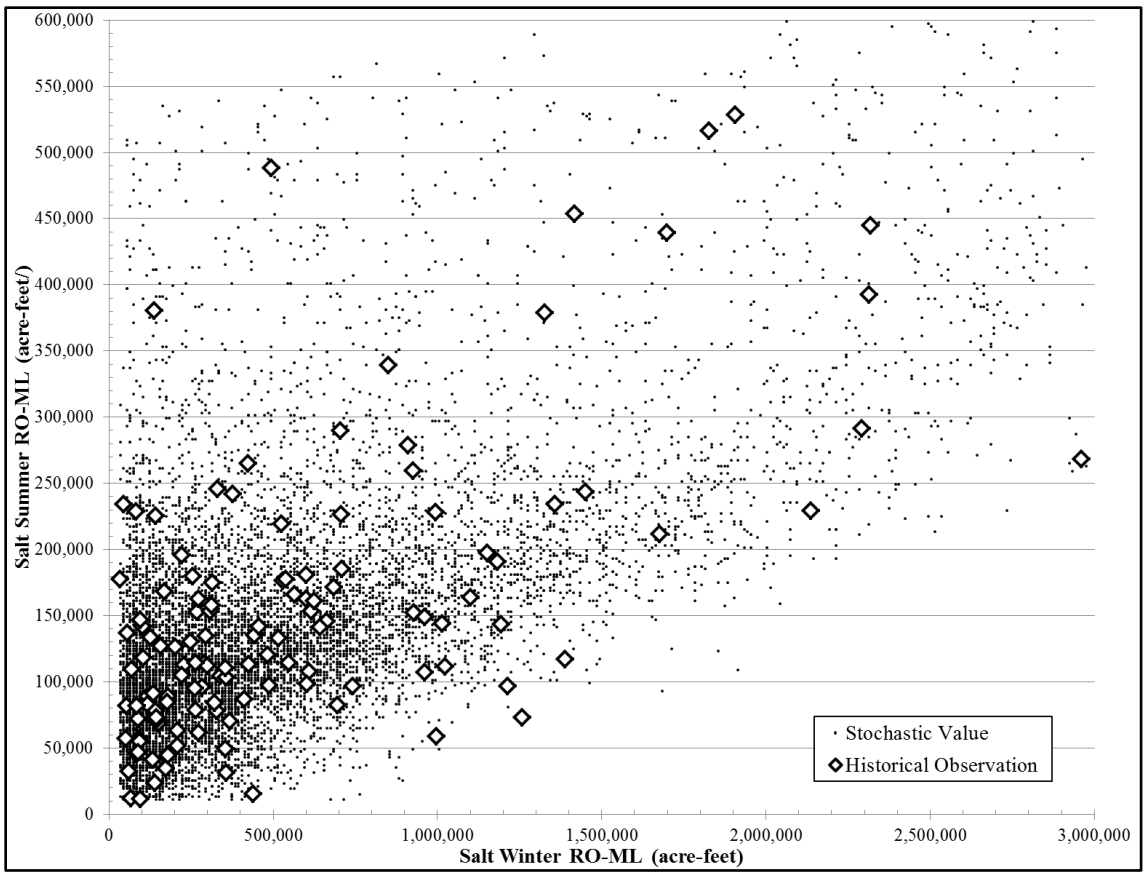

Figure 3.4.15. Salt in Summer vs Salt in Winter; 10,000-Years of Stochastically Generated NBS Values in Comparison to Historical Observations.

The scatterplot of generated values representing the Salt watershed's winter-to-summer seasonal dependency (r=0.613) is shown in Figure 3.4.15. The generated values overlay the field of historical observations reasonably well and extend to the high-side in summer due to their exponential distribution above the trend. The scatterplots for the other seasonal correlations are not included here (Salt summer-to-winter, Verde for each) because at their low correlations there no evidence of relationships in scatterplot patterns. A comparison of the simulated NBS probability distribution to the historical record at the aggregate level is shown in Figure 3.4.16 with close alignment of the cumulative distribution functions. It is satisfying to observe that at the aggregate level the

cumulative probability of generated values is in close agreement with the historical series, indicating that the random generation methodology is hierarchically representative top-down as well as bottom-up.

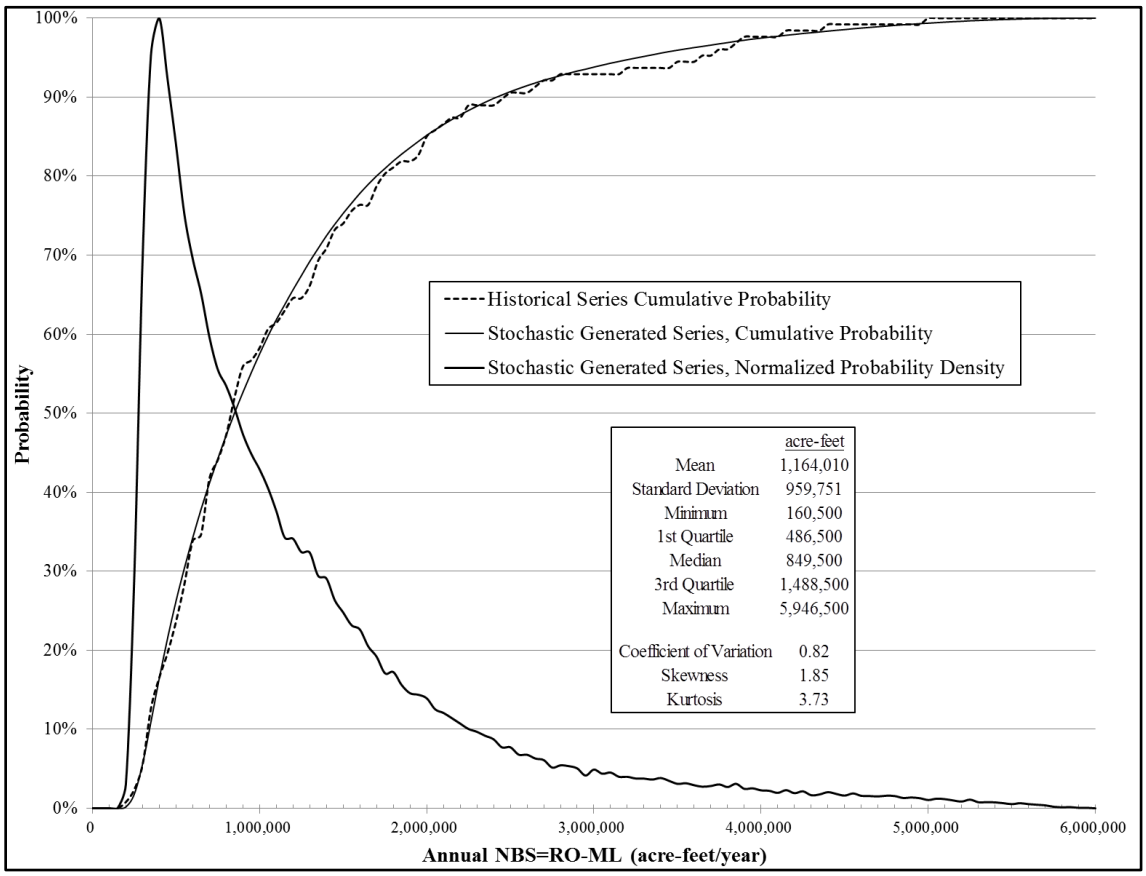

Figure 3.4.16. Probability Distributions of the Historical Record and 120,000 Years of Stochastically Generated Annual NBS.

An example of temporal variability in a generated series is shown in Figure 3.4.17. All 120,000 years cannot be displayed in one graphic, so just one 500-year sample segment of model output is shown. The data have been smoothed with the Lanczos filter to suppress high-frequency components so that decadal variability of the underlying trend-cycle is revealed. The filter-smoothed historical series is also overlaid for comparison purposes. Roughly similar periodicity and amplitude variations between

the generated and historical series can be observed. Every portion of the series is unique in its particular pattern of variability, but all cycle in one fashion or another around the long-term median. The generated series contains periods similar to what has been historically experienced but also reveals higher and lower extremes of shorter and longer temporal duration, as suggested by tree ring data. The historical series is but one manifestation of all possible outcomes that the climatically-driven watersheds can yield for net inflows to the reservoir system. The dozen 10,000-year generated series provide a more thorough, detailed exploration of many characteristics and impacts – enabling a complete assessment of system vulnerability and resilience once passed through the reservoir operations model.

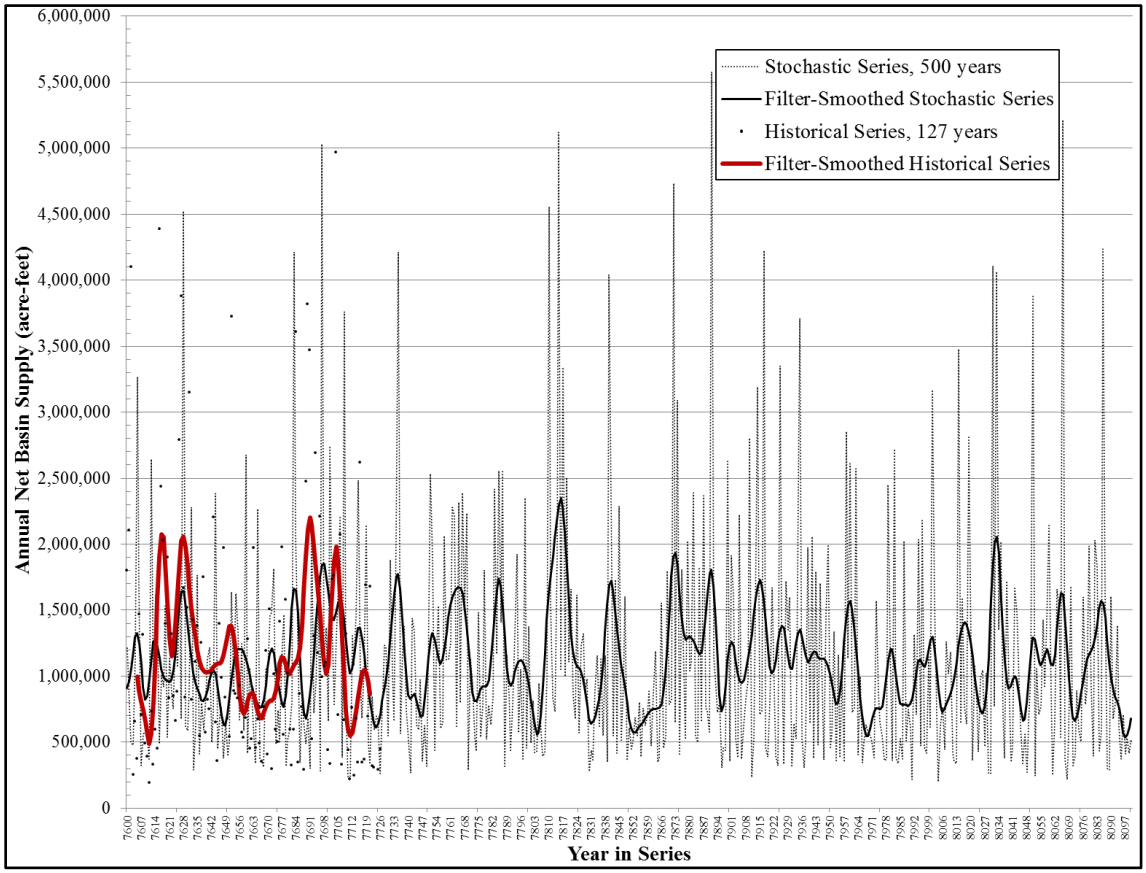

Figure 3.4.17. A 500-Year Sample from the Stochastically Generated 120,000 Years, Compared to the 127-Year Historical Record.

3.5 Hydrologic Sensitivities to Climate

3.5.1 Abstract

Once forecasts of future precipitation and temperature changes are developed, the influence of those climate conditions must be translated to forecasts of change in net basin water supply (NBS) from the watersheds. Quantification of the sensitivity of runoff to climate change has been reported in the literature through modeling studies of hydrologic processes that entail considerable rigor but often with uncertain, unsatisfactory, and incomplete results. These have typically been pursued by computationally-intensive land surface hydrology models (LSHMs) involving complex parameterizations (Schaake 1990; Risbey and Entekhabi 1996; Vano et al. 2012). Findings are often specific to the watershed studied, and a watershed is chosen in part for well-behaved hydrologic response (Gaussian, constrained, seasonal simplicity). The Salt and Verde watersheds are uniquely noncompliant in these regards, with limited quantification of land-atmosphere dynamics in the region. For this investigation, not only precision but accuracy of results is important to investigative validity. And, interpretations must be applicable to the key probability distributions underlying the stochastic simulation methodology so that alternative NBS sequences can be generated and passed to reservoir operation simulations. The literature indicates that a satisfactory LSHM solution is elusive in these regards.

An alternative approach was demonstrated by Vano and Lettenmaier (2013, 2014) employing a pair of heuristic runoff dependency parameters that have been central to many research investigations. They showed that calculations applying a precipitation elasticity (ratio of %-runoff change to %-precipitation change) and temperature

sensitivity (%-runoff change per 1^{o}C temperature change) yielded sufficiently comparable results to variable infiltration capacity (VIC) land surface hydrology modeling of Colorado River watersheds to provide viable assessments of water resource impact. The heuristics can be derived empirically from the observational record in keeping with the overall approach of this investigation. Regression analyses and kriging methods have been employed to develop seasonal heuristics for each watershed and at the SRP reservoirs.

While results align with expectations at the mean, non-linear trends were revealed across key variables, posing important stream flow implications depending on relative position within probability distributions. Winter temperature sensitivity is nearly indistinguishable at low evapotranspiration response, while it is significant in summer with overland flow impairment and reservoir losses. It is lessened by an active monsoon season, which also dilutes the loss contributions at reservoirs. Precipitation elasticity of runoff in semi-arid regions is often assumed to be approximately 2.0, but this study revealed higher values in winter and lower ones in summer, with smaller elasticity when approaching the base flow level and in the upper range of precipitation and runoff. Descriptive algorithms have been derived that can be readily applied to NBS distribution functions with any climate change assumption to assess stream flow impact and water resource sustainability for the region.

3.5.2 Literature Review

Risbey and Entekhabi (1996) pointed out the large uncertainties in climate model simulated precipitation fields (which persist today) that create a basic weakness in the approach of coupling climate with hydrologic models. This can be significant at the

basin level, particularly with the orographic character of the western United States. Nonlinearities in elasticity response noted by all researchers further weaken confidence in that approach. Sankarasubramanian et al. (2001) reported that most prior hydrology research used conceptual watershed models for climate sensitivity studies and that model validation has been an ongoing challenge. Application of different models to the same watershed was leading to significantly different results. And, quite remarkably, analyses of the same basin using the same model could also lead to different results due to differing model parameter estimates and calibration differences resulting in altered model sensitivities. They observed that, if the correct form of the hydrologic model is unknown, then the accuracy of elasticity estimations derived from them are questionable. Vano et al. (2012) came to the same finding upon conducting simulations of the CRB with five LSHMs. They reported streamflow outcomes at Lees Ferry with a wide span of precipitation elasticities, ranging from 2 to 6. And, differences in annual temperature sensitivities between models were revealed, with S_T ranging from -2% to -9% per ^{o}C. There were substantial seasonality and streamflow magnitude differences among the models along with varying and highly nonlinear sensitivity responses. Differences among the LSHMs were larger than the precision required for valid application to this investigation.

Elasticity of runoff in proportion to precipitation is a concept borrowed from the field of economics and introduced to hydrology by Schaake (1990). Elasticity is a quantification of the proportional change in one variable relative to the proportional change in another. For the case of runoff relative to precipitation –

$$\Delta R/R = \varepsilon_p \, (\Delta P/P) \tag{3.12}$$

where R = runoff, P = precipitation,

ΔR = marginal change in runoff, ΔP = marginal change in precipitaiton,

and ε_p = precipitation elasticity of runoff (unitless)

The changes, ΔR/R and ΔP/P, are typically expressed in percentage terms. So, for example, an elasticity, ε_p = 2.0, indicates that a 10% change in precipitation will result in a 20% change in runoff. With the recognition that temperature also influences the relationship, runoff response to both variables is often graphically represented with iso-contours of percentage runoff change according to percentage precipitation change on the abscissa and temperature on the ordinate axes (Risbey and Entekhabi 1996; Fu et al. 2007a). An example from this investigation is given in Figure 4.1.5 of Chapter 4. When the graph is examined in the vertical direction, a percentage change of runoff for one degree of temperature change is defined as temperature sensitivity of runoff, S_T (Fu et al. 2007a) –

$$S_T = (\Delta R/R) / \Delta T \qquad \text{(units: \% per } ^{o}\text{C)} \tag{3.13}$$

Vano et al. (2012) examined the interaction of the ε_p and S_T terms in LSHM simulations of the CRB and found their combined effect to be additive within modest ranges of temperature and precipitation change. The interactive term was quite small, and the heuristics may be assumed orthogonal and simply additive when considered in combination.

Conceptual hydrological models and observational studies of the Sacramento

River basin of California conducted by Risbey and Entekhabi (1996) came to some general findings subsequently confirmed by other researchers. Streamflow amounts are strongly sensitive to precipitation but relatively insensitive to mean seasonal temperature. This is consistent with many regression analyses that show most runoff variance explained by precipitation with only modest additional variance explained by temperature, although this can be seasonally dependent. Response to precipitation exhibits substantial nonlinearity in that it depends on the precipitation volume change and the mean climate state. There are greater changes in streamflow response during very wet years so that a larger precipitation change results in a greater nonlinear streamflow response. Higher soil moisture and larger snowpack increases the amount of runoff relative to precipitation. During dry years a weak linear to nonlinear relationship can be present. They found that the seasonal climate cycle in the Sacramento basin is typically strong enough to essentially re-initialize the basin's hydrology every year by erasing long-term surface moisture storage that would provide hydrologic memory. The Salt and Verde basins behave similarly if even more so considering their higher potential ET throughout the summer season.

Risbey and Entekhabi also observed that streamflow timing is sensitive to temperature. Interestingly, this leads to a buffering effect that reduces streamflow volume sensitivity to temperature. Losses from sublimation of snowpack and evapotranspiration are typically the main temperature effect, but in marginal snow regions an earlier melt will tend to occur when it is cooler and energetic potential for those effects are closer to their annual minimum. If runoff occurred later in spring the energetic potential would be higher. This was also noted by Jeton et al. (1996). Either

streamflow timing or amount, but not usually both, are sensitive to changing mean temperatures. Vano et al. (2012) also reported that some sub-basins in their LSHM simulations showed increasing winter-spring runoff with increasing temperature, and the mechanism seemed most prevalent in transitional locations with a temperature-sensitive snowpack. As will be noted below (Fig. 3.5.5), some manifestation of this effect appears in analysis of the Salt River watershed.

Sankarasubramanian et al. (2001) pointed out that since elasticity is a function of runoff & precipitation, elasticity findings can be expected to be complex across the span of runoff and precipitation regimes. That complexity makes inter-basin comparisons challenging, and they simplified doing so by just examining the mean precipitation level for basins having Gaussian variability (Sankarasubramanian and Vogel 2003) and skirting acknowledged nonlinearity issues.

Fu et al. (2007a) reminds us that full climate elasticity of streamflow is really a conditional precipitation elasticity accounting for the effects of temperature. To accommodate that, they introduced the two-parameter indices defined earlier: precipitation elasticity and temperature sensitivity. In a comparative study of these with a VIC hydrologic model applied to the UCRB, Vano and Lettenmaier (2014) confirmed that these heuristics provide viable estimates of climate sensitivity that avoid LSHM simulation complexities and allows the influence of temperature and precipitation to be segregated for a better understanding of the drivers of hydrologic change. Fu et al. explored how to reflect the complicated non-linear relationship among runoff, precipitation, and temperature for assessment of future climate scenarios. This included various methods by which to graphically and parametrically express climate elasticity

(Fu et al. 2007a; Fu et al. 2007b), and they searched for those which have the best fitting error to observational data records. They found that kriging methods were best at providing multivariate interpolations with observational data from which functional expressions of elasticity and sensitivity can be calculated. This methodology was employed for this investigation along with guidance from prior research, as will be explained below. Fu et al. concluded that important but complicated nonlinear response is not easily captured in a single elasticity value, and multi-dimensional representations must be employed, often with seasonal differences specific to the watershed. And, they warn that while exploration of temperature and precipitation changes at the margin may illuminate a watershed's climate response, results are a function of the data set explored. More data is better, limited data leads to low confidence in results, and care should be exercised in extrapolations too far beyond the range for which data records are available.

3.5.3 Temperature Sensitivity

While temperature increases are readily observed in the historical record, manifestations of effects on the hydrologic cycle have remained elusive to-date (Murphy and Ellis 2014). However, temperature-induced changes might have been small and as-yet unresolvable in their effects. The Hurst-Kolmogorov analysis in Section 3.3.12 was conducted to further examine the possibility of recent subtle impairments. It provided little indication of winter effects but did show the possibility of emerging summer runoff impairment and some contributions to miscellaneous loss coinciding with recently elevated temperatures. While Vano et al. (2012) deduced a general temperature sensitivity from LSHM modeling of the UCRB of -6.5±3.5%/ ^{o}C, further work by Vano and Lettenmaier (2014) revealed the seasonal dependence of temperature sensitivity (and

for precipitation elasticity as well). Summer values were several times what were found for the coolest winter months. They also observed slightly higher sensitivity once temperature had been elevated. Their aggregate finding of S_T = -6.5%/ ^{o}C is similar to results of water budget runoff modeling of LCRB watersheds by Ellis et al. (2008), which averaged 6%/^{o}K. These values are close to expectations from PE relationships such as the Hamon equation which has exponential temperature dependence, going as $e^{0.062T}$ (Ellis et al. 2008). As such, PE is small at low temperatures, but increasing at 6.4%/ ^{o}K. Assuming an annual value similar to these and small winter sensitivity, then the balance of summer sensitivity could be a double digit percentage.

If this has emerged in the Salt and Verde watersheds with rising temperatures during the 1980s-90s, then a comparative calculation between pre- and post-rise periods can provide a bounding estimate to the sensitivity assessment. Instrumented miscellaneous loss data has only been available since the reservoirs were placed in service, so the pre-rise period for the Salt side of the system is 1935-1979 and for the Verde it is 1946-1979. Temperatures appear to have paused since 2000 (Fig. 3.3.1). Comparative calculations are shown in Table 3.5.1, coming to a summer temperature sensitivity estimate of approximately -20%/^{o}C. However, the short recent period has been relatively dry with an ongoing drought, and this calculation is not controlled for precipitation. It therefore provides only a maximum estimate of summer S_T. The kriging analysis below rectifies this deficiency. The calculations in Table 3.5.1 also reveal a larger miscellaneous loss increase on the Salt side of the system than the Verde, probably attributable to relative reservoir sizes. Further examination of ML time series (not

shown) does show that average ML levels appear slightly elevated in recent years. The Verde exhibits no recent ML trend while there may be some for the Salt. Elevated ML emerged as the runoff and NBS curves appear to undergo slight declines and average ML between periods was found to have a statistically significant difference for both the Salt and Verde sides of the system.

Table 3.5.1. Comparison of Recent to Early Periods for Estimates of Maximum Expected Temperature Sensitivity.

	Summer Season		
	Salt	Verde	
Early period	1931-1979	1946-1979	
Recent period	2000-2015	2000-2015	
ΔT between periods	~ +1.3°C	~ +1.5°C	
Runoff (RO)			
mean, Early	161,900	68,700	
mean, Recent	115,000	49,000	
ΔRO between periods	-46,900	-19,700	
	-29%	-29%	
Temperature Sensitivity, S_T:	*-22%*	*-19%*	*per °C*
MiscLoss (ML)			
mean, Early	13,600	-500	
mean, Recent	44,100	5,500	
ΔML between periods	30,500	6,000	
NBS (=RO-ML)			
mean, Early	148,300	69,200	
mean, Recent	70,900	43,500	
ΔNBS between periods	-77,400	-25,700	
of which, ΔRO is:	61%	77%	
of which, ΔML is:	39%	23%	

These are maximum expectations only, a bounding calculation.

Similar calculations were performed for the winter season. HK analyses were essentially equivalent between runoff and NBS at low values, and ML distributions between time periods are not statistically different, indicating negligible temperature sensitivity of runoff and no evidence of changing ML contributions in winter.

Regression analyses of runoff and miscellaneous loss also show no temperature dependence of those variables in winter. 81% of Salt winter runoff variance is explained just by in-season precipitation, with an additional 5% explained by antecedent season precipitation and runoff. 84% of Verde winter runoff variance is explained just by in-season precipitation, with another 1% explained by antecedent season runoff. Temperature does not enter the step-wise winter regression relationships and its correlation with both runoff and miscellaneous loss are small and statistically insignificant.

This is not the case in summer when temperature effects are evident. Explained variances are smaller than seen for the winter season (40% Salt, 55% Verde); and although precipitation explains most of the variance, temperature does enter the step-wise regression relationship for both watersheds. It was noted, however, that when Salt summer runoff is above about 200,000 acre-feet in the season, temperature is absent from the regression relationship. Those are typically wet years when there is carry-over streamflow from April into May and temperature effects appear dampened. Correlations of summer temperature with runoff and miscellaneous loss were found to be statistically significant. Runoff impairment dynamics occur on the watershed, but it is believed that most miscellaneous loss mechanisms in summer are at the reservoirs. Therefore the analysis of summer NBS temperature sensitivity was conducted for those variables separately as well as in combination.

The regression equations for summer runoff can be differentiated with respect to temperature for a sensitivity estimate applicable at the center of the runoff distribution (in

the vicinity of the mean/median/mode). These were calculated for comparison to other results and found to be:

Salt-Summer S_T = ~ -11%/^{o}C Verde-Summer S_T = ~ -10%/^{o}C

These estimates align well with the nominal sensitivity (~ -10%/^{o}C) found by Vano and Lettenmaier (2014) for the UCRB in May-September. However, such values only apply at the average; and with so much of the research literature indicating nonlinear response, a more sophisticated analysis methodology is required.

Following the guidance of Fu et al. (2007a; 2007b) and other hydrologists (personal communications), kriging methods were employed to explore the three-dimensional space of runoff response (z) to temperature (y) and precipitation (x). Kriging is an optimal interpolation method that gives the best linear unbiased estimate of intermediate values within a domain of irregularly sampled data. Interpolating methods based on other methods' criteria have been shown to not necessarily yield the most likely intermediate values. The technique is also known as Wiener–Kolmogorov prediction and was originally developed based on the Masters thesis work of Daniel G. Krige who sought to estimate the most likely distribution of gold ore based upon data from a limited set of boreholes. Different types of kriging may apply depending on the properties of the data examined, and for this investigation ordinary kriging was employed as coded in Python by Murphy (2015). Specific runoff interpolation points were not of interest since S_T and ε_p are relative metrics assessed by orthogonal slopes within the 3-dimensional field. Therefore the temperature-precipitation space was examined granularly with 100x100 cells for slope analysis, and cell size did not affect results. The krige solution

for Salt runoff in winter is given on Figure 3.5.1 and for summer in Figure 3.5.3. The Verde solutions are given in Figures 3.5.2 & 3.5.4. Some variability due to contributions of individual years can be seen, but the general patterns reveal the major difference between winter and summer. Little vertical trend with temperature is evident in winter while it is clearly present in summer.

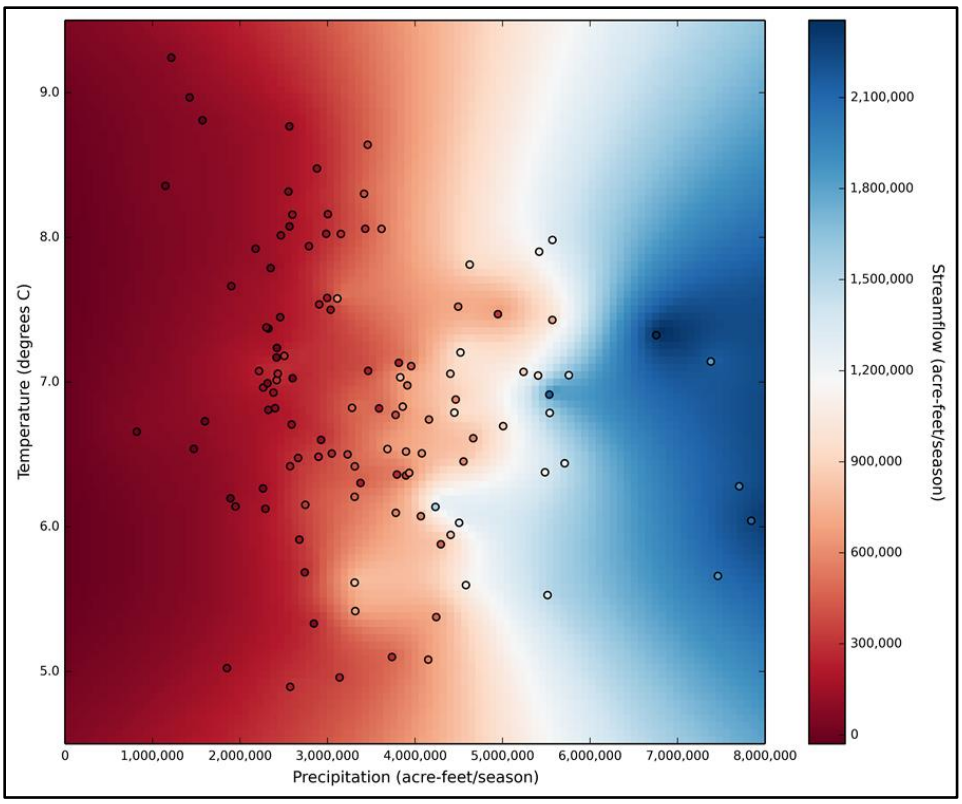

Figure 3.5.1. Kriging Solution for Salt Watershed Runoff Response in Winter.

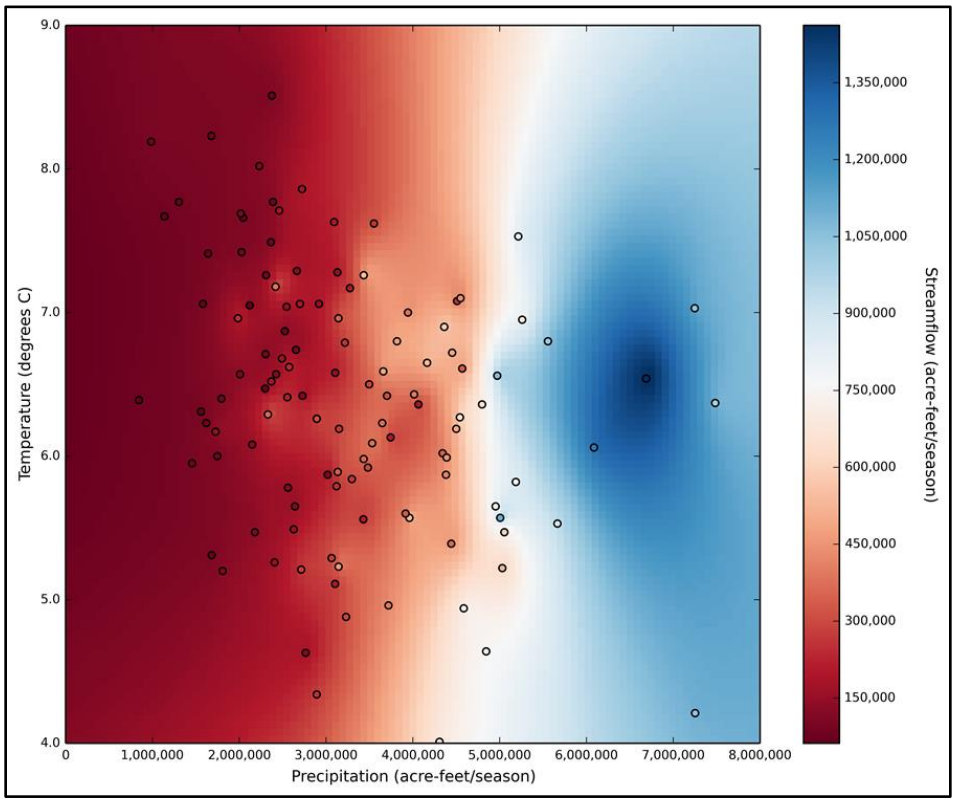

Figure 3.5.2. Kriging Solution for Verde Watershed Runoff Response in Winter.

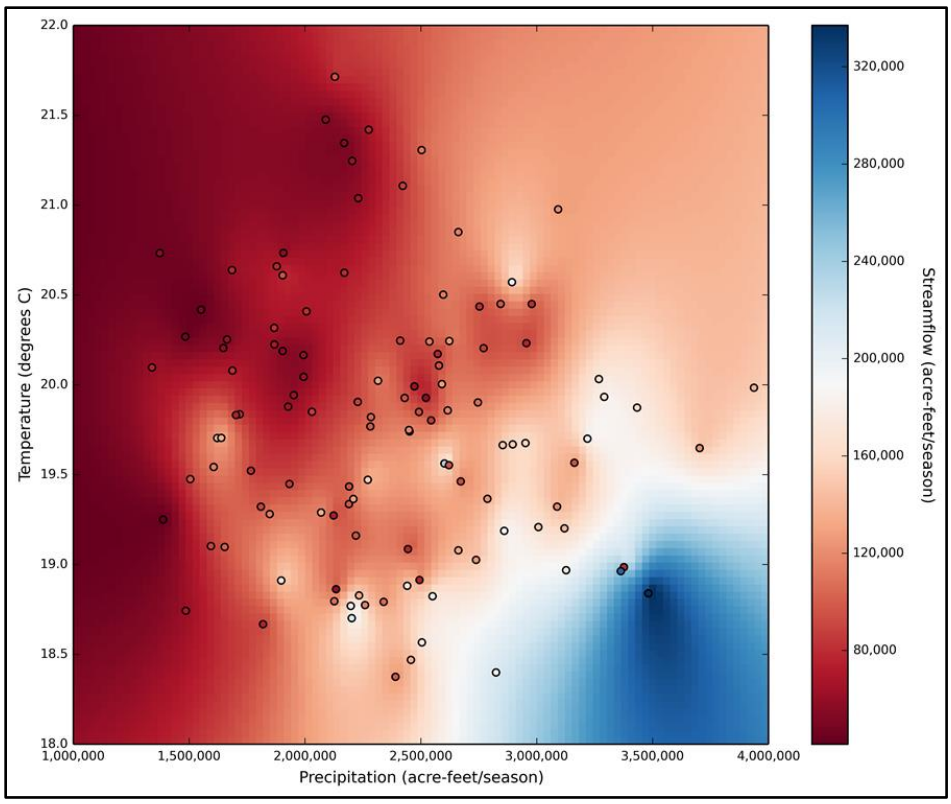

Figure 3.5.3. Kriging Solution for Salt Watershed Runoff Response in Summer.

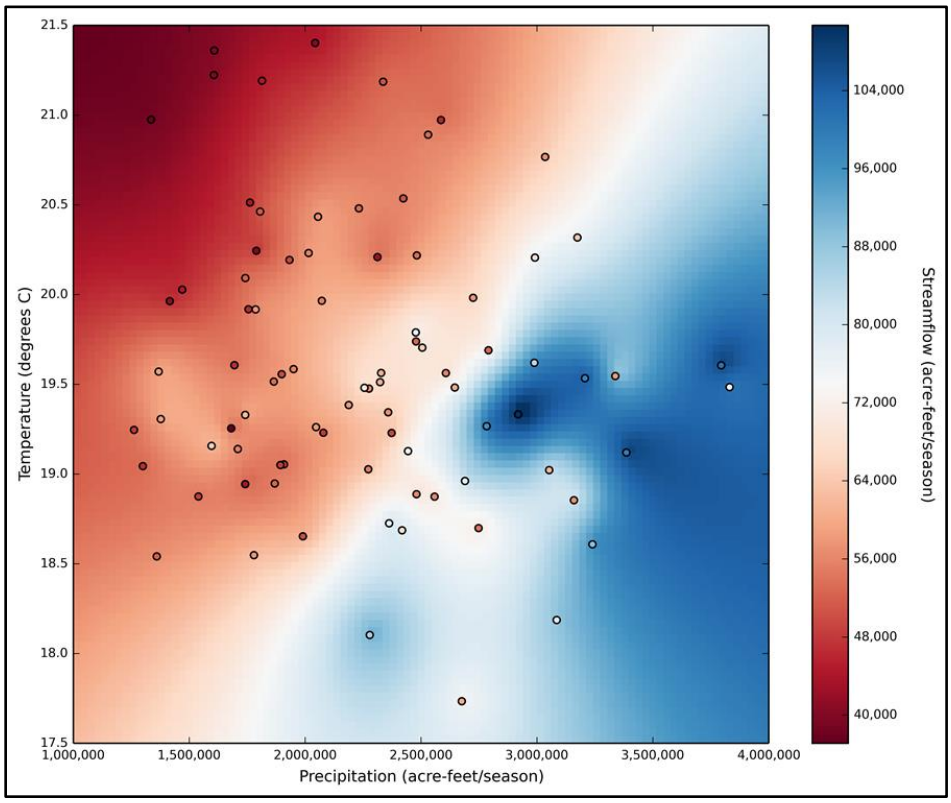

Figure 3.5.4. Kriging Solution for Verde Watershed Runoff Response in Summer.

A maximum amount of observational data is desired for assessing hydrologic response. But, it must be acknowledged that across the ~120 years of data, various changes both transitory and transformative may have occurred on the watersheds aside of temperature and precipitation and that those might show up in hydrologic response. Examples include land cover changes with settlement, agriculture expansion or retirement, cessation of logging and reforestation, fires, one-time meteorological events, etc. Where data indicated such a possibility, kriging was conducted with and without anomalous observations and among data subsets to assess their influence on temperature sensitivity and precipitation elasticity estimates. The goal was quantification of typical climate elasticity that represents a watershed-season's current behavior.

Evapotranspiration dynamics are different when water traverses a land surface before finding its way into a protected streamflow channel. Thereafter, larger channels sustain riparian areas that influence evapotranspiration, and reservoir evaporative losses are different still. Water passing a reservoir input gage will have originated either in baseflow from spring-fed groundwater sources or overland flow from precipitation. The relative contributions among all these differences are reflected in nonlinear sensitivity. In the limit as precipitation approaches zero only baseflow is subject to temperature impairment which is smaller than effects on overland flow. Regression relationships show inverse collinearity of temperature with precipitation. Large precipitation events are not only cooler but large runoff volumes across fully saturated soils experience diminished temperature sensitivity towards some minimal value in the limit of high precipitation. All the above considerations were evaluated with the expectation that temperature sensitivity will be a minimum at baseflow without precipitation, rising to its

maximum effect in typical runoff regimes, and then diminish towards high precipitation and runoff levels.

Once a kriging solution is calculated, precipitation level can be controlled to explore temperature sensitivity by vertical iso-precipitation cuts through the krige surface. Multiple curves were extracted and plotted for runoff vs temperature. Temperature levels were examined for difference of slope, and sensitivities were calculated using various slope segments. In most cases continuity of behavior could be identified across the sample temperature range, and the recent upper temperature range was of primary interest since it is the basis from which future temperature changes will

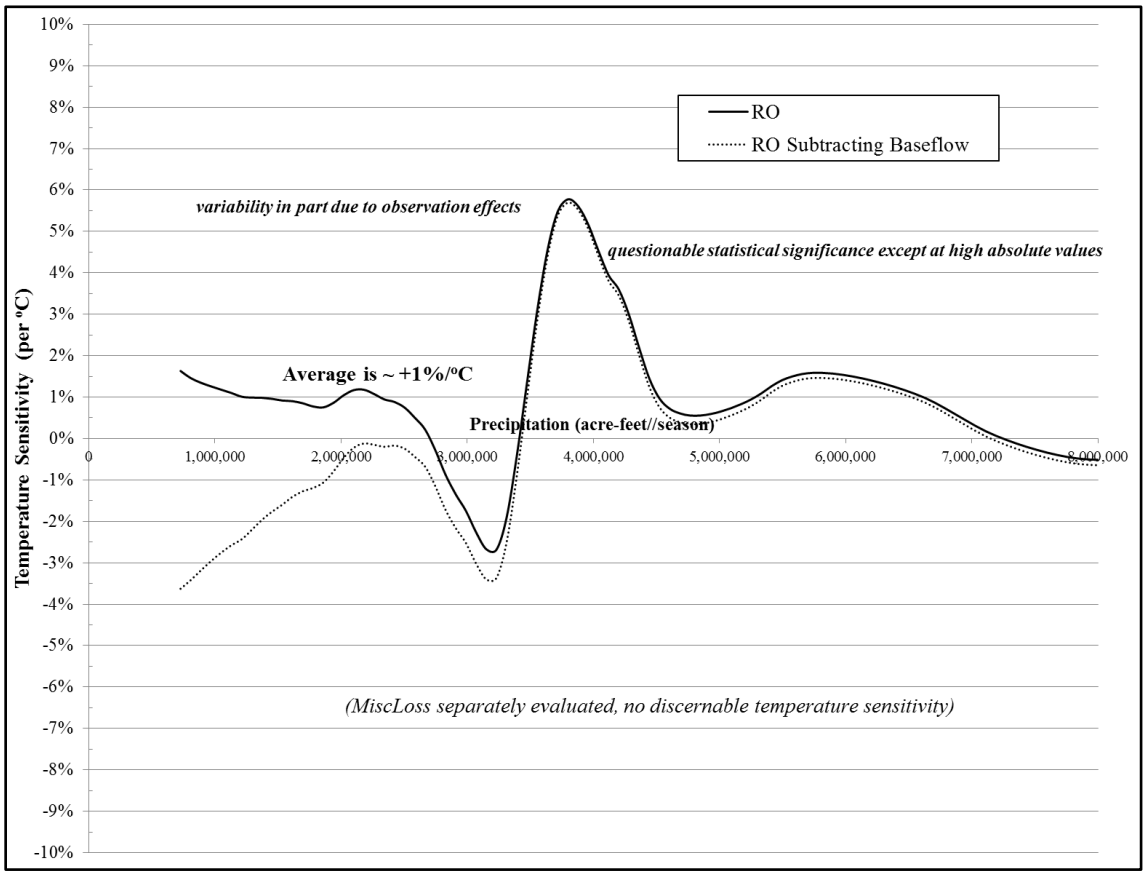

Figure 3.5.5. Salt-Winter Temperature Sensitivities by Precipitation Level per Krige Solutions. A uniform 0%/^{o}C was adopted .

occur. Sensitivity by precipitation level (and corresponding average runoff level) is then plotted and a pattern across levels is identified. Some Salt-winter krige results are shown in Figure 3.5.5. There is variability around an average +1%/^{o}C sensitivity, but with indeterminate statistical significance. This positive sensitivity was mentioned in the literature review above, and reverses to a negative sensitivity if winter season definition is extended through May to include late-season runoff and warmer temperatures. No trend by precipitation level is evident and for the purposes of this investigation a uniform 0% or +1% could be applied. A zero value was adopted. Verde results are shown in Figure 3.5.6 with small sensitivities of unclear statistical significance. Upon various

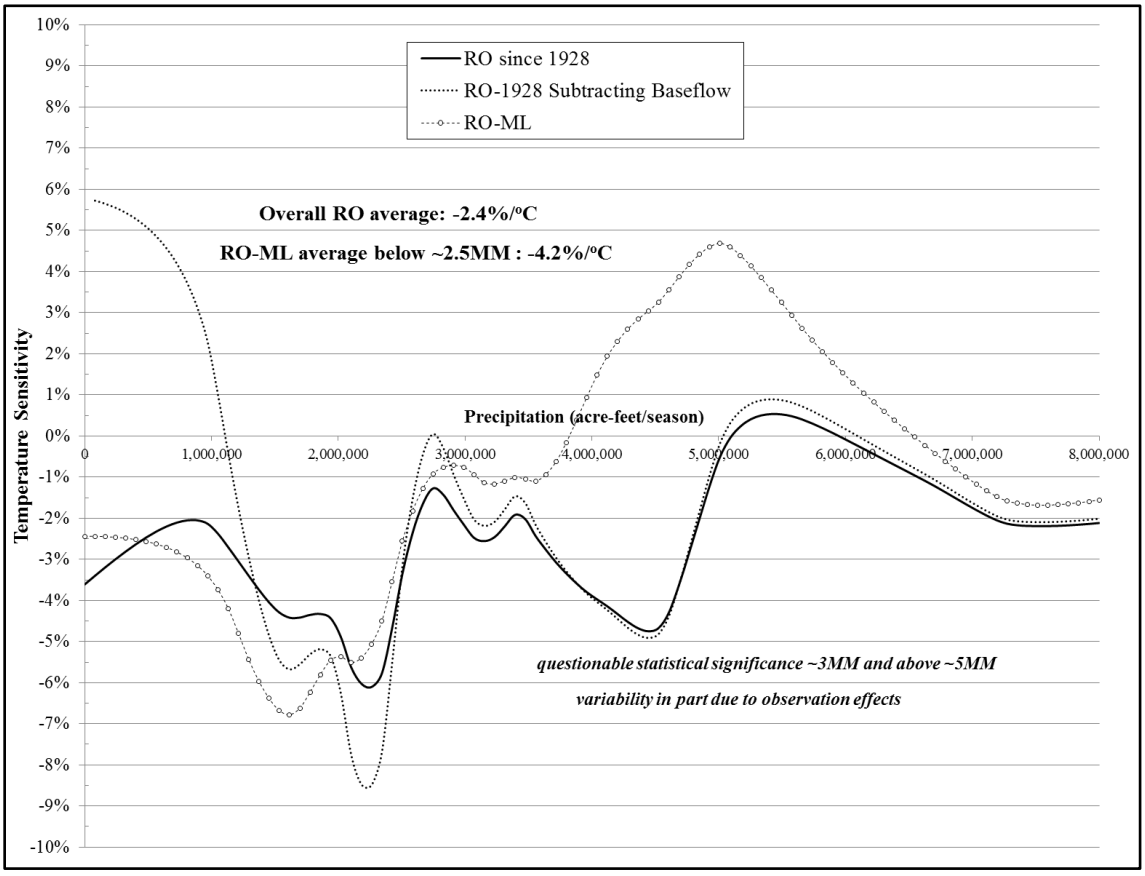

Figure 3.5.6. Verde-Winter Temperature Sensitivity by Precipitation Level per Krige Solutions. A uniform -3%/^{o}C was adopted for NBS below 182,000 acre-feet/season (P<2.5E06) and 0%/^{o}C above that level.

analyses of the data, it appeared that a nominal -3%/^{o}C could be assumed for precipitation below 2,500,000 acre-feet/season (NBS<182,000) and 0%/^{o}C above that level.

Very different krige results were obtained for the summer season. Iso-precipitation curves display diminishing runoff with increasing temperature. Sensitivity calculations had to be made with various data subsets and combinations of variables to resolve a pattern, in part because summer runoff efficiencies are very low so that precipitation-dependent findings only weakly translate to runoff levels. The Salt-summer curve in Figure 3.5.7 was derived for runoff in its upper distribution and baseflow

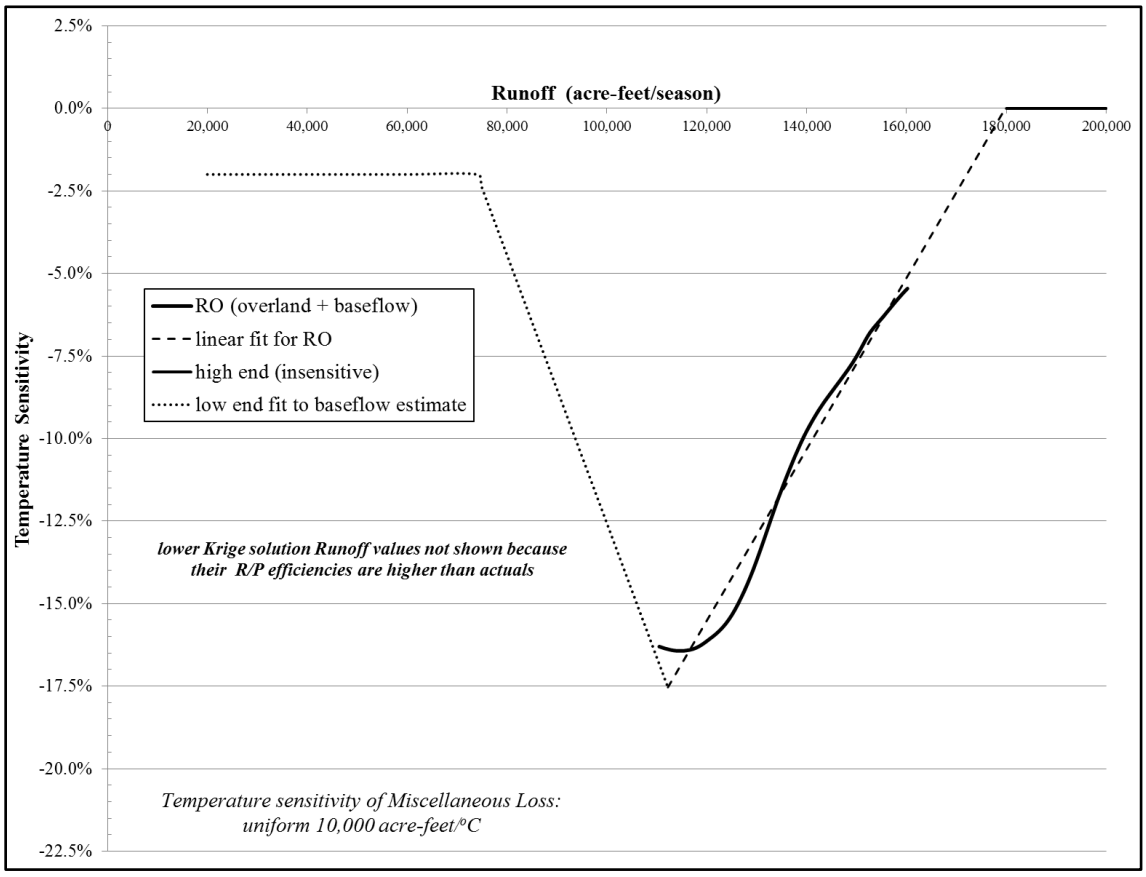

Figure 3.5.7. Salt-Summer Temperature Sensitivities by Runoff Level per Krige Solutions.

sensitivity was estimated, allowing the intermediate portions of the curve to be identified. Comparative analyses also revealed temperature dependence for miscellaneous loss of 10,000 acre-feet/^{o}C, a significant but understandable value considering the surface area of Lake Roosevelt susceptible to evaporative loss. This was smaller for the Verde side of the system as shown in Figure 3.5.8 where it is a function of NBS level. Verde S_T follows a similar inverted-triangle pattern as the Salt. Nominal temperature dependence in the center of the runoff probability distribution is close to the -10%/^{o}C estimate from the regression analysis above. Now that the seasonally distinct and nonlinear temperature dependencies are revealed, it is clear that the result of their pairings with NBS probability

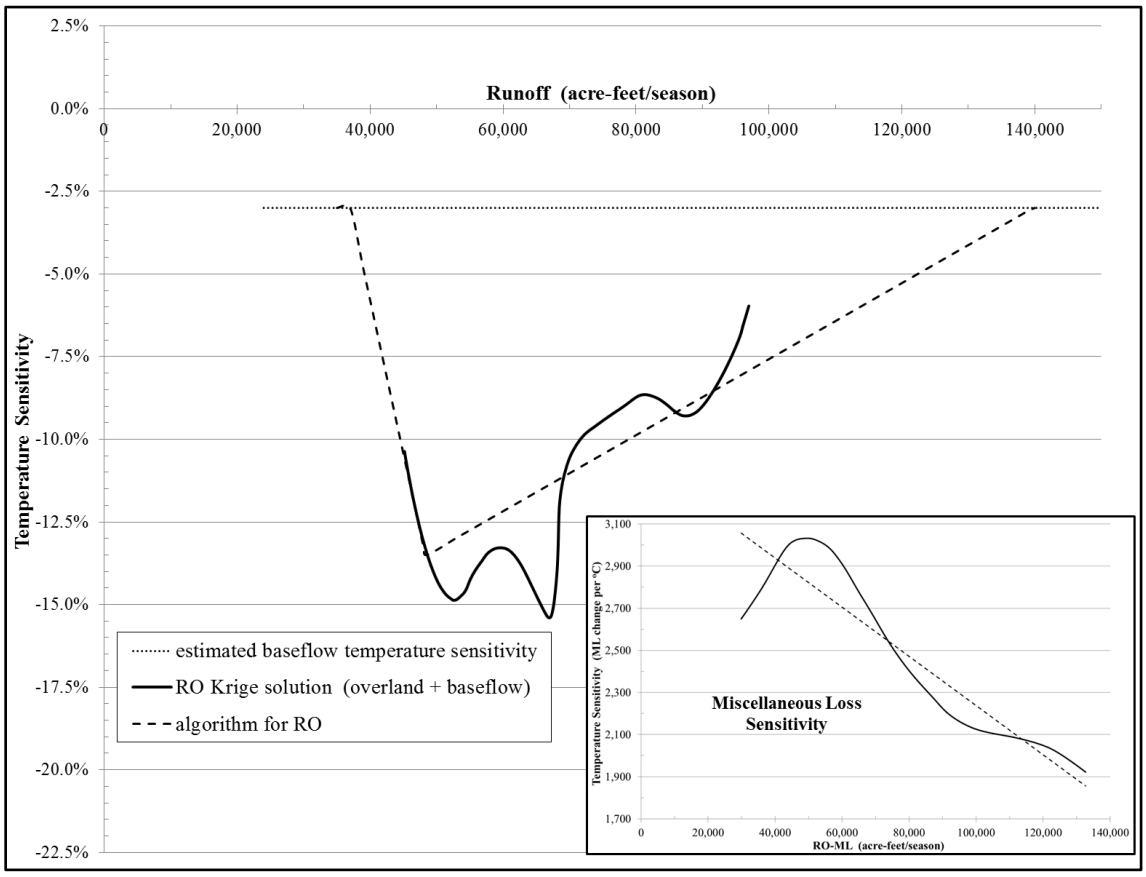

Figure 3.5.8. Verde-Summer Temperature Sensitivities by Runoff Level per Krige Solutions.

distributions will result in significant differences from what might be assumed by a naïve, homogeneous sensitivity assumption. All of the temperature sensitivity algorithms derived from this analysis are tabulated in Appendix D.

3.5.4 Precipitation Elasticity

As discussed earlier, precipitation elasticity of runoff is defined as the marginal change of runoff in proportion to the marginal change of precipitation for the hydroclimate R-P regime being examined:

$$\varepsilon_p = (\Delta R/R) / (\Delta P/P) \tag{3.14}$$

which can be rearranged to

$$\varepsilon_p = (\Delta R/\Delta P) / (R/P) \tag{3.15}$$

and we see that this is the slope of the runoff-vs-precipitation relationship divided by runoff efficiency. An aggregate elasticity estimate can therefore be made by an overall R-vs-P slope calculation divided by average runoff efficiency. These are shown for the Salt and Verde watersheds in winter in Figures 3.5.9 and 3.5.10, with aggregate $\varepsilon_p = 2.39$ for the Salt in winter and 2.01 for the Verde. It is also evident that the relationship has changed over time, with higher runoff and efficiency in wetter times than dry. Nonlinearities are therefore expected, and this calculation is not controlled for temperature, so it is only a preliminary estimate.

Estimates were also attempted for the summer season, but runoff efficiencies and slopes from R-vs-P scatterplots are very small with weak correlations (not shown). Slope and efficiency were approximately equal so that ε_p appeared close to 1.0. But at such low runoff levels baseflow constitutes an important portion of the streamflow that is

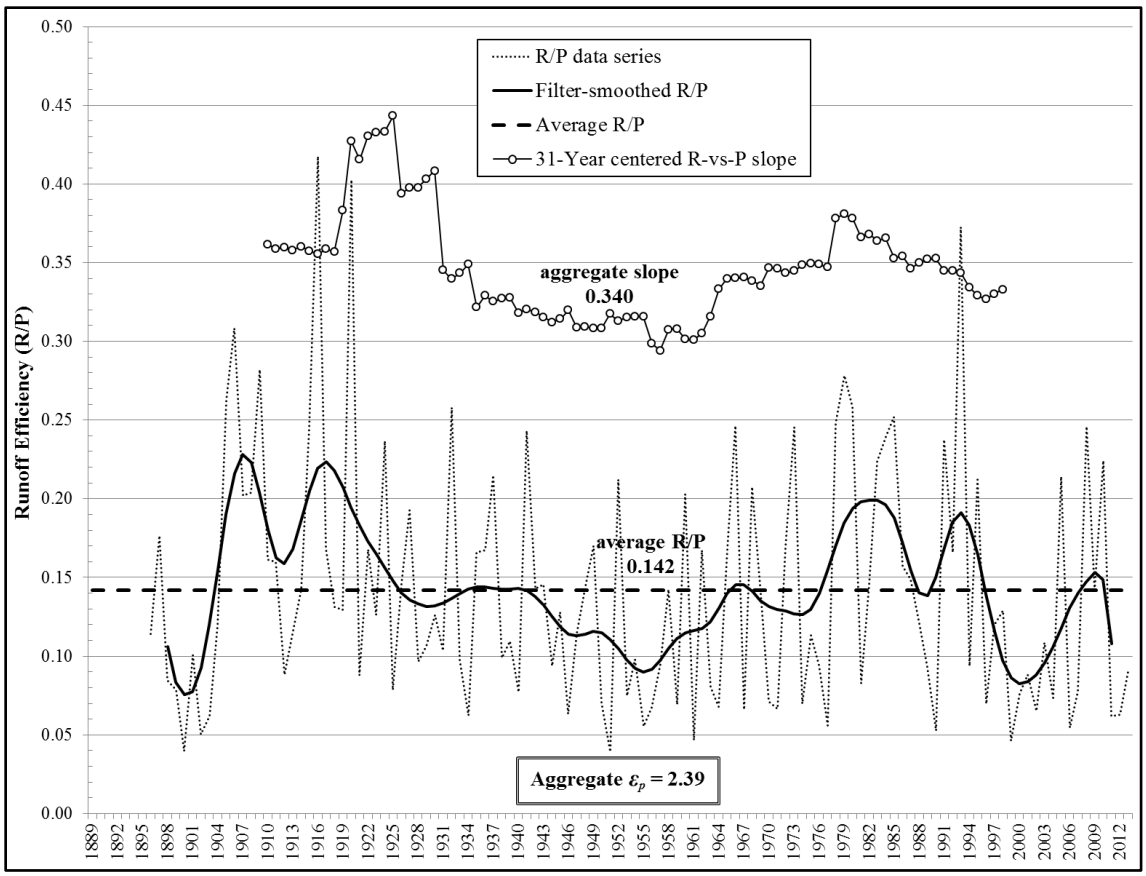

Figure 3.5.9. Salt-Winter Aggregate Elasticity by Precipitation-Runoff Slope and Efficiency.

uninfluenced by precipitation. It became clear that overland flow elasticity can only be accurately assessed by subtracting a baseflow estimate from runoff data before the elasticity calculation is made. Baseflow was estimated from minimum levels in the stream gage record and checked at low precipitation in kriging solutions. At the opposite extreme, at high runoff, net gain contributions from heavy precipitation have been documented that are not captured by the stream gage. Runoff efficiency might therefore be under-estimated and influence the elasticity calculation in those regimes. Multiple versions of each dataset were therefore evaluated – with and without baseflow, with and without net gains – to best identify the precipitation-dependent streamflow.

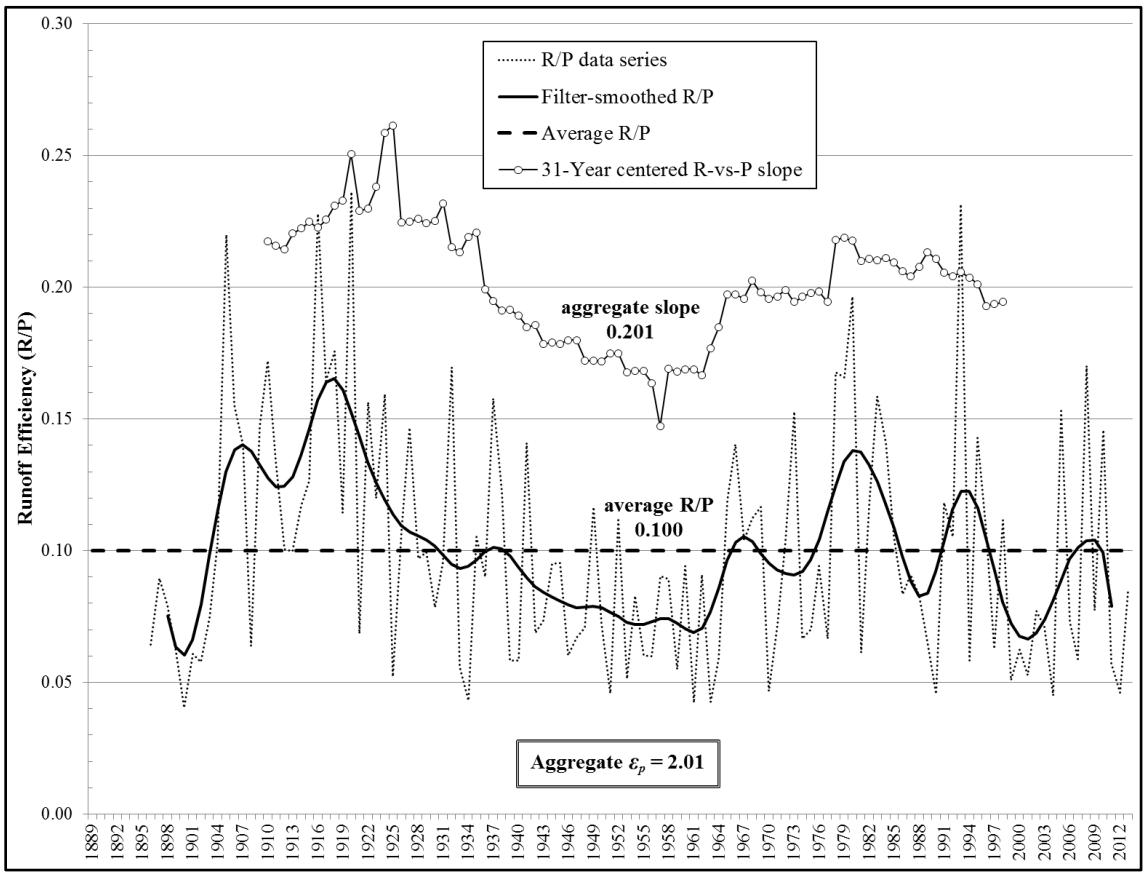

Figure 3.5.10. Verde-Winter Aggregate Elasticity by Precipitation-Runoff Slope and Efficiency.

Analyses of the kriging solutions (modified Figs. 3.5.1 – 3.5.4) were examined by horizontal iso-temperature cuts of the interpolated surface. Consistency of the curves across temperature levels was examined and those from higher temperature levels used if trends were apparent. Local slopes, efficiencies, and elasticities were calculated across the range of precipitation and runoff. At the low and high limits of precipitation, R/P efficiency should approach minimum and maximum values (see Figs. 3.5.11, 3.5.12). With baseflow subtracted, elasticity starts at 1.0 in the limit of zero precipitation and increases towards a maximum value mid-range at typical precipitation-runoff levels. It

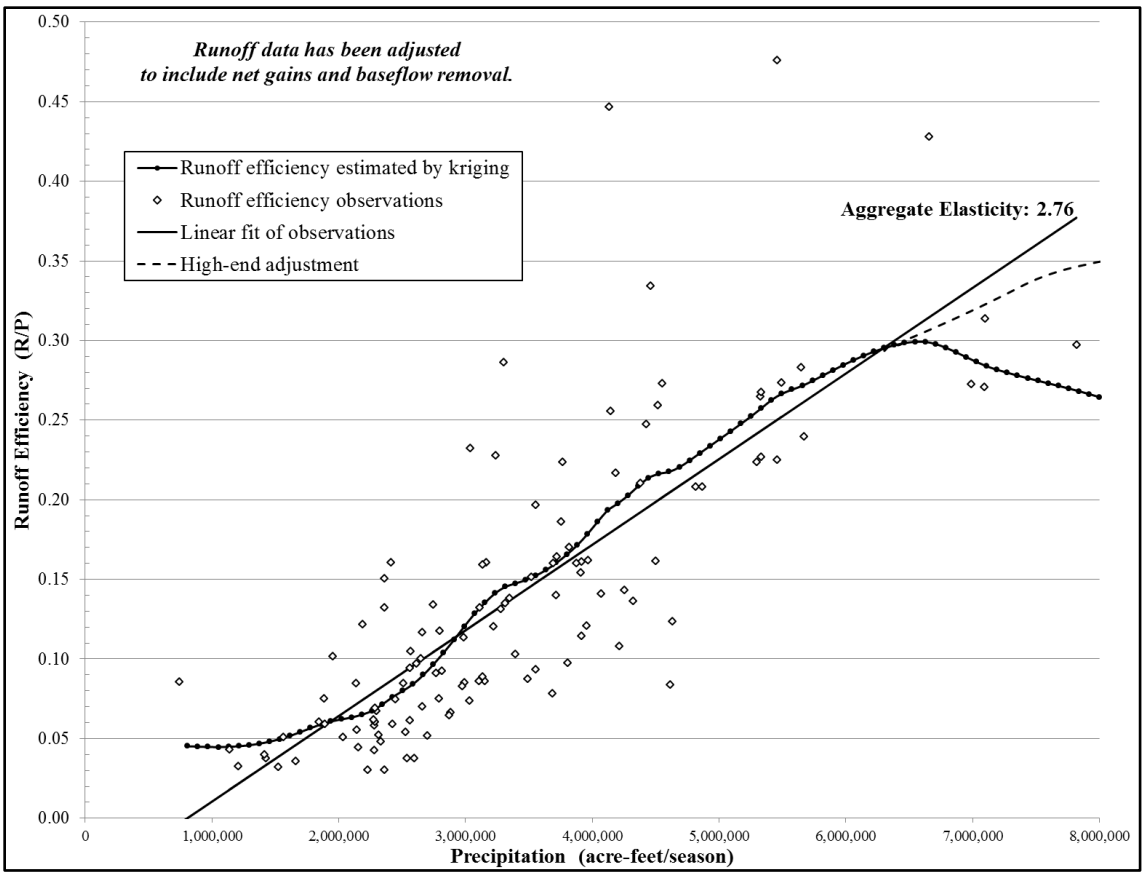

Figure 3.5.11. Salt-Winter Runoff Efficiency by Precipitation Level, Adjusted for Baseflow and Net Gains.

then declines towards high precipitation levels as runoff efficiency approaches a maximum value and incremental runoff occurs in equal proportion to further increases of precipitation. It was discovered that efficiencies at the high end calculated from the krige solution were sometimes inconsistent with observational data, probably due to too few observations for kriging at the edge of the interpolation space. The ends of efficiency curves for the solutions were therefore re-estimated where needed such that elasticity did approach 1.0 rather than droop as shown at the high-ends in Figures 3.5.13, 3.5.14. The triangular shape of the elasticity curve became apparent across all data sets examined. And, as shown in Figures 3.5.13 and 3.5.14, low- and high-end segmented linear fits were

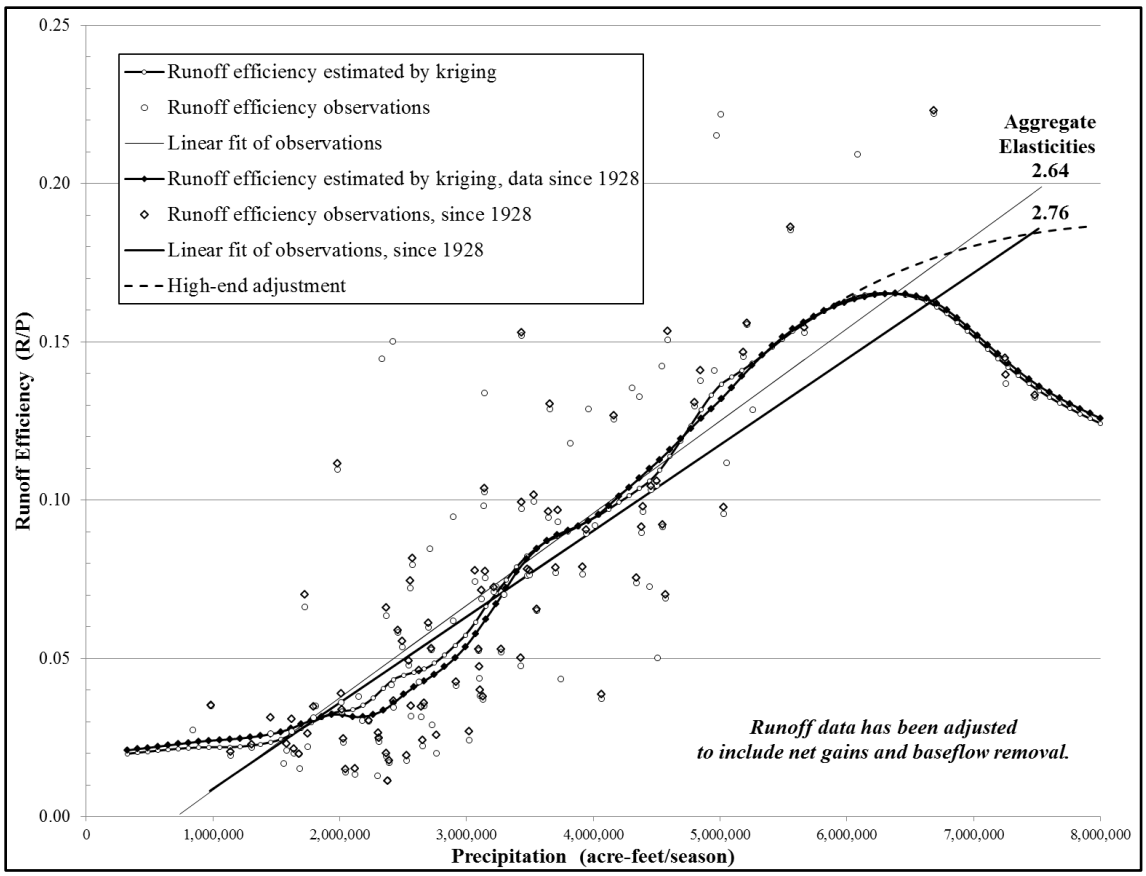

Figure 3.5.12. Verde-Winter Runoff Efficiency by Precipitation Level, Adjusted for Baseflow and Net Gains.

calculated using data from the portions where there was confidence in krige results. These fits are the algorithm solutions used for this investigation. Aggregate elasticity was re-calculated from data modified for baseflow and net gains, and those values correspond well to the peak values of the triangular winter curves as noted in Figures 3.5.13 and 3.5.14.

Summer season elasticity proved to be a more tenuous challenge. Runoff efficiency is very low on both watersheds in summer and even lower when baseflow is subtracted from the data. ET is so high in summer that little precipitation is translated to NBS (Salt ~2.5%, Verde ~1%). As can be seen in Figures 3.5.15 and 3.5.16, there is

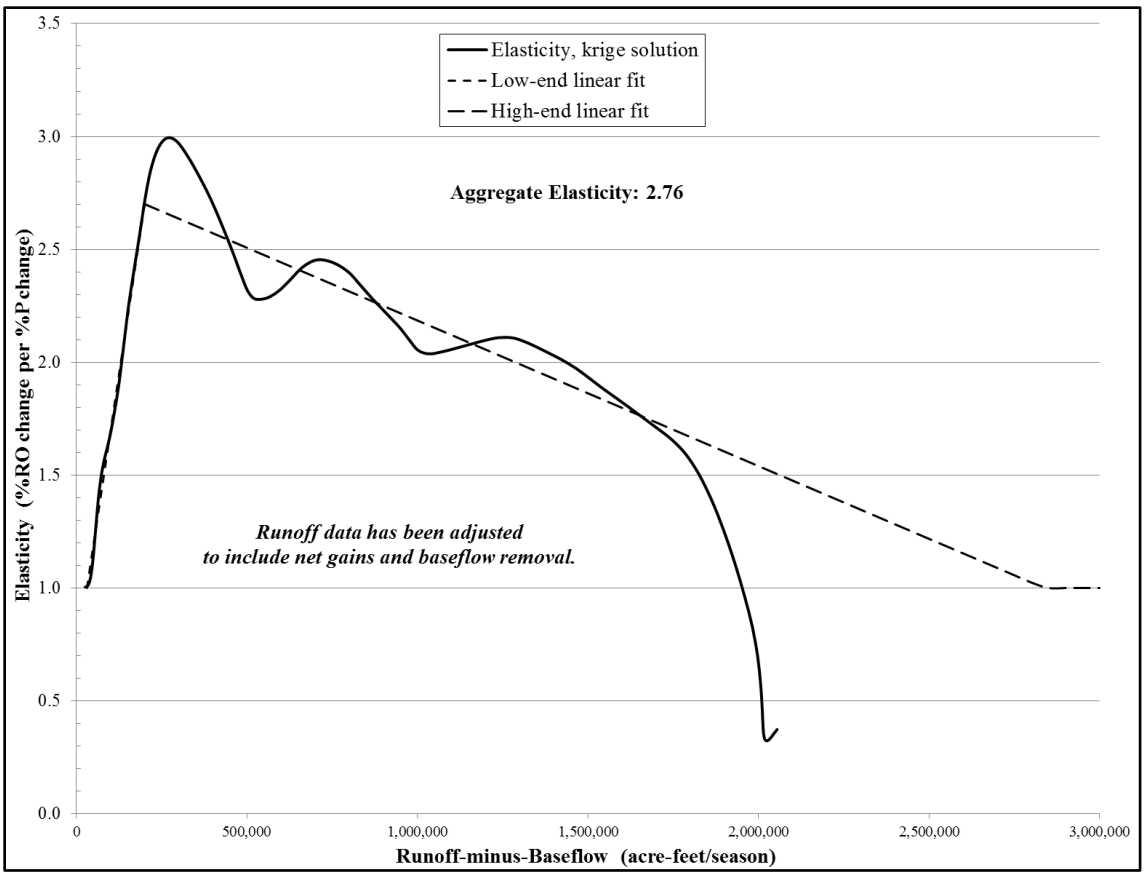

Figure 3.5.13. Salt-Winter Precipitation Elasticity of Runoff, by Runoff Level Adjusted for Baseflow.

nearly no relationship of efficiency with precipitation. In the case of the Salt, watershed aggregate elasticity can essentially not be estimated (Fig. 3.5.15). The addition of a few new data points could readily change the estimate of ~1.0. Fortunately, kriging was able to identify more of a relationship and a solution was found in Figure 3.5.17. But, the elasticity curve is lower than for other watershed-seasons. The Verde summer krige solution (Fig. 3.5.18) shows high variability due to the wide and variable scatter of efficiency with precipitation (Fig. 3.5.16), but a fitted solution was derived and an aggregate value was calculated (see Fig. 3.5.18).

The elasticity solutions thus far are a function of the level of watershed runoff less

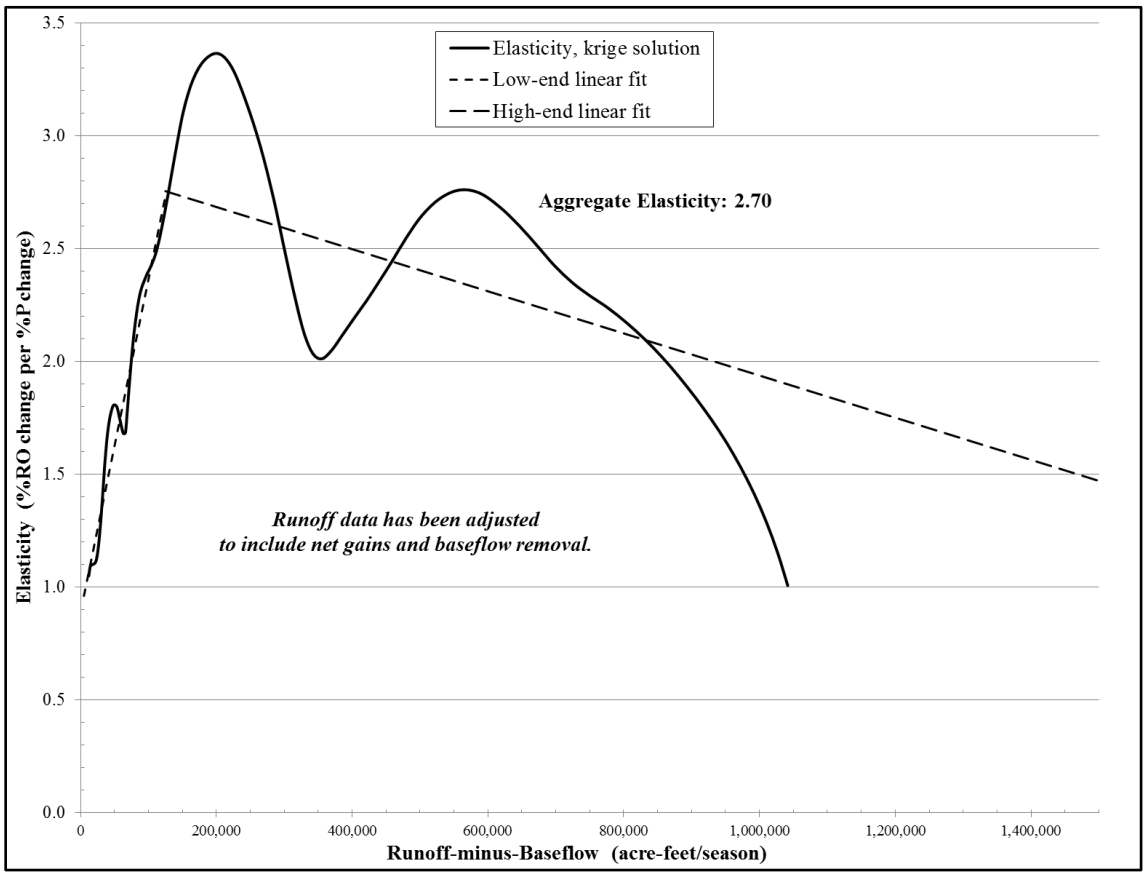

Figure 3.5.14. Verde-Winter Precipitation Elasticity of Runoff, by Runoff Level Adjusted for Baseflow.

baseflow. In addition, net basin supply change also includes any marginal contribution to miscellaneous loss from precipitation change at the reservoirs. This was examined to find no incremental ML at precipitation below the average level, but small net gain contributions were evident above the mean precipitation level. To develop the relationship of ML change to marginal precipitation change, a couple simple relationships can be examined.

First, a simple regression is performed with data above the mean value, and its solution can be differentiated to get – $\Delta ML/\Delta P = c$ or $\Delta P = \Delta ML/c$ (3.16)

When NBS is plotted as a function of precipitation at the reservoirs a linear relationship is found that can be expressed as –

$$NBS = m\,P + b \quad \text{or} \quad P = (NBS - b)/m \tag{3.17}$$

And, we can define marginal precipitation change as $\Delta P/P = \delta$, a fractional value. Combining these,

$$\delta = \Delta P/P = (\Delta ML/c) / ((NBS - b)/m) \tag{3.18}$$

And, upon rearranging obtain –

$$\Delta ML = \delta\, c\, (NBS - b) / m \quad * \tag{3.19}$$

(*only applicable above mean precipitation or corresponding NBS)

The constants c, b, and m are empirically derived from the data set for a watershed-season. The incremental ΔML per precipitation change, δ, is then added to baseflow (assumed fixed) and change of runoff ($\delta x \mathcal{E}_p x R$) to arrive at a new NBS value in total response to the precipitation change. Although the ΔML net gain mechanism applies mostly in winter, small contributions were also identified for the summer season. All of the precipitation elasticity algorithms derived from this analysis are tabulated in Appendix D.

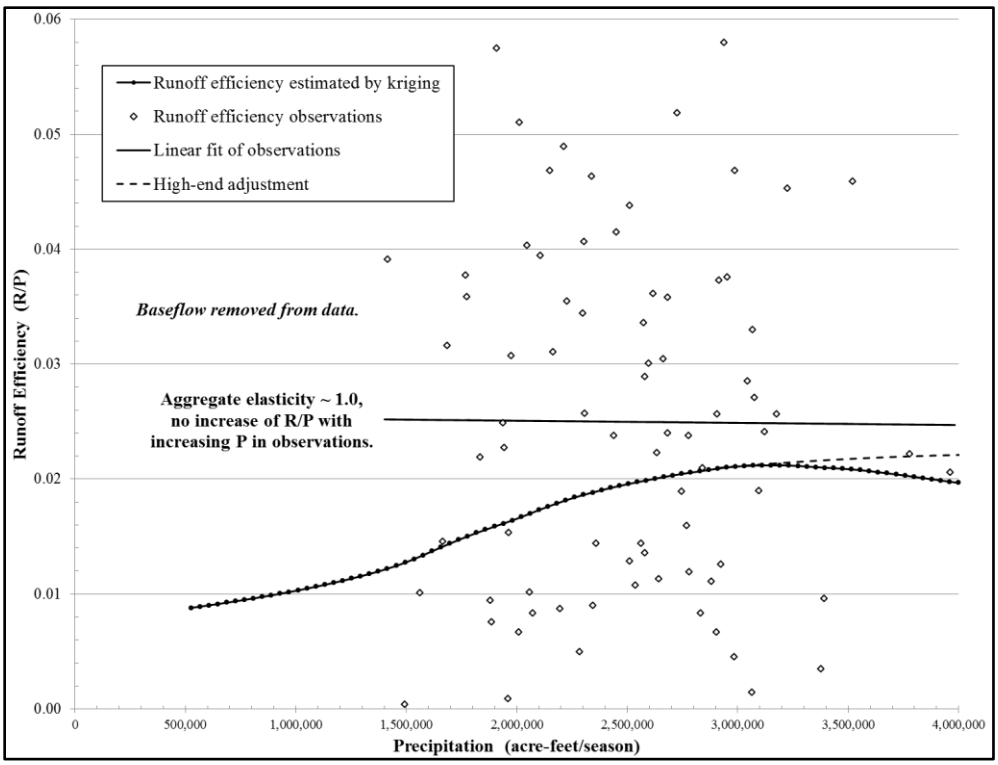

Figure 3.5.15. Salt-Summer Runoff Efficiency by Precipitation Level, Adjusted for Baseflow.

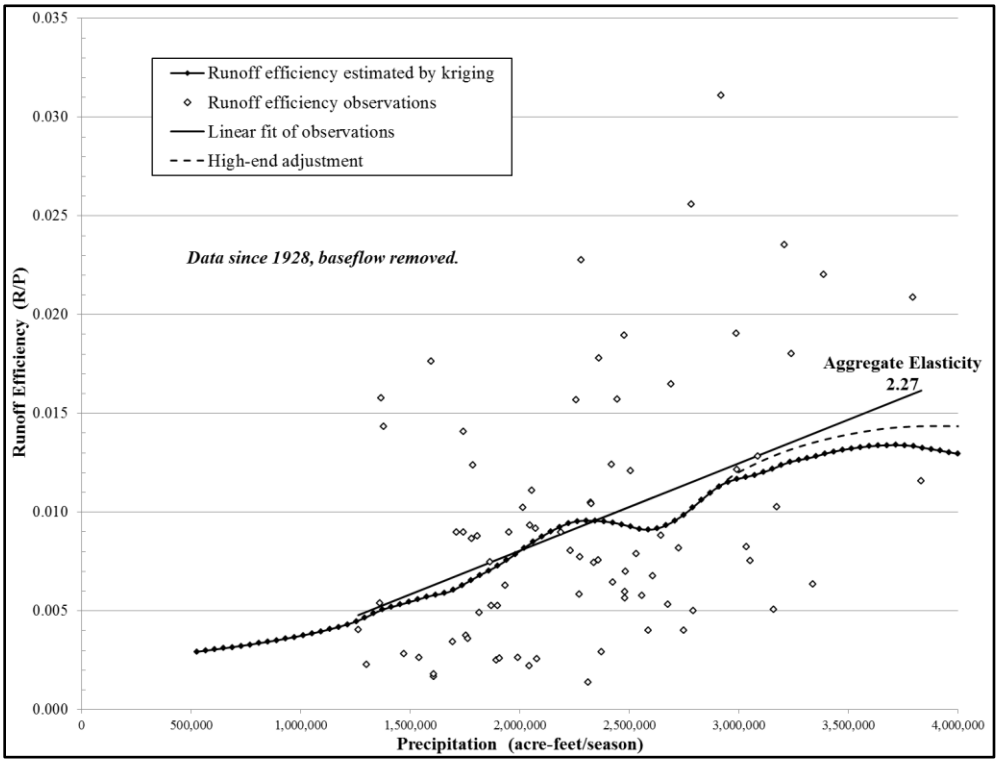

Figure 3.5.16. Verde-Summer Runoff Efficiency by Precipitation Level, Adjusted for Baseflow.

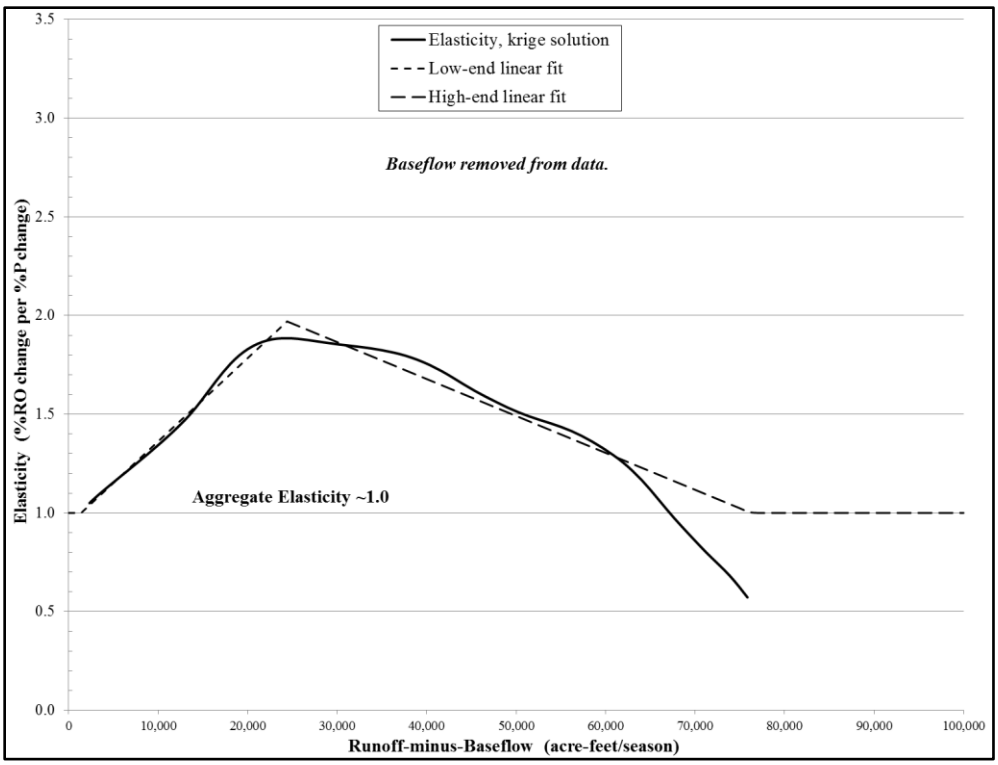

Figure 3.5.17. Salt-Summer Precipitation Elasticity of Runoff, by Runoff Level Adjusted for Baseflow.

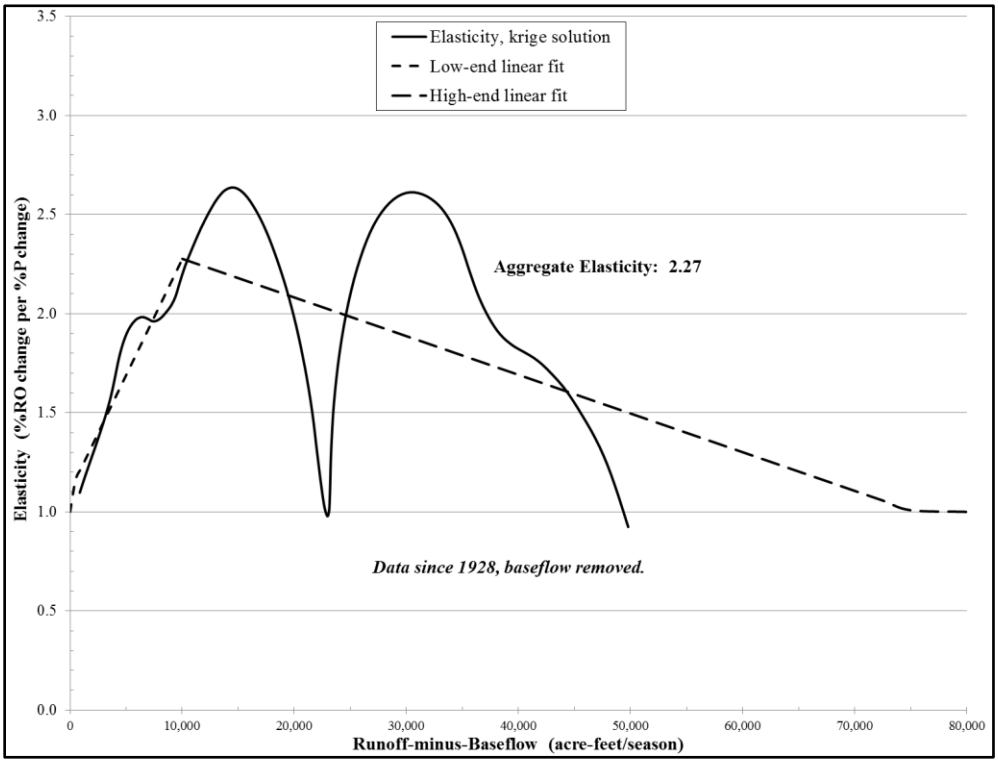

Figure 3.5.18. Verde-Summer Precipitation Elasticity of Runoff, by Runoff Level Adjusted for Baseflow.

3.6 Multi-Decadal Climate Change Forecasts

"…; a simple model with well-understood flaws may be preferable to a sophisticated model whose correspondence to reality is uncertain." - Lins & Cohn, 2011

Water operations management is concerned with two long-range planning time horizons: 30 years ahead for operational issues, and 100 years for infrastructure investments. If a case could be made that the climate and stream flow distributions in the Salt and Verde watersheds will remain unchanged over those timeframes, then the baseline statistical characterization would provide a sufficient vulnerability assessment. However, this is not expected. Considerable uncertainties persist about exactly how climate changes might evolve over the coming decades and modify expectations of net basin water supply. The climate modeling community has been resistive to describing their model results as a forecast, asserting that their findings are only a set of possible 'projections' of the future (Kundzewicz 2009; Trenberth 2010). Pielke and Wilby (2012) remind us that "downscaling has practical value but with the very important caveat that it should be used for model sensitivity experiments and not as predictions." "It is inappropriate to present downscaled results to the impacts community as reflecting more than a subset of possible future climate risks." If the water management community had identified and endorsed a projection it could serve as a forecast. But, this has not been the case (WUCA 2009) and uncertainties surrounding downscaled results persist (Vano et al. 2014).

The thrust of this research has been to develop an alternative to shortcomings inherent in the standard top-down climate modeling approach for assessment of change projections and impacts. While the alternative methodology is not confined to any

specific climate change projection, the objective of this research is the analysis of a limited, manageable and relevant number of projections. To that end, this investigation assesses (1) a most-likely forecast of future climate in the watersheds based in empirical statistical forecasting methods and (2) a higher projection based upon mean temperature changes cited in IPCC AR5.

3.6.1 Literature Review and Forecast, Precipitation

As is demonstrated by the runoff characterizations conducted for this study, the majority of runoff variance is explained by precipitation. Without it, hydrologic processes have little to work with. Expectations of precipitation change therefore dominate forecasts of net basin water supply. Assessment of precipitation time series was conducted for watersheds of the CRB to confirm whether or not they have become non-stationary (Murphy and Ellis 2014). Non-stationary temperature was revealed but stationary precipitation was concluded through analysis against statistical criterion. Subsequent to that work, further study performed under hydrologist considerations of stationarity reinforces findings of highly variable but stationary precipitation in the Salt and Verde watersheds. This is consistent with a similar conclusion by Hoerling (2014) for California that "… it can be said with high confidence that there is no trend toward either wetter or drier conditions for statewide average precipitation since 1895 …". This is not to say that pluvial periods of heavy precipitation and historical drought intervals are absent from the historical record and should not be expected to occur again. They will, as are reflected in the stochastic simulations employed in this study. However, temporal determinism is fleeting amidst no long-term trend. Particular periods of excess or deficit are often attributed to sea surface temperature (SST) variations affecting ocean-

atmosphere coupling, although they provide only a partial explanation of variability and remain a difficult basis from which to make precipitation predictions (Balling and Goodrich 2007; Thomas 2007; McCabe and Wolock 2012; Nowak et al., 2012).

The primary attribution of drying in CRB watersheds as projected by climate models is an expectation of broadening Hadley cell circulation resulting in a pole-ward expansion of the subtropical dry zones and a northward forcing of the average storm track, thereby resulting in altered precipitation patterns (Seager and Vecchi 2010). GCM-based analyses for the 21st century are predicated upon the assumption of strengthening mean flow moisture divergence accompanied by reductions in transient eddy moisture convergence per the projected pole-ward shift of storm tracks under global warming. The critical reliance of surface water resources in Southwest North America (SWNA) on the transient eddies is well-known in the form of major Pacific winter storm systems tapping atmospheric river moisture that provide major contributions to surface runoff. While these transient events have been characterized meteorologically (Ralph et al. 2011), their climatic dependencies remain poorly understood beyond recognition of a relationship with SSTs and expectations of increasing moisture delivery capacity proportional to increasing temperatures (per the Clausius-Clapeyron relationship). Acknowledging the SST dependency, Seager and Vecchi (2010) state that aside of warming contributions to drying "the future hydroclimate of SWNA will also depend, to an important extent, on the pattern of SST change", which has been shown to drive natural modes of variability. They go on to state: "… the severity of drying of SWNA that will occur in the near-term future will depend on tropical Pacific climate change, but the current generation of climate models simulates the tropical Pacific very poorly. We have little confidence in

their widely varying projections of how the tropical Pacific climate system will respond to radiative forcing."

The extent of Hadley cell widening and its attribution is an ongoing subject of research, with researchers noting the lack of a unified theory of Hadley cell circulation. Recent empirical evidence does not agree well with climate model simulations (Hoerling and Quan 2012) and assessments indicate that any changes observed to date are not statistically significant, remaining within the envelope of natural variability originating in SST transients. Recent modeling research by Hoerling and Quan (2012) has identified extra-tropical SST change to be the strongest potential driver to Hadley cell circulation change. Acknowledging the low detectability of such change against the background of natural variability and considering the oceanic heat sink's long response time, Hoerling indicates that detectability of a persistent Hadley cell circulation change is low and probably lies beyond the end of this century.

The total precipitation upon and runoff out of the watersheds of the CRB occurs primarily during the winter season when evapotranspiration is at a minimum due to dormant vegetation and low temperatures. In efforts to better represent the topographic complexity and small-scale interactions in the CRB, the use of higher-resolution regional climate models (RCMs) bounded by constraints originating in large-scale GCMs has revealed some instructive findings. Spatial and seasonal differences were seen resulting in lower temperatures, colder headwaters, higher precipitation with more of it as snow, larger snowpacks, higher soil saturation conditions, and less precipitation sensitivity to climate change effects (Gao et al. 2011; Dominguez et al. 2012; Vano et al. 2014). Relative to their host GCMs, RCMs resulted in smaller, single digit percentage decreases

in LCRB winter precipitation by mid-century accompanied by increases in extreme precipitation event intensity, while statistically insignificant changes were found for the interior west. Single-digit precipitation reductions are unresolvable against coefficients of variation an order of magnitude larger. Even if the commonly-estimated global change of precipitation with temperature of about 2%/^{o}K is applied, it is readily evident that, even with the temperature changes of the past century, a corresponding change of precipitation is unresolvable from natural variability.

Questions of detectability of precipitation changes at regional scales amidst interannual variability have been investigated by Mahlstein et al. (2012) using GCMs to estimate the global temperature change required for a precipitation change signal to emerge above natural variability. Their analysis focused on regional wet seasons because detectability was found to be more challenging in the dry season. They found that emergence of the precipitation change signal is not generally anticipated in the near future. At least a 1.4^{o}C warmer overall climate relative to early 20th century temperatures was found to be required for detectability in any climate region of the world, which is approximately twice the global warming experienced to date. Their results for the western United States indicate that a global temperature increase in excess of 3.5 ^{o}C is required before a precipitation change might be detected, leading the researchers to conclude no emergence of a signal in the region before the year 2100.

Specific to the Salt and Verde watersheds, Ellis et al. (2008) developed a water budget runoff model for these basins and used several GCM outputs to estimate mid-century runoff. When only GCM temperature changes for the region were applied, modeled runoff reductions fell within a sufficiently small standard deviation that

statistical significance testing could demonstrate a difference from zero. When the widely variable precipitation changes were then applied, substantial runoff uncertainties were introduced, broadening the range of outcomes, leaving the average essentially the same and placing statistical significance in question. This inability to conclude a definitive role for precipitation change many decades in the future is also reflected in other studies which employ even larger numbers of scenarios for estimating ensemble averages. If ensemble members were independently generated, each outcome would contribute to narrowing the confidence limits of a change expectation. However, Knutti et al. (2013) have traced the genealogy of CMIP5 and earlier models, revealing significant common ancestry and cross-pollination. Outcome independence is therefore hard to establish beyond the handful of independent originators which limits the extent to which statistical significance testing of ensemble averages can conclude a forthcoming change different from zero. Knutti and Tebaldi's (2013) review of CMIP5 findings concludes that there is a low confidence in any indication of modeled precipitation change for the Southwest United States. This is evident in downscaled climate model data passed through hydrologic models (Gangopadhyay et al. 2011) in support of the U.S. Bureau of Reclamation's Colorado River Basin Water Supply & Demand Study (2012). The CMIP5 projections contain new emissions scenarios and many more model simulations than previous iterations. While the CMIP5 model projections embody significantly greater complexity, they have not yet incorporated evolving understandings of important physical processes such as clouds and aerosols which play a key role in climate feedback mechanisms (Boucher et al. 2013). While it has been noted that, in general, CMIP5 results are not significantly different than CMIP3 (Knutti and Sedlacek

2013), expectations of precipitation change have shifted in some regions, including the Southwest United States and the Salt & Verde watersheds. While CMIP3 models on average indicated small reductions in precipitation, CMIP5 results now depict no change (Reclamation 2013). Such a shift is indicative of the inability to conclude any precipitation change in the future. This conclusion was echoed by Trenberth (2014) during a AGU Falling Meeting presentation. To paraphrase his comment: 'Given the wide range of precipitation representation and projections in the models, I don't see why anyone would use them to make assertions about future precipitation.'

Drawing upon the scientific forecasting knowledge base can provide instructive guidance to constructing a forecast for this investigation. Several decades of forecasting research has identified those practices which have been shown to result in better forecast outcomes. That is not to say that by their implementation the forecast will be perfect (as none are) – but it is more likely to result in lower forecast error than would have otherwise been the case. Much of the research literature was compiled by Armstrong (2001), and has been made available to practitioners through the International Institute of Forecasters (IIF) at www.forecastingprinciples.com. Two principles are particularly relevant to this study: (1) how to forecast in situations of high uncertainty, and (2) the importance of forecast validation.

In situations of high uncertainty the principles recommend forecasting conservatively. In climatology this is termed a persistence forecast while in forecast science it is called a naive forecast. The principle recommends that if there is not a clear and supportable basis on which to apply a forecast trend, then none should be used. As discussed above, there has been no long-term trend in precipitation over the Salt and

Verde watersheds and research into driving mechanisms indicate that if an influence does evolve it will not do so before the end of this century. As has been concluded by Guntzler et al. (2012), caution should be exercised in the attribution of projected SWNA drying to anything other than temperature, as precipitation considerations are too uncertain. A precipitation forecast of persistence is therefore appropriate and quite straightforward, although the timing of pluvial and drought periods should be considered. But, for the purpose of future-state probability distributions for stochastic simulation study, precipitation contributions can be held constant through the balance of this century with no NBS probability modifications forced by precipitation change.

3.6.2 Literature Review, Temperature

As reported by Murphy and Ellis (2014), temperature was found to be persistently nonstationary in both winter and summer on the Salt and Verde watersheds. Increases have been non-monotonic with statistically significant trend-cycle behavior which must be incorporated to the construction of forecasts. Cyclicality can be considered once the overall trend is accurately assessed. As was shown, average temperature in the Salt and Verde watersheds increased approximately 1^{o}C between 1979 and 2000 (Fig. 3.3.1). Since then average temperatures have remained essentially level without further increase. The rate of increase during the 1980s-90s was temporarily at its highest, at 0.5^{o}C/decade, while it was 0.155^{o}C/decade over the full instrumented history. Assuming the high rate of increase immediately commences again, a projection ahead to the year 2050 calculates to a total temperature rise of 2.8°C since 1979. This aggressive assumption is at the lower bound of GCM-based projections. A linear extrapolation using all long-term data places average 2050 temperature just 1.4°C higher than 1979 values, well below the

GCM-based range. When Ellis et al. (2008) applied downscaled GCM model-scenario combinations to their Salt-Verde water budget runoff model the mean temperature rise for the study area was projected to range from 2.4° to 5.6°C with an average of 3.7°C for the year 2050. These ranges lie well above indications from the empirical evidence and thereby infuse uncertainty to identification of future temperature changes for use in this investigation.

This divergence of climate model projections from outcome has been demonstrated in other studies, often assessed at the global level. Fyfe et al. (2013; 2014) reported that "recent observed global warming is significantly less than that simulated by climate models". They studied trends in global mean surface temperature from 117 climate simulations by 37 CMIP5 models to find that the average modeled rate of temperature increase is twice the observed global warming rate over 1993-2012. The observed warming rate was even lower from 1998-2012 at one-quarter the average modeled trend and not significantly different from zero, suggesting a temporary 'hiatus' in global warming. Statistical significance testing rejected the null hypothesis that observed and modeled trends are equal over the past 20 years, with the divergence beginning in the early 1990s. They speculate that the difference might be explained by some combination of unaccounted external forcings such as stratospheric aerosols or water vapor, inaccurate model response of which transient climate sensitivity is one possibility, or an unusual period of internal climate variability. From a forecasting perspective, it appears unlikely that an offsetting period of climate variability might arise by 2050 to align outcomes with modeled temperature change. For global warming to reach levels suggested by the IPCC (2013), it would need to resume at rates in excess of

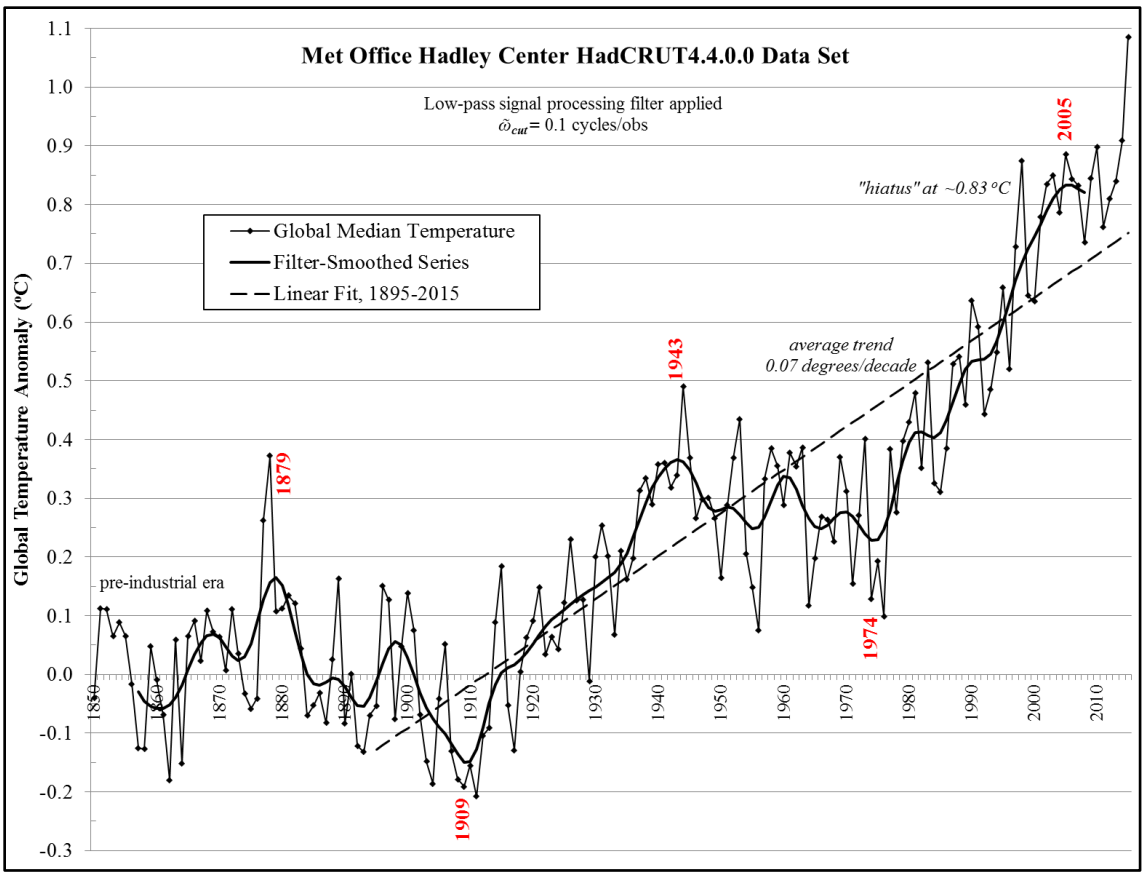

Figure 3.6.1. History of Global Annual Surface Air Temperature Anomalies.

0.25°C/decade on a sustained basis for the next 35 years and beyond. There is no historical precedent for that rate over long durations. Global surface temperature anomalies reported by the U.K. Met Office Hadley Centre (Morice et al. 2012) are shown in Figure 3.6.1, where anomalies are calculated relative to a stable cumulative average level in the pre-industrial era (0.339°C offset vs 1961-1990). As seen in Figure 3.6.2, a sustained warming rate of about 0.26°C/decade is required to attain the future IPCC RCP4.5 or RCP6.0 temperature projections, while RCP8.5 requires 0.45°C/decade. An analysis of the data set for all warming rates by duration since 1895 using linear regressions is shown in Figure 3.6.3. The rate-durations required to attain the mean temperature increases projected by AR5 are well outside the historical envelope.

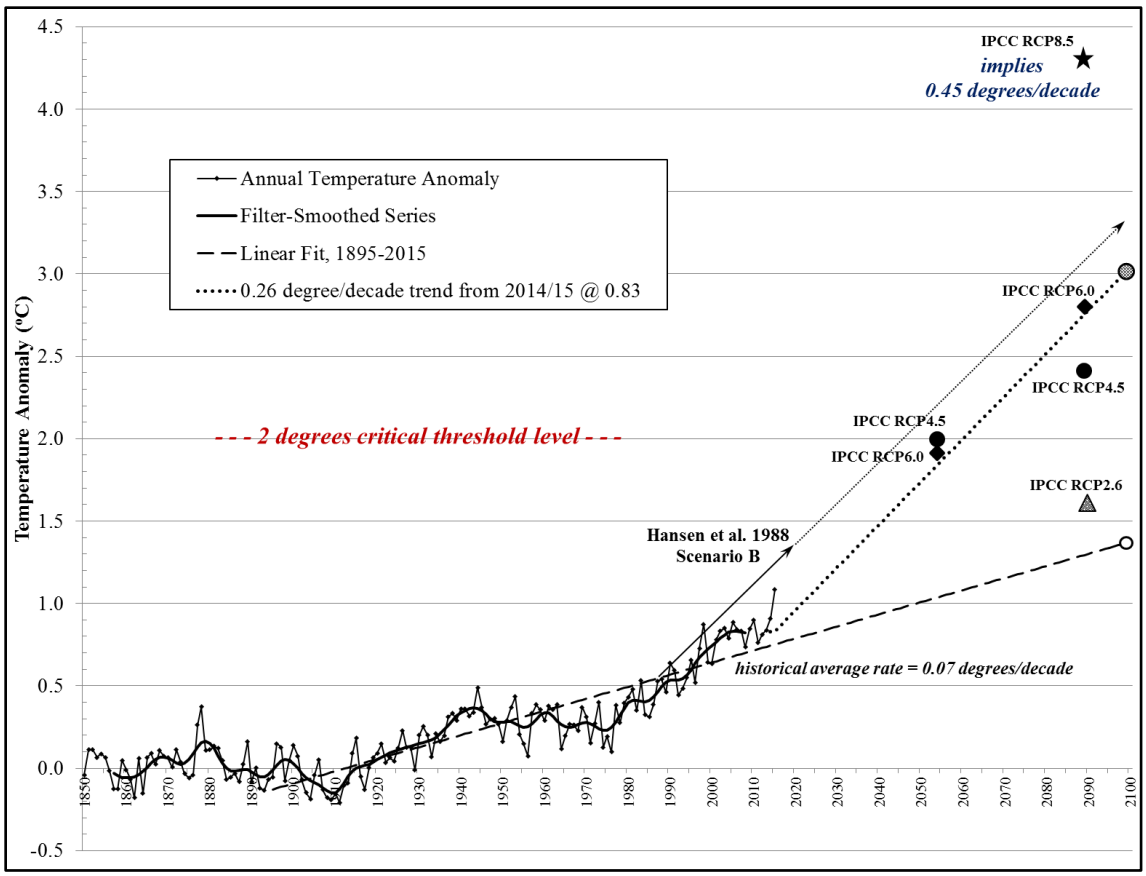

Figure 3.6.2. Global Temperature Anomaly Projections.

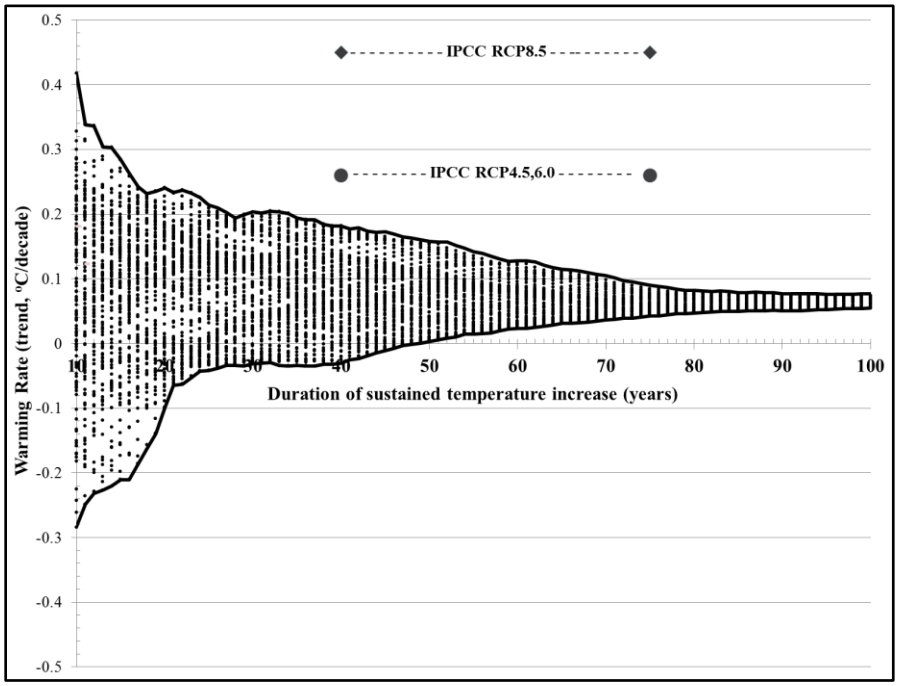

Figure 3.6.3. All Historical Global Warming Rates by Duration, 1895-2015.
The rates required to attain IPCC AR5 projected average warming levels are indicated.

Privalsky and Yushkov (2015) studied the statistical properties of 47 CMIP5 model simulations of average annual surface temperature for the continental United States, 1889-2005, and compared them to the HadCRUT4 observational record. If a simulated time series has the same basic statistical properties as the observed time series, one may regard the climate model as reliable at the spatial scale examined. And, conversely, a model generating data whose major statistical properties differ significantly from the observed record may be considered inadequate. They found that most CMIP5 models adequately reproduce the time and frequency domain behavior of the observed time series, which is close to a white noise sequence (frequencies > 0.05/yr). However, the more fundamental statistical characteristics, and those most relevant to the investigative objectives of this dissertation, were found to be unsatisfactory. Mean temperature values for the model-simulated data varied up to 6.8^{o}C and were all statistically different from the observed historical mean annual temperature. Temperature trend rates of the models ranged from zero to 0.15^{o}C/decade and were generally biased high, exceeding the observed rate by as much as 220%. 25 of the 47 model trend rates fell beyond a 95% confidence interval for the estimate of observed warming. So, if all models cannot correctly assess the level of the historical time series, and the majority of them cannot reproduce the historical warming rate, the basic parameters upon which to base a forecast into the future are absent. The situation cannot be expected to be better for CMIP5 simulations of the smaller-scale Salt and Verde watersheds considering the statistical benefit bestowed by spatial aggregation to the continental scale. There might be some subset of CMIP5 simulations whose statistics fortuitously average to a closer representation of watershed history, but there is little basis upon which to scientifically

identify that group, thereafter leaving the investigator with no assurance that the subset does not suffer the same deficiencies identified by Privalsky and Yushkov.

3.6.3 Most Likely Temperature Forecast

Considering the uncertainties identified above, this investigation chose to take on the development of an evidence-based multi-decadal temperature forecast model that incorporates current research findings for the key components of the temperature record which are: (a) climate sensitivity to anthropogenic forcing and (b) the primary modes of natural internal variability. As articulated by Koutsoyiannis (2011), for hydrologic modeling to incorporate nonstationarity information, change(s) must be described by a deterministic function(s), which reduces uncertainty by explaining part of observed variability. He states that:

> "a claim of nonstationarity is justified and, indeed, reduces uncertainty, if the deterministic function of time is constructed by deduction, and not by induction (direct use of data). Thus to claim nonstationarity, we must: (1) establish a causative relationship, (2) construct a quantitative model describing the change as a deterministic function of time, and (3) ensure applicability of the deterministic model into the future."

He then concludes, based on previous analyses (Kousoyiannis et al 2008; Anagnostopoulos et al 2010), that climate models have been unable to reproduce known statistical characteristics of past climate important to hydrology and are unable to provide validated predictions for the future. In contrast, the deterministic forecast model described below does meet their criteria. The model development is first applied to the

HadCRUT4 global temperature record for proof-of-concept and then employed for the Salt and Verde watersheds and reservoirs.

As can be seen in Figure 3.6.1, the data indicate modulation of an anthropogenic trend by internal variability that can be modeled and is likely to continue into the future. An explanatory model incorporates time series methods as outlined by forecasters (e.g., Makridakis et al. 1998). A data time series pattern is composed of (i) the level of the series, (ii) a long-term trend, (iii) cyclicality, (iv) seasonality, and (v) irregular components (error). These components align with the additive temperature anomaly model proposed by Lovejoy (2014)

$$T(t) = T_{anth}(t) + T_{nat}(t) + \varepsilon(t) \tag{3.20}$$

where
$T(t)$ is the measured temperature anomaly at time, t,
$T_{anth}(t)$ is the anthropogenic contribution forcing an up-trend,
$T_{nat}(t)$ is natural variability composed of spectrally identifiable cycles,
and $\varepsilon(t)$ is the error term.

The anthropogenic term is considered deterministic and monotonically increasing as greenhouse gas (GHG) concentrations rise. It is the forcing element to the trend and elevated level of the time series. The natural variability term is often assumed to be stochastic; however, research into its role in the warming hiatus reveals at least one and possibly two predictable low frequency components. Those with demonstrated timing and amplitude can be incorporated into a forecast model while other modes of variability are relegated to the error term.

Temperature variability scales widely with time, and the objective is to assess it climatologically, therefore seeking to suppress sub-decadal weather and macro-weather

components (Lovejoy 2013). The band-pass filter described in Section 3.1 is applied for this purpose to filter-smooth the data series (Fig. 3.6.1).

3.6.3.1 Natural Variability

Multi-decadal temperature variations have been thoroughly analyzed over the past few decades. Using spectral analysis methods, Schlesinger and Ramankutty (1994) identified non-random 65-70 year oscillations in multiple data records. Their analysis found it strongest in the North Atlantic and suggested it arises from predictable internal variability of the ocean-atmosphere system. Delworth and Mann (2000) compared the instrumental record with proxy-based reconstructions and coupled ocean-atmosphere models to show a distinct oscillatory mode centered in the North Atlantic Ocean operating on a ~70 year timescale over the past 330 years. They identified thermohaline circulation variability as the driving mechanism and noted the links between the North Atlantic and Pacific Oceans through atmospheric bridging via teleconnection patterns. Kerr (2000) published a review of the evidence for a 60-year temperature oscillation in the climate system, stating that "some researchers suspect that oscillations in the heat-carrying currents of the North Atlantic are to blame for this natural mode". He noted "the challenge of disentangling greenhouse warming from natural warming". Schlesinger and Ramankutty (2000) responded to Kerr's article, referring to their previous and ongoing research by stating

> "We found that while the anthropogenic effect has steadily increased in size during the entire 20th century, such that it presently is the dominant external forcing factor of the climate system, there is a residual factor at work within the

climate system. This residual factor is quite likely the 65- to 70-year oscillation of the North Atlantic Ocean. “

Gray et al. (2004) developed a tree-ring reconstruction of the Atlantic Multidecadal Oscillation (AMO) index which demonstrated that strong, low-frequency variability similar to the recent instrumental record has been a consistent climate feature for the past five centuries. Knudsen et al. (2011) examined a set of high-resolution climate proxy records from the region bounding the North Atlantic Ocean to show that a quasi-persistent 55- to 70-year oscillation characterizes North Atlantic ocean-atmosphere variability over the past 8000 years, corresponding to the AMO in instrumental records. Knight et al. (2005) came to the conclusions that the AMO pattern lends predictability to temperatures several decades into the future and has been large enough to modify anthropogenic warming rate estimates.

Zhen-Shan and Xian (2007) decomposed temperature data at the global, Northern Hemisphere, and China levels and identified four oscillation modes on an underlying trend. Two operate on sub-decadal time scales while the others have ~20-year and ~60-year periodicity. The trend plus 60-year mode dominate the lower strength 20-year mode. Having also observed non-uniform warming in the global temperature record, Tung & Zhou conducted an attribution study using empirical mode decomposition and multiple regression analysis – coming to the observation of a recurrent multi-decadal oscillation likely related to the AMO (Zhou and Tung 2013; Tung and Zhou 2013). They conclude that this low-frequency component of internal variability accounts for 40% of the recent warming trend, it is superimposed on an underlying GHG warming rate since

1910, and that previously-deduced GHG warming rates should be substantially revised downwards. Their finding is similar to what was reported by Wu et al. (2011), who conducted an enhanced empirical mode decomposition study to also conclude that the late-20th century high warming rate was a consequence of an upward swing of multi-decadal variability in combination with a GHG warming trend. They estimate that as much as one-third of the warming reported by the IPCC may have been due to multi-decadal variability.

Yao et al (2016) similarly applied empirical mode decomposition methods to three global temperature anomaly data sets and identified a quasi-60 year oscillatory mode on a monotonically increasing trend, along with a weaker mode with 24 year mean periodicity and four weak high frequency modes. They found multi-decadal fluctuations of the AMO to be largely in phase with the 60-year variability while the Pacific Decadal Oscillation (PDO) index was found to lead the cycle by about 16 years. Considering the findings, they conclude that the hiatus is likely to extend for several more years. Li et al (2013) came to a similar conclusion for northern hemisphere temperatures, indicating the hiatus will extend to 2027 before North Atlantic cooling weakens relative to anthropogenic-induced warming. The combination of a secular warming trend and internal oscillatory variability has now been thoroughly characterized by a number of researchers to conclude that natural variability contributions have been underestimated, resulting in over-estimation of the anthropogenic contribution to the warming trend in the late 20th century, although debate persists about the driving mechanisms (e.g., Zhang et al. 2013).

From their decomposition analysis Zhen-Shan and Xian (2007) projected a continued 20 year cooling period using a combined temperature mode extrapolation. Keenlyside et al. (2008) anticipated a pause in global temperature rise as North Atlantic and tropical Pacific cooling dynamics offset anthropogenic warming. This has come to pass with numerous investigations into the ongoing hiatus, widely attributed to cooling of the eastern tropical Pacific with ongoing investigations of the role of the trade winds, increasing subsurface heat uptake, the role of deep-water and upper-ocean thermal exchanges, and cyclical phase reversals (Balmaseda et al. 2013; Meehl et al. 2013; Kosaka and Xie 2013; Xie and Kosaka 2013; Held 2013; Hu et al. 2013; Trenberth and Fasullo 2013; England et al. 2014; Kosaka 2014; Trenberth et al. 2014; Watanabe et al. 2014; Dai et al. 2015; Trenberth 2015; Fyfe et al. 2016; Meehl et al. 2016). However, Chen and Tung (2014) do not support the Pacific-centric view, recalling the primary location of multi-decadal variability in the North Atlantic and secondarily the Pacific with atmospheric bridging between. Barcikowska et al. (2015) find that Pacific cooling is a leading phase of an overall 66-year global pattern which precedes the major cooling mode by about 16 years, similar to the Yao et al. (2016) finding. The lagged synchronicity of climate indices was explored in instrumental and 300 years of proxy data by Wyatt et al. (2012) to show an AMO signal propagation through the northern hemisphere via a sequence of atmospheric and lagged oceanic teleconnections which they term the “stadium wave”. Wyatt and Curry (2014) identified the Eurasian Arctic shelf-sea region as a strong contender for generating and sustaining propagation of a northern hemisphere climate signal with further stabilization of the oscillatory system by co-varying Pacific Ocean atmospheric circulations. Analyses by Mazzarella and Scafetta

(2012) confirm natural temperature variability from a dominant ~60-year climate cycle since 1650, and they suggest a linkage to solar-astronomical origins. Even weak astronomical influences are sufficient to drive a resonant frequency in the earth system, which Kurtz (2014) has calculated by modeling the Atlantic meridional overturning circulation (AMOC) as a thermosyphon loop cooler. He developed the governing equations for North Atlantic heat flow and, by analogy with an electrical LRC circuit, calculated the natural frequency at which the system oscillates in response to a disturbance (perhaps astronomical). The AMOC flow oscillation period was calculated to be approximately 65 years, in close agreement with the observed AMO frequency. Based upon the first principles employed in his derivation, Kurtz emphasizes that the oscillation is a permanent feature of the Earth's climate system due to the specific configuration of the Atlantic basin, and not simply stochastic variability.

In summary, the cumulative literature has clarified that the cyclical variability is deterministic, and there are indications of causative relationships. These are two prerequisites stipulated by Koutsoyiannis (2011) for modeling of nonstationary phenomena. It remains then to construct a quantitative model as a function of time (and ensure its applicability into the future, done below in Sec. 3.6.3.5, Model Structure and Validation).

The low frequency temperature variability is often evident in a filter-smoothed anomaly curve (Fig. 3.6.1) where local minima and maxima occur around 1879, 1909, 1943, 1974, and 2005. An oscillatory cycle approximation can be made with the simple sinusoidal expression –

$$T_{nat}(t) = (A/\sqrt{2}) \cos[2\pi(t-t_o)/P] \quad (3.21)$$

where
A is the peak amplitude of local minima and maxima,
P is the cycle period,
and t_o sets the temporal phase of the function at one of the local maxima.

A can be calculated from the average of identified minima and maxima. Cycle strength is $A/\sqrt{2}$, the average power (RMS value) of the sinusoidal function. A is set negative or positive per sign of the last minima or maxima. Periodicity, P, is twice the average of intervals between all minima and maxima (typically 63±3 years). t_o is a chosen minima/maxima year setting the phase relationship of the forecast to the historical series. Preliminary estimates of A, P, and t_o (for de-cycling the anomaly series) are calculated relative to linear regressions of the historical series. Final values (Fig. 3.6.4) are calculated from the filter-smoothed de-trended series once the anthropogenic trend is identified.

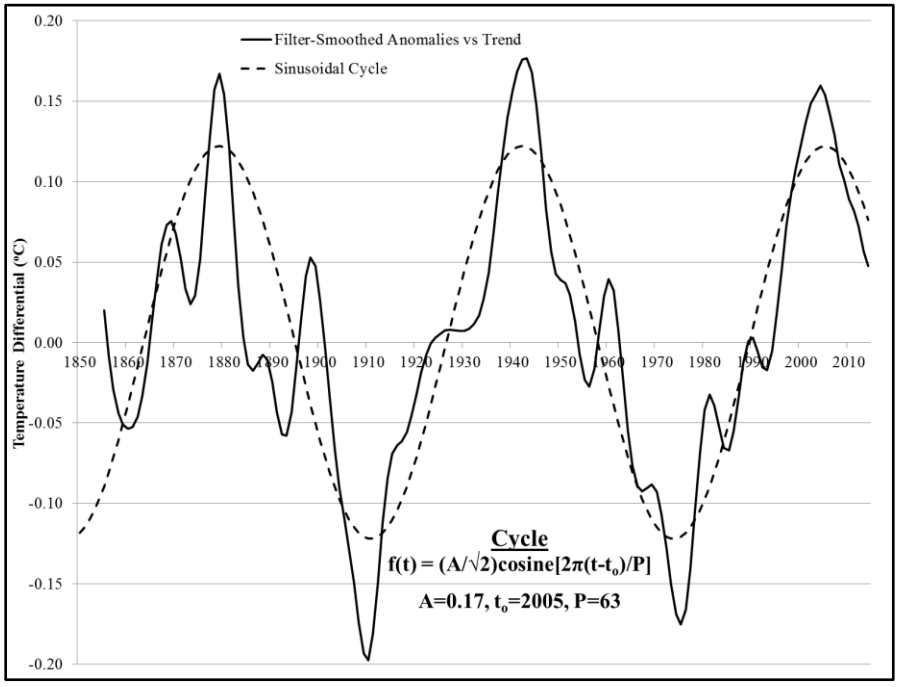

Figure 3.6.4. Sinusoidal Cycle Fit to Primary Mode of Natural Variability.

3.6.3.2 Anthropogenic Trend

Radiative forcing by atmospheric carbon dioxide has been recognized since the time of Arrhenius (1896) to be proportional to the logarithm of the gas concentration relative to an unperturbed state (Hartmann 1994, 337-340), which is typically taken to be the pre-industrial concentration level of 278±5ppm (IPCC 2013). Climate sensitivity to CO_2 doubling from this level is a key question around which future warming trends have been vigorously debated. Transient climate response (TCR) is a practical sensitivity measure that can be observationally assessed after several decades of CO_2 forcing.

Chylek et al. (2007) studied empirical climate sensitivity through observed rates of change in aerosol optical depth, global surface temperature, and GHG concentrations. They found climate sensitivity is reduced by half when observed decreases of aerosol optical depth are included in radiative forcing calculations. Their estimates of TCR fall in the range of 1.1 to 1.8^{o} C per doubling of atmospheric CO_2 concentration. TCR analyses by other researchers have been conducted through global energy budget approaches using forcing estimates for all components. Otto et al. (2013) reported a best-estimate of 1.3^{o}C (5-95% c.l. range: 0.9-2.0^{o}C); the mean estimate by Skeie et al. (2014) is 1.4^{o} C (range: 0.8-2.2^{o}C); and Lewis and Curry's (2015) median estimate is 1.33^{o} C (range: 0.9-2.5^{o}C). These researchers note that observation-based estimates are moving lower as sequential data are acquired and CO_2 forcing becomes larger relative to uncertainties. IPCC GCM-based estimates are generally higher than observational findings, and research continues into forcing uncertainties (e.g., Shindell 2014). The IPCC 5th Assessment Report stated the range of possible values is from 1.0^{o} to 3.0^{o}, but declined to provide a definitive value "because of a lack of agreement on the best

estimate across lines of evidence" (IPCC 2013). The mean TCR embodied in CMIP models is 1.8^{o}C per CO_2 doubling.

The divergence between observational estimates of long-term equilibrium climate sensitivity (ECS) from CMIP models is even more pronounced. Otto et al. report a most likely estimate of 2.0^{o}C (range: 1.2-3.9^{o}C); Skie et al. report 1.8^{o}C (range: 0.9-3.2^{o}C); and Lewis and Curry's median ECS estimate is 1.64^{o}C (range: 1.05-4.05^{o}C). IPCC AR5 states that the likely range is 1.5-4.5^{o}C, while CMIP models typically reflect the common ECS assumption (Hansen 2013) of 3^{o}C per doubling (range: 2.2-4.7^{o}C). The difference between models and observational estimates creates projections with very different temperature change expectations later in this century. The narrowing of ECS versus TCR values also indicates a faster climate response time than assumed in models, which is consistent with the observation of fast transient response (a few years) to volcanic and ENSO events.

If climate sensitivity has been over stated then it is more likely closer to a direct CO_2 warming contribution without feedback effects (~1.0^{o}C/2xCO_2). Climate models do not explicitly implement climate sensitivity, but rather do so through parameterization of mechanisms which act to amplify the warming. A central one is enhanced counter-radiation from the increased water vapor holding capacity of the atmosphere with rising temperature per the Clausius-Clapeyron relationship. This is implemented in climate modeling through an assumption of constant relative humidity through upper layers of the atmosphere which amplifies upper layer counter-radiative warming. Douglass et al. (2008) examined temperature trends for the satellite era to find that since 1979 there is no significant long-term amplification factor in the troposphere relative to the surface.

Paltridge et al (2009) examined tropospheric humidity using NCEP reanalysis data to find negative trends in specific humidity in the upper troposphere for the period 1993-2007. Specific humidity trends were positive below 850mb as might be expected in a mixed layer over a moist surface with rising temperatures. They note that "…increases in total column water vapor in response to global warming do not necessarily indicate positive water vapor feedback, since very small decreases of water vapor in the mid-to-upper troposphere can negate the effect of large increases in the boundary layer." Their tentative conclusions suggest the possibility that water vapor feedback might reduce rather than positively amplify climate system response to increasing GHG, in opposition to common assumptions and what is parameterized in models. To examine how well water vapor at high altitudes is understood, Jiang et al. (2015) have compared satellite observations over 2004-2014 to three reanalysis data sets which provide climate modelers with estimations of upper troposphere and lower stratosphere water and its dynamics. They found the reanalyses overestimated the amount of annual global mean water in the upper troposphere by up to ~150% compared to observations. Substantial differences were also found in water vapor transport, both vertically and horizontally. The researchers conclude: "Significant H_2O biases in the upper troposphere and lower stratosphere produced by the reanalyses could complicate efforts to improve the representation of moist processes and humidity transport in climate models and thus affect the accuracy of climate projections."

Since past temperature change is the manifestation of all forcings, and temperature data are more certain than current forcing estimates, direct analysis of the temperature record is a viable approach to forecast model development. However, other

anthropogenic effects besides CO_2 are represented in the record, including other long-lived GHGs, aerosols, land cover changes, and climate feedbacks; and some of those vary regionally. As has been analyzed by Lewis and Curry (2015) and Lovejoy (2014), key anthropogenic effects are functions of economic activity correlated with CO_2 levels, so that CO_2 concentration provides a useful variable for evaluating the temperature trend. To distinguish a climate response inclusive of all anthropogenic effects from TCR with CO_2 alone, an effective climate response (ECR) to CO_2 doubling is defined and employed for $T_{anth}(t)$. Its logarithmic relationship is

$$T_{anth}(t) = \text{ECR} \times \log_2[CO_2(t)/CO_2(pre\text{-}ind)] \qquad (3.22)$$

Any two or more points in a temperature-CO_2 response curve can, in principle, identify ECR. While a regression slope after log-CO_2 transformation could readily serve this purpose, data cyclicality obscures the relationship and results in highly variable estimates (see Fig. 3.6.5). De-cycling and smoothing the time series is therefore necessary, and steps in identifying the underlying anthropogenic trend's ECR then become

a) filter-smooth the anomaly time series,
b) relative to a trend estimate (starting with a linear approximation), identify cycle parameter estimates of A, P, and $t_{o,}$
c) subtract the cycle (Fig. 3.6.4), from the anomaly series,
d) filter-smooth the decycled series,
e) apply sequential linear regressions of length P to the series and extract fitted temperature at the year corresponding to phase $3\pi/2$ (Fig. 3.6.6),
f) match the years' CO_2 with fitted temperatures,

g) identify ECR as suggested above and map the data to iso-ECR curves (Fig. 3.6.5),

h) repeat from step (b) using a trend calculated from the updated ECR solution.

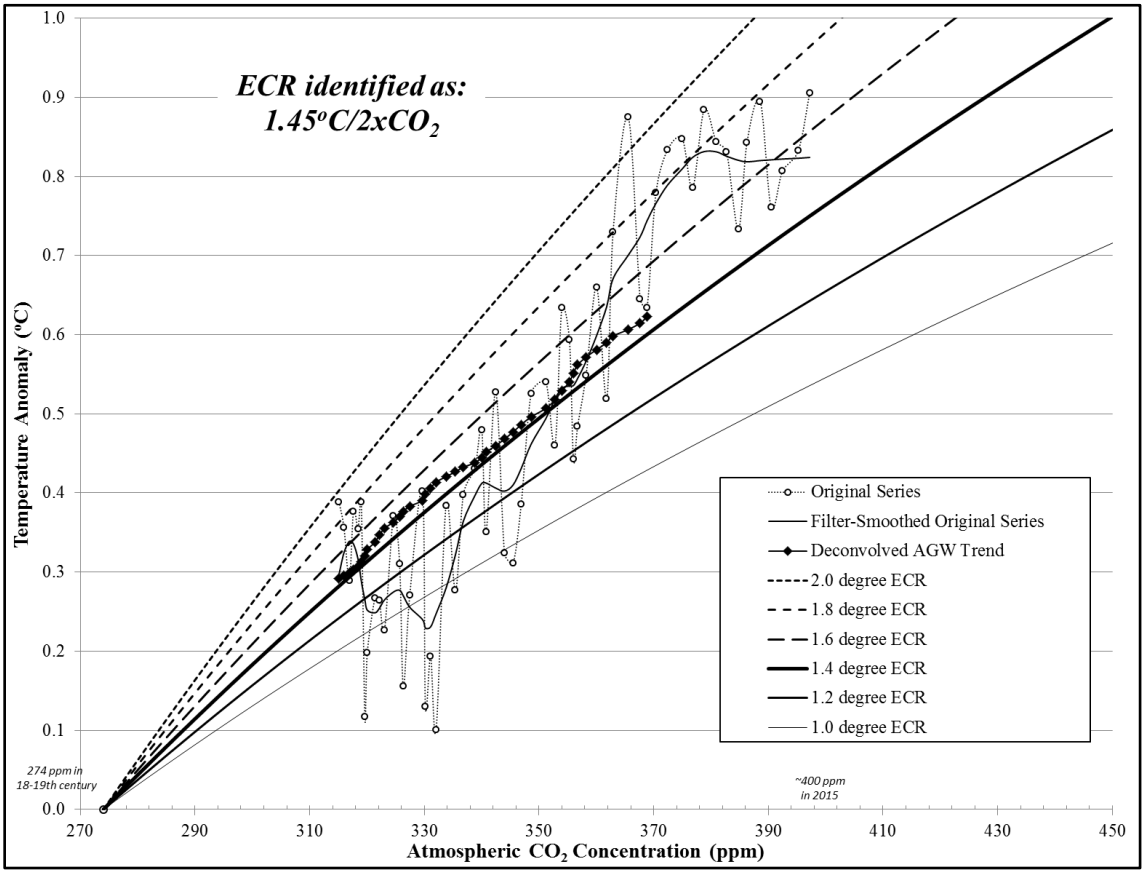

Figure 3.6.5. Identification of Global Effective Climate Response (ECR).

In step (e) the linear regressions of length *P* are intended to capture one cycle of natural variability. The underlying exponential trend is higher than a linear fit at the ends of the regression and below it at midpoint. However, they intersect at approximately the $\pi/2$ and $3\pi/2$ positions (points 16 and 48 in a 64-point regression), so that is where an anthropogenic temperature estimate can be extracted (Fig. 3.6.6) and matched to that year's CO_2 concentration. Convergence to an ECR solution is quickly found, along with

final cycle parameters once the identified ECR trend is subtracted from the temperature anomaly series and it is filter-smoothed.

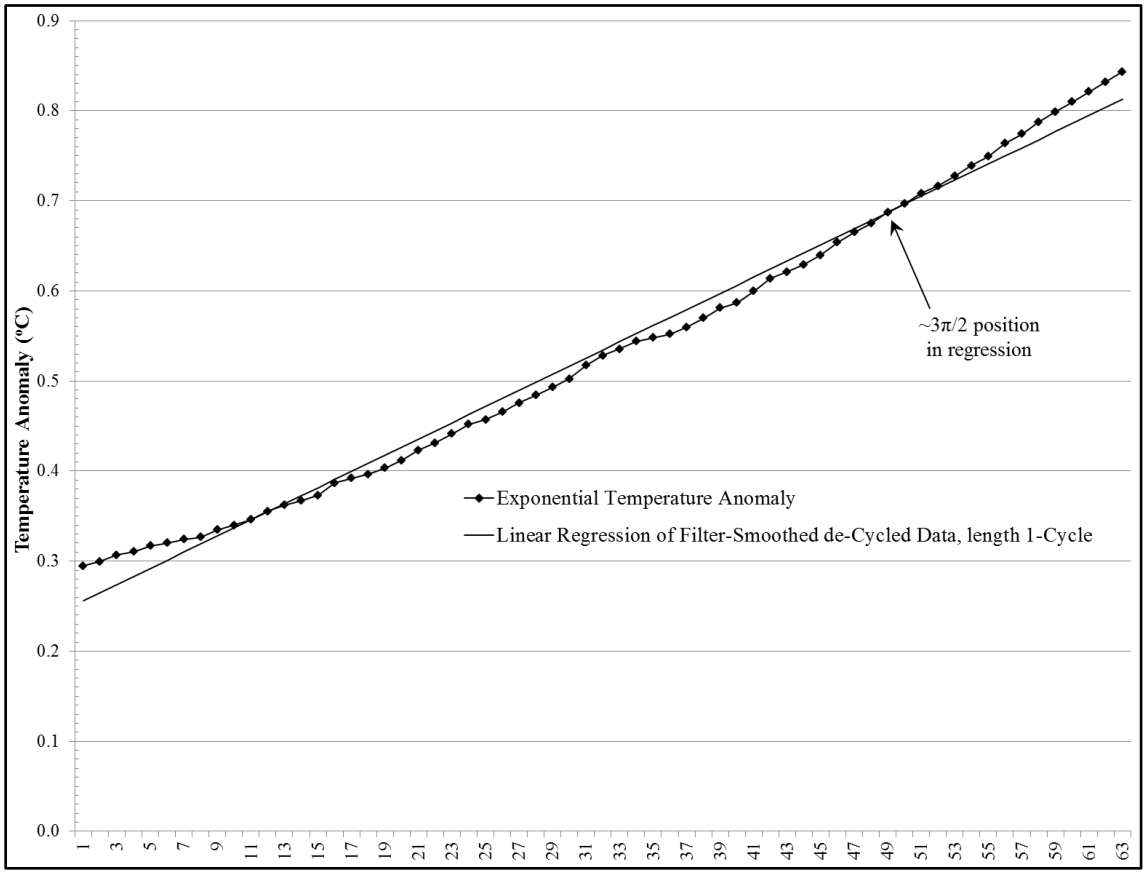

Figure 3.6.6. Identification of AGW Temperature Contribution by Sequential Regressions.

3.6.3.3 Model Results

Exploratory data analysis (Fig. 3.6.1) has revealed the 'stair-step' fashion in which temperatures have risen with low frequency natural variability and anthropogenic forcing, and their relative contributions can now be graphically displayed as shown in Figure 3.6.7. The ECRs per increasing CO_2 level are identified (Fig. 3.6.5), and a best estimate of $1.45^oC/2xCO_2$ is found. A global ECR of 1.45^oC is at the low end of climate model estimates and just a few tenths of a degree higher than what could be expected

solely from a CO_2 radiative response, indicating small net additions from other anthropogenic forcing and feedbacks in the climate system. This indicates through observational evidence that climate models are "running too hot" in the manner in which forcing and feedbacks are internalized within the models.

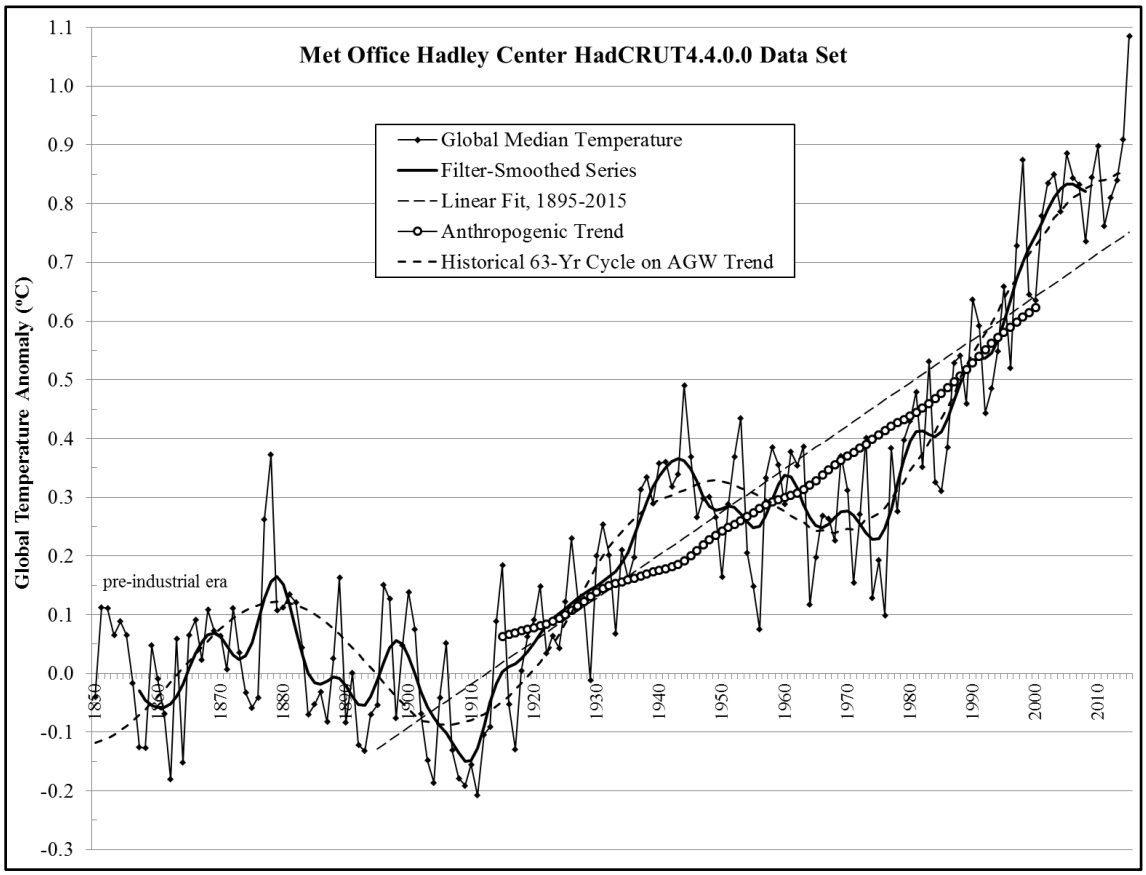

Figure 3.6.7. Global Temperature Anomaly History and 2-Component Model Fit.

As revealed in Figure 3.6.7, a 63-year cycle has been present throughout the instrumental record, superimposed upon the underlying anthropogenic global warming (AGW) trend. The cycle is shown in Figure 3.6.4 where the average cycle amplitude, $A=0.17^{o}$ over the instrumental record; at an average period, P=63 years; and t_o can be set to the last local maxima in 2005. The anthropogenic warming trend emerged early in the

20th century which combined with a rising phase of the cycle, resulting in an accentuated 1920s-30s temperature increase. The down-slope of the cycle was sufficient to offset the anthropogenic contribution into the 1970s, explaining the discussions of global cooling in that decade. The cycle slope reversed again and contributed to accelerate warming in the 1980s-90s. While the warming rate in those decades has been widely attributed solely to anthropogenic origin, this deconvolution of the data record places that in dispute and clarifies the relative contributions of AGW and natural variability (Fig. 3.6.7). The current warming hiatus has ensued due to another reversal of cycle slope shortly after 2000 while the AGW trend continues to monotonically rise, nearly offsetting each other.

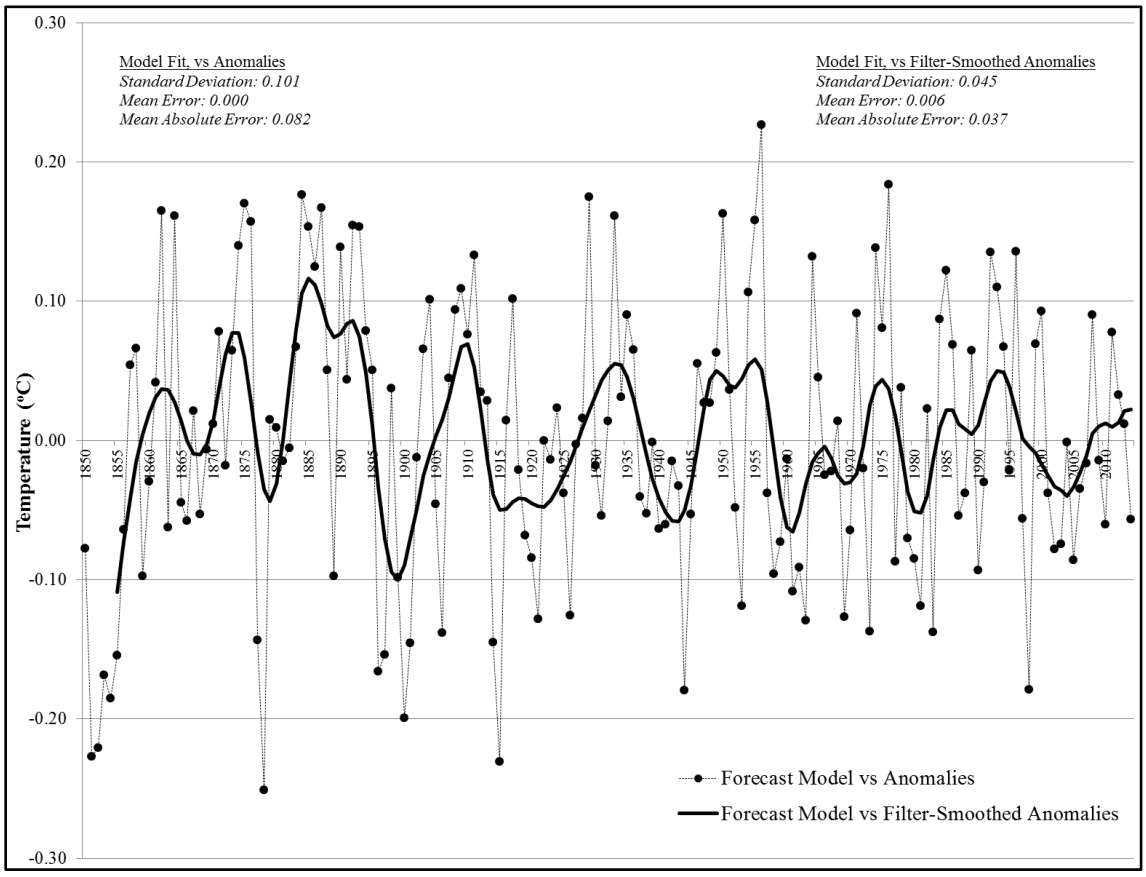

Figure 3.6.8. Residuals of 2-Component Model Fit to Historical Series.

Residual errors of the model versus HadCRUT4 history are normally distributed with a standard deviation of 0.10^{o} for the anomaly series and 0.045^{o} for the filter-smoothed series (Fig. 3.6.8). These are 21% and 48% reductions versus a trend-only model not including the cycle. Model residuals versus the filter-smoothed series (Fig. 3.6.8) reveal the second natural variability cycle indicated by spectral analyses reported in the literature. It has a periodicity of approximately 20 years and is ~30% the strength of the primary cycle. The ECR derivation was re-run using both the primary and secondary cycles, and an ECR=$1.43^{o}C/2xCO_2$ was calculated. This is not very different from the $1.45^{o}C$ solution using only the primary 63-year cycle.

3.6.3.4 CO_2 Forecast

The application of any temperature forecast method is dependent upon a forecast of future CO_2 emissions and atmospheric concentration. While CO_2 concentration appears to be rising exponentially, a close examination reveals notable consistency in its rate-of-change, increasing from zero in pre-industrial times to a 0.75ppm/year rate in the late-1950s, to a recent 2.1ppm/year (Fig. 3.6.9). This can be fit and extrapolated with a logistic function, as is often applied in technology diffusion studies (Armstrong 2001). The logistic formulation by Fisher and Pry (1971) has been applied with its parameters calculated from recent data, preferably of the last 30 years, and with exploratory sensitivity evaluation of the logistic solution. It is assumed that the logistic curve's central inflection point has not been reached as of 2015 and will not be in the near-term, which is mathematically accommodated by a high limiting rate value.

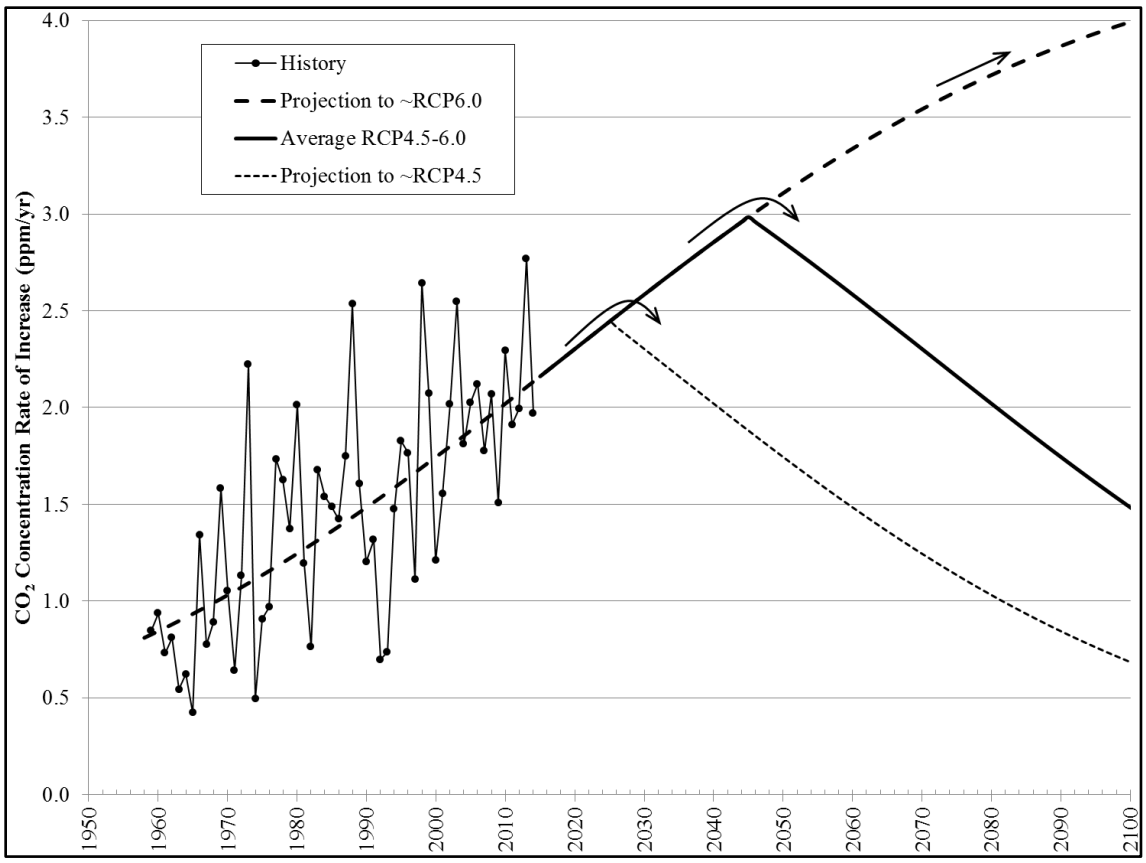

Figure 3.6.9. Annual Net Additions to Atmospheric CO_2 Concentration.

The best-fit logistic curve yields a CO_2 concentration extrapolation in the year 2100 which closely approximates the representative concentration pathway (RCP) scenario RCP6.0 concentration in the IPCC AR5 report (Fig 3.6.10). The result is very consistent to mid-century regardless of logistic equation parameterization. Potential demographic, economic, and technological changes could readily modify the CO_2 rate of increase in upper portions of the logistic curve, eventually slowing or reversing it in coming decades. Possible rate reversals in future years might slow CO_2 evolution to a long-term RCP4.5 concentration (Figs. 3.6.9, 3.6.10). A concentration pathway midway between RCP4.5 and RCP6.0 is used in this study for the most-likely forecast, and sensitivity results are provided.

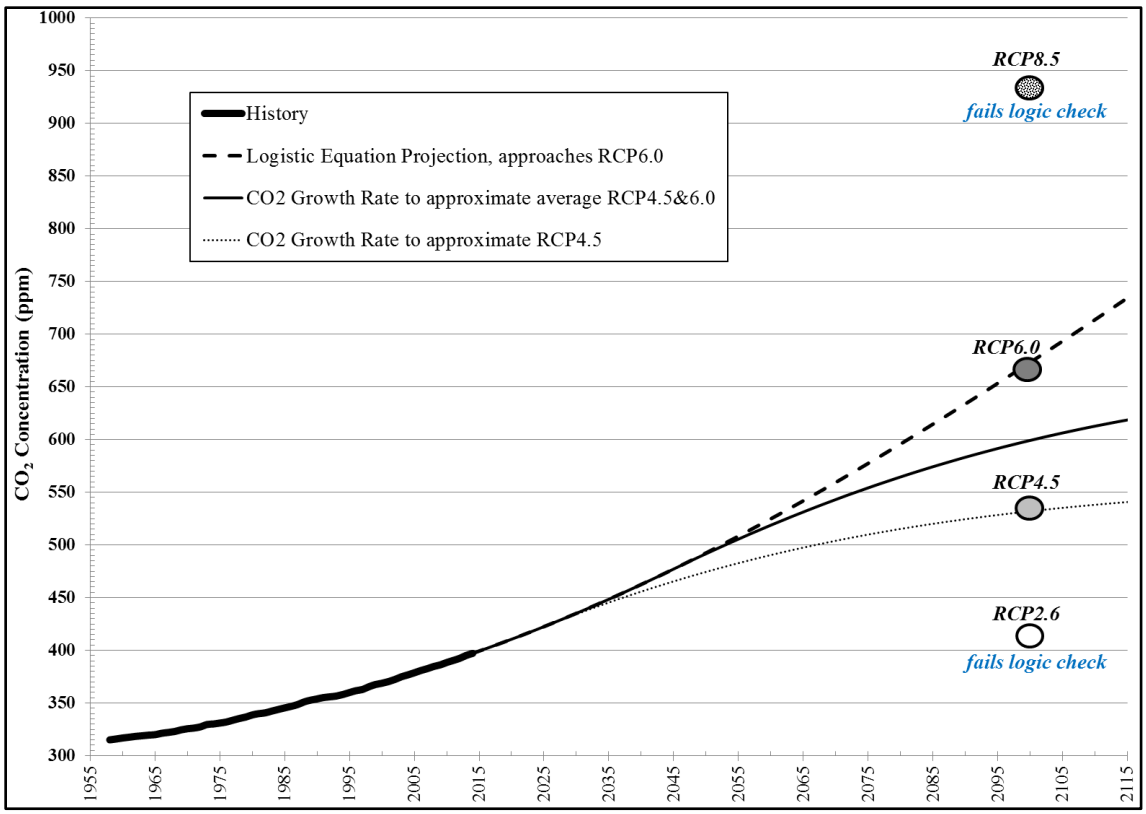

Figure 3.6.10. History and Forecasts of Atmospheric CO_2 Concentration.

It was found that the RCP2.6 and RCP8.5 scenarios for future CO_2 concentrations are mathematically improbable. With the current rate-of-increase >2ppm/year, it will take less than a decade to exceed the CO_2 levels of RCP2.6 (421ppm in 2100). An examination of the growth rate of annual CO_2 increments reveals that the rate has, on average, been declining and is currently in the range of 1.0 to 1.5%/year as shown in Figure 3.6.11. This was recognized by other researchers and served as their basis for CO_2 forecasts (e.g., Hansen et al. 1988). Such growth rates place CO_2 projections well below the 936ppm of RCP8.5 at the end of this century. It would require a sustained 2.25%/year growth rate of the annual increment to mathematically reach that level, which is inconsistent with the demonstrated trend over recent decades. A 'business as usual'

description of RCP8.5 is therefore illogical, and the term more appropriately applies to RCP6.0. While RCP2.6 and RCP8.5 can serve as research test cases for climatological investigations at extreme limits, they should clearly not be considered in a forecasting context.

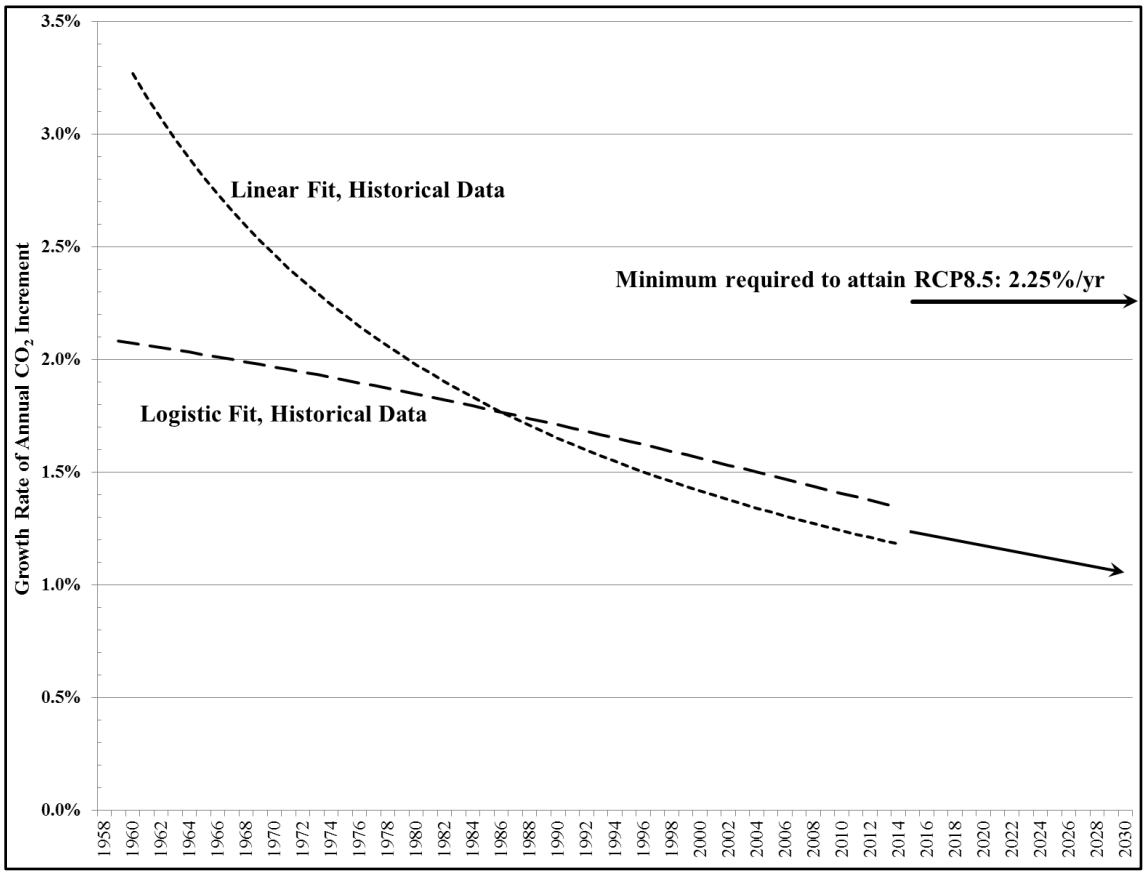

Figure 3.6.11. Growth Rate of Annual Additions to Atmospheric CO_2 Concentration.

3.6.3.5 Model Structure and Validation

From the earlier discussion, the form of the temperature forecast model is composed of the anthropogenic contribution, one or two natural variability cycles, and error. The first of these is the most important for positioning the trend of a long-range forecast, while the cycles provide a decadal modulation which may be important

depending on relevance of its features to the investigative purpose. The forecasting science literature (Armstrong 2001) counsels practitioners to not forecast cycles due to the lack of research evidence that it improves accuracy, unless there is knowledge based on physical laws that they will occur and good information about them is available. Small uncertainties can accumulate to large error over the forecast time horizon if the forecasted cycle gets out of phase with the actual cycle. So, there should be good confidence in cycle length and fairly sure knowledge of cycle amplitude if it is to be employed. The period estimation for the primary temperature cycle over the instrumental record is approximately 63 years ±5%, while the 20-year secondary cycle's period can be estimated to approximately ±20%. The amplitude of the primary cycle appears consistent within the instrumental record, although there is debate over data from the paleoclimate record. There is more amplitude variability in the secondary cycle which is just 30% the strength of the primary cycle. The mid-century lies just 2/3^{rds} of a primary cycle into the future, and the relevant late-century 2081-2100 window is 1.2 primary cycles ahead. Secondary cycle forecasts would entail three times the number of primary cycles involved. As indicated in the natural variability literature review above, a significant amount of research has investigated the origins of the primary cycle while there is less knowledge of the secondary cycle. The primary cycle explains most of the relevant trend modulation, and ECR with it alone is very close to ECR calculated with both cycles. Compliance with forecasting principles therefore indicates that while there may be a sound basis upon which to include the primary cycle in a forecast, the secondary one should be set aside. This is the approach used for the 2-component (AGW+63yrCycle) temperature forecasts used in this study.

Now that the methodology has been developed by which to identify the key components of an empirical model, we must assess its applicability for temperature forecasting into the future. As mentioned earlier, forecast validation is a central tenet of forecasting principles (Armstrong 2001) and is a chief concern for the application of models to predictive climate purposes (Schneider 1992). Model residuals alone are an incomplete assessment of expected forecast error that should instead be calculated through a validation analysis employing hold-out forecasts measured against historical outcomes (Makridakis 1998; Armstrong 2001; Fildes and Kourentzes 2011). As stated by Pielke (2008), "Forecast verification can provide a valuable test of knowledge and predictive capabilities." He recommends that the IPCC clearly define the key variables which are important for projection assessments and the corresponding verification (observational) datasets. Validation analyses were reported from the standpoint of the hydrology community by Koutsoyiannis et al. (2008) and by Anagnostopoulos et al. (2010) for a selection of regional watersheds – finding that IPCC models perform poorly for hydrologic projections. Fildes and Kourentzes (2011) took a forecaster's perspective in a validation study conducted at global and regional levels using a Hadley Center GCM model projection together with a set of statistical time series models they constructed and evaluated in comparison to the GCM. They concluded that climate simulation-based forecasts could benefit by being combined with statistical models. Their work also indicated a climate sensitivity half of that estimated through GCMs. Similar conclusions were reached in an analysis by Suckling and Smith (2013) –

> "… that empirical forecasts can improve decadal forecasts for climate services, … It is suggested that the direct comparison of (climate) simulation models with

> empirical models becomes a regular component of large model forecast evaluations. Doing so would clarify the extent to which state-of-the-art simulation models provide information beyond that available from simpler empirical models and clarify current limitations in using simulation forecasting for decision support."

Forecast validation by hold-out analysis objectively constructs a suite of parameterized forecasts positioned across the historical record using only the information available at the point in time that the forecast is made. The structural form of our empirical model is parameterized by analysis of the data available at the hold-out year. The forecast is constructed and errors per time horizon are measured against the actual historical outcomes. Forecast errors can be compared to other methods applied from the same starting year. There will always be some non-reducible forecast error even with the best of methods, so the objective is comparative error assessment of methods and quantification of expected error for a forecast horizon. For our purposes absolute forecast error (|Actual-Forecast|) is of secondary importance to mean forecast error over long time horizons, which captures bias. Cumulative mean error provides an assessment of a model's accuracy of trend representation – the important metric, since it is the long-term trend that determines cumulative climate change impacts. The objective is to examine whether mean forecast error has been minimized more with the model under evaluation than by alternative methods. This is often evident in graphical comparisons.

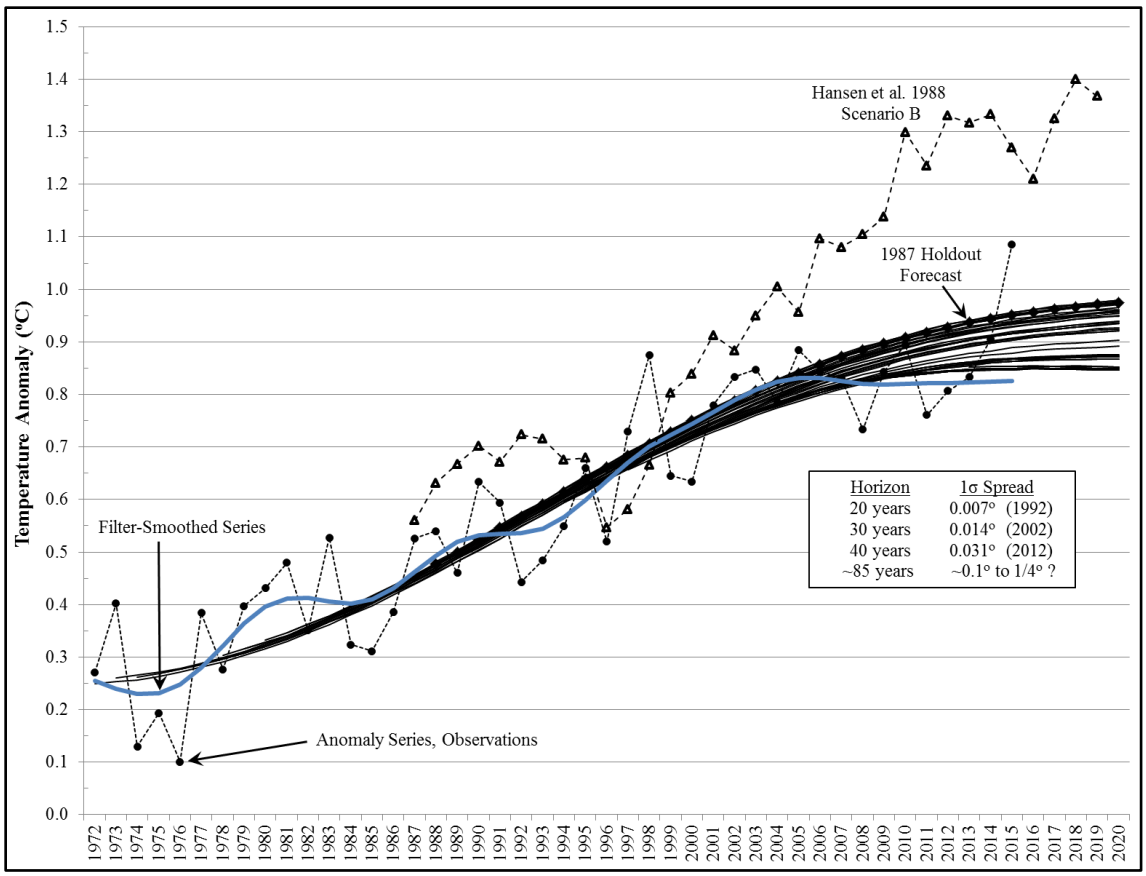

Figure 3.6.12. Hold-Out Forecasts with 2-Component Empirical Model, Using Only the Data Available at the Year in Which Forecast Is Made.

Long-range forecasts were constructed by the 2-component empirical model starting with 1972 when sufficient instrumental data were available to assess ECR, P, and A, and make a CO_2 forecast. Others were then made from 1973 and every subsequent year, as shown in Figure 3.6.12. Forecast error can be evaluated out to a 42-year horizon, and their spread is shown. The ECR estimate is consistent over the chronology, and estimates of period and amplitude are only updated after additional minima or maxima occur in the filter-smoothed series (mid-‘70s and mid-‘00s). The spread in hold-out forecasts is therefore due largely to CO_2 forecast variability with each additional year’s CO_2 record. As can be seen, the forecasts cluster reasonably well within evolution of the

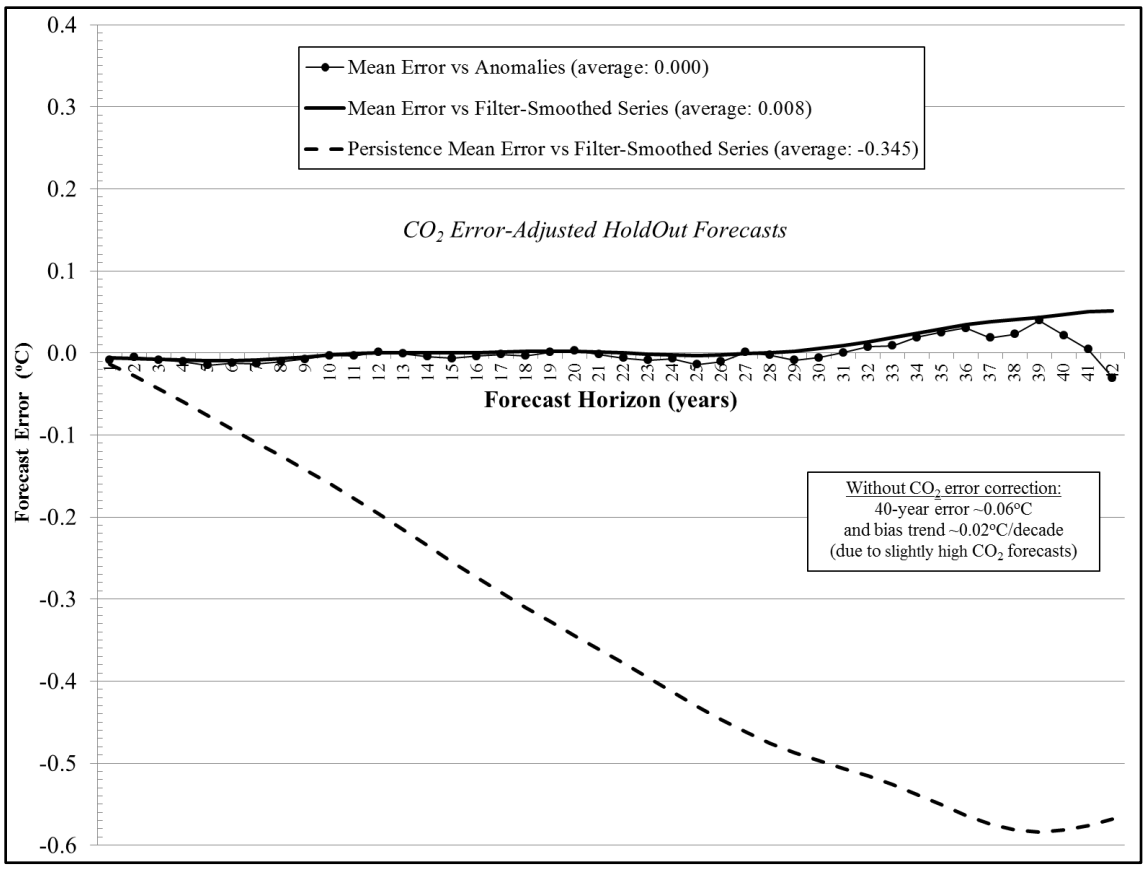

Figure 3.6.13. Hold-Out Forecast Mean Error by Horizon for the 2-Component Empirical Model Forecasts (CO_2 error-corrected) and Persistence Forecasts.

actual anomaly series. Mean forecast error is essentially zero by time horizon (Fig.3.6.13) and cumulatively with the forecasted years (Fig. 3.6.14).

Also reported in Figure 3.6.12 is the temperature anomaly forecast produced by the Goddard Institute for Space Studies climate model with data as of 1987 and published by Hansen et al. (1998). The authors identified their emissions Scenario-B as the most-likely outcome, which was the case. This is the oldest available climate model forecast of global warming that can be evaluated for multi-decade forecasting accuracy against actual outcomes. It is well-documented and served as the basis for J. Hansen's June 1988 congressional testimony (Hansen 1988), once it had become clear that AGW was forcing

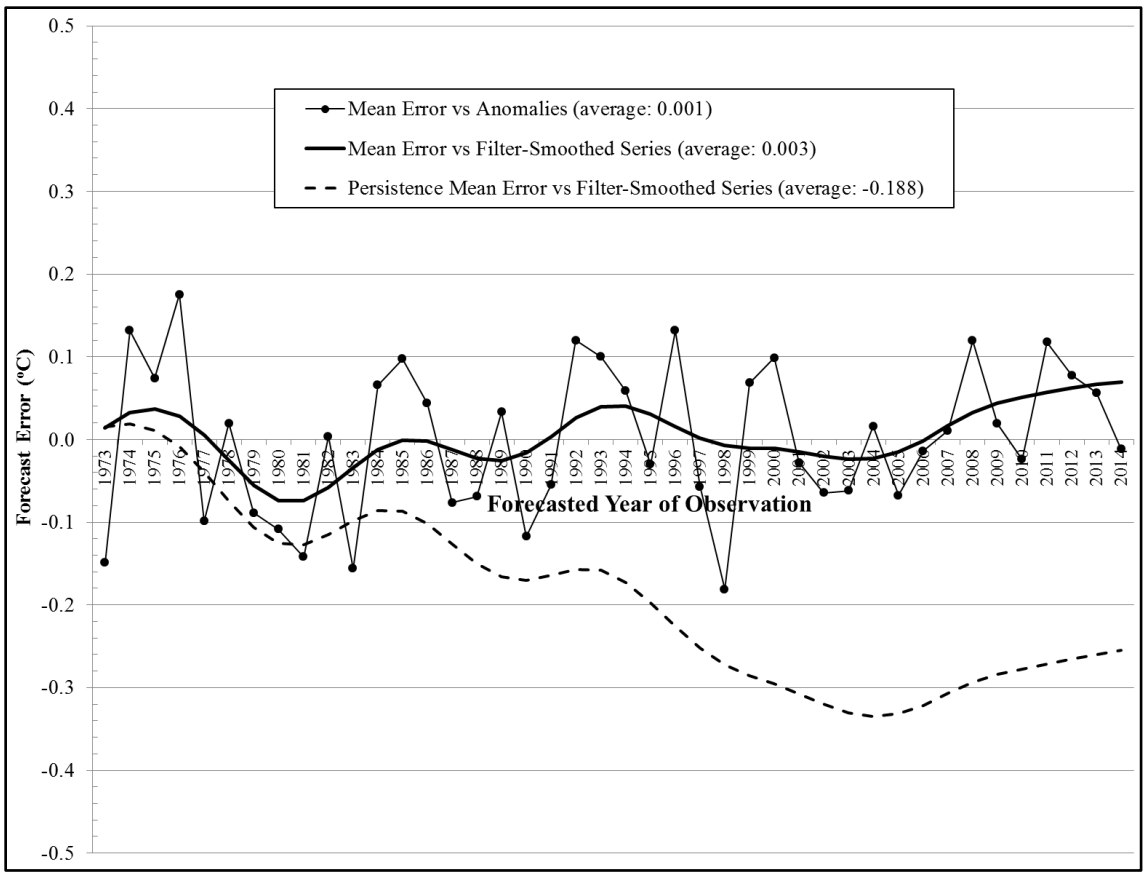

Figure 3.6.14. Hold-Out Forecast Mean Error by Year of Observation for the 2-Component Empirical Model Forecasts (not CO_2 error-corrected) and Persistence Forecasts.

temperature anomalies above natural variability. The divergence from actual observations is seen to emerge in the early 2000s. Error in the Hansen et al. forecast arises from a combination of CO_2 forecast error and internal climate model error. It is straightforward to correct for CO_2 forecast error by examination and adjustment of adjacent years' CO_2 and temperature. This was done and the remaining forecast error attributable to the climate model is shown in Figure 3.6.15. The 1998 El Niño temperature transient caused the temporary drop in all errors that year, and a Scenario-B error trend becomes obvious around 2005. CO_2 error correction removes approximately 20% of the rising forecast bias. Total forecast error has been increasing at approximately

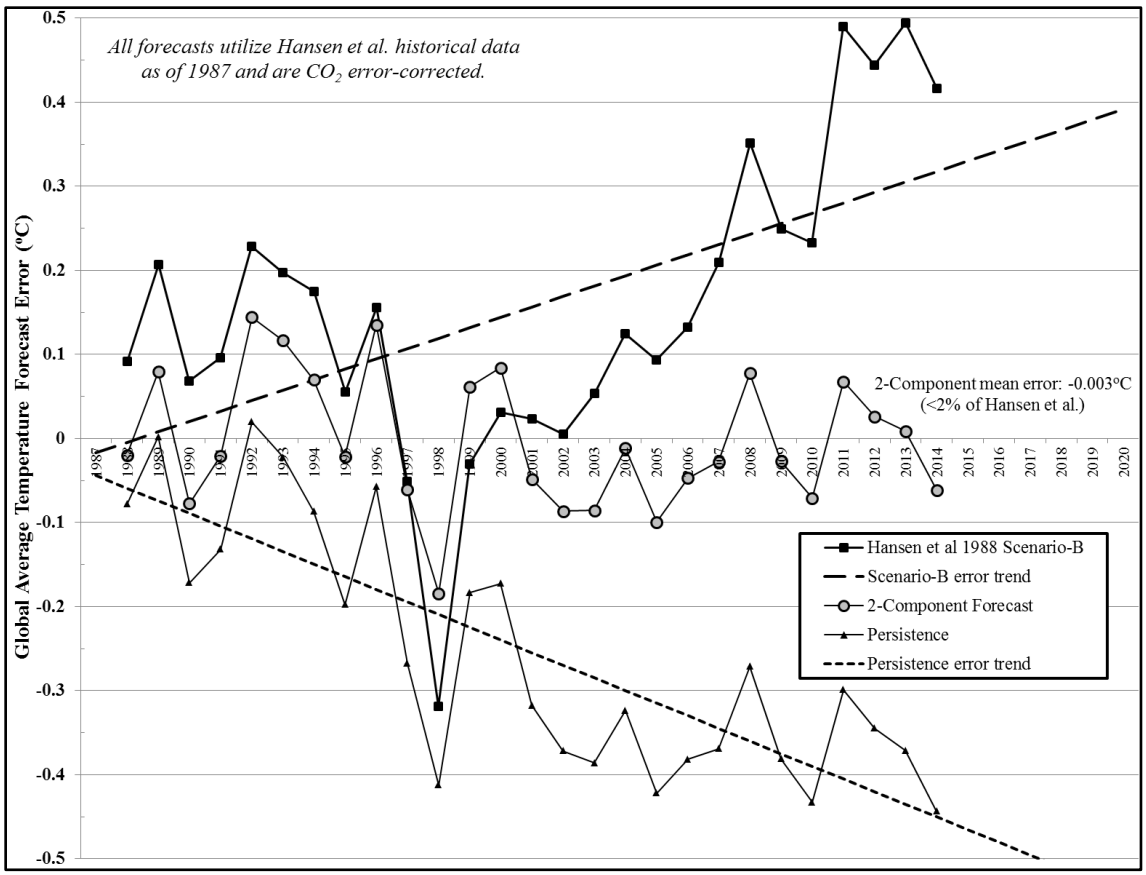

Figure 3.6.15. Comparison of Three Forecast Methods from 1987. Only the empirical 2-component method has minimal mean forecast error and no error trend.

0.15°/decade, but at 0.12°/decade once CO_2 error correction is applied. Such model-only error can accumulate substantially over long time horizons. Persistence forecast error from 1987 is also shown in Figure 3.6.15. It has an error bias trend as well, but in the opposite direction to Hansen et al. since it under-forecasts rather than over-forecasts.

A 2-component empirical forecast is constructed from the Hansen et al. 1987 data and its error is also shown in Figure 3.6.15. Annual errors lie within approximately ±0.1°C over time, and cumulative mean error is a miniscule -0.003°C. In conclusion, the empirical model is demonstrably better than a climate model and better than persistence, and its multi-decade error expectations have been quantified.

3.6.3.6 Global Temperature Anomaly Forecast

The global temperature anomaly forecast using the current estimates of CO_2(preind)=274ppm, ECR=1.45°C, A=0.17°C, P=63yrs, t_o=2005 applied to the model equations is shown in Figure 3.6.16. The CO_2 forecasts of Figure 3.6.10 corresponding to late-century RCP4.5 and RCP6.0 concentrations are used to bracket the most-likely temperature anomaly forecast, and roughly correspond to 95% confidence limits derived from hold-out forecast errors. The anthropogenic contribution is predicted to continue its monotonic upward trend, modulated by natural variability. The forecast range is notably more constrained than the wide range of AR5 projections, dissipating the large

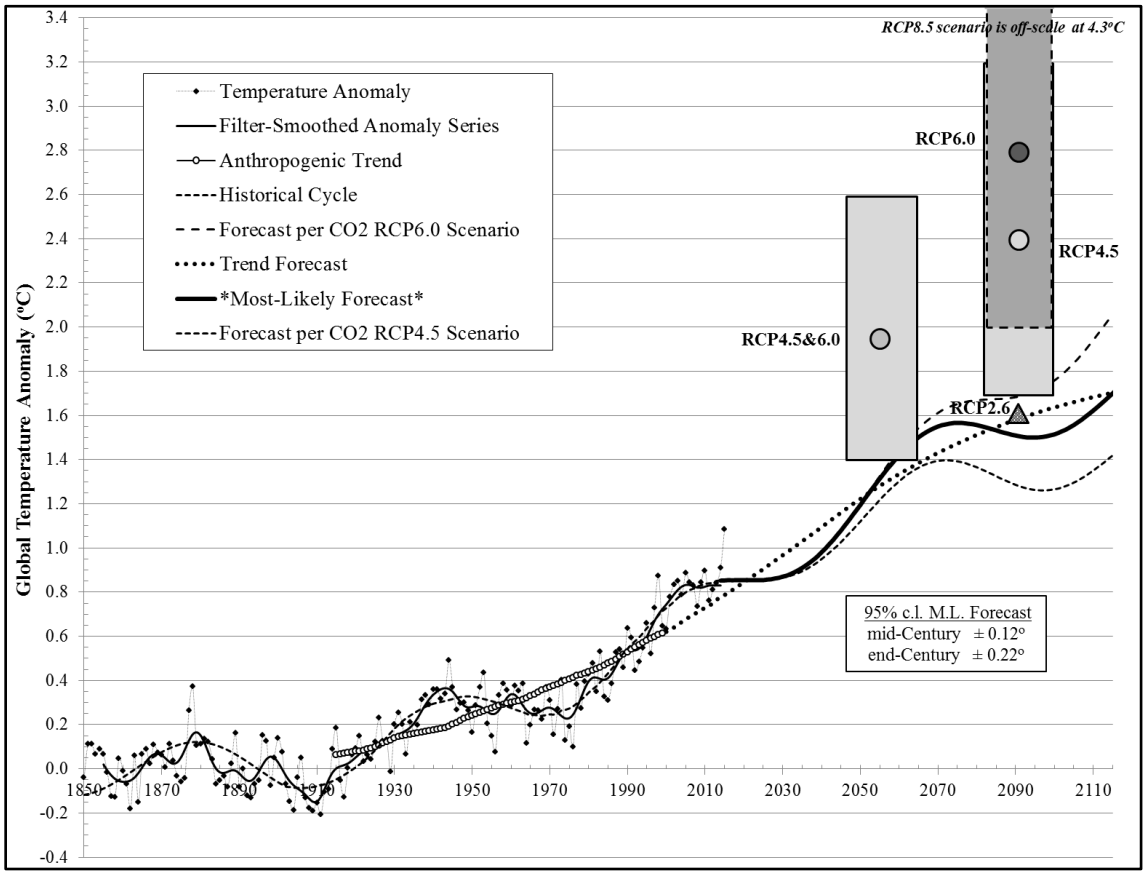

Figure 3.6.16. 2-Component Global Temperature Anomaly Forecasts Compared to AR5 Change Projections.

uncertainties suggested by the IPCC. The forecasts are at the low end of the ranges indicated by IPCC climate model simulations, both at mid-century and at end-century. About half of AGW that is expected by end-century has already occurred. The forecast reveals how relative contributions of the $T_{anth}(t)$ and $T_{nat}(t)$ terms evolve over time. During the 1920s-30s and 1980s-90s the warming was emphasized by the rising phase of cycles in $T_{nat}(t)$. The reverse prevailed during the cooling period into the 1970s and at the present time. The current down-cycle in $T_{nat}(t)$ is forecasted to counteract rising $T_{anth}(t)$ for most of the next two decades. When the error term is taken into consideration, a rising temperature ramp may not be detectable again until the mid-2030s when another significant warming period similar to the 1980s-90s ensues into the 2060s. CO_2 concentration will have doubled from its preindustrial level by 2070, at which time another hiatus is forecasted that persists through the end of the century. A 1.45^{o} ECR maintains global temperature change below 2^{o}C through this century, which is IPCC's critical limit beyond which significant impacts may occur. Uncertainties in the CO_2 rate-of-change later in this century are the most sensitive long-term assumption of the forecast model within reasonable parameterizations, although they only contribute about 0.15^{o} to 0.25^{o}C in uncertainty. The next temperature rise two decades away provides decision makers more time for adaptation planning and implementation, which is fortuitous because all impacts of the last warming have not yet been fully assessed amidst all other climate and meteorological variability. Those should clarify with time, enabling informed preparatory actions in anticipation of the next temperature increase.

3.6.3.7 Salt-Verde Temperature Anomaly Forecast

Chylek et al. (2013) examined the past century's temperature and precipitation in the Southwest United States for the purpose of identifying major drivers of regional climate change. They found that early 20th century warming was dominated by transitions in the AMO while the late part of the century was influenced by both the AMO (concurrent with the PDO) and increasing greenhouse gas concentrations. They attribute regional warming of the past few decades equally between the AMO-PDO and GHG drivers and thereby reach the conclusion that CMIP model sensitivity to GHG has been overestimated by approximately a factor of two. The climate conditions predicted for the Southwest by CMIP simulations are supported in their analysis only in the case of the climate indices returning to their late-20th century rate of change and sustaining that mode. They consider this highly unlikely considering the long-term AMO-PDO cyclicality imprint on the region.

All elements of the 2-component empirical model can be readily derived regionally to support applicability of the methodology to the Salt and Verde River watersheds and reservoirs utilizing their instrumental records. Climate sensitivity and response to large-scale circulation dynamics differ between global and regional data sets but reflect similar periods of warming and cooling in temperature trend-cycles, including the 1970s cooling period and the current hiatus. This can be seen in Figure 3.6.17 where ECR=2.89^{o}C/2xCO_2 for the combined watersheds has been calculated for the forecast. ECR is generally expected to be higher over land than the global value. Uniqueness of a regional ECR is expected and due to localized influence of aerosols, land cover interactions, and feedbacks. Similarly, the unique imprint of multi-decadal variability in

the Southwest United States (Nowak et al. 2012; Chylek et al. 2014) is reflected in local effects of large-scale circulation dynamics, although consistency of cycle period is evident in the watersheds.

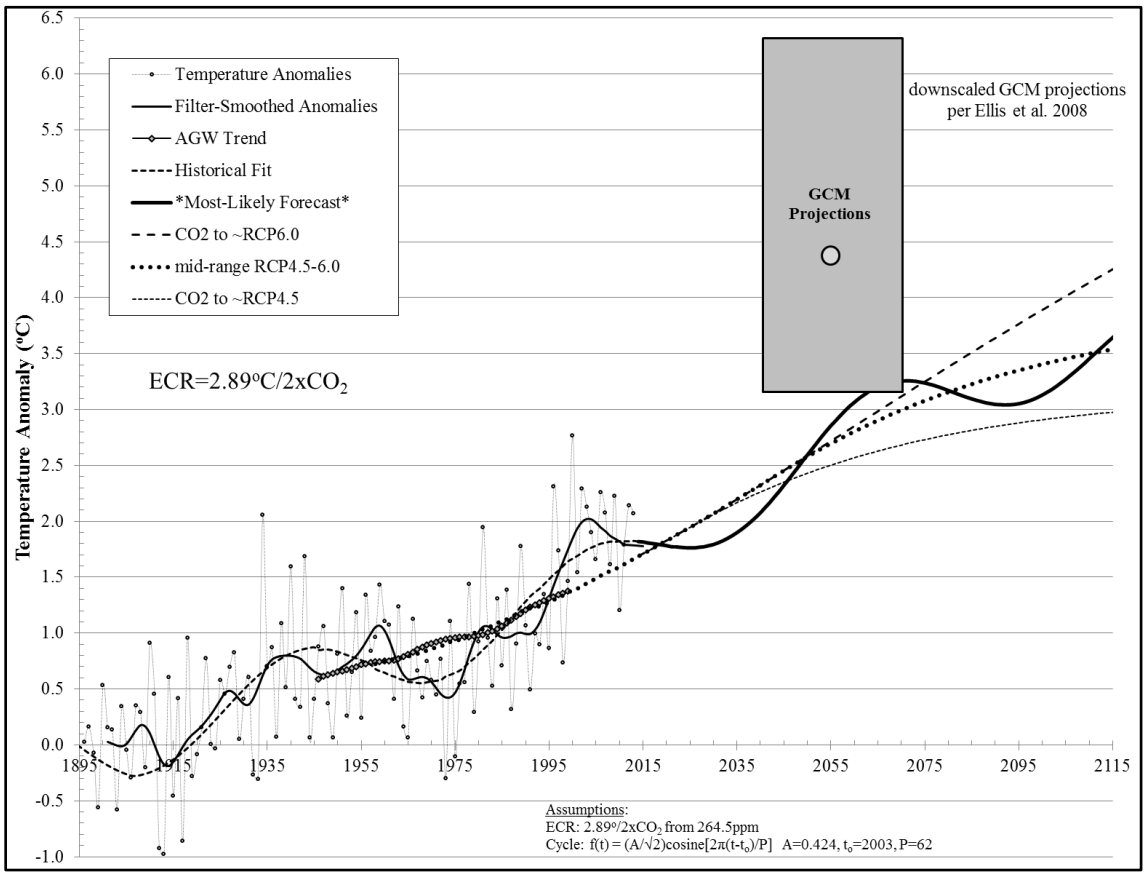

Figure 3.6.17. Temperature Anomaly Forecasts of Combined Salt and Verde River Watersheds Compared to Downscaled Climate Model Change Projections.

Since the central Arizona climate sensitivity is twice the global value, the current and future hiatus periods will occur at temperature anomaly levels twice what is seen at the global level. The hiatus intervals provide a convenient temperature differential over which to calculate a single-number temperature change forecast for analysis of the SRP system. As can be seen in Figure 3.6.17, the temperature change to arrive at the future hiatus (2065-2095 average) relative to the current level (2000-2030 average) is

approximately 1.5°C. But, if there is a unique regional ECR there may also be unique ECRs for each watershed-season and the reservoirs, and this was found to be the case. They are summarized in Table 3.6.1, along with the temperature differentials that are the most likely forecasts of future temperature change applied for this research investigation. Among the forecasts, it is noted that the Verde watersheds and reservoirs in summer have a climate sensitivity and hence a temperature change forecast notably larger than other watershed-seasons. The reason for this is unclear and merits further investigation. Nevertheless, the identified temperature forecast values are used for this research, and conclusions are not very sensitive to Verde summer values due to the relatively small summer runoff contributions from the Verde River.

Table 3.6.1. Effective Climate Response (ECR) and Temperature Change from the Current Hiatus (2000-2030) to the Future Hiatus (2065-2095).

	Most Likely Forecast		AR5 Projection
	ECR ($^oC/2xCO_2$)	future temperature change	future temperature change
Global Water-Year	1.45	0.6 °C	1.57 °C
Salt & Verde Water-Year	2.89	1.5 °C	3.1 °C
Watershed-Season			
Salt Winter	2.87	1.34 °C	3.1 °C
Verde Winter	2.20	1.02 °C	3.1 °C
Salt Summer	2.90	1.35 °C	3.1 °C
Verde Summer	3.97	1.86 °C	3.1 °C
Reservoir-Season			
Salt Winter	1.80	0.82 °C	3.1 °C
Verde Winter	2.95	1.37 °C	3.1 °C
Salt Summer	2.55	1.18 °C	3.1 °C
Verde Summer	3.97	1.85 °C	3.1 °C

3.6.4 Temperature Projection Based in IPCC AR5

The climate modeling community, globally and regionally, has been resistive to providing what can be relied upon as a forecast, asserting that their findings are only possible 'projections' of the future. As previously discussed, those projections over-state temperature trends compared to current observational analyses and span an irreducibly wide and uncertain range of expectations. Nevertheless, a succinct temperature change originating in AR5 models is desired for this investigation of the SRP system to explore what those implications might be. This was derived based upon –

1) AR5 global mean temperature changes, 2046-2065 & 2081-2100, for RCP4.5 and RCP6.0
2) regional climate sensitivity at twice global sensitivity
3) current regional hiatus at ~1.8^{o}C relative to preindustrial
4) trend calculation to identify temperature changes in the same comparative time interval as the empirical forecast

The calculation yields an AR5-derived temperature change projection of 3.1^{o}C for late-century, as compared to the empirical model's ~1.5^{o}C forecast (Table 3.6.1). The 3.1^{o}C change has been uniformly applied to the watersheds and reservoirs in both seasons for an AR5 temperature change projection.

3.7 Reservoir System Operations Simulation Model

3.7.1 Abstract

Successful water management outcomes are largely a function of the design and operation of a reservoir system matched to the hydroclimate of its watersheds. Such systems are built to buffer against hydroclimatic variability and differentials between supply and demand, thereby assuring continuity in water delivery and flood protection. The cumulative interaction of runoff variability with reservoir system design and operation greatly affect the response and status of the system at any point in time. The interplay is essential to understanding impacts on water availability, which is the bottom-line measure of resilience.

To perform that assessment, a reservoir system operation simulation model (ResSim) was developed with the cooperation of the Water Resource Operations group at SRP. The model incorporates a customer water demand schedule, system replenishment through climate-driven runoff from the Salt and Verde watersheds and losses at the reservoirs, and the web of decision rules used to manage an integrated six-reservoir system with groundwater backup and operating protocols. A wide range of NBS time series scenarios can be efficiently exercised through the model which reports status of all key variables at seasonal time steps for the very long time series needed for detailed probabilistic assessments of key performance metrics. System implications of climate change in the NBS series can then be readily assessed from the system response differentials and findings can inform adaptation measures.

3.7.2 ResSim Model in FORTRAN

Some analysis of the SRP reservoir system capabilities was previously performed by SRP's Water Resource Operations group (Phillips et al. 2009). Using their Long-Term Drought Planning Model (LTDPM) and monthly data in 50 year intervals they analyzed the effect of long-term drought on the reservoir system if managed under current operational guidelines. Flow reductions in fixed percentages of the historical median were analyzed to determine what it would take to deplete reservoir storage. As well, extended periods of drought from the historical record were tested with percentage reductions in runoff to assess effects on storage. The findings provide important insights to the resilience of the SRP reservoir system as well as its vulnerability in periods of drought. However, results were incomplete because they dealt only with established runoff time series without consideration of alternative temporal variability. The historical runoff record is unlikely to exactly repeat itself in the future, so consideration should be given to the full range of other possible sequences. Since droughts occur in the Southwest United States with multi-decadal return frequency, very long time series must be studied to thoroughly assess them in a statistically rigorous manner, and this can be performed by passing stochastic simulation series (from Sec. 3.4) through a reservoir operations model. Modeling at seasonal or annual rather than monthly time steps is more computationally efficient for the long, repeat executions required to explore numerous scenarios, and the LTDPM did not lend itself to this purpose.

Consequently, this investigator developed full flowcharting of a seasonal, deterministic reservoir operations simulation model to enable evaluation of the cumulative impact of numerous watershed flow sequences on SRP water storage,

groundwater pumping requirements, and management action thresholds. Investigator's advisor, A.W. Ellis, programmed the model in FORTRAN, and it was tested to demonstrate accurate and representative outcomes. The web of decision rules within ResSim were established from SRP's operational information (SRP-a, SRP-b) and published research work (Phillips et al. 2009). It was found that, although the system is managed day-to-day, the key operational decisions can be well-represented in modeling on a seasonal basis. ResSim was therefore built on a winter-summer basis, simplifying calculations into two seasons per water year and making it feasible to quickly execute a nearly infinite string of years for estimates of statistics from very large sequence outcomes. The model's configuration of operating rules and parameterizations of the reservoir system were reviewed with SRP Water Resource Operations personnel for representativeness and completeness, and inputs from those consultations were incorporated to the final version of ResSim which was used for this investigation. Complete details of the model and flowcharts are documented in Appendix F.

The main features of the ResSim model can be summarized as:

- Water year start date of October 1st and winter-to-summer runoff transition on May 1st.
- Six Salt and Verde reservoirs, rated per current storage capacities (Table 2.1.1).
- Fixed water delivery schedule of 900,000 acre-feet/year (representative monthly customer demand schedule provided by SRP, Appendix F).
- Groundwater pumping per SRP storage planning diagram, which is a function of reservoir storage status (Appendix F).

- Model inputs as runoff and miscellaneous loss, or as net basin supply (NBS=RO-ML).
- Miscellaneous loss directly input or calculated per localized climate at the reservoirs.
- Priority to water supply for the Salt reservoirs' hydroelectric generation.
- Seasonal depletion and replenishment sequences per balance of surface water demand versus net basin supply.
- Reservoir positioning rules for winter runoff.
- Defined depletion/replenishment sequences within and between the Salt and Verde sides of the reservoir system.
- Spillage monitoring and correction between the Salt and Verde sides of the system.
- Reduced water allocation rules (2/3^{rds} of season demand) implemented below 600,000 acre-feet of total remaining reservoir storage.
- Reservoir system depletion shutdown at 50,000 acre-feet remaining storage which persists until Salt reservoir storage recovers to 450,000 acre-feet, with user-defined recovery options.

The ResSim model outputs 28 characteristics of the reservoir system per season, including all volumes of water in and out of the system, water stored in each of the six reservoirs, the customer water demand and the amount of demand that is met, the amount of groundwater pumped to supplement surface water, and coded messages associated with significant thresholds (e.g., reduced allocation, system depletion). Surface and

groundwater deliveries are identified in ResSim by season, but the downstream water distribution agreements between SRP and the various water users are not. For this investigation a baseline assumption of 367,000 acre-feet of water delivery in winter (over 7 months) and 533,000 acre-feet in summer (over 5 months) is used, which was typical in the several years (2003-2011) preceding initiation of this study (delivery history in Appendix F). To the extent that actual water deliveries do not follow this assumption, cumulative modeled results will deviate accordingly. The implications of larger or smaller deliveries, while an interesting question that can be explored with the toolset developed for this investigation, is an analysis outside the scope of this report.

3.7.3 Model Evaluation

Verification testing of the ResSim model was conducted and reported to SRP by Ellis and Murphy in 2012. This included replicating Phillips et al.'s (2009) analyses, an assessment of the model's ability to replicate the recent historical progression of reservoir storage, and model execution with the full historical NBS record since 1889 to assess how the system would have responded if it had been in place with the current configuration and operating rules. The model effectively reproduced anticipated behaviors and confirmed the suitability of ResSim for the anticipated purposes of this research investigation (Ellis and Murphy 2012).

Model evaluation intends to test the model's ability to replicate operational outcomes using the stream gage and climate data records for the years since the SRP system was fully in operation. However, ResSim is built according to current system configuration and operating rules, and many of those have changed appreciably over time, making comparisons inexact. For example, upon examination of the historical

storage record it is evident that there were significant ongoing modifications of reservoir operations into the early 1970s. In particular, water storage in the smaller Salt reservoirs was inconsistent with what would now be expected under current operating guidelines. As well, there have been documented changes in SRP's storage planning guidelines since 1971 (Phillips et al. 2009), and simulation of the historical record is complicated by other changes, including:

- Expansion of Roosevelt Lake reservoir capacity by 305,000 acre-feet in 1996 (simulations use post-1996 storage capacity throughout).
- Revision of operational safety-of-dams rules that accompanied the extension of Roosevelt dam.
- Revision of groundwater pumping guidelines in the mid-1990s and again in 2006 (simulations use the current algorithm).
- Revision of water allocation reduction rules in 2006 (simulations use current rules).
- SRP's purchase of approximately 500,000 acre-feet of water from the Central Arizona Project (CAP) in the early 2000s (simulations consider no outside water sourcing).
- Delivery of water to a changing demand schedule through time, including a decline in deliveries over the past few years (simulations use a constant annual 900,000 acre-feet).

Nevertheless, as can be seen in Figure 3.7.1, ResSim renders a seasonal storage series reflecting the historical progression, although with attributable periods of offset. Co-

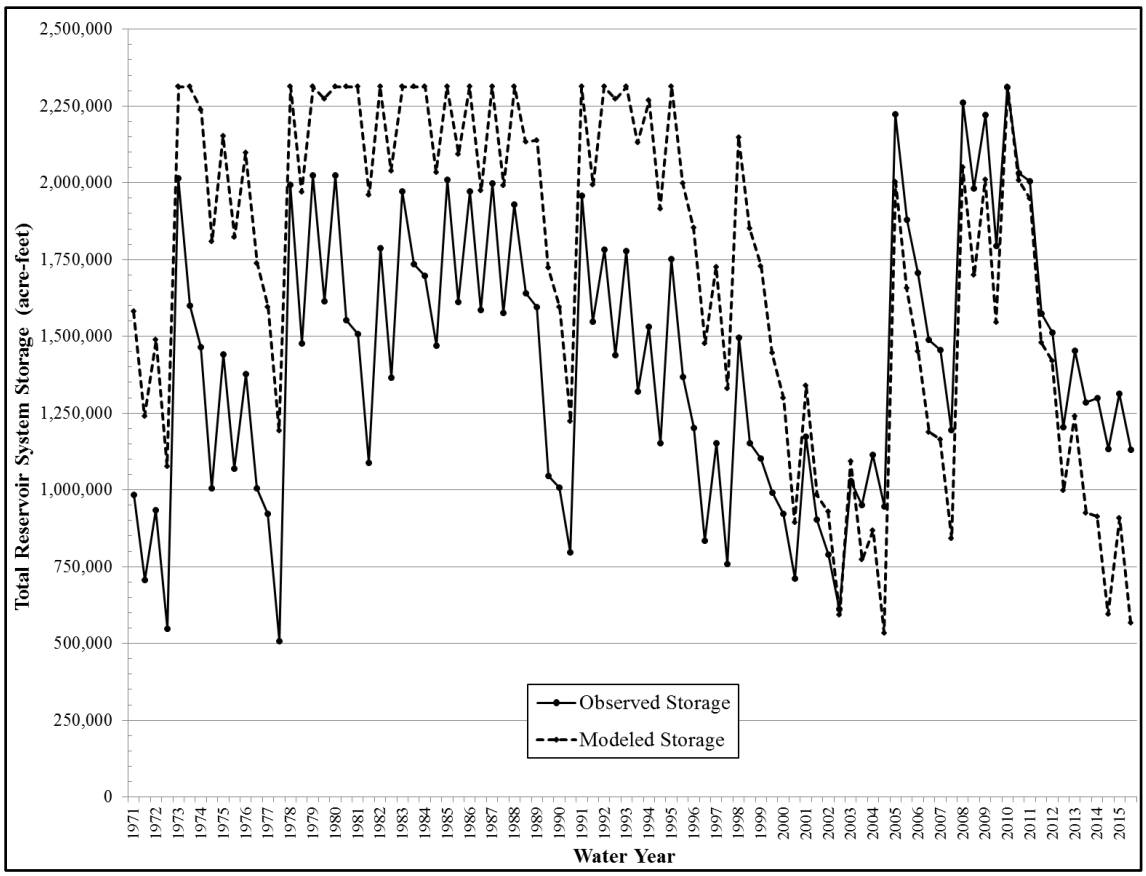

Figure 3.7.1. Observed and ResSim-Modeled Total Reservoir Storage at End-of-Seasons (April 30, September 30) Since 1971.

variability of simulated and observed reservoir storage is evident with a systematic offset owing to the use of the larger post-1996 storage capacity (at Roosevelt Lake) in ResSim with updated operational rule revisions. This results in a continuing offset until the drought of 2002-2003. That threatening drought period triggered reduced water allocation deliveries to customers and water sourcing outside the system from CAP, which closes the bias between modeled and observed results. After the depth of that drought period, simulated storage is consistently less than observed storage, which is in part a product of the carryover effect of the CAP water purchase. Then, more recently, a

sequence of deliveries below modeled demand (Fig. F1 in Appendix F) has kept storage at higher levels than would be expected.

The only full system replenishment since the 1996 Roosevelt Dam extension occurred in the winter of 2010, so only since then should ResSim modeling be expected to align with observed outcomes. But, the differential of lower actual water deliveries than 900,000 acre-ft/yr has left the system with a cumulative storage benefit of approximately 500,000 acre-ft at the end of 2015. As discussed in Chapter 4 (Results) of this document, the SRP system is well-matched to its watersheds' NBS for delivery of 900,000 acre-ft/yr. Any reduction in water delivery readily benefits reservoir storage because the probability of reservoir inflows sufficient to sustain the system is readily enhanced when withdrawals are below the median of the skewed NBS probability distribution (Fig. 3.4.16). In other words, there is a significant enhancement of system resilience during drought periods by even modest delivery demand reductions, as has been demonstrated over the last five years.

The modeled storage response to the entire historical NBS series is shown in Figure 3.7.2. Total system storage is maximized during periods of high inflows and depleted during cumulative deficits. The NBS time series has a high coefficient of variation with periodic high flows which quickly refresh the reservoir system. The sharp and deep 1890s drought is readily apparent, briefly resulting in total remaining storage below 600,000 acre-feet, which would call for reduced water deliveries under conservation measures. It ended abruptly with a very wet 1905 followed by the pluvial 1910s-20s period during which the system would have been repeatedly topped off and spilled excess water. A shallower but longer dry period is seen across the 1950s followed

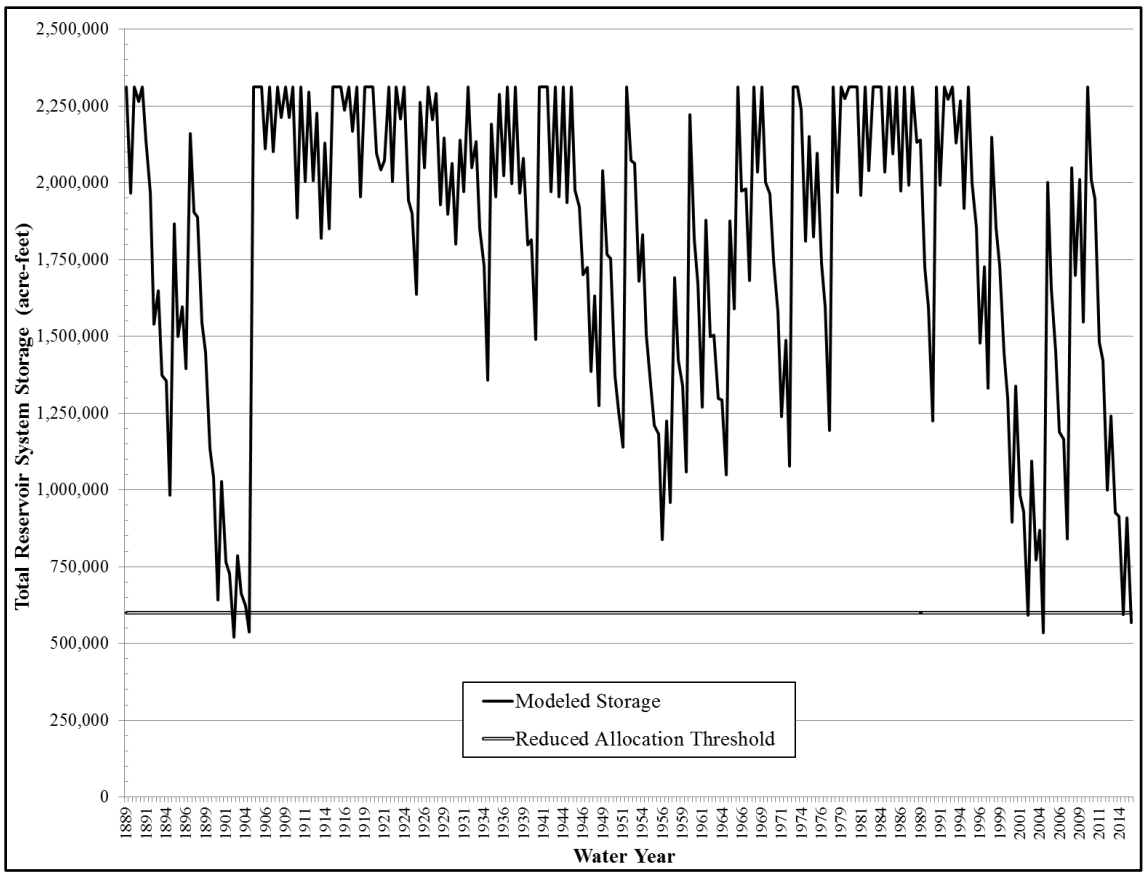

Figure 3.7.2. Modeled Total System Storage Response to Historical Watershed Inflows for the Period 1889-2015.

by another pluvial period centered in the 1980s. The model renders a couple seasons of storage below 600,000 acre-feet at the beginning of the 2000s which did trigger changes in water allocation and the purchase of CAP water. Although drought relief came briefly with the El Niño winters of 2005, 2008, & 2010, below-median NBS over the last five years places modeled storage again at the 600,000 acre-feet storage threshold. But, as discussed above, declining demand over the same period has made the imposition of allocation reductions moot.

No depletion of the reservoirs was found in this ResSim analysis of the historical record. The reduced allocations and groundwater pumping would have buffered against

the reservoirs reaching a depleted condition during dry periods within the past 127 years. Furthermore, it seems that if only a few hundred thousand acre-feet of conservation or other water is sourced at the opportune time, total storage can be kept above 600,000 acre-feet until larger inflows return for reservoir replenishment. Alternatively, if additional reservoir capacity were available, some spillage could have been captured during periods of high flow. This would essentially raise the curve in Figure 3.7.2 away from the trigger level for reduced allocations. In this sense the 1996 modification of Roosevelt Dam was a wise storage capacity addition. Another similar capacity addition could further reduce chances of triggering allocations in the future, which is an option to consider if realistic climate change scenarios raise probabilities of deeper or longer droughts to an unacceptable level of recurrence that cannot be addressed by conservation measures.

To perform a further stress test of the system, a uniform percentage NBS reduction can be applied to the historical series and assessed by ResSim (Ellis and Murphy 2012). This is a coarse method by which to analyze the system; but, such a practice raises a persisting divergence of opinion among practitioners over whether it is sufficient to assess changes through such simple adjustments to an overall probability distribution or whether resilience is more reliably assessed through detailed statistical constructs (Katz 2010). An entire distribution shift may be appealing in its simplicity but it leaves unresolved concerns whether there may be different drivers to different parts of the NBS distribution. This is an important distinction in hydrologic modeling with potentially significant differences for results. This investigation took the choice of

examining effects as a function of NBS distribution; and important implications to analysis findings were found as will be discussed in Chapter 4.

As illustrated by the above analysis, the ResSim reservoir simulation model provides a key tool by which to assess cumulative impacts of highly variable inflows of seasonal NBS from dual, correlated watersheds. While examination of historical record effects are instructive, they are not the complete story – which can now be completed by passing very long time series generated by the stochastic simulation methodology through the ResSim model.

CHAPTER 4

RESULTS

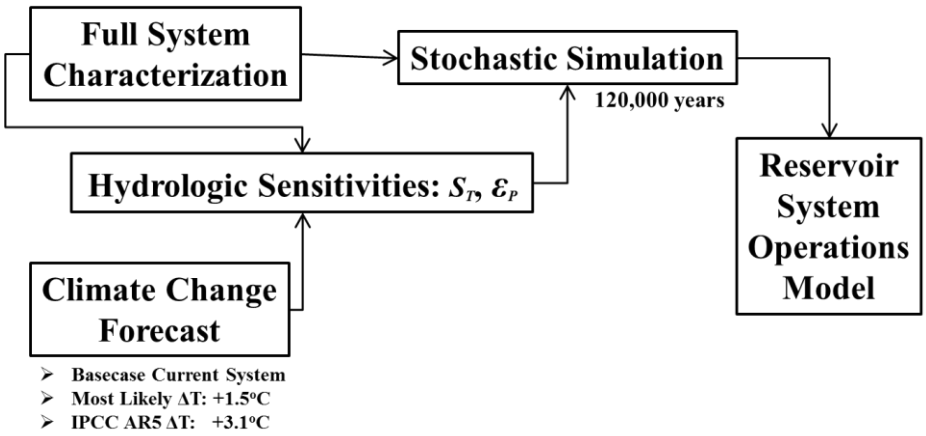

Figure 4.0.1. Integration of the Components of this Research Investigation.

The methodological components described in the last chapter provide the tools necessary to conduct an integrated analysis of the SRP system based in its long historical data record. Interfacing of the analytical components is diagrammatically outlined above in Figure 4.0.1. A full system characterization (Sec. 3.2) enabled the development of the stochastic simulation methodology (Sec. 3.4) and calculations of the hydrologic sensitivities of the watersheds and reservoir system (Sec. 3.5). Details of the stochastic simulation algorithms are documented in Appendix C, from which a dozen 10,000-year time series were generated for this investigation, for a total of 120,000 years of dual-season, dual-watershed NBS. The resultant distribution of total annual NBS is given in Figure 3.4.16. Any transformation of that pdf due to forthcoming climate change is translated according to the hydrologic sensitivity algorithms documented in Appendix D. Two climate change forecasts for the later part of this century (2065-2095 vs 2000-2030) were developed (Sec. 3.6). These are the author's most likely forecast and a projection

based in AR5 from the IPCC (Table 3.6.1). The latter is approximately double the average temperature change of the former. The 120,000 years of simulation data were transformed for each of the two change cases per S_T findings. ε_p algorithms were not applied for the change cases as no precipitation trend is anticipated within those temperature ranges, but they were applied for the sensitivity analyses described below.

While there are numerous questions about the three 120,000-year time series that can be examined, the central ones regarding differences in net basin water supply and drought occurrence are analyzed and reported below. All generated series and the historical record were passed through the reservoir operations model that was developed (Sec. 3.7; details in Appendix F), and system response in key respects is also reported below.

4.1 Net Basin Supply

The NBS probability distribution function previously shown in Figure 3.4.16 is reproduced in Figure 4.1.1 in comparison to the resultant pdfs for the temperature change cases (summary statistics are documented in Table G1 of Appendix G). The annual median NBS of the current system's generated series is 849,500 acre-feet, which, when combined with a nominal 50,000 acre-feet of groundwater, matches the 900,000 acre-feet of annual water deliveries from the SRP system around which the ResSim model is exercised. In this regard the watersheds are well-matched to the rest of the system. As can be seen in Figure 4.1.1, the effect of the temperature changes is a downward shift of the pdfs. The degree of NBS change is nonlinear and a function of position examined

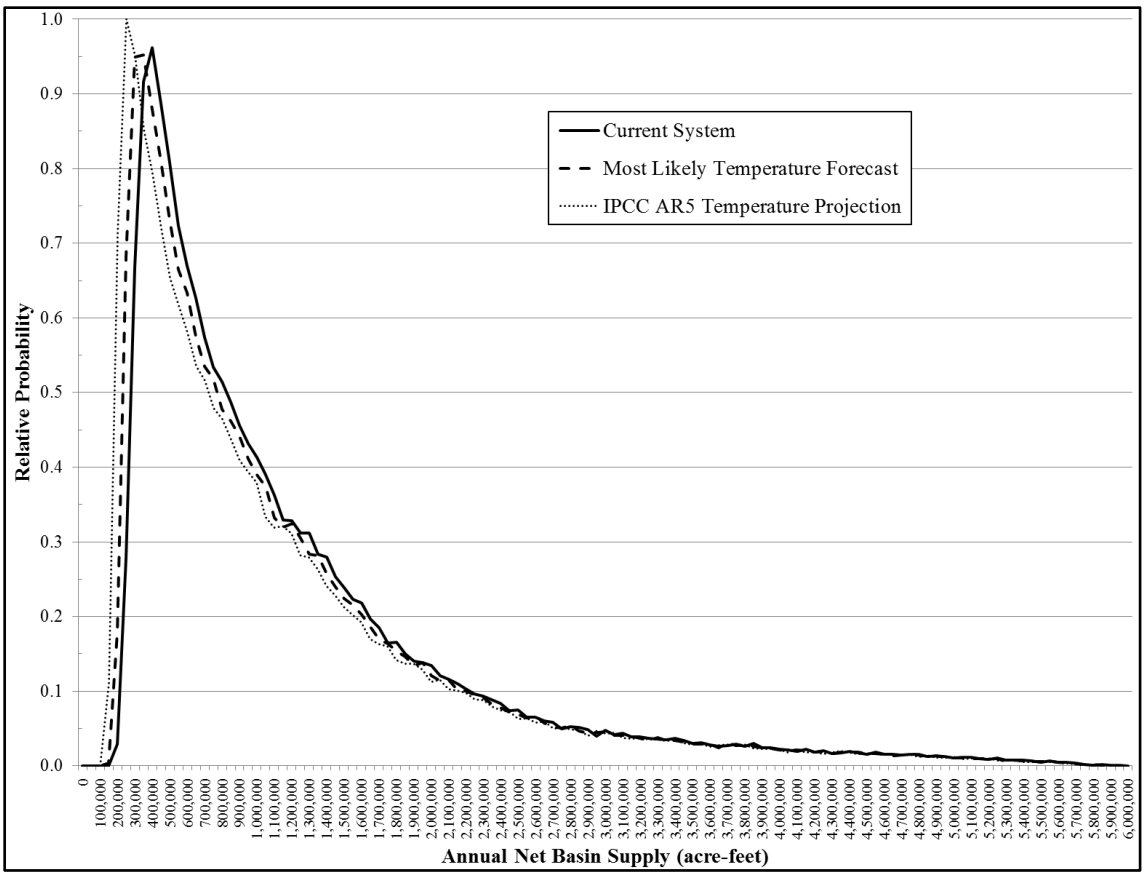

Figure 4.1.1. Annual NBS Probability Distribution Functions for the Current System and the Two Temperature Change Cases.

Table 4.1.1. Change of Annual NBS as a Function of Position within the NBS Probability Distribution. The most likely temperature change is about 1.5°C; the AR5 change is 3.1°C.

	Most Likely Forecast vs Current System	IPCC AR5 Projection vs Current System
10th percentile	-13%	-28%
25th percentile	-9%	-19%
Median	-5%	-10%
Mean	-3%	-7%
75th percentile	-2%	-5%
90th percentile	-1%	-3%

within the pdf. Some quantification of this is provided in Table 4.1.1. The most likely temperature case results in about a 4% reduction in the vicinity of the median and mean NBS, while the larger AR5 temperature change induces about double that reduction.

However, more illuminating is what occurs in very low and high flow regimes. Recall that temperature sensitivity was found to be minimal in winter but with discernable summer effects upon flows from the watersheds and losses at the reservoirs. The system is primarily dependent on winter precipitation for reservoir refresh; so, if that is deficient, annual NBS is comprised more of the summer flows and losses that are temperature sensitive. If, instead, winter runoff is the dominant portion of annual NBS and subject to minimal temperature sensitivity, summer effects are diluted within the annual impairment. Productive El Niño winters can result in upper-quartile NBS, and their annualized temperature sensitivity is only ~1% to 2%/^{o}C. With non-productive winters, annual NBS impairment is expected to be in the range of 6% to 10%/^{o}C. Previous research (Fu et al. 2007b; Vano and Lettenmaier 2014) has identified seasonal dependence of temperature sensitivity and hinted at nonlinear response. But the findings of this investigation are the first specific quantification of those for any watershed based in observational evidence, and it reveals a more detailed expectation of only modest streamflow impairment.

The differentials between temperature cases were examined to identify the origin of NBS reductions, and their average apportionment is shown in Table 4.1.2. Only a few percent is due to winter runoff impairment, which can be readily lost amidst high year-to-year precipitation variability. It is during the summer season that future temperature changes will have an effect; and, of those NBS impairments, roughly half of it occurs

during runoff to streamflow and half of it as additional miscellaneous loss at the reservoirs (52%/45% in most likely forecast, 45%/51% for AR5 projection). So, evaporative water loss from the reservoirs is as important as what will happen on the watersheds, and it becomes a larger percentage with more elevated temperatures. This finding might be expected, and it is difficult to envision a manner in which to suppress such natural loss.

Table 4.1.2. Origins of NBS Reductions at Typical NBS Levels.

	Most Likely Forecast	IPCC AR5 Projection
Winter	3%	4%
Summer		
Salt Runoff	20%	20%
Verde Runoff	32%	25%
Salt MiscLoss	32%	40%
Verde MiscLoss (at reservoirs)	13%	11%

The nonlinear reductions in annual NBS due to future temperature change are composed of unique nonlinearities for each watershed-season (not shown), and any NBS level can be comprised of varying watershed-season contributions per the stochastic constructs (developed in Sec. 3.4). Consequently, their changes are also stochastically distributed in a nonlinear fashion across NBS level. This can be seen in Figure 4.1.2 for the most likely temperature forecast and in Figure 4.1.3 for the IPCC AR5 projection. NBS impacts are clearly more pronounced at low levels where summer contributions are more heavily weighted, as was discussed above. There is also a broad probabilistic distribution of potential outcomes at low levels. At high NBS levels, which are due to

wetter winters, reductions are much smaller and the distribution is more constrained. It becomes clear that the totality of nonlinear interactions becomes difficult to encapsulate in simple expressions or graphical display.

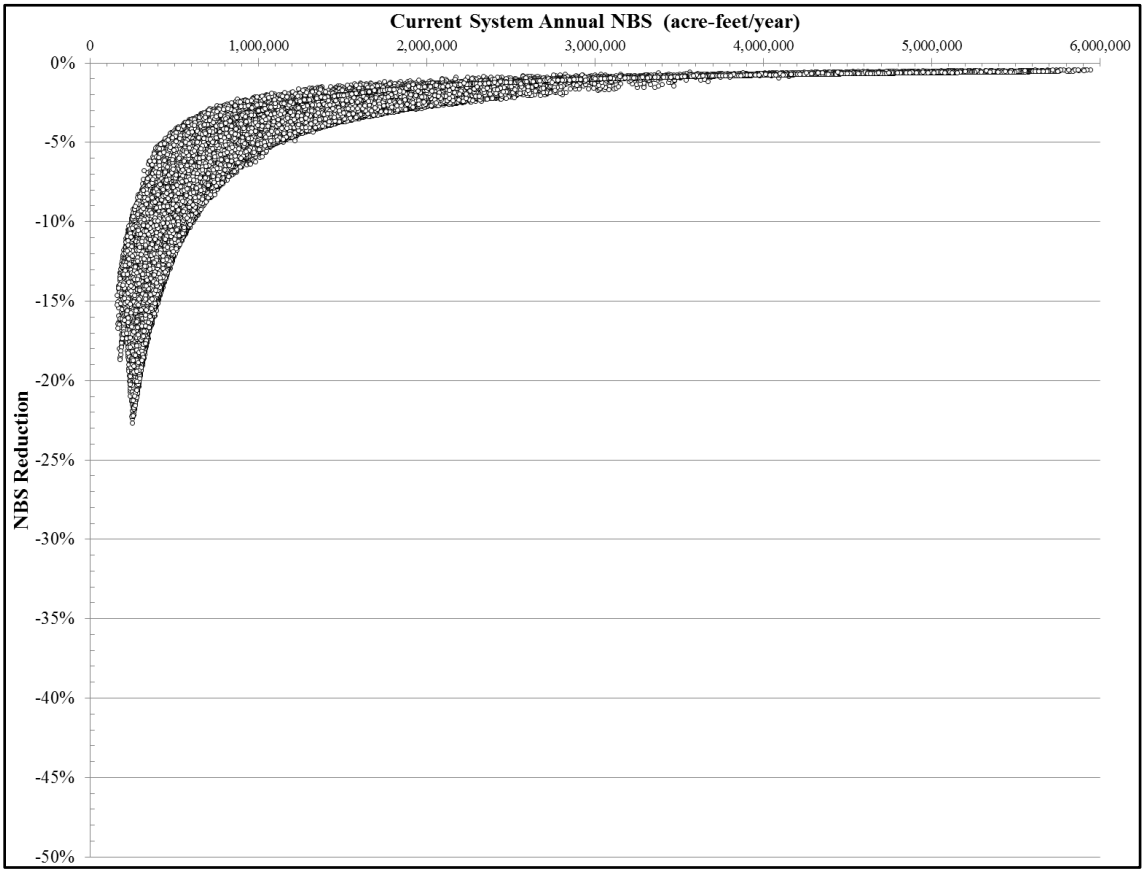

Figure 4.1.2. Distribution of NBS Reductions from Current Levels for the Most Likely Temperature Forecast.

The effects of precipitation variability are also nonlinear as was clear from the findings for precipitation elasticity of runoff, ε_p (Sec. 3.5.4). A given percentage precipitation change is amplified by nonlinear elasticity (although typically around 2.0) to create a runoff change as a component of total NBS. The amount of precipitation increase required to offset average temperature-induced NBS reductions at any level (or

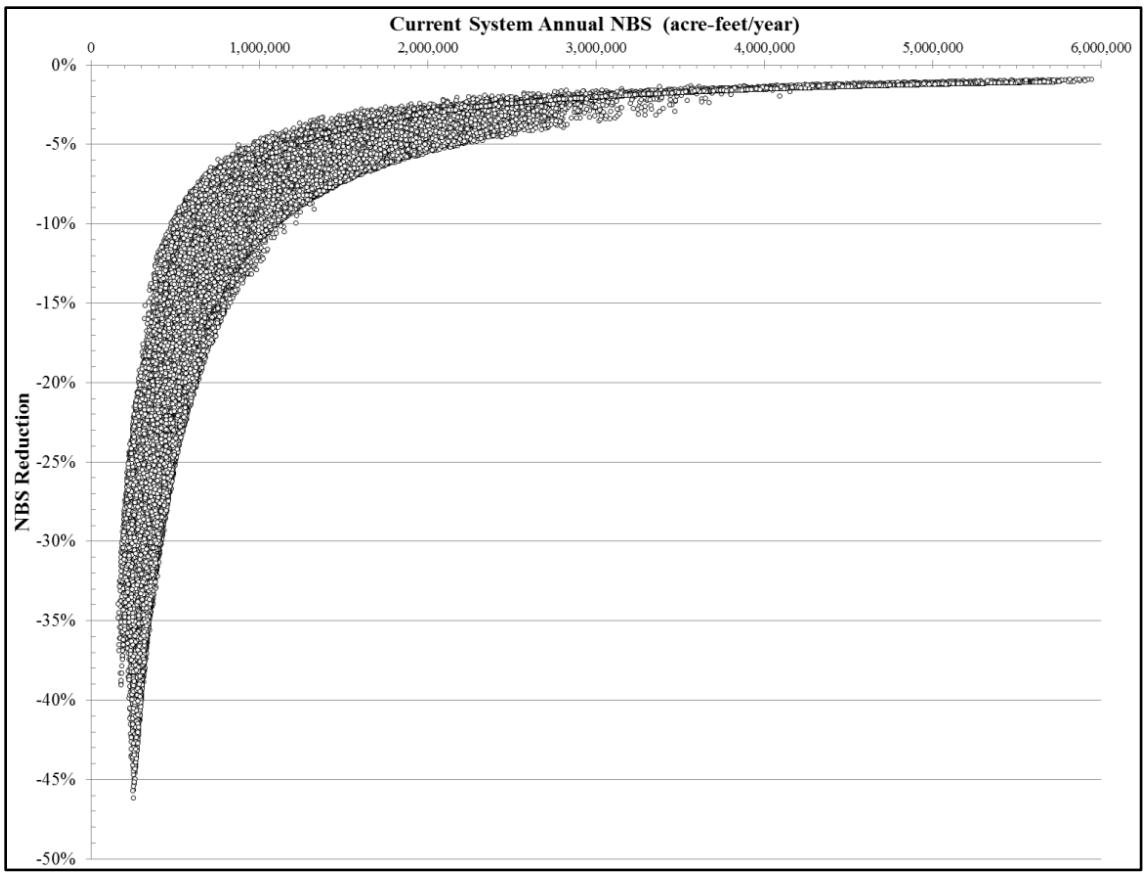

Figure 4.1.3. Distribution of NBS Reductions from Current Levels for the IPCC AR5 Temperature Projection.

any point in the distributions) can be solved for, and this was done at median NBS for the most likely temperature forecast, and is displayed in Figure 4.1.4. A uniform and modest 2.5% precipitation increase is sufficient to establish an equalizing offset. The effect of the temperature change on NBS from Figure 4.1.2 is reproduced in dark gray in Figure 4.1.4, and changes from a +2.5% precipitation change alone are shown in light gray. The net of the two acting together is shown in combination, which has a new and different nonlinear distribution. NBS levels below median tend to still show reductions, although with a widened distribution of outcomes. NBS levels above median, and certainly above the mean (~1.16MM), show an NBS increase up to a ceiling of about +3%. The same

analysis was conducted for the IPCC AR5 temperature change which can be offset at the median for ΔNBS=0 by a precipitation increase of approximately 5%. The scatter of those distributions is widened in both directions but of similar shapes to Figure 4.1.4.

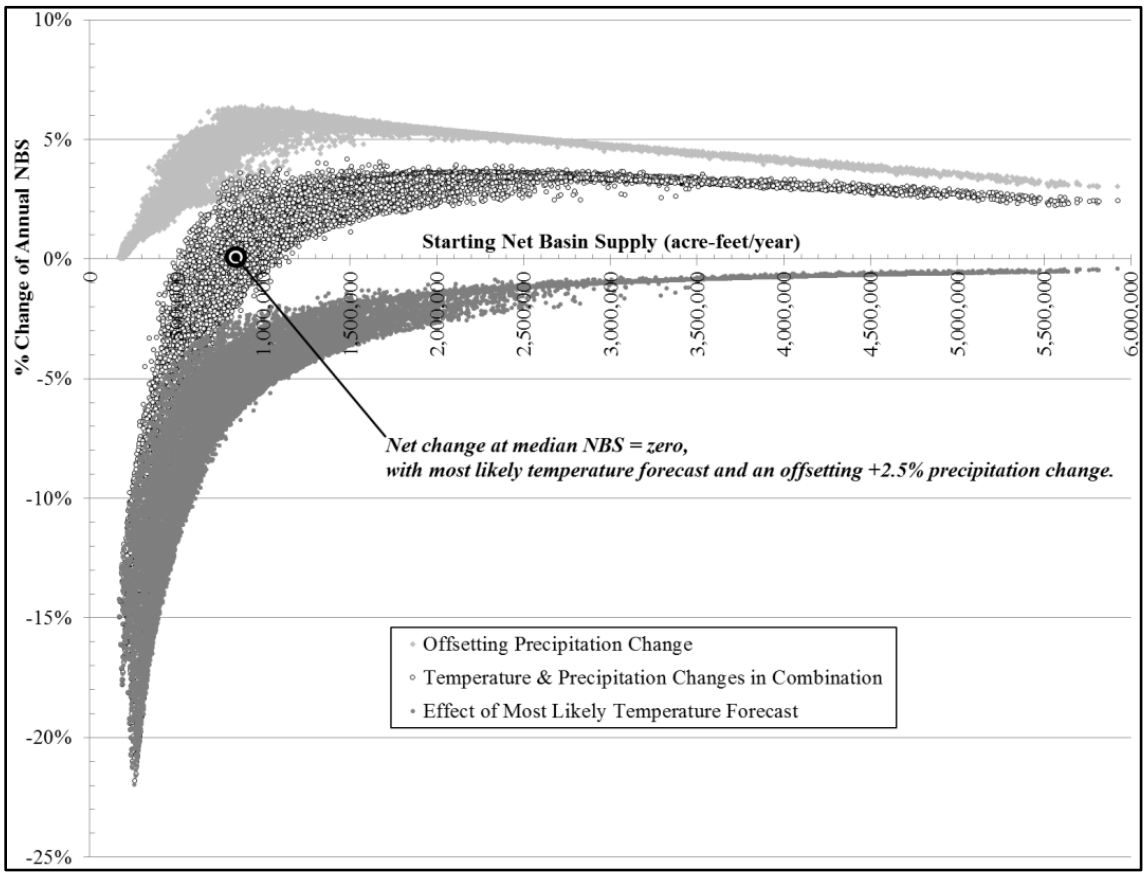

Figure 4.1.4. Change in NBS Due to the Most Likely Temperature Forecast (reduction), Due to an Offsetting +2.5% Precipitation Change (increase), and from the Temperature and Precipitation Changes in Combination.

One way that hydrologic research findings are sometimes reported is to identify lines of equivalent streamflow change across a field of temperature and precipitation changes. An example is reluctantly provided in Figure 4.1.5 with the caution that it is an incomplete over-simplification. The findings of this investigation make it readily apparent that doing so in a single plane at one NBS level is inadequate to the evidence.

Multiple planes in a third axis are required to capture the complexity, and each of those is a probabilistic function scaling with NBS having distribution breadth which can overlap the change examined.

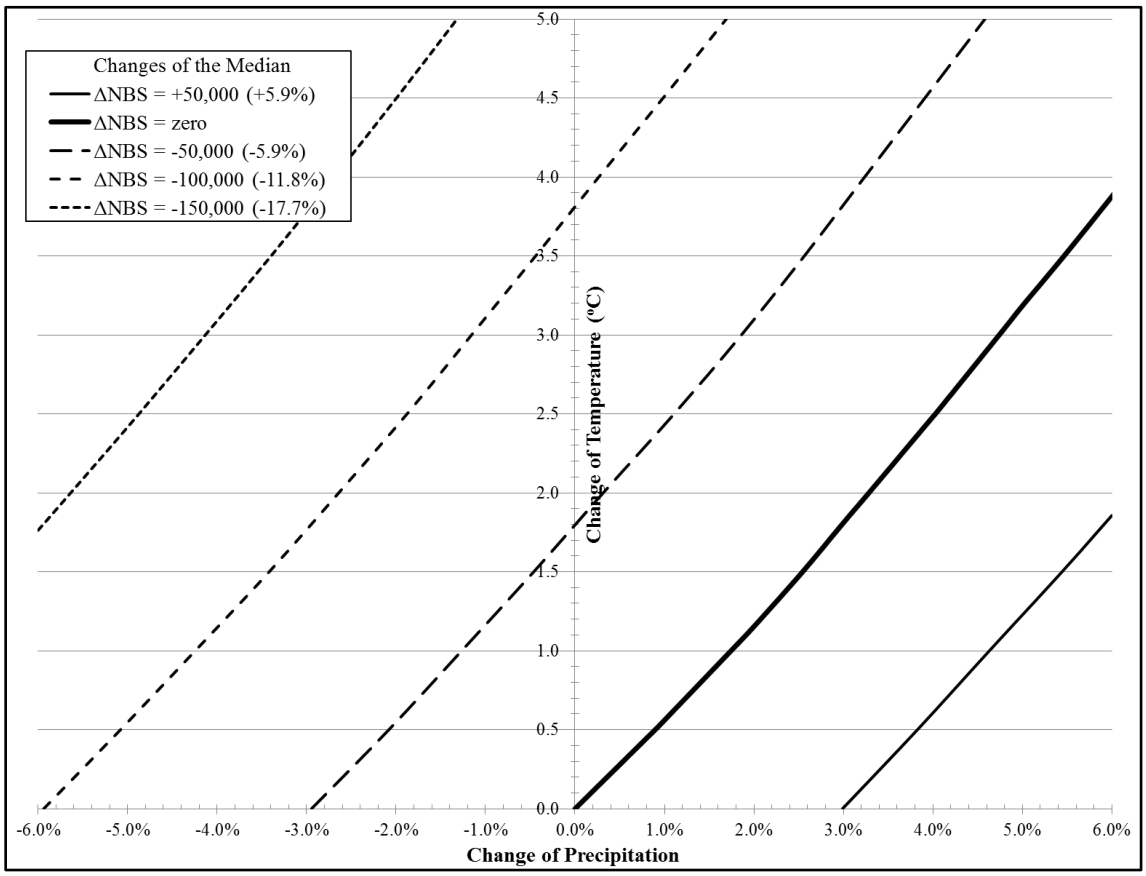

Figure 4.1.5. Lines of Constant NBS Change per Changes of Temperature and Precipitation. These apply ONLY relative to median NBS and at the center of the stochastic distribution.

Multiple ΔT-ΔP combinations are now available for ΔNBS=0 at the median which provides a quantification of offsetting average effects at one point in the distribution. These amounts of precipitation change which range only up to 5% can be compared to natural variability that was quantified in Figure 3.2.9 (30-year climate-normal precipitation). While there has been no long-term trend in precipitation, there

have been periods of temporal variability both above and below the long-term average. It was above early in the 20th century, below at mid-century, significantly above in the 1980s-90s, and now again below. The precipitation climate-normal values have ranged from -5% to +10%, with winter ranges being even wider. If and when above-normal levels again return, the precipitation change will be more than sufficient to offset the temperature change cases across most of the NBS distribution. Only at the lowest NBS and precipitation levels will a ΔP change be insufficient to offset temperature impacts. This is consistent with the explained variances from regression analyses using these climate variables. It therefore appears very likely that anticipated temperature changes of the future may be unresolvable and in question for their impact amidst natural precipitation variability.

4.2 Drought

The research questions motivating this investigation deal primarily with drought occurrence and its statistical properties. Multi-year periods of low flow within an NBS time series below a criterion level are of primary interest because they represent threatening time periods for the reservoir system that require detailed impact assessment. The following section provides a definition of drought relevant to the SRP system, identifies drought occurrences within the 120,000 years of stochastic simulation time series, and analyzes key drought characteristics before their impacts are interpreted through ResSim modeling.

4.2.1 Drought Definitions

In general, the onset and the end of a drought are notoriously difficult to determine specifically and, in retrospect, are usually defined relative to a particular impact. A wide variety of impacts arise due to drought, making it difficult to establish a single working definition having universal meaning. Consequently, a variety of criteria can often be applied to an instance, each having relevance for the specific impact under consideration. For this study consideration is only given to hydrologic drought relevant to the SRP system, referring to a period with deficient net basin supply of surface water that challenges ongoing management operations of the system. And, rather than simply conceptual, an operational definition is required if quantified comparisons are to be made for metrics such as drought frequency, severity, and duration (Mishra and Singh 2010). The basic element required for assessing drought metrics is a threshold level for the key relevant variable. With large natural variability inherent in NBS history and in expected simulation series, an explicit and consistent threshold is needed against which comparisons can be conducted. While thresholds may conceptually be a function of time or other changing conditions, the SRP system circumstances (fixed deliveries and operating rules) call for a fixed criterion to highlight periods of interest with an objective standard.

The total water delivery requirement of 900,000 acre-feet/year modeled in this study is satisfied by a mix of surface water and groundwater. The minimum groundwater pumping rate is 50,000 acre-feet/year when reservoir storage is full (Phillips et al. 2009), which is essentially the rate when pumping is at near-idle. This condition leaves the 850,000 acre-feet balance of delivery requirements to be satisfied by surface water. If

NBS is consistently 850,000 acre-feet/year or larger, then the reservoir system maintains or increases storage, surface water delivery requirements are met, and there is no drought. A drought threat exists if NBS remains below this level for a multi-year period over which reservoir storage would progressively decline. As noted in Table 3.4.2, the historical median annual NBS has been 836,000 acre-feet and the stochastic simulation 10,000-year medians range from 830,500 to 866,500 with an overall 120,000-year median of 849,500 acre-feet. When median supply approximately equals demand the system is well-matched to the watersheds supporting it. The analyses conducted for this report have therefore used an 850,000 acre-feet/year NBS criterion for drought threshold assessments.

The high year-to-year variability of the NBS time series (Figs. 3.4.17, 4.2.1) brings into question how to treat individual years above (or below) the threshold amidst a clustering below (or above) threshold. Should such occurrences define the end of a period to be evaluated or somehow averaged into adjacent years? Simple trailing averages could be applied, but those are length-dependent and still contain elements of variability affecting drought identification. This is particularly problematic when the threshold is in the middle of a highly skewed probability distribution, which is the case for the SRP system. Application of a decadal smoothing filter removes length-dependent variability and provides a smoothed series within which threshold crossings can be identified. This method was utilized in Ellis and Murphy (2012) with satisfactory results. However, the chosen frequency response of the filter can influence the temporal and amplitude character of the smoothed series and hence how a drought is categorized. A review of the drought literature did not reveal uses of averaging or smoothing methods,

instead finding run theory to be the commonly applied method for drought identification. It simply identifies sequences with all adjacent values in a time series below (or above) a critical threshold level (Mishra and Singh 2010). Therefore the analyses below use continuous runs-of-years below 850,000 acre-feet/year to identify a drought, which makes calculations from time series straightforward.

Once a run of years in drought is identified, the key parameters to be calculated are:

- Initiation time (first year of shortage).
- Termination time (first year after initiation that NBS is again above threshold).
- Duration, time during which NBS is below the threshold criteria (Termination time minus Initiation time).
- Severity: cumulative deficiency below the threshold level.
- Intensity: average value below the threshold level (severity divided by duration).
- Depth: minimum value below the threshold criteria in the duration.

The history of NBS by water-year is shown in Figure 4.2.1 where drought periods below the threshold criteria are indicated. Their height position is average NBS (intensity) during a drought. While 2016 water-year data is incomplete at the time of this writing, it appears annual NBS will be approximately 600,000 acre-feet if a typical summer occurs, and the current drought will have extended to its 6^{th} year. Over the 128 year instrumental record there will have been one 7-year, one 5-year, and two 6-year

droughts, for an occurrence rate of 3.125 droughts per century. No 4-year drought occurred, and 3-year droughts are not identified in Figure 4.2.1. SRP water operations staff has indicated that 3-year events are of little consequence, but they begin to be concerned after 4 years (personal communication). The analyses below are therefore concerned with drought durations 4 years and longer.

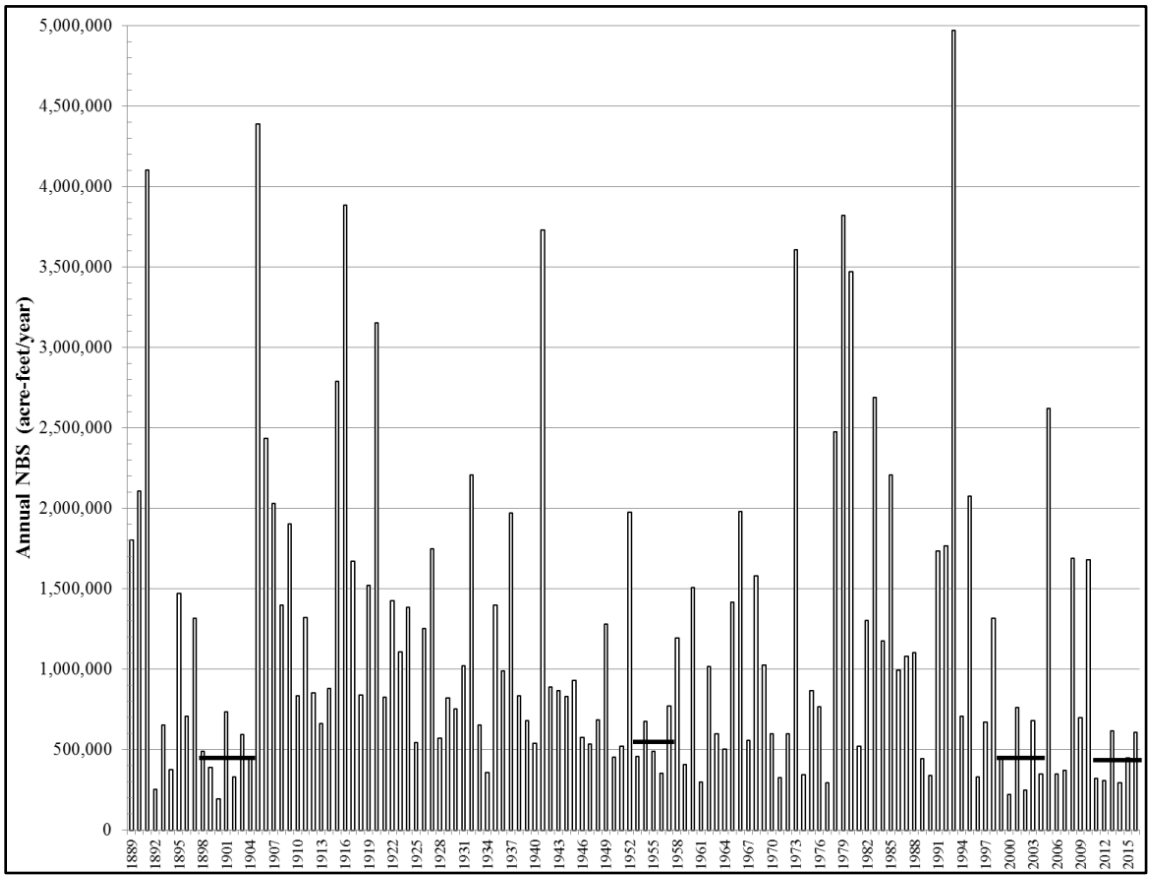

Figure 4.2.1. Droughts ≥4 years Duration and Their Intensity in the NBS Historical Record.

4.2.2 Drought Characterization

Probabilistic characterization is very important to any consideration of drought risk. Risk is typically defined as the probability of one or more defined events during a

stipulated timeframe, such as a decade, century or lifetime (Mishra and Singh 2011). Drought's probabilistic behavior can really only be analytically derived from long simulations assuming a certain stochastic structure of the underlying hydrologic system, since the historical record usually lacks sufficient occurrences of the phenomena of interest from which to make substantiated probability statements.

Drought is a multivariate event characterized by its duration, intensity, and depth which can be correlated in some fashion (Mishra and Singh 2011; Katz 2010). Portrayal of their joint characteristics is therefore an informative analytical tool as shown in Figures 4.2.2 and 4.2.3. All droughts from the 120,000-year simulation of the current system are shown, in comparison to those from the historical record. It is readily apparent that the instrumental record is a limited random sample from what could have occurred. The longest drought found in the stochastic simulation of the current system was 16 years in duration, but its probability of occurrence is a vanishingly small 0.083%/century. Most drought durations are $\leq$ 11 years, similar to the longest identified in the tree ring record (Hirschboeck and Meko 2005, 2008). The simulation of a long 120,000-year series has enabled the assessment of very small probability events. It is interesting to note that the intensity and depth of long droughts are consistent with asymptotes identifiable from probability distributions in shorter drought data. The next sections of this document quantify the probability distributions of drought duration, intensity and depth.

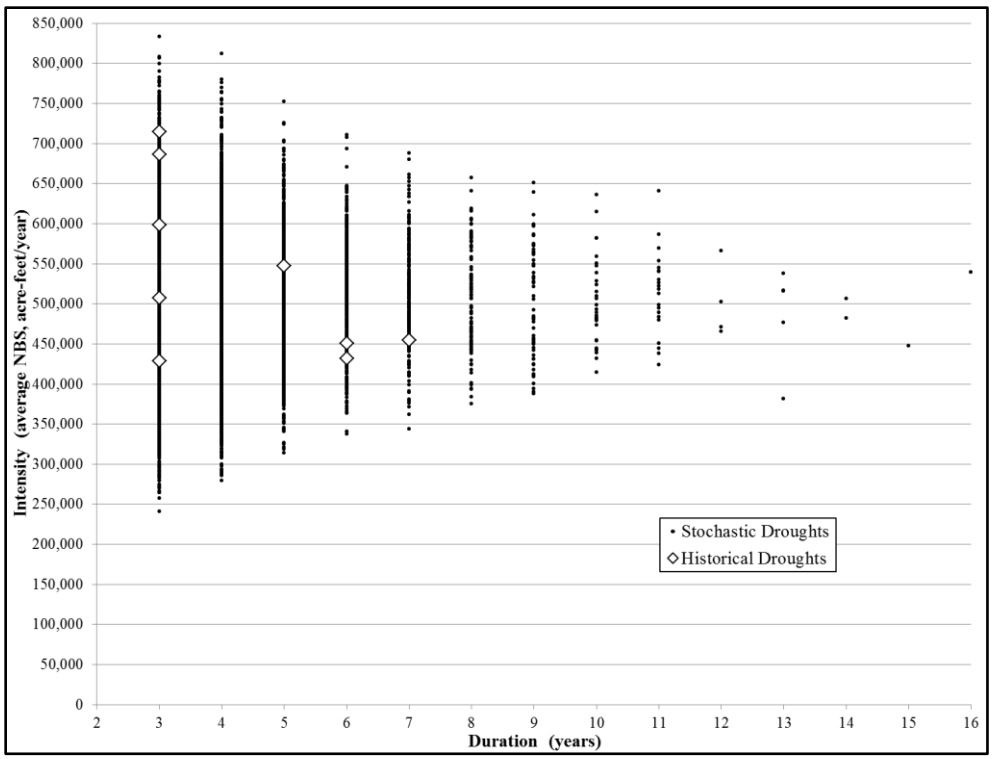

Figure 4.2.2. Duration and Intensity of Historical and Stochastically Generated Droughts (current system case).

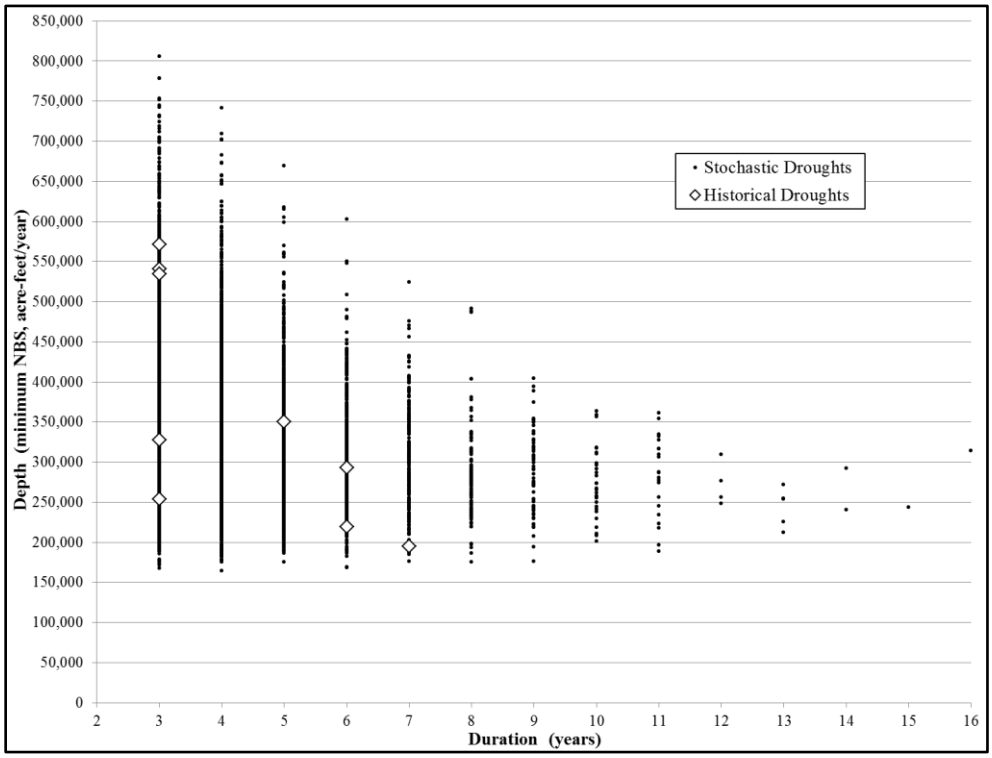

Figure 4.2.3. Duration and Depth of Historical and Stochastically Generated Droughts (current system case).

4.2.2.1 Probability Functions, Duration

Statistical modeling methods from extreme value theory can be applied to illuminate the probabilistic character of drought parameters (Gumbel 1958; Coles 2001; Katz 2010; Mishra and Singh 2011; DeGroot and Schervish 2012). A review of examples in the literature comes to the central observation that the probability of the number of drought occurrences within a time interval is described by the Poisson distribution, which is related to the exponential distribution that describes the probability distribution of time until a drought occurrence.

Three conditions of a random variable must be met for these probability functions to apply:

1) The number of occurrences in any two disjoint intervals of time must be independent of each other. (This condition is satisfied by noting that there is zero autocorrelation in the historical runoff time series and outcomes are i.i.d. (independent and identically distributed). There is no memory in the system, and a drought period can be expected to occur independently of other droughts.)
2) The probability of an occurrence during any particular very short interval of time must be approximately proportional to the length of that interval. (The chance of a drought occurrence is clearly lessened as one considers smaller and smaller time frames.)
3) The probability of two or more occurrences in any particular very short interval of time must be of a smaller order of magnitude than the probability of just one occurrence. (A drought is rarer as the time period under consideration is shortened, and the chance of more than one occurrence is significantly rarer still.)

This application of the Poisson distribution to phenomena occupying a finite time interval of several years is unique, but valid, so long as drought occurrence is i.i.d and sufficiently infrequent within a 100-year timeframe that droughts do not influence one another. The i.i.d. conclusion at the annual level based upon stationarity analysis and as embodied in the stochastic simulation methodology is sufficient to establish that a sequence of drought years is also i.i.d. Sample statistics compiled to date are sufficient to demonstrate the relatively low occurrence frequencies for the hydrologic droughts of interest (Fig. 4.2.1). The probability of one occurrence is independent of all others and therefore of where in the series it is considered; so, the statistics analyzed here apply at any point in the time series. To confirm that the findings of this investigation do conform to this assumption, statistics of all drought occurrences that arose across the 120,000 year simulation of the current system are compared to theoretical expectations from the NBS p.d.f. (Fig. 4.1.1). Each sequential simulation year is generated from the p.d.f. having a median matching the drought threshold (850,000 acre-feet). So, theoretically, the probability of the next year being in drought is 0.50, the probability of two more years in drought is 0.50^2, three more years is 0.50^3 , …, to 0.50^n for n years ahead. As can be seen in Figure 4.2.4, the simulation outcomes closely track this expectation, confirming i.i.d. drought outcomes. Water management may employ this simple calculation to assess the probability of a continuing drought based upon any drought definition in comparison to the NBS p.d.f.

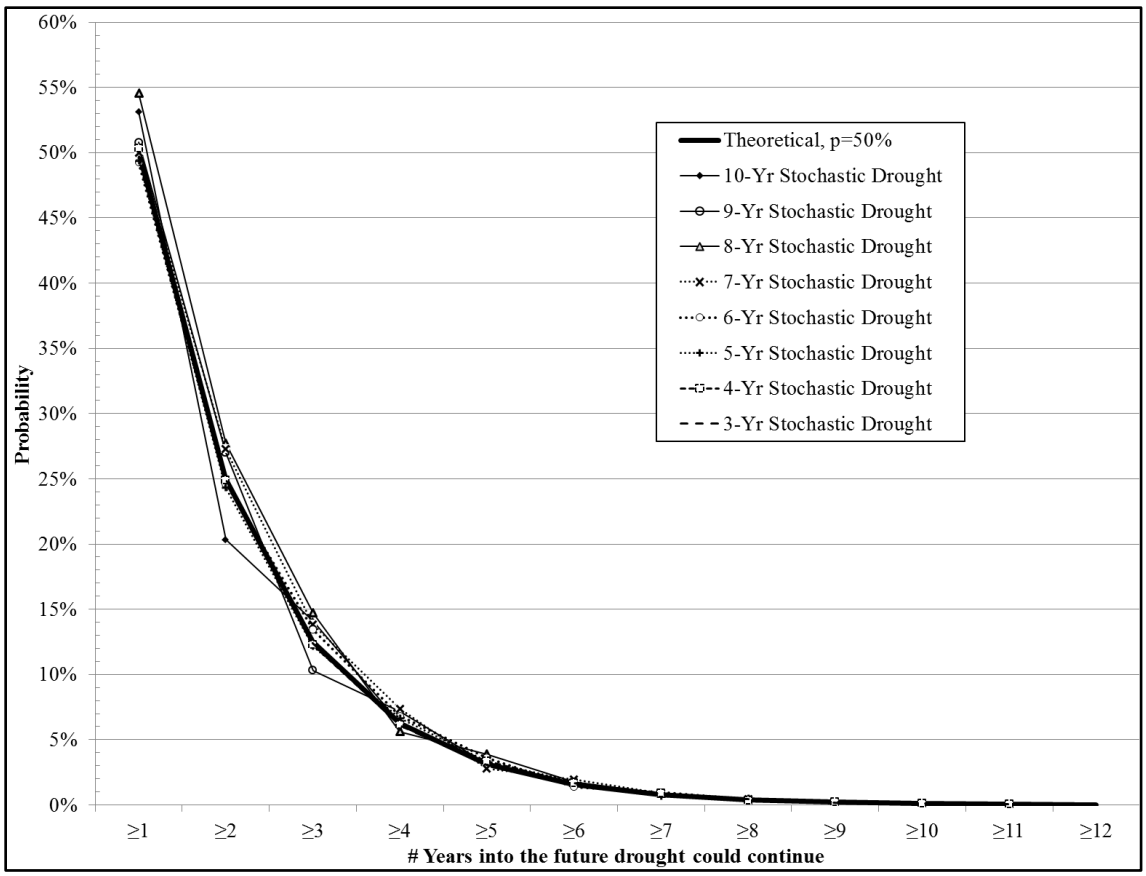

Figure 4.2.4. Expected Probability of a Continuing Drought Compared to Statistics from Stochastically Generated Droughts; Drought Threshold and NBS Median = 850,000 acre-feet.

A Poisson process is distributed as:

$$f(x|\lambda) = e^{-\lambda} \lambda^{x} / x! \quad \text{for positive integers } x = 0, 1, 2, \ldots \tag{4.1}$$

where it can be shown that the mean, E(x), and the variance, Var(x), are equal to the parameter, λ.

The exponential distribution is:

$$f(x|\beta) = \beta e^{-\beta x} \quad \text{for all } x > 0 \tag{4.2}$$

where it can be shown that the mean, E(x), and the standard deviation StDev(x) are equal to the inverse of the parameter, $1/\beta$. By an integral of this equation from any time, t, to ∞ it can be shown that the probability distribution of time until an occurrence is described by $\Pr(x \geq t) = e^{-\beta t}$ for all $t > 0$ (4.3)

The Poisson and exponential probability functions are closely related through λ and β, each of which is essentially a representation of average time until occurrence of a drought. Values for these parameters were derived from the drought population in the current system's stochastically generated time series. λ_n as a function of two expressions of duration are shown in Figure 4.2.5. λ_n can be calculated from the data for a specific duration, n, or it can be calculated for all droughts of duration ≥ n. They are additive in n and have a similar functional relationship. To simplify presentation of results, obtain larger sample sizes for statistical testing, and align with how drought is often considered, most calculations herein are presented in terms of duration ≥ n years.

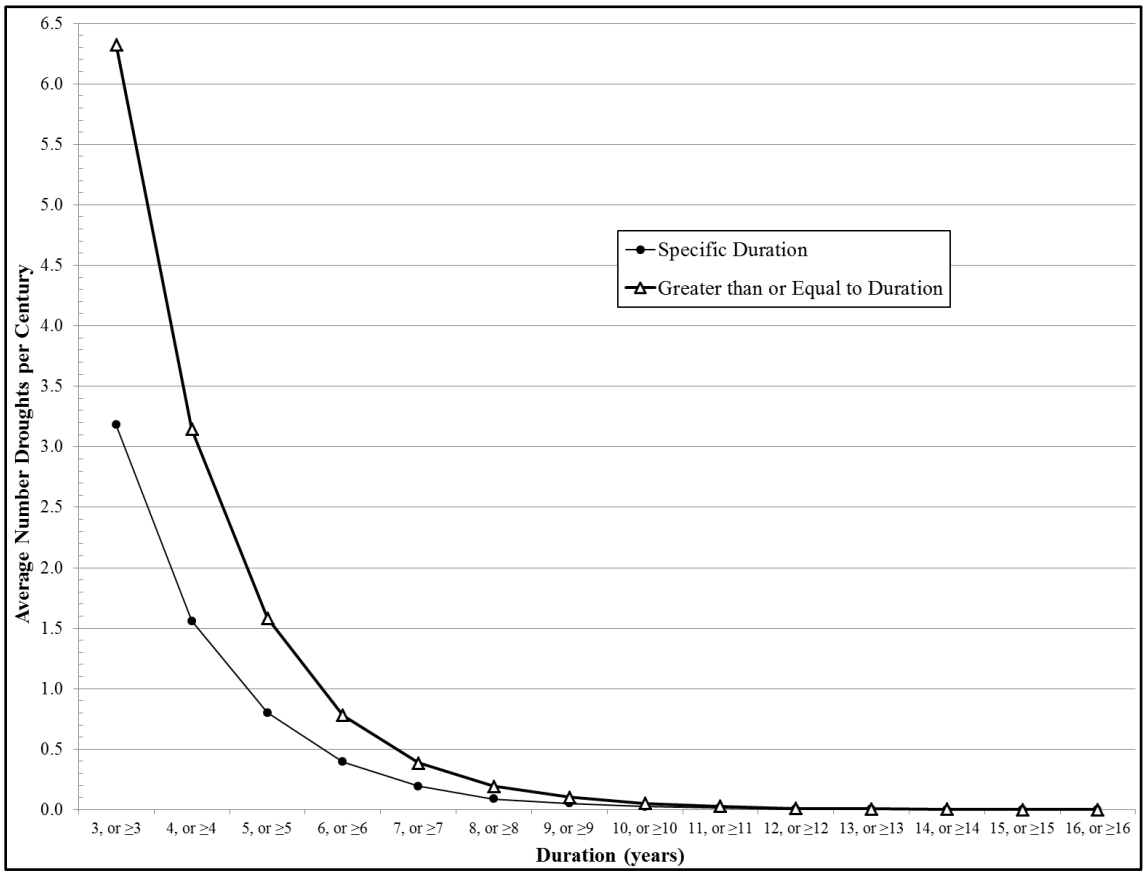

Figure 4.2.5. Current System Poisson Parameter, λ (average number of droughts per century), as a Function of a Specific Duration and as ≥ Duration.

All drought parameters were calculated from the 120,000-year current system simulation and then were recalculated for simulations of the most likely temperature forecast and the IPCC AR5 temperature projection. The calculated Poisson parameters are tabulated in Table 4.2.1. The Poisson parameter curves for the three cases are given in Figure 4.2.6, showing marginal increases in the average number of droughts per century as temperature increases.

Table 4.2.1. Poisson and Exponential Distribution Drought Parameters: λ_n (average number of occurrences per century) and $1/\beta_n$ (average time to occurrence), Calculated from the Three 120,000-Year Stochastic Simulation Cases.

	Mean Number of Droughts per Century									
Drought Duration (yrs)	≥3	≥4	≥5	≥6	≥7	≥8	≥9	≥10	≥11	≥12
Current System	6.33	3.14	1.58	0.78	0.39	0.19	0.11	0.05	0.03	0.01
Most Likely Forecast	6.86	3.53	1.87	0.96	0.50	0.27	0.14	0.08	0.04	0.02
IPCC AR5 Projection	7.39	3.99	2.18	1.17	0.62	0.34	0.19	0.11	0.06	0.03

	Mean Time to Drought Occurrence (years)									
Drought Duration (yrs)	≥3	≥4	≥5	≥6	≥7	≥8	≥9	≥10	≥11	≥12
Current System	16	32	63	128	260	519	952	1875	3529	9231
Most Likely Forecast	15	28	54	104	200	377	719	1290	2308	5455
IPCC AR5 Projection	14	25	46	85	160	293	533	938	1690	3429

With values of λ_n for all durations having been identified, the Poisson process probability function was applied to the three simulation cases to calculate the probability of any number of drought occurrences of any duration in a century (Table 4.2.2). Longer droughts are likely to occur more rarely within a century relative to the shorter ones and the Poisson formulation allows this to be quantified. Table 4.2.2 can be employed by water management for drought risk decision-making. For example, if the decision is taken to accept a 5% drought risk level over the coming century then the system should

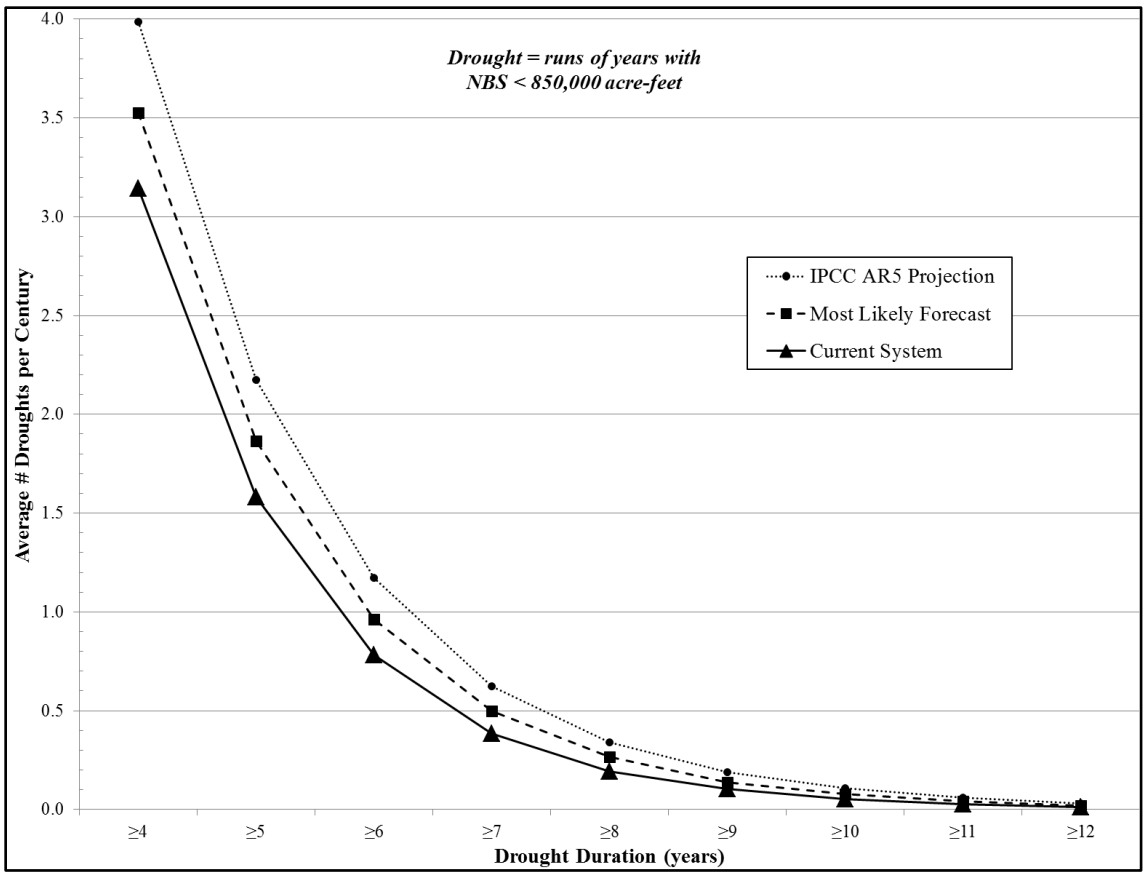

Figure 4.2.6. Drought Poisson Parameter, λ_n, from the 120,000-Year Stochastic Simulation; for the Current System, the Most-Likely Temperature Forecast, and the IPCC AR5 Temperature Projection.

be managed in anticipation of any combination of six droughts ≥4-years, four (of the 6) ≥5-years, two (of the 6) ≥7-years, and one drought (of the 6) ≥ 10-years. When considering a future temperature increase, the probabilities increase by 1% to 4% across the matrix of Table 4.2.2 for the most likely temperature change forecast. Similar marginal increases occur for the AR5 temperature change projection relative to the most likely forecast. Using this risk matrix, water management can adopt a climate expectation of their choosing and plan for the number of drought occurrences by duration per their risk comfort level. But, since temperature change forecasts contribute only

small incremental probability differences, a planning guideline is relatively insensitive to temperature expectations. The same set of decisions would probably be taken regardless of temperature forecast. For example, the decision might simply reduce to planning for a 5% chance of a 10- or 11-year drought over the next century along with an expectation of a few 5- to 8-year droughts.

Table 4.2.2. Probability of the Number of Drought Occurrences in a Century by Duration; for the Current System, the Most Likely Temperature Forecast, and the IPCC AR5 Temperature Projection.

	# Occurrences	Drought Duration (years)								
	per Century	≥ 4 Yrs	≥ 5 Yrs	≥ 6 Yrs	≥ 7 Yrs	≥ 8 Yrs	≥ 9 Yrs	≥ 10 Yrs	≥ 11 Yrs	≥ 12 Yrs
CURRENT	0	4%	21%	46%	68%	82%	90%	95%	97%	99%
SYSTEM	1	14%	33%	36%	26%	16%	9%	5%	3%	1%
	2	21%	26%	14%	5%	2%	0%	0%	0%	0%
	3	22%	14%	4%	1%	0%				
	4	18%	5%	1%	0%					
	5	11%	2%	0%						
	6	6%	0%							
	7	3%								
	8	1%								
MOST LIKELY	0	3%	15%	38%	61%	77%	87%	93%	96%	98%
FORECAST	1	10%	29%	37%	30%	20%	12%	7%	4%	2%
	2	18%	27%	18%	8%	3%	1%	0%	0%	0%
	3	21%	17%	6%	1%	0%	0%			
	4	19%	8%	1%	0%					
	5	13%	3%	0%						
	6	8%	1%							
	7	4%	0%							
	8	2%								
IPCC AR5	0	2%	11%	31%	54%	71%	83%	90%	94%	97%
PROJECTION	1	7%	25%	36%	33%	24%	16%	10%	6%	3%
	2	15%	27%	21%	10%	4%	1%	1%	0%	0%
	3	20%	19%	8%	2%	0%	0%	0%		
	4	20%	11%	2%	0%					
	5	16%	5%	1%						
	6	10%	2%	0%						
	7	6%	1%							
	8	3%	0%							

The differences in Poisson parameters among the two temperature change cases and the current system can be tested for statistical significance to ascertain whether the methodology has, in fact, revealed an impact to the number of drought occurrences.

While this could be done on the basis of λ_n values for each of the dozen 10,000-year sequences, a normality assumption is important when sample size is just 12. λ_n values are small and bounded by zero which places normality in question. The test is therefore instead conducted for the mean number of droughts in a 10,000-year sequence so that t-statistic hypothesis testing may be applied. The number of droughts for all dozen sequences by duration and for the three temperature cases is given in Table G2 of Appendix G. The table shows the t-statistics that were calculated for hypothesis tests of whether the mean number of droughts is different between temperature cases. The null hypothesis is rejected for drought durations out to approximately ≥11 years (95% confidence level). Droughts longer than this from the stochastic simulation are so few in number (<30 in 120,000 years) that it is not possible to test whether their mean rate of occurrence has changed between climate cases. But, as discussed above, the risk of those droughts to water operations is sufficiently small that they are not a major issue. The higher-risk drought events (up to ~11 years) are shown by the hypothesis tests to occur with greater frequency under the most likely temperature forecast and the IPCC AR5 temperature projection. Their differences in Poisson parameter values may therefore be considered statistically significant.

As discussed above, another way to examine drought occurrence statistics is by the time between droughts, which is exponentially distributed. The corresponding exponential parameter values (average time to a drought occurrence, $1/\beta$) are given in Table 4.2.1. Some probability distributions are calculated per $1/\beta_n$ and displayed in Figure 4.2.7 with average time to occurrence noted. As can be seen, the average time to occurrence alone is an incomplete representation of possible outcomes because, for any n,

the probability of occurrence within a shorter time interval is higher than at the average periodicity. This is accentuated for the shortest duration droughts, but long duration droughts have lower and more uniform probability distributions in time, resulting in an increasingly longer average return period.

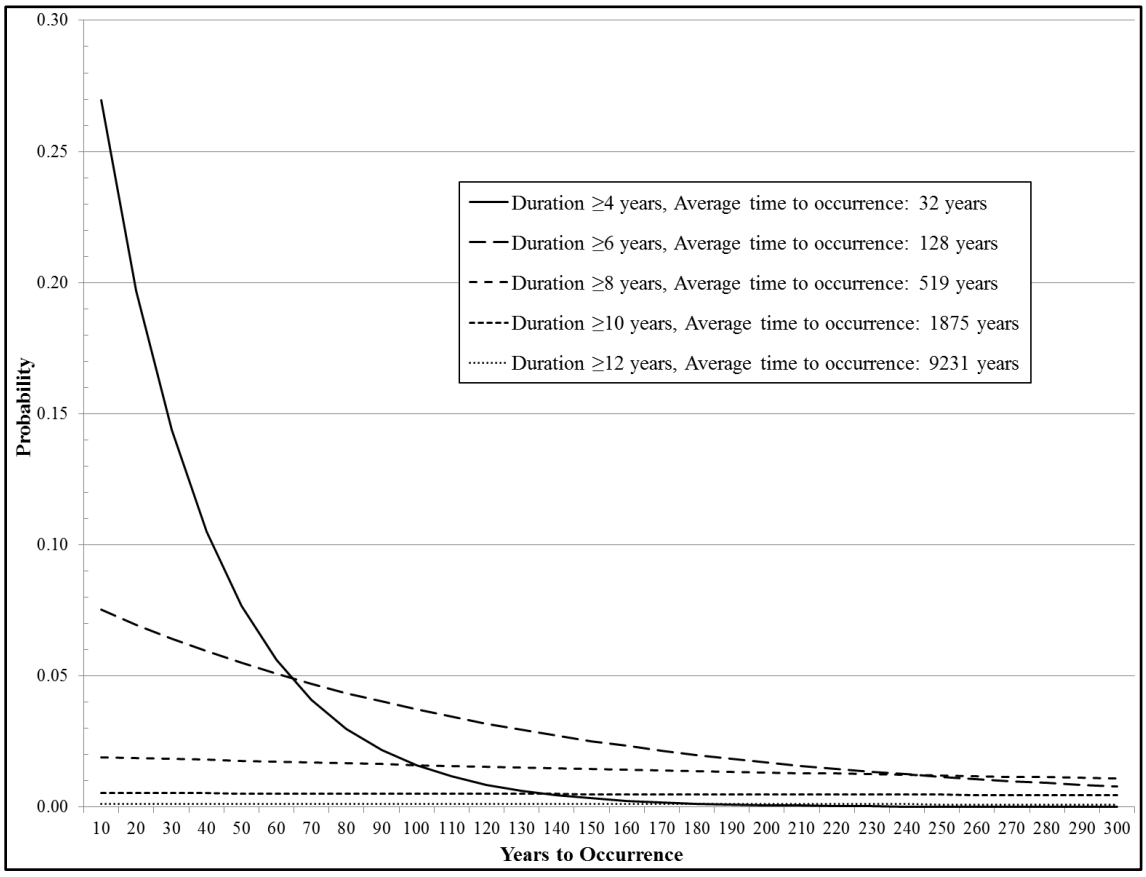

Figure 4.2.7. Exponential Probability Distributions of Time to Occurrence of Various Duration Droughts.

As for the Poisson parameter, exponential distribution parameters were also calculated for simulations of the most-likely temperature forecast and the IPCC AR5 temperature projection. The probability distribution results for duration ≥5 and ≥9 years are shown in Figure 4.2.8. While average time to occurrence shortens with increasing

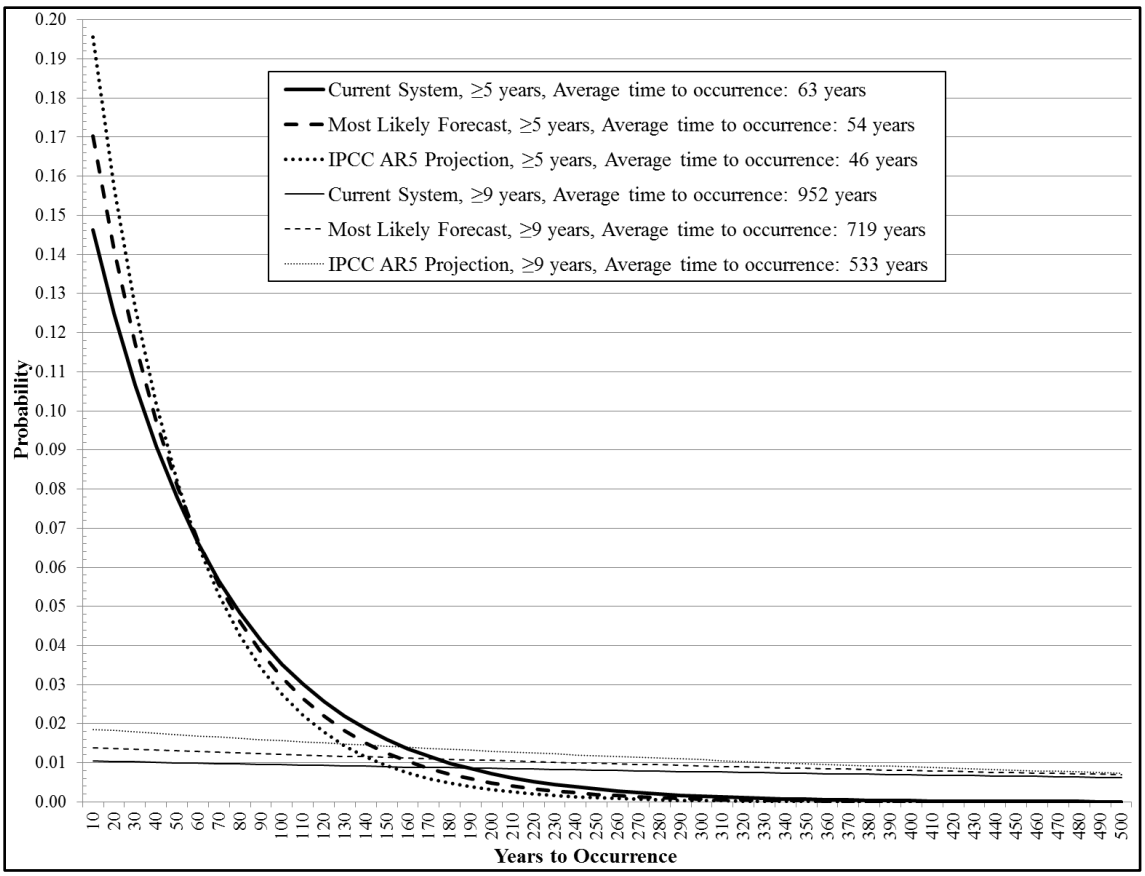

Figure 4.2.8. Exponential Probability Distributions of Time to Occurrence of a Drought ≥5 and ≥9 Years for the Current System, the Most-Likely Temperature Forecast, and the IPCC AR5 Temperature Projection.

temperatures, the shifts in probability distribution are non-uniform. Shorter horizon probabilities rise, but longer horizon probabilities fall. This characteristic diminishes with long-duration, rarer drought such that their probability by time horizon is uniformly small with weak temperature dependence. All values of λ_n and $1/\beta_n$ for the three temperature cases are given in Table 4.2.1 and graphically compared in Figure 4.2.9. By examination of Figure 4.2.9 at any level of either λ_n or $1/\beta_n$ the sensitivity of duration between the temperature curves is seen to be small. At most, the impact is a difference of only one year in drought duration. Taken together with the observations above on risk

data in Table 4.2.2, the variability in actual drought outcomes over the course of a century is likely to be similar to or even larger than the change induced by increasing temperatures. Managing for variability will therefore also address the drought impact of any future temperature increase.

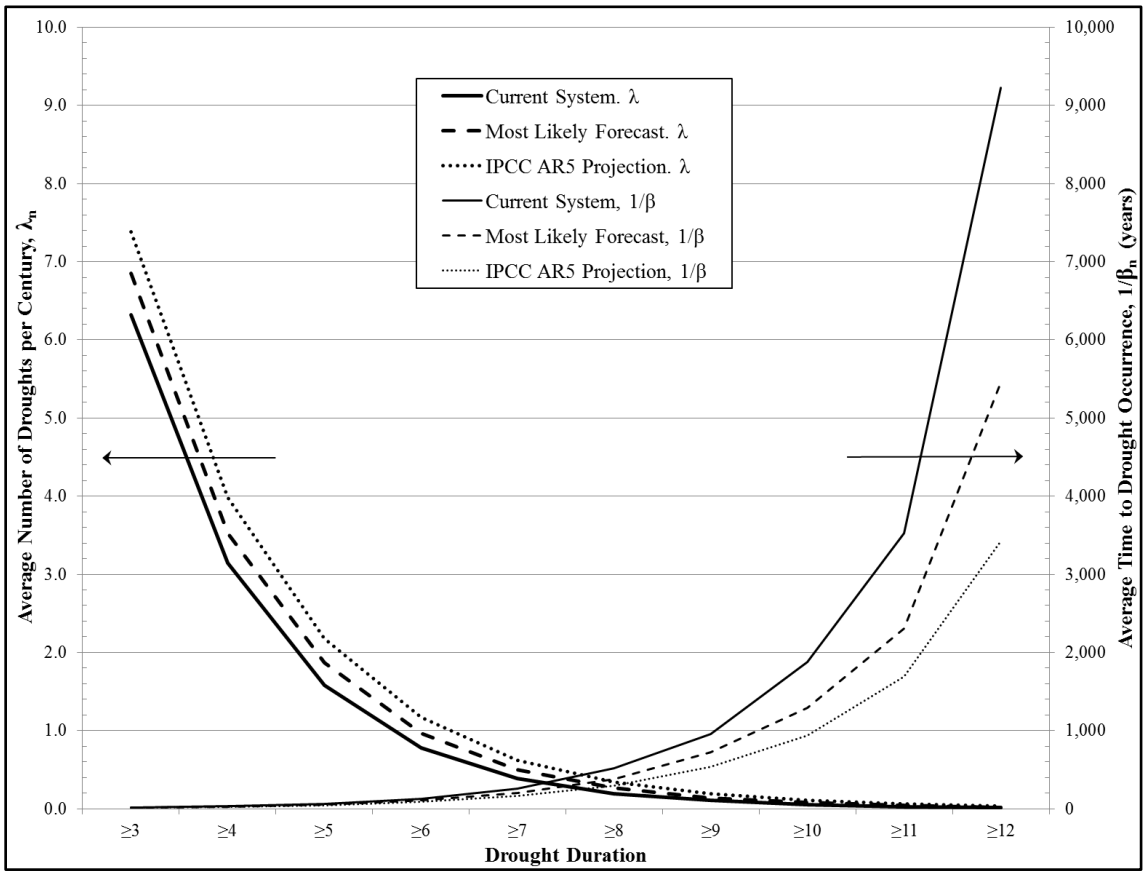

Figure 4.2.9. Poisson and Exponential Distribution Parameters: λ_n (average number of occurrences per century) and $1/\beta_n$ (average time to occurrence), for the Three Temperature Cases.

4.2.2.2 Probability Functions, Intensity and Depth

The preceding analyses on the basis of duration in Figures 4.2.6 to 4.2.9 are representations for all severities of drought. Katz (2010) suggests that severity can also be analyzed simultaneous with duration to achieve a full, dual-variable characterization

of drought events. The dozen 10,000-year series were developed in this study to have sufficient simulation data to achieve such a characterization. The severity dimension of drought is mathematically represented by intensity (average NBS below the threshold level; intensity times duration = severity), and it can also be instructive to examine drought depth (minimum annual value below threshold). The distributions of drought in these dimensions were shown above in Figures 4.2.2 and 4.2.3 for the current system case. It is readily apparent that drought intensity is symmetrically distributed about a common central value at all durations and a narrowing variance with increasing duration (Fig. 4.2.2). Drought depth variance also declines with duration (Fig. 4.2.3), but the distribution is upwardly skewed with a low bounding value. Mean/median depth declines with increasing duration. There is sufficient structure evident that these distributions were analyzed to identify their functional forms. Their key statistics are compiled in Table G3 of Appendix G and graphically displayed in Figures 4.2.10 (intensity) and 4.2.11 (depth).

The drought intensity data distributions were tested and found to be, for the most part, normally distributed. The only exceptions are in the low tail of the distributions for short duration droughts. Those tails are bounded so that normality is slightly distorted in the lowest 5^{th} percentile. The longer duration drought distributions do not display this effect. Means of the distributions across duration were tested to find them all statistically equivalent. There is, however, a downward trend in standard deviation with duration as can be seen in Figure 4.2.10 that can be readily described by a linear fit. Considering the behavior across duration, it is very feasible to assign a parameterized normal distribution, N(*mean*, $S_x(D)$), to the intensity variable.

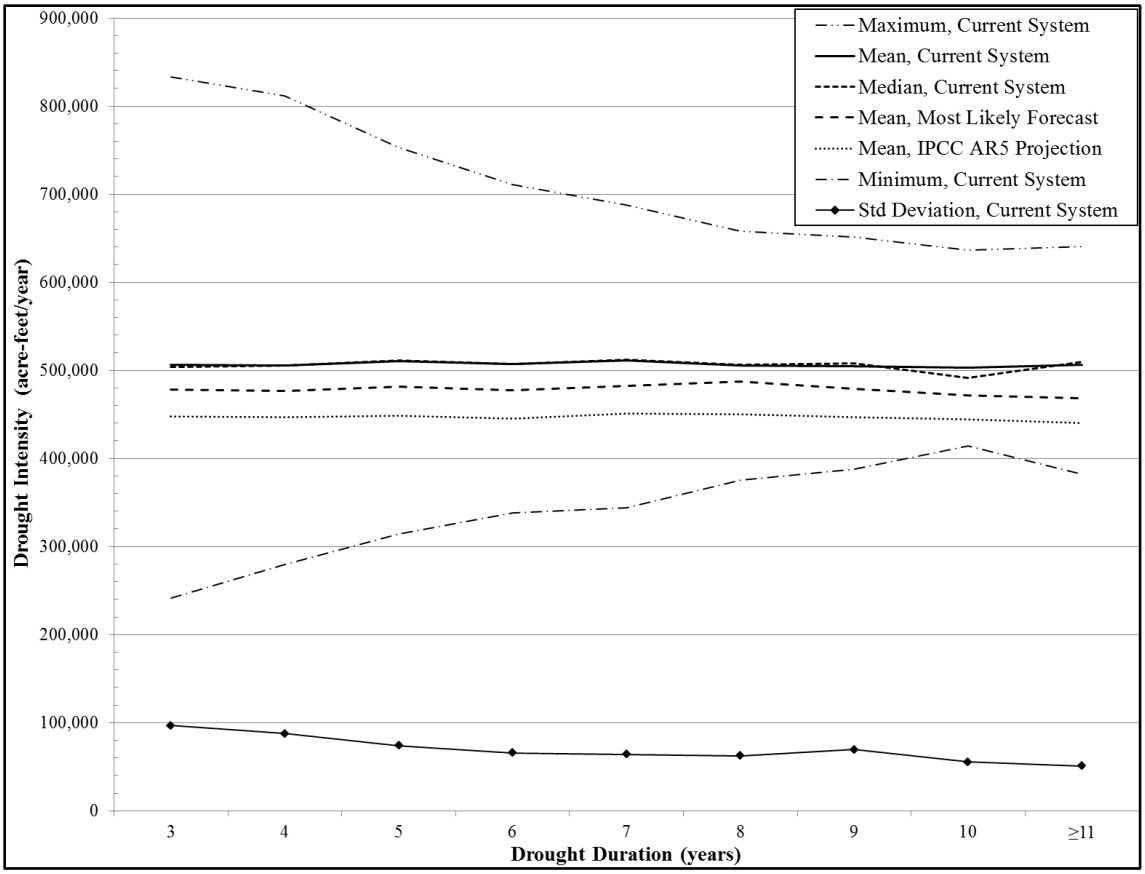

Figure 4.2.10. Distribution of Drought Intensity as a Function of Duration. Mean intensities are also shown for the most likely temperature forecast and the IPCC AR5 temperature projection.

The drought depth data distributions were also tested but found to not be normally distributed. As shown in Figure 4.2.11 (and Fig. 4.2.3), the distributions are skewed upwards and their behavior can be represented by a gamma distribution, a two-parameter family of continuous probability distributions. The two descriptive parameters for the gamma function, shape and scale, can be established by fit to empirical distributions. Those will also be a function of duration as indicated by Figure 4.2.11. So, as for intensity, the depth probability distribution can be readily parameterized. The stochastic linkage between intensity and depth is then all that remains to have established a complete statistical characterization of drought in its key dimensions.

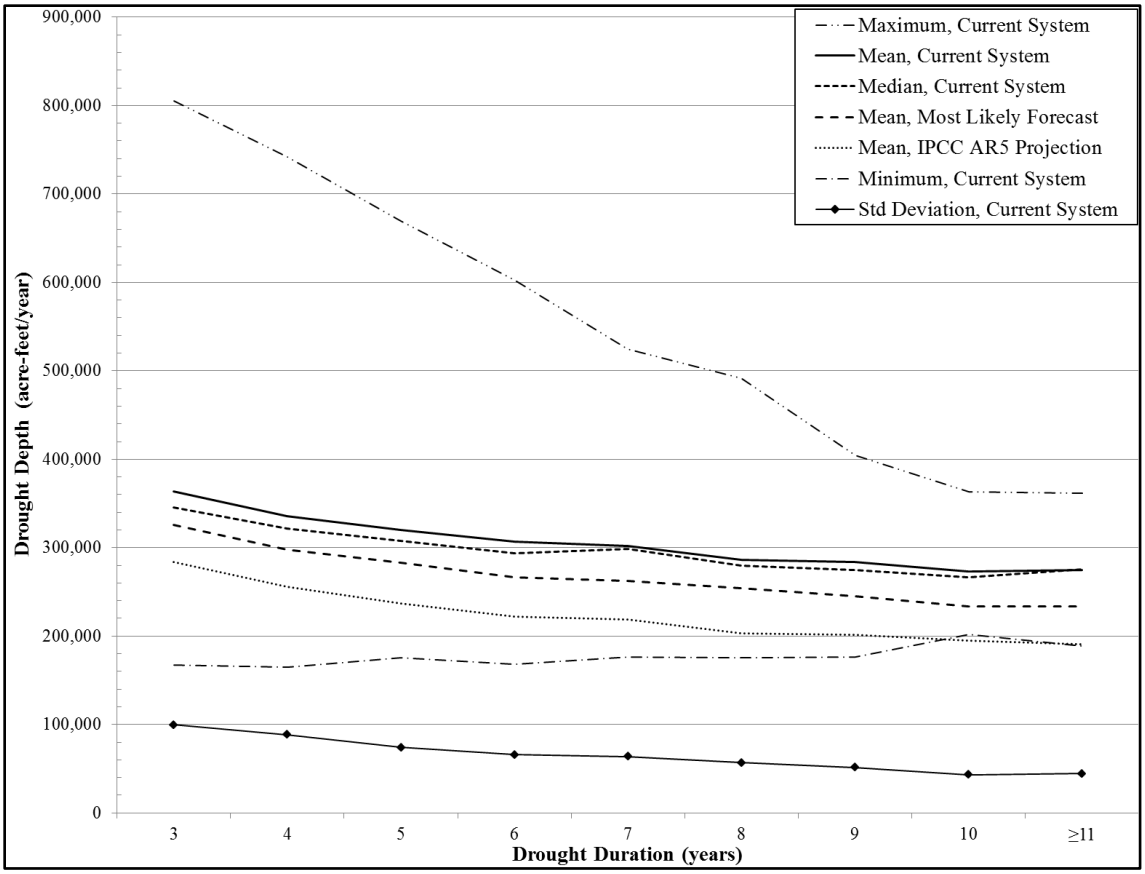

Figure 4.2.11. Distribution of Drought Depth as a Function of Duration. Mean depths are also shown for the most likely temperature forecast and the IPCC AR5 temperature projection.

4.2.2.3 Discussion

There is a temperature dependence of severity which is shown in Figures 4.2.10 and 4.2.11 for the most likely and IPCC AR5 cases in comparison to the current system behavior. The intensity and depth distributions shift downwards with increasing temperature. The hypothesis testing for the difference-of-mean between cases is documented in Table G3 of the appendix, and changes are shown to be statistically significant. An interesting result occurs when the offsetting precipitation change discussed in Section 4.1 is also applied (+2.5% with +1.5^{o}C, +5% with +3.1^{o}C). Drought occurrences by duration return to numbers similar to the current system case before

temperature changes were applied, such that changes in Poisson parameter are no longer statistically significant. However, drought intensity and depth are still adversely affected. Even with complex nonlinear effects, the increased risk of drought occurrence from ΔT can be reversed by an offsetting ΔP. But, when a drought does occur it will still be a more severe one. This result can be traced to the way the offsetting values interact. The offsetting values were calculated to balance at the median as shown in Figure 4.1.4. Temperature impairment primarily has its impact on the NBS distribution below the median, its effect diminishing at higher NBS. Precipitation change effects occur with an opposite influence, enhancing NBS above the median. Hence, each sequential year has a 50/50 chance of being either more influenced by ΔT or by ΔP. Since the drought threshold criteria has the same value as median NBS the stochastic outcomes for runs of years returns to probabilities as they were before ΔT was applied, and drought risks return to the current system case. When a stochastically generated year is from the lower part of the distribution it will be impaired by the temperature change with less precipitation change influence. Hence the same runs of drought years will occur (although perhaps at different locations in the time series) but with lower NBS. So, droughts will be more severe than for the current system case. ΔT-ΔP combinations balancing each other at other positions in the distribution obviously have different implications, and the choice of what constitutes a drought also bears upon the results. These are not stochastic simulation artifacts. The methodology and the specific hydrologic sensitivities are representing the variable nature of the watersheds and illuminating natural complexities of the system.

For the purpose of assessing hydrologic impacts of climate change, the relationships of the key drought descriptors – duration, intensity, depth – to rising temperatures can now be statistically expressed upon a set of underlying deterministic assumptions. Whether then, from a hydrological science standpoint, temperature impacts should be considered nonstationary can be answered in the negative. As Koutsoyiannis and others have pointed out (Koutsoyiannis et al. 2009), theirs is a more sophisticated interpretation of the stationarity concept than simply a change in a time series. What matters is whether temperature's effects can be expressed and studied in a statistical manner relevant to its impact, and this analysis has demonstrated a path to doing so for drought vulnerability of the SRP system. Let there be no lingering doubt, stationarity is not dead in the relevant sense of the word.

4.3 Reservoir System Response

4.3.1 Depletion Risk

All stochastically-generated time series of net basin supply by watershed-season were successfully passed through the ResSim model to evaluate reservoir system response. Response to the historical series was previously examined in Section 3.7 with the evolution of reservoir water storage given in Figure 3.7.2. There are two important storage thresholds to be examined. The first is reservoir depletion and shutdown (at 50,000 acre-feet of remaining storage), and the second is when total remaining storage reaches 600,000 acre-feet and subsequent water deliveries follow a reduced allocation protocol (1/3rd reduction). Reduced allocations are discussed in the next section below.

There were no depletions of the reservoir system across all 120,000 years of the current system simulation. The minimum storage level reached was at 11% of system capacity and storage replenishment quickly followed. At the modeled level of customer demand (900,000 acre-feet/year), it appears that the system is sufficiently robust to remain operable even through some very severe drought periods. This is made feasible by reduction of customer water allocations with conservation measures when called for and the utilization of groundwater pumping which scales up with declining storage. It appears that SRP's reservoir system design and operating rules are well-matched to climate outcomes, and surface water depletion is highly unlikely when demand matches nature's supply.

Future elevated temperatures result in NBS reductions as previously quantified, and therefore the severest droughts are expected to result in lower minimum storage levels. This was found to be the case for the most likely forecast as shown in Table 4.3.1. Nevertheless, there were no system depletions under the most likely future temperature expectations. For the case of the IPCC AR5 projection, two depletions did occur over the 120,000 years for an average rate of one in 600 centuries. The Poisson process assumption can be applied to this rate to calculate the depletion probabilities given in Table 4.3.1. As can be seen, the probability of system depletion is negligible, and the small modeled probability of an occurrence can be readily addressed. In fact, it already has. Recent actual deliveries by the SRP system below modeled demand has shown that resulting cumulative incremental storage (Fig. 3.7.1) can be significant enough to further buffer minimum storage relative to critical thresholds. One of the depletion examples is examined in detail in Section 4.4.1 (Examples of Drought and System Response) to find

that a ~50,000 acre-feet/year delivery reduction is sufficient to counter the small depletion risk. This has already been more than attained in recent deliveries. This research therefore concludes that the SRP system is not endangered by depletion risk.

Table 4.3.1. System Depletions and Minimum Total Remaining Water Storage for the Current System, the Most Likely Forecast, and the IPCC AR5 Projection.

	Current System	Most Likely Forecast	IPCC AR5 Projection	
# System Depletions:	0	0	2	in 120,000 years
Poisson parameter, λ			1.67E-03	per century
probability of 0 depletions in a century:			99.8%	
probability of 1 depletion in a century:			0.166%	
probability of ≥2 depletions in a century:			~ 0%	
Minimum Storage:	248,402 11% of capacity	156,833 7% of capacity	< 50,000	acre-feet

4.3.2 Reduced Water Allocations

The SRP system is, in part, resilient because conservation measures are an important part of management operations. As total remaining reservoir storage approaches 1/4th of system capacity (600,000 acre-feet) the protocol is stated to be a 1/3rd reduction in water delivery allocations (Phillips et al. 2009). In practice those measures will not be taken lightly by management and reductions might be phased in or in other ways subject to staggered or sustained actions. Nevertheless, for the purposes of ResSim modeling, water deliveries are reduced by 1/3rd in the season after which the 600,000 threshold is crossed. When total storage is again above threshold at season's end the delivery rate is returned to the modeled 900,000 acre-feet/year level for the next season.

ResSim modeling also encountered rare instances (< once per thousand years) when reduced allocations had not yet been implemented and a dry season's water delivery requirement from Lake Roosevelt was not yet balanced with the other three full reservoirs on the Salt side of the system (for hydroelectric generation). ResSim was built seasonally and so does not capture finer timescale actions that would balance Lake Roosevelt with the full reservoirs and prevent its depletion. For modeling purposes these instances are treated as a reduced allocation season and the reduction is the shortfall of what Lake Roosevelt did not deliver. The next season balances all reservoirs on the Salt side of the system and again checks status of the system against the reduced allocations threshold.

As mentioned, in practice management is unlikely to intermittently implement and withdraw conservation measures as storage hovers near the threshold level. Rather, such actions might be planned with the outlook for a few seasons in advance. Consequently, actual reduced allocation periods would be longer than modeled although fewer in numbers. Instances would essentially be concatenations of clustered short intervals below threshold. Therefore two methods were applied to quantify reduced allocation results. The first is as-modeled by ResSim. The second method identifies one or more seasons below threshold within a sliding 6-season window to be reduced allocation period along with a criteria that total storage return again to ~50% of capacity (1.2MM acre-feet) before the period is considered over. This is the preferred analytic method because its statistics are more reflective of likely management situations. Similar definitions to those for characterization of drought periods (duration, intensity, depth) were applied to total storage data during periods of reduced water allocations.

Reduced allocation periods were assessed for their number of occurrences per century and the percentage of time that the system delivered less than full modeled volume. The two analysis methods did show the expected difference in these measures. As-modeled by ResSim, the current system's 120,000-year stochastic series had 1.1 reductions per century and the system was in a reduced allocation mode 1.2% of the time. The second method resulted in 0.65 reductions per century and reduced allocation mode 1.7% of the time. The differences were statistically significant although the data set is the same, which reinforces the importance of specific definitions when statistically assessing these outcomes. The rest of the results reported below are calculated from the second method which is more relevant to management action.

Once the reduced allocations data was compiled for the historical series and the three stochastic temperature cases it was readily evident that its analysis can follow what was previously performed for drought occurrences. The occurrence statistics are compliant with the criteria for the Poisson and exponential probability functions, so rate parameters were calculated and are given in Figure 4.3.1 and Table 4.3.2. Reduced allocation periods can begin and end with either season (although most of the time after summer and winter, respectively). So, with that seasonal resolution the percentage of time on reduced allocation can be calculated and is also tabulated. As would be expected, the mean number of occurrences and the time on reduction increase with warming temperatures, and those differences are statistically significant (data in Table G.4 of Appendix G).

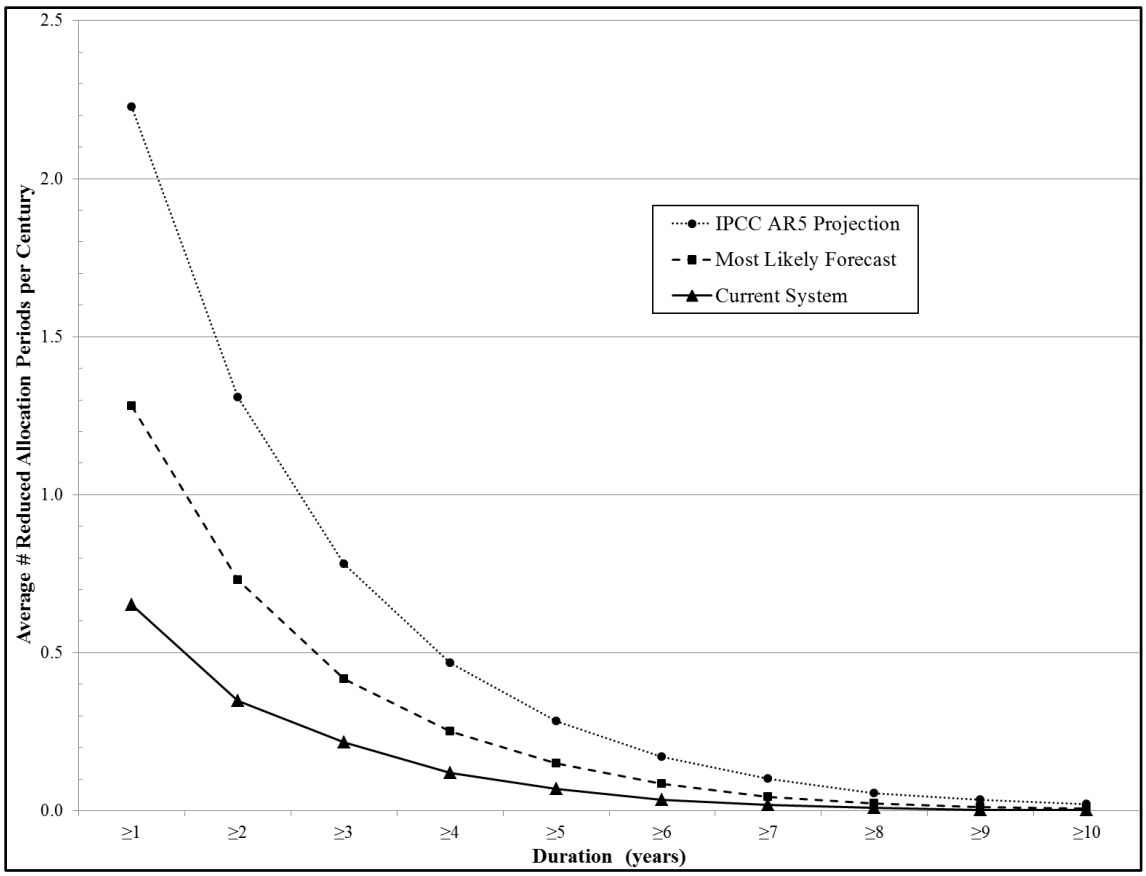

Figure 4.3.1. Poisson Parameter, λ_n, for Reduced Allocation Periods from the 120,000-Year Stochastic Simulation; for the Current System, the Most-Likely Temperature Forecast, and the IPCC AR5 Temperature Projection.

Table 4.3.2. Summary Statistics for Reduced Allocation Periods, Historically and for the Three Stochastic Series Cases.

	% of the time on reduced allocations	Mean # occurrences per century	Storage During Reduced Allocation Periods			
			Intensity (ave storage)		Depth (min storage)	
			Median	99th %-tile	Median	99th %-tile
per Historical Data	5%	2.3	697,000	- - -	520,000	- - -
per Stochastic Series						
Current System	1.7%	0.65	687,536	434,290	463,451	367,892
			30%	19%	20%	16%
Most Likely Forecast	3.5%	1.28	665,871	416,270	426,068	244,391
			29%	18%	18%	11%
IPCC AR5 Projection	6.4%	2.23	637,492	356,673	405,809	167,663
			28%	15%	18%	7%

Total reservoir capacity = 2,313,000 acre-feet

It is interesting to note, however, the comparative response of the historical data series. There have been three periods in system history with reduced allocations per ResSim model analysis: (a) 1902-1904 during the 1890s drought, (b) 2002-2004 when conservation measures were actually imposed, and (c) in the current period of 2014 to present when reduced allocations have been averted owing to lower water demand. These incidents calculate to a mean occurrence rate (2.3/century) similar to the average anticipated for the AR5 projection (2.2/century). Historical time on reduction would have been 5%, midway between the most likely forecast value (3.5%) and AR5 projection (6.4%). The historical values are perhaps slightly overstated because the incidents have fallen at the beginning and end of the historical period without more periods of higher storage in the data to balance the calculation. But nevertheless, the system has been managed through periods analogous to what may be encountered in a warmer future by the same application of conservation measures when required, depletion risk is avoided, and water services are sustained.

Table 4.3.3. Probability of the Number of Reduced Allocation Occurrences in a Century of any Duration for the Current System, the Most Likely Temperature Forecast, and the IPCC AR5 Temperature Projection.

# per century:	0	1	2	3	4	5	6	7
Current System	52%	34%	11%	2%	0%	0%	0%	0%
Most Likely Forecast	28%	36%	23%	10%	3%	1%	0%	0%
IPCC AR5 Projection	11%	24%	27%	20%	11%	5%	2%	1%

Table 4.3.3 applies the Poisson function to calculate probabilities for any number of reduced allocation occurrences of any duration within a century. Similar to drought risk results, this information provides management with risk assessments for threatening

periods of low reservoir storage. As indicated by the data, consideration should be given to the risks in the current system of ~2 occurrences/century, which increases to ~3 or 4 with the most likely forecast and ~5 with the AR5 projection. So, while the actions that would be taken are similar, indications are that they may need to be applied more frequently in the warming future.

Reservoir storage levels during reduced allocation periods have been also characterized and are shown in Figures 4.3.2 and 4.3.3 for the current system case. Storage intensity (Fig. 4.3.2) is typically higher than the 600,000 acre-feet threshold due to storage fluctuations that can exceed threshold during a reduced allocation period. The

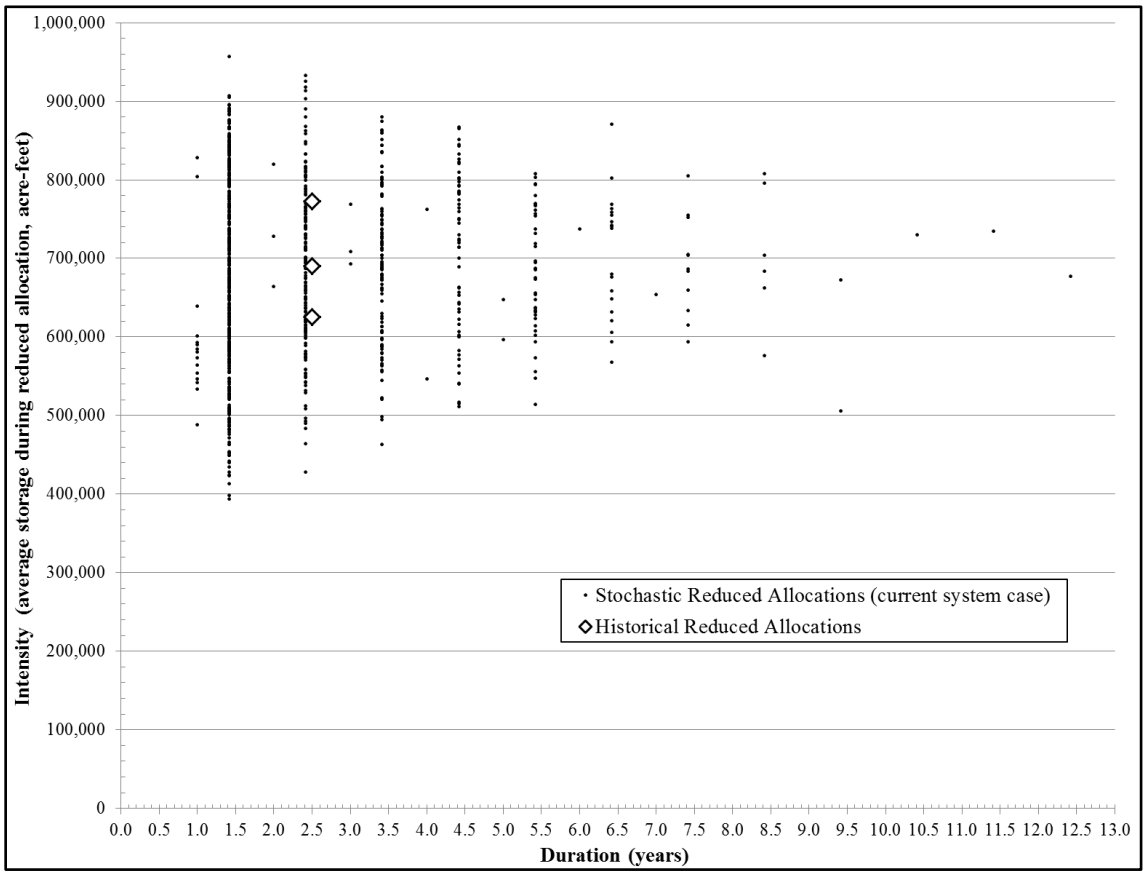

Figure 4.3.2. Storage Intensity During Reduced Allocation Periods as a Function of Duration.

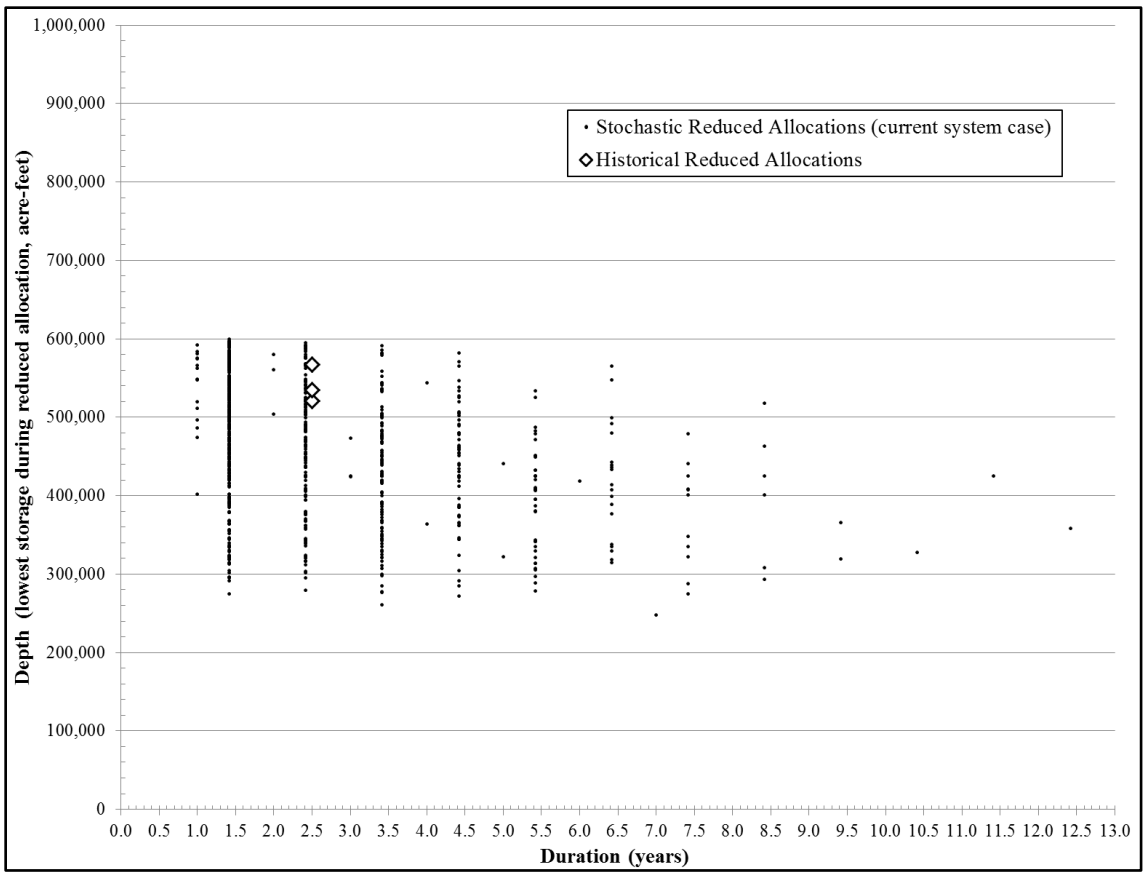

Figure 4.3.3. Storage Depth During Reduced Allocation Periods as a Function of Duration.

lowest storage levels during the periods (Fig. 4.3.3) are, of course, below the threshold. Those also become lower with warming temperatures as given in Table 4.3.2 and constitute depletion risk as the low tail of their distribution approaches zero. As was previously discussed, there were no depletions in the most likely forecast, and two in the AR5 projection for a very low risk of occurrence. The lowest modeled storage for the historical series is 520,000 acre-feet as shown in Table 4.3.2, which is not far below threshold and sufficient to maintain hydroelectric generation.

4.3.3 Groundwater Pumping

As previously discussed and as built into the ResSim model, the SRP system relies upon groundwater to supplement surface water deliveries and this supports sustainability of the system when reservoir storage is progressively depleted. The algorithm by which this occurs (Phillips et al. 2009) is given in Table F2 of Appendix F. Even when reservoirs are full some nominal amount of groundwater pumping takes place. That rate is ~50,000 acre-feet/year or 5.6% of the modeled 900,000 acre-feet annual water deliveries. Total pumping capacity probably exceeds the maximum annualized rate of 325,000 acre-feet/year; but, assuming that maximum limit is followed, 36% of deliveries could be from groundwater as reservoir system storage falls below ~800,000 acre-feet. Then, when storage falls below the 600,000 acre-feet reduced-allocation threshold, conservation measures are imposed to reduce water deliveries by 1/3rd. In that rare circumstance the maximum pumping rate would then constitute 54% of water deliveries. The 120,000-year simulations provide data by which to calculate the probability of a pumping level as a percentage of deliveries and those are plotted in Figure 4.3.4. As can be seen, the probability of higher pumping rates exponentially diminishes to low levels. When the historical NBS series was passed through ResSim, groundwater made up an average of 10.9% of deliveries. The current system simulation series result was 10.6% on average. Because elevated temperatures result in some NBS impairment and lower storage levels, the most likely forecast indicates that groundwater will increase to a mean of 12.2 % and the IPCC AR5 projection to 14.2% of deliveries.

So, a warmer future calls for incrementally more groundwater to balance diminished surface water, and the extra amount required in the future can be readily

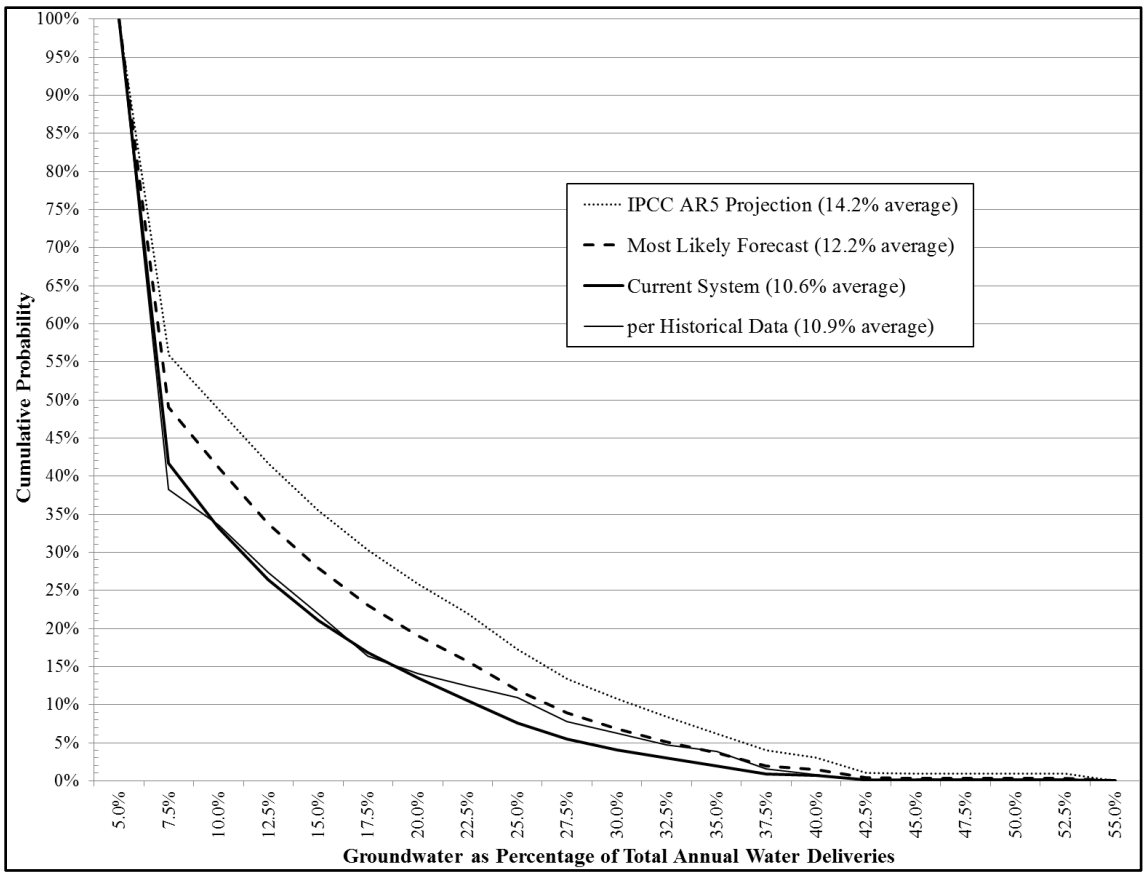

Figure 4.3.4. Probabilistic Representation of the Percentage of Annual Water Deliveries Sourced from Pumped Groundwater.

calculated. The most likely forecast differential is 1.6%, and the differential for the AR5 projection relative to the most likely case is another 2%. At deliveries of 900,000 acre-feet/year these differentials clarify that an extra 14,400 acre-feet/year (or another 18,000 for AR5) of groundwater will be required later in this century. Groundwater banking for future withdrawal has been conducted on an ongoing basis for many years with surplus water when it is available. The calculated differentials for extra withdrawal requirements provide water management with the banking planning data by which to balance groundwater input-output and maintain safe yield in a warmer future. The author is unfamiliar with the capacity of banking infrastructure; but, relative to ongoing water

flows through the system, including spillage (discussed below), it would seem that many years of these extra groundwater requirements can be accommodated.

4.3.4 Pluvial Events and Spillage

This investigation was initiated with the goal of assessing current and future sustainability of the SRP system over concerns of drought and consequent threats to water deliveries. But, in addition to potential water shortages, the research methodology also provides information for pluvial events that may threaten to overwhelm system infrastructure. Within recent memory, the winter of 1993 was such an event that challenged water management with its excessive flows. That year and all others are shown in Figure 4.3.5 for their actual winter NBS and how the ResSim model responds had the present reservoir system been in place at the time. 1993 winter NBS was approximately twice total reservoir system capacity and most of that water did spill, doubtlessly with some of it reaching the main stem of the Colorado River. The stochastic simulation time series were examined for winter NBS levels similar to what occurred that year. Winter NBS >4,000,000 acre-feet (annual >4.5MM) has an average return rate of 1.44 times per century for the current system, or ~1.4% chance of happening in any year as indicated off-scale in Figure 4.3.6. If lesser pluvial levels are of concern, they can be examined in Figure 4.3.5, and spillage probability can be evaluated by Figure 4.3.6. For example, the labeled historical years in Figure 4.3.5 would have spilled more than ~1.5MM acre-feet, with an annual probability under 7% (return rate = 6.19/century). The average rates decrease slightly with future elevated temperatures as shown in Figure 4.3.6 (average spillage reduction ~6% for a future temperature increase). These average return rates are the Poisson process parameters for pluvial events, allowing the probability of

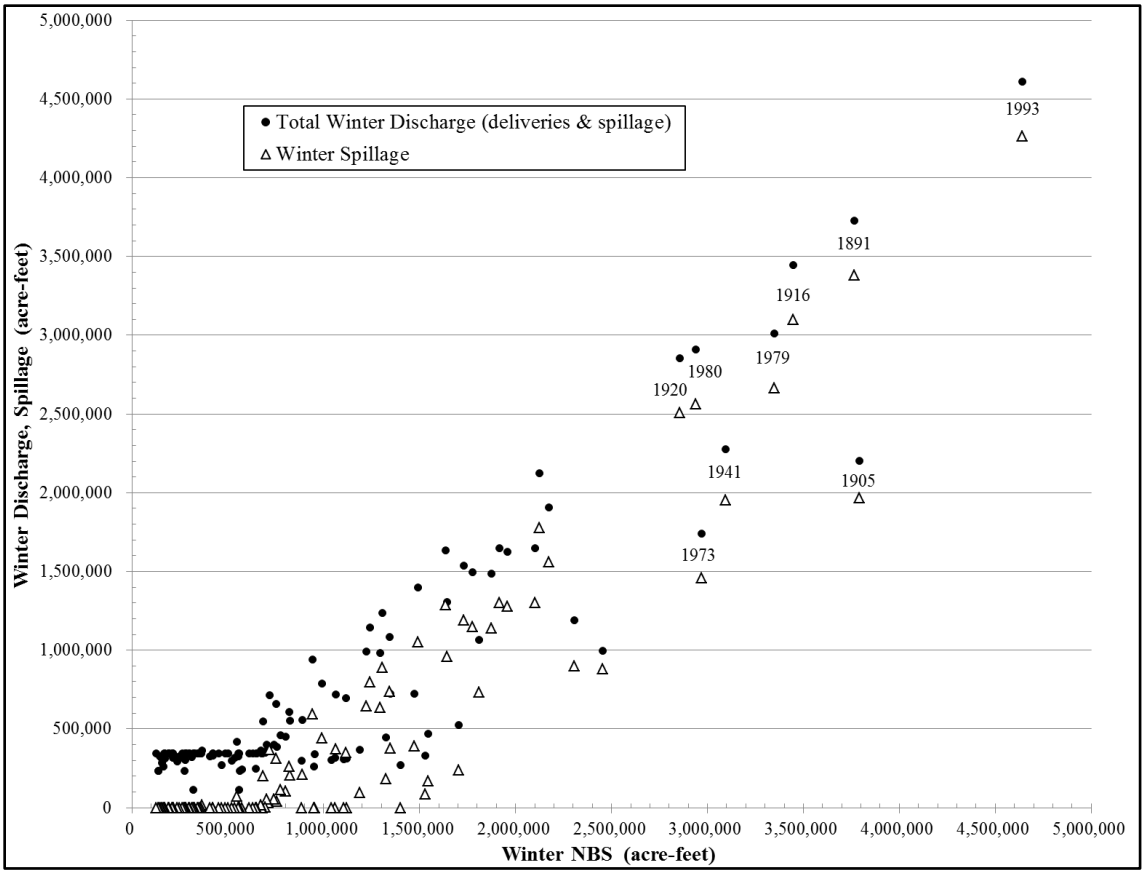

Figure 4.3.5. Historical Winter NBS and Expected Discharge and Spillage Volumes as Assessed by ResSim for the Present System Configuration and Operating Conditions.

any number of occurrences to be calculated as was previously performed for droughts.

Observational data for extreme precipitation events are rare by nature, so that expectations of how they will change in a warmer future are unclear and challenging to verify. But, the data revealed by this study provides a basis on which to conduct sensitivity analyses in two parts: return frequency and intensity. For example, return rates for the pluvial thresholds suggested above can be modified according to an assumption that extremes will occur more frequently. Using the example above, the 1.44/century average occurrence rate (69-year average return) could be modified to alternative values such as 2.0/century (50-year return), and then the consequences to

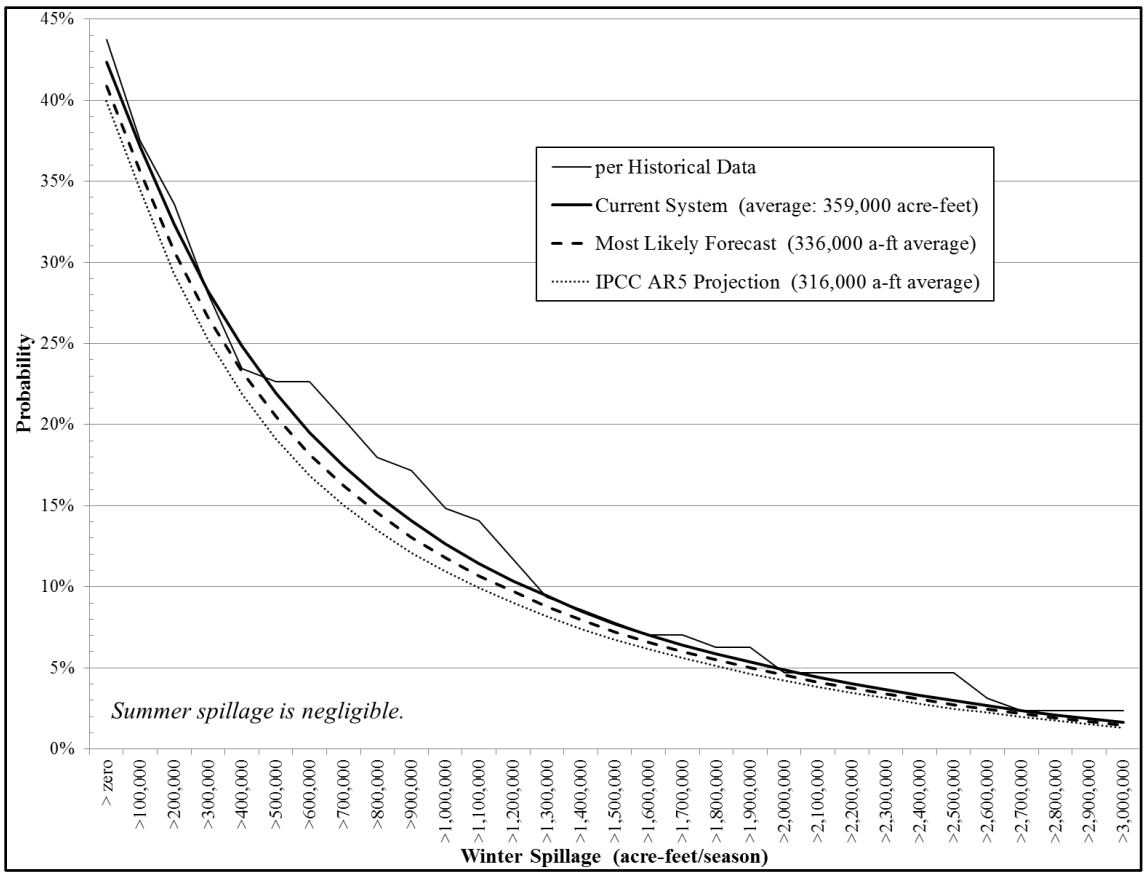

Figure 4.3.6. Probability of Winter Spillage from the Reservoir System.

preparedness assessed therefrom. Such an assumption acts, of course, in opposition to the curve shift identified in Figure 4.3.6. The low and relatively insensitive probabilities of extreme occurrences would very likely result in similar preparedness measures. In practice, actions taken in anticipation of a 50-year event are likely to be the same taken when it had a 69-year expectation.

Intensity considerations might be assessed as anticipated enhancements of precipitation yield that is predicated upon the increasing moisture carrying capacity of warmer air. This is quantified by the Clausius-Clapeyron equation, which is an exponential function of temperature approximating 7%/^{o}K at average temperature as discussed in Section 3.3.11. With this and the precipitation elasticity and runoff

efficiency results shown in Figures 3.5.11 to 3.5.14, feasible ranges of NBS increase can be calculated at high NBS levels where elasticity is low and efficiency high.

Figure 4.3.6 also provides information for the probability that spillage from the SRP reservoir system might pass down the Salt River, join the Gila River, fill any holding systems such as Painted Rock Dam, and eventually deliver water to the main stem of the Colorado River. It is outside the scope of this research, but an examination of historical spillage events might identify the spillage threshold at which this can happen. Figure 4.3.6 then readily provides the probability of that occurring in the future.

4.4 Additional Results and Discussion

4.4.1 Examples of Drought and System Response

The reservoir system's response to specific droughts of interest within an NBS sequence can be examined for insight to system resilience and vulnerability, providing guidance to management operations and adaptation considerations. Of course, there are hundreds of these from the simulations that can be examined. One would expect the longest and deepest droughts to more likely trigger a period of reduced allocations as total system storage drops below 600,000 acre-feet. This was generally found to be the case, but how each situation evolved was unique because outcomes are subject to the cumulative effects of prior years. Total storage may have been gradually depleted before a short drought occurs which is sufficient to trigger reduced allocations; or an extended shallow drought may begin when storage is high enough to sustain the system through the dry times without adversely affecting customer deliveries. Some very long, although shallow, dry periods can be endured without reducing water deliveries. This was the case

during the actual 1950s drought. The periods of greatest concern are droughts which are either deep or of long duration, or both. Two examples of this which provide some insight are given in Figures 4.4.1 and 4.4.2 where alternating winter-summer values for total NBS and total storage are plotted for each of the temperature simulation cases.

In Figure 4.4.1 the sequence begins with a very wet winter which fills reservoirs to capacity, followed by a few weak NBS years and then a 6-year drought (indicated by the 'DDD…'s). In general, as can be seen, winter NBS is larger than summer NBS (same for storage), and temperature impairments of NBS are most evident in summer. The temperature impairments in the most likely and AR5 cases are sufficient to cause the drought to begin two years earlier, making it an 8-year drought. Total storage is progressively depleted; but, since it began from a full condition, reduced allocations are not implemented until late in the drought (indicated by the 'RRR…'s). Only 3 seasons of reduction result for the current system and most likely forecast cases, which extends to 5 seasons in the AR5 case. The drought is then ended by three wet winters that fully refill the reservoirs and relieve the reduced allocation period. As can be seen, remaining system storage responds on a lagged delay to declining inflows and will tend to "bottom out" with more groundwater pumping and reduced allocations until flows recover (seen more completely in Fig. 4.4.2). In other examples (not shown) an occasional year of slightly-above-average inflow was sufficient to sustain the system until a complete reservoir refill was eventually attained. Storage recovery can be seen to occur with a much faster response time than the decline. Given the similar scale of storage capacity to potential high winter NBS, this makes for a fast-refresh system when a wet winter does occur.

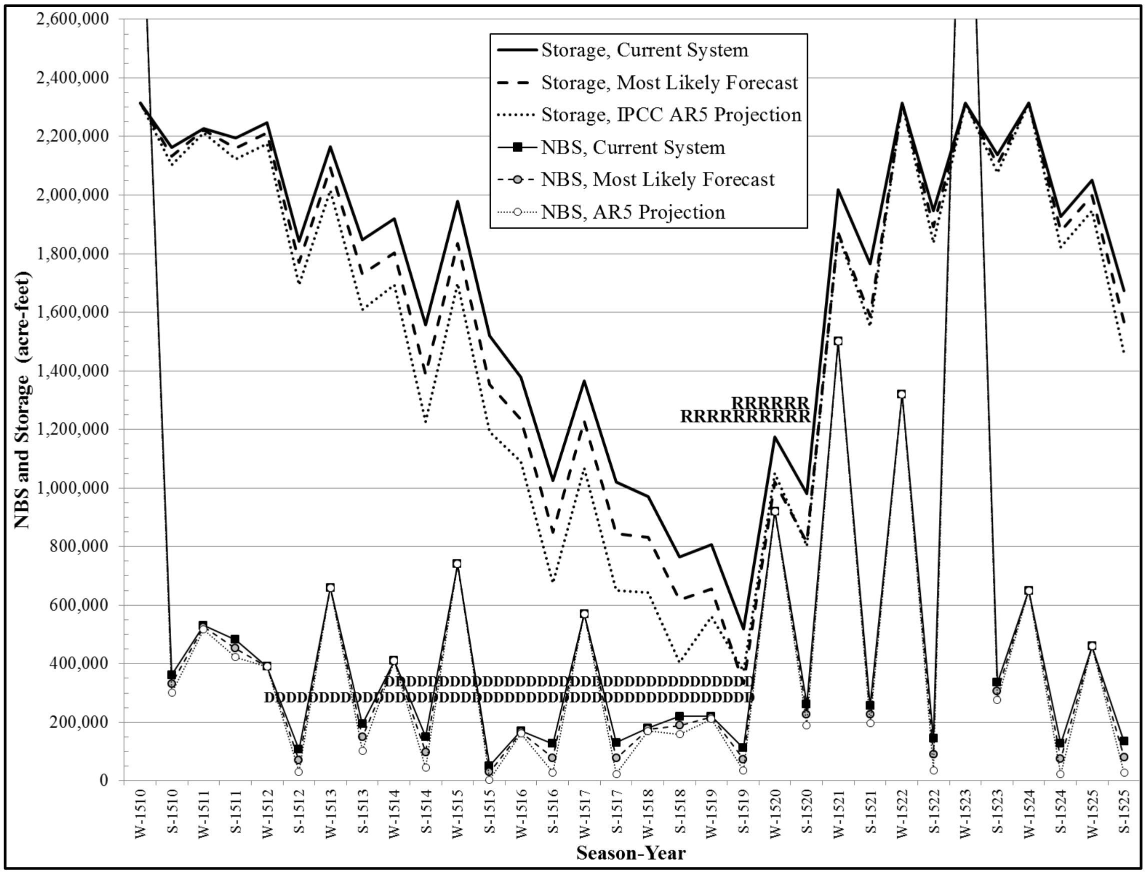

Figure 4.4.1. An Example of a Pluvial-to-Drought-to-Pluvial Period from the Simulations Having a Short Interval of Reduced Allocations.

The example in Figure 4.4.2 is one of the two instances in 120,000 years of simulation where reservoir depletion occurred for the AR5 temperature projection. The sequence begins with storage at about 80% of capacity when a 9-year drought occurs. Reduced allocations are implemented four years into the drought and last 11 seasons. Winter NBS becomes so repeatedly weak that when summer NBS contributions are impaired by elevated temperatures the reduced allocation period begins earlier (13 seasons for the most likely case, 15 seasons for the AR5 case), and the drought extends to 10 years. The depletion at ~35,000 acre-feet of remaining end-of-summer storage only occurs in the case of the AR5 projection (large black diamond in Fig. 4.4.2), and only

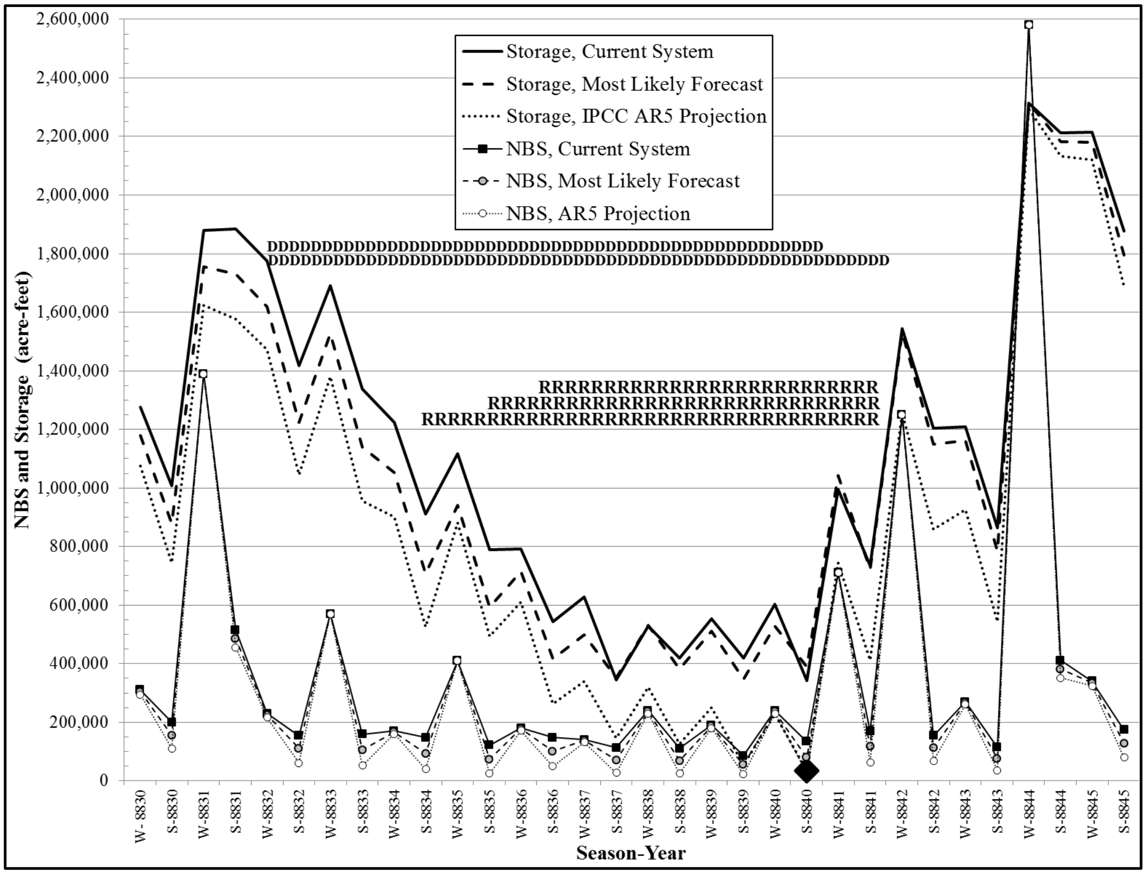

Figure 4.4.2. A Worst-Case Example from the Simulations of a Long Drought with an Extended Period of Reduced Allocations. Reservoir depletion occurs only for the case of the IPCC AR5 temperature projection.

because summer inflows are repeatedly impaired amidst high evaporative losses at the reservoirs and no assistance from five sequential years of unusually low winter inflows. The NBS impairments in the most likely forecast case are not as severe which manages to keep the remaining storage at around 400,000 acre-feet until recovery begins. The NBS differential between the AR5 and most likely cases averages 53,000 acre-feet/year over the 10 drought years. One anticipatory action water management could take to avoid reservoir depletion is more groundwater pumping than the self-imposed rate limit of 325,000/year. If 378,000/year is technically feasible then surface water storage would

remain at the most likely levels of Figure 4.4.2. Alternatively, as previously discussed in Section 4.3.1 (Depletion Risk), water delivery reductions like those of the past few years are more than sufficient to counter any depletion risk.

4.4.2 Decadal Variability

An important assumption underlying the entirety of this research investigation has been the demonstrated assumption that annual net basin supply outcomes are independent and identically distributed. The stationarity investigation showed this to be the case, as there were no autocorrelations across all time horizons. The stochastic simulations employed this fortuitous result for the methodology used to generate sequential years in long time series. An i.i.d. assumption at the annual level establishes validity of extending the concept to the statistics of multi-year droughts, reduced allocations, and pluvial periods that can be expressed on a per-century basis. It was shown in Figure 3.4.17 that the resultant NBS time series demonstrate periods of clustered variations above and below the long-term mean very similar to the historical record, assuring confidence in methods. But what can be said of those variations above and below the long-term mean that are highlighted by filter-smoothing the time series? They are, by definition, stochastic events by the way they have been generated. But the historical series may reflect more than that.

There is a significant body of research into drought and pluvial periods in the CRB (Balling and Goodrich 2007; Thomas 2007; McCabe and Wolock 2012; Nowak et al. 2012), with general findings that ENSO, the PDO, and the AMO play a role not only for temperature, as discussed in the forecast development section of this document, but perhaps also for precipitation and streamflow. Nowak et al. (2012) identified the low-

frequency 64-year mode of variability in Lees Ferry streamflow and linked it primarily to the AMO as was suggested by other research. Balling and Goodrich (2007) found that the PDO explained more variance for a drought index than did ENSO or the AMO, but found all to play some role in explaining LCRB precipitation. Explained variances in their analysis were modest at best, leaving ample uncertainties for drought forecasting. It is generally believed that higher probabilities for a wet winter in the lower CRB are aligned with the occurrence of an El Niño in a consistent positive phase of the PDO. It is not the purpose of this discussion to incorporate that in the results of this investigation, which would regardless not be possible in a rigorous forecasting sense since only two ambiguous precipitation cycles are present in the observational record. These can be seen in Figure 3.2.18 where generally elevated NBS was present from 1905 into the early 1920s and then again from the mid-1970s into the early 1990s, the eras separated by about 65 years in time. When examined in comparison to cyclicality in historical temperature records (global in Fig. 3.6.1, Salt-Verde in Fig. 3.6.17), temperature cycle minimums can be seen to occur near the outset of these wet periods (~1909, ~1974). The onsets correlate with the temperature cycle switch to a warming phase.

So, if one were to extrapolate these observations, the current drought might abate by the early 2030s if timing is correlated to a phase reversal of the AMO. If a warming rate switch is more related to a Pacific phase shift there are suggestions it may come sooner (Trenberth 2015; Meehl et al. 2016). It would appear that wetter years could accompany the forthcoming warming period portrayed in the most likely forecast. That would last for no more than a couple decades while an elevated temperature level would persist thereafter. As was discussed in Section 4.1, this would disguise temperature-

induced NBS impairments until perhaps they become more evident during the ensuing drought period in the next hiatus after mid-century. Of course, these are somewhat speculative at this time but do integrate the various research contributions to a possible outlook that can be considered when addressing the temporal decadal variability question raised above.

CHAPTER 5

CONCLUSIONS

Large natural climate variability and expectations of climate change have raised serious questions about the vulnerability and resilience of surface water resources in the Southwest United States. A number of research investigations have worked to address these concerns. The investigation reported in this dissertation was motivated by the observation that over the last several years the predominant assessment path based in climate modeling scenarios has not provided satisfactory results suitable for water management facing complex risk-based decisions. In the face of climate variability masking uncertain findings and unsettled conclusions over forthcoming changes in climate forcing mechanisms, the research paradigm of GCM downscaling with hydrologic translation is not reducing uncertainty for water managers despite application of exhaustive efforts. Such research often does not reach the stage of specific impact assessment when any projection within a wide span of possibilities cannot be supported with convincing and useful guidance. This study responds to the challenge by inverting the investigative approach, placing primary attention on the system under consideration, and developing an integrated toolset to assess climate risks.

The Salt River Project system is endowed with one of the longest hydrologic data records in the western United States. This facilitated a thorough characterization resulting in a stochastic simulation methodology used to generate long, synthetic time series of net basin water supply from highly skewed distributions of the dual-watershed system in winter and summer seasons. A dozen 10,000-year series were generated for a total simulation sample size of 120,000 years. This is sufficient to enable detailed

probabilistic risk assessments per relevant management criteria. The data record was also employed to establish two key measures of hydrologic response to climate: temperature sensitivity and precipitation elasticity of runoff. These dual heuristics enable translation of any climate change scenario to a modified time series of net basin supply. While many future scenarios could be evaluated, two were developed and investigated in detail: (1) a most likely forecast using empirical statistical methods rooted in forecasting science and climate research findings, and (2) a projection based in AR5 of the IPCC. All three dual-watershed, dual-season time series cases (current system, most likely, AR5) were passed through the ResSim reservoir operations model developed for this investigation to assess impacts on operational metrics. All the methodological components required for completion of this research investigation were successfully developed with effective data interfaces and internally consistent assumptions. Their basis in prior research and the underlying assumptions have been articulated in this report. This successful integration of multidisciplinary methods yielding specific findings demonstrates that immediate progress can be made in response to the needs of water management aside of inconclusive hydroclimate modeling while that approach matures.

The results reported in Chapter 4 are a subset of analyses that could be conducted on the data available from this investigation. Exploratory data analysis readily revealed that natural variability plays a significant role in the SRP system's outcomes and that the region has endured periodic drought over the entirety of its instrumental and paleoclimate record. While many definitions of drought are possible, the one relevant to this study looks for runs of years below the annual NBS required to sustain surface water delivery requirements. Deliveries have been taken to be the 2003-2011 average of 900,000 acre-

feet/year, which requires 850,000 from surface reservoirs when groundwater pumping is at its minimum rate. By coincidence, the median of the highly-skewed NBS distribution is also approximately 850,000 acre-feet/year. An important measure of long-term system sustainability is whether water withdrawals are below median NBS, and this system meets that criteria. When the most likely climate change scenario is applied the median NBS shifts to 809,000 acre-feet/year and water deliveries of 859,000 acre-feet/year are supportable over the long-term (816,000 in the AR5 case). Actual delivery requirements have continued a long-term decline and are now below the 900,000 acre-feet/year modeled in this study and so are already positioned for the most likely forecast and the AR5 projection. By this measure the reservoir and delivery system is well-matched to the watersheds supporting it.

Studies of tree ring data previously provided some evidence of decade-long drought in the pre-instrumental era of these watersheds. This study confirmed that those are indeed possible and provides a detailed risk assessment for the current state of the system, answering one of the central research questions of this investigation. Analysis of simulation series revealed droughts up to 16 years duration but those have a vanishingly small probability of occurrence. Most are ≤ 11 years, similar to the longest identified in the tree ring record. Drought that long is rare but possible. Results from the long simulation time series indicate that there is a 99% probability of a drought ≥ 12 years not occurring in a century (1% that it will), and 95% probability for droughts ≥ 10 years. A complete risk matrix has been calculated for the number of occurrences of drought of any duration in a century. The probabilities increase by 1% to 4% across the matrix when each future temperature increase scenario is considered. These marginal risk changes are

probably smaller than the risk level water management might want to consider (10%, 5%, other?), so a planning guideline might be relatively insensitive to future temperature expectations. The decision could reduce to planning for a 5% chance of one decade-long drought over the next century along with an expectation of a few 5- to 8-year droughts. The severity statistics accompanying such droughts have also been revealed by this investigation.

A drought might result in the imposition of conservation measures where water allocations to the user service area must be reduced. The operational protocol calls for this when reservoirs fall below 600,000 acre-feet of total remaining storage. These instances have been quantified from the ResSim operations model output. Again, the results provide quantitative risk assessments and indicate that at least 2 such periods should be planned for within a century. This increases to 3 or 4 under the most likely temperature change forecast and up to 5 periods with the AR5 projection. These are not average expectancies, which are lower, but rather outcomes having a risk just large enough to deserve attention for planning purposes. Whether total reservoir storage falls to the 600,000 acre-feet threshold is a sensitive function of the cumulative balance of system inflows and outflows. ResSim modeling of the recent historical record indicates the system should have fallen to that threshold and be in reduced allocations at the present time. But this is not what happened, and mid-summer 2016 storage is twice that level. This is attributable to declining water deliveries while ResSim was run at constant 900,000 acre-feet/year deliveries, resulting in a large cumulative differential which is also sufficient to buffer against the future climate change cases which were modeled. So, one possible adaptation response was demonstrated in practice before this investigation was

completed. Another response might be the addition of a few hundred thousand acre-feet of storage capacity to the system as was done at Lake Roosevelt in the mid-1990s. This would increase the minimum remaining storage levels revealed by this study, as starting storage would have begun at a higher level and storage depths would be less likely to cross the reduced allocation threshold. This study has revealed that current operational protocols result in a slow progression of storage reduction and a fast refresh when inflows do rebound. Measures which have the effect of extending the progression before thresholds are crossed provide more time for replenishments to reoccur.

The risk of reservoir system depletion under current management guidelines is zero. There were no depletions across all 120,000 years of the current system simulation and none for the most likely climate change forecast. There were two depletions in 120,000 years for the AR5 projection, calculating to a 0.17% probability of depletion in a century. This goes to zero when the lower level of recent water deliveries is taken into consideration. The conservation measures and groundwater pumping protocols have their desired effects, and it appears the system design and operating rules are well-matched to climate outcomes. This research concludes that the SRP system is not endangered by depletion risk now or in the future under the assumption set used in this study. The system can be managed through periods of climate risk, provided that no constraints are imposed which would compromise resilience and limit flexibility of the protocols modeled in this analysis.

The SRP system has been in operation for more than a century with the vulnerabilities that this simulation methodology has revealed in detail. The examined risks are present in the current system and climate change will act to increase those, but

only marginally. Planning assumptions therefore only need be adjusted to take those into account, provided, of course, they are being adequately addressed in the first place. Perhaps some of the expressed concerns are that current risks have not been thoroughly examined so that climate change might expose those vulnerabilities. If so, data from this analysis can close that gap.

As Matalas (1990, 149) stated, "Though the matter of climate change is not to be taken lightly, climate variability has perhaps greater bearing on the uncertainties in water management." After examining the interacting sensitivities of climate with streamflow and reservoir safe yield, Schaake (1990, 201) wrote "Two general conclusions can be drawn about the sensitivity of safe yield to climate change. First, safe yield is less sensitive to climate change than is the average annual runoff or measures of low flow. Second, storage reservoirs built to buffer climate variability also provide a buffer against the effects of climate change." The findings of this investigation confirm those statements of 25 years ago in *Climate Change and U.S. Water Resources*. In another chapter Rogers and Fiering (1990, 218) evaluated sensitivities within a stochastic basin model coming to the observation that "… (simulation) outcomes are relatively more sensitive to residual errors in estimating the basin model parameters than to changes … induced by climate change. In others words, model error masks the "real" effects of climate change." This investigator observed the same in many discussions of water resources in the Southwest when mis-parameterized models or over-simplifications exaggerate uncertainties and confuse decision makers. This investigation has rigorously developed all methods, assumptions, and intermediate findings required to arrive at the reported results and reveal system vulnerability and resilience in specific detail rather

than vague generalities. Minimum complexity has been employed sufficient for complete representation but also comprehension by the user who will be informed and may confidently challenge some assumptions and findings. The methodology is available to evaluate alternative assumptions. Some might address the stationarity, hydrologic sensitivity, and forecast assumptions employed in this investigation.

The stationarity analyses in this study came to the conclusion that while the temperature time series for this region has displayed non-stationarity over the last 80 years, the precipitation series is stationary. There have been periodic variations around the long-term mean, perhaps in part a function of decadal climate variability, but there is no persistent precipitation trend and no case can be made from research to date that one will emerge within the rest of this century. The guidance from forecasting science for this situation is clear: if no trend can be established, none should be forecasted. Otherwise, forecast error can be expected to increase significantly. Therefore precipitation variability has been treated in a sensitivity analysis coming to the finding that it is the primary independent variable influencing runoff with sufficient effect to obscure runoff impairments from increasing temperature. So, if future periods of temperature increase are accompanied by precipitation variability, it will be difficult to differentiate their effects just as it has been in the historical realization.

Derivations of the hydrologic sensitivity functions in this study show that an increase in winter temperature has essentially no effect on runoff and net basin water supply. However, important temperature impairments are present in summer, both on the watersheds and at the reservoirs with highly nonlinear effects that have now been quantified. Precipitation elasticity of runoff is also highly nonlinear in both the winter

and summer seasons. The hydrologic response functions differ between seasons and between watersheds and are a function of the precipitation and runoff level analyzed. The over-simplifications or inaccurate parameterization of hydrologic response by other studies are at the center of the Rogers and Fiering observation noted above.

As would be expected, the chosen forecast of future climate change influences the outcome of an analysis, primarily for net basin supply and to a lesser degree for system impacts. A large set of scenarios could be taken from the uncertain range of projections prepared for the region. However, none appear to have been endorsed thus far by the water management community. Many are inconsistent with current observational data, which motivated this investigation to develop a multi-decadal temperature forecast using empirical statistical methods. The approach incorporates current understanding of anthropogenic warming and circulation dynamics in the coupled ocean-atmosphere system, reconciles the observational record, dissipates the uncertainties of climate model projections, is validated against 40^{+} years of the historical record, and provides a simple but clarifying representation of the future grounded in forecasting principles. The result indicates the current warming slowdown will continue for another two decades followed by an accelerated warming period towards another hiatus in 2065-2095. The temperature differential between that timeframe and the present (approximately 1.5^{o}C) was used as the most likely temperature change forecasted for this study. This is about half what is inferred for the Salt-Verde region by the IPCC AR5 mean global temperature change scaled by observed climate sensitivity. The results forced by these temperature changes were found to be statistically significant in all key dependent variables; but, as discussed above, changes must be assessed relative to current system risks. Others may consider

whether these forecasts and their implications are a reasonable set of assumptions to utilize, or whether other alternatives should be considered.

This research was undertaken with the goal that results be interpretable within the context of decision-making for drought planning and adaptation, building long-lasting knowledge to manage water resources through extreme drought periods, and bringing a clearer meaning of climate change projections for the region. This work is an important and unique contribution to climate change adaptation. It stands in sharp contrast to ever more detailed but ever more uncertain fine-scale simulations of water resource systems under downscaled hydroclimatology. From a theoretical perspective, general suggestions of this approach have been touched upon in the climate adaptation community but without clear articulation to date. Perhaps this is because development of the complete methodology necessitated incorporation of disparate tool sets from climatology, hydrology, systems analysis, probability and statistics, forecasting science, and water management. This integration of multidisciplinary methods for assessing vulnerability of a system to forthcoming change is a new contribution to climate change science, standing apart from top-down hydroclimatic modeling. It is anticipated that the impact of this research will be long-lasting, particularly for SRP. Its transferable example serves as an approach for water planners in other regions facing similar needs for specific vulnerability assessments and decision support for drought and climate change adaptation planning.

5.1 Possible Future Analyses

During the course of this research a number of avenues for further investigation were revealed. Some are given below, with the expectation that they can be addressed in the future with the tools developed for this research.

A couple drought examples were examined in Section 4.4.1, but other variations are available for detailed analysis, and assessments of their impacts could be useful for drought planning purposes.

Some variables must be held constant in a study such as this. But the implications of water deliveries both larger and smaller than the modeled 900,000 acre-feet/year are clearly significant. Impact analyses across a range of delivery levels can provide management with important information on the full capabilities and limitations of the SRP system.

The benefit of the Roosevelt Lake storage capacity expansion in 1996 became clear during this study. Without it, system risks would have been larger than has been characterized and in that way it was a wise investment. While the possibility of further reservoir storage additions to the SRP system might appear remote at this time, the risk-reduction benefits in certain future system scenarios are worthy of consideration.

The tools developed for this investigation can perform an assessment of near-term risks conditional upon reservoir system storage levels at a point in time. This could aid decision making situations that water management might confront in the future.

The effect on groundwater pumping requirements under two climate change scenarios was reported in Chapter 4. To address the safe yield imperative of Arizona

groundwater management more detailed assessments under other scenarios may help inform long-term water banking and withdrawal plans.

There is a probability of winter season water spillage from the system that has a number of downstream consequences, both positive and potentially negative. Further analysis of those instances could be conducted to determine their implications.

The historical record of the summer season on the Verde River watershed has displayed anomalous behavior in streamflow and in temperature. Perhaps there have been some manner of water diversions; the watershed-season has the highest climate sensitivity of those examined; and possible interactions of these are unclear. While this was not of major consequence to research findings, it could portend further change on the watershed that should be investigated.

The Four Forest Restoration Initiative, an effort to restore forest ecosystems in the Coconino, Kaibab, Apache-Sitgreaves, and Tonto National Forests with tree thinning is expected to soon be underway. The effect on runoff in the Salt and Verde watersheds is speculative at this time, but could potentially increase streamflow in the timeframe at which climate change impairments may occur.

5.2 Postscript – The Hubris of the Climate Model

The scientific method relies upon challenges from alternative theories. The confrontation of criticisms and rigors of reconciliation should be welcomed in climate science despite numerous vested political, economic, commercial, and career interests. Unfortunately the facts and the science are often overshadowed in the ensuing political debate without periodic reappraisal of underlying assumptions, especially as new

information comes to light. From the time this author embarked upon the program of which this dissertation is the final requirement, important new information has emerged. This is sufficient to place in question many of the assertions of eight years ago. For example: hiatus – there is one; role of natural variability – larger than assumed; climate sensitivity – smaller than expected. One can expect more in the future. Some might say that discoveries were not forecastable (possible response: think harder, don't discount alternatives until investigated). But, what ***was*** forecastable and will continue to be so is that exaggerated claims will eventually be found out. Unfortunately climate science is rife with them at this time, and there is little sign of any sobriety which is so urgently needed.

One of the literature references for this study is titled "Are climate models 'ready for prime time' in water resources management applications, or is more research needed?" (Kundzewicz and Stakhiv 2010). Quite simply, an unbiased review of the current state of climate modeling comes to the conclusion that they are not ready. To expect very complex models to be capable of uncertainty reduction when their completeness is not established (Trenberth 2010; Vano et al. 2014) and accuracy of their formulations have not be demonstrated (Koutsoyiannis et al. 2008; Anagnostopoulos at al. 2010; Beven 2011; Fildes and Kourentzes 2011; Suckling and Smith 2013; Frigg et al. 2015; Privalsky and Yushkov 2015) is sufficient to conclude that climate model ambiguity remains a fundamental limit to that expectation.

Weather models took decades to develop to a level that can reasonably inform us about the 10-day weather forecast. Likewise, it will be many years before climate models can make reliable forecasts of the climate decades ahead. At present it is questionable

even whether their hindcasts capture key variables in a manner satisfactory to desired objectives. Despite calls for progress measurement criteria (Pielke 2008), none have been defined. This is indicative of an immature discipline. Until then, and as counseled by those who teach us these topics, the models are best suited for gaining insight by sensitivity analyses and not as policy-informing tools, as they have no skill for forecasting-prediction-prognostication. Many in the modeling community indicate such unnoticed reservations deep within unread portions of assessment reports. The resistance to presenting model output as a forecast, but rather as nothing more than one possible projection, is a sufficient basis for setting them aside and awaiting their eventual maturation a few decades hence.

Some of the reactions in response to alternative contributions that bring scientific rigor to bear or come to differing indications of the future have demonstrated a surprising degree of hostility considering the supposedly cherished emphasis on interdisciplinary science. The personal experiences of rejection recounted by several prominent leaders in the decades-old field of forecasting science suggest that much progress has yet to be made for incorporating fundamental and valuable ideas from other disciplines. Forecasters know by parallel experiences in other applications that when climatologists assert "this situation is different" and outside advice may be ignored, at some point the folly of such assertions will become evident. But by then those at fault will have slipped into retirement or obscurity with their cloak of invincibility forgotten and never revisited but casting a long shadow over the profession. A one-note science risks the loss of public credibility for science-based policy when its weaknesses are eventually exposed and viable alternatives were ignored.

REFERENCES

Alam, J. 1997. *Irrigation in the Verde Valley: A report of the irrigation diversion improvement project*. Verde Natural Resource Conservation District.

Anagnostopoulos, G.G., D. Koutsoyiannis, A. Christofides, A. Efstratiadis, N. Mamassis. 2010. A comparison of local and aggregated climate model outputs with observed data. *Hydrological Sciences Journal* 55(7):1094-1110. doi:10.1080/02626667.2010.513518.

Arrhenius, S.A. 1896. On the Influence of Carbonic Acid in the Air Upon the Temperature of the Ground. *Philosophical Magazine and Journal of Science* 41:237-276.

Armstrong, J.S., Ed. 2001. *Principles of Forecasting: A Handbook for Researchers and Practitioners*. Boston: Kluwer Academic Publishers.

Baillie, R.T., S-K. Chung. 2002. Modeling and forecasting from trend-stationary long memory models with applications to climatology. *International Journal of Forecasting* 18:215-226.

Balling Jr., R.C., G.B. Goodrich. 2007. Analysis of drought determinants for the Colorado River Basin. *Climatic Change* 82:179-194. doi:10.1007/s10584-006-9157-8.

Balmaseda, M.A., K.E. Trenberth, E. Kallen. 2013. Distinctive climate signals in reanalysis of global ocean heat content. *Geophysical Research Letters* 40:1754-1759. doi:10.1002/grl.50382.

Barcikowska, M., T. Knutson, R. Zhang. 2015. Global imprint of a 70-yr oscillatory-like behavior in sea surface temperature: possible implications for the 'hiatus' in global warming. *American Meteorological Society 2015 Annual Meeting and 27th Conference on Climate Variability and Change, Phoenix AZ*, Paper 3.1A, Poster 535.

Barnett, T.P., D.W. Pierce. 2009. Sustainable water deliveries from the Colorado River in a changing climate. *Proceedings of the National Academy of Sciences* 106(18):7334-7338. doi:10.1073pnas.0812762106.

Barnett, T.P., D.W. Pierce, H.G. Hidalgo, C. Bonfils, B.D. Santer, T. Das, G. Bala, A.W. Wood, T. Nozawa, A.A. Mirin, D.R. Cayan, M.D. Dettinger. 2008. Human-Induced Changes in the Hydrology of the Western United States. *Science* 319:1080-1083. doi:10.1126/science.1152538.

Beven, K. 2011. I believe in climate change but how precautionary do we need to be in planning for the future? *Hydrological Processes* 25:1517-1520. doi:10.1002/hyp.7939.

Boucher, O., D.A. Randall, P.P. Artaxo, C.S. Bretherton, G. Feingold, P. Forster, V-M. Kerminen, Y. Kondo, H. Liao, U. Lohmann, P.J. Rasch, S.K. Satheesh, S.C. Sherwood, B.B. Stevens, X-Y. Zhang, G. Myhre, D.T. Shindell. 2013. Importance of clouds and aerosols in assessing climate change. *American Geophysical Union 2013 Fall Meeting, San Francisco CA*, paper U22A-05 (invited).

Brown, C., R.L. Wilby. 2012. An Alternate Approach to Assessing Climate Risks. *EOS, Transactions, American Geophysical Union*, 93(41):401-403.

Brown, C., Y. Ghile, M. Laverty, K. Li. 2012. Decision scaling: Linking bottom-up vulnerability analysis with climate projections in the water sector. *Water Resources Research* 48:W09537. doi:10.1029/2011WR011212.

Burt, J.E., G.M. Barber. 1996. *Elementary Statistics for Geographers, 2nd Edition.* New York: The Guilford Press.

Chen, X., K-K. Tung. 2014. Varying planetary heat sink led to global-warming slowdown and acceleration. *Science* 345(6199):897-903. doi:10.1126/science.1254937.

Christensen, N.S., D.P. Lettenmaier. 2007. A multimodel ensemble approach to assessment of climate change impacts on the hydrology and water resources of the Colorado River Basin. *Hydrology and Earth System Sciences* 11(4):1417-1434.

Christensen, N.S., A.W. Wood, N. Voison, D.P. Lettenmaier, R.N. Palmer. 2004. The effects of climate change on the hydrology and water resources of the Colorado River Basin. *Climatic Change* 62:337–363. doi:10.1023/B:CLIM.0000013684.13621.1f.

Chylek, P., U. Lohmann, M. Dubey, M. Mishchenko, R. Kahn, A. Ohmura. 2007. Limits on climate sensitivity derived from recent satellite and surface observations. *Journal of Geophysical Research* 112:D24S04. doi:10.1029/2007JD008740.

Chylek, P., M.K. Dubey, G. Lesins, J. Li, N. Hengartner. 2013. Imprint of the Atlantic multi-decadal oscillation on southwestern U.S. climate: past, present, and future. *Climate Dynamics* 23(1):119-129. doi:10.1007/s00382-013-1933-3.

Coles, S. 2001. *An Introduction to Statistical Modeling of Extreme Values*. London: Springer-Verlag.

Dai, A., J.C. Fyfe, S-P. Xie, X. Dai. 2015. Decadal modulation of global surface temperature by internal climate variability. *Nature Climate Change* 5:555-559. doi:10.1038/nclimate2605.

Daly, C., R.P. Neilson, D.L. Phillips. 1994. A Statistical-Topographic Model for Mapping Climatological Precipitation over Mountainous Terrain. *Journal of Applied Meteorology* 33:140-158.

Daly, C., W.P. Gibson, G.H. Taylor, G.L. Johnson, P. Pasteris. 2002. A knowledge-based approach to the statistical mapping of climate. *Climate Research* 22:99-113. doi:10.3354/cr022099. Available at http://prism.oregonstate.edu. Last accessed 30 October 2015.

DeGroot, M.H., M.J. Schervish. 2012. *Probability and Statistics, 4th Edition*. Boston: Addison-Wesley, Pearson Education Inc.

Delworth, T.L., M.E. Mann. 2000. Observed and simulated multidecadal variability in the Northern Hemisphere. *Climate Dynamics* 16(9):661-676. doi:10.1007/s003820000075.

Dlugokencky, E., P. Tans. NOAA, Earth Systems Research Laboratory, Global Monitoring Division. Available at www.esrl.noaa.gov/gmd/ccgg/trends/. Last accessed 15 January 2015.

Dominguez, F., J. Cañon, J. Valdes. 2010. IPCC-AR4 climate simulations for the Southwestern US: the importance of future ENSO projections. *Climatic Change* 99(3-4):499-514. doi:10.1007/s10584-009-9672-5.

Dominguez, F., E. Rivera, D.P. Lettenmaier, C.L. Castro. 2012. Changes in winter precipitation extremes for the western United States under a warmer climate as simulated by regional climate models. *Geophysical Research Letters* 39:L05803. doi:10.1029/2011GL050762.

Douglass, D.H., J.R. Christy, B.D. Pearson, S.F. Singer. 2008. A comparison of tropical temperature trends with model predictions. *International Journal of Climatology* 28:1693-1701. doi:10.1002/joc.1651.

Ellis, A.W., K.W. Murphy. 2012. *Analysis of the Sensitivity of the Salt River Project Reservoir System to Climate Variability and Change*. Project Report to SRP, 5/1/2012.

Ellis, A.W., T.W. Hawkins, R.C. Balling, Jr., P. Gober. 2008. Estimating future runoff levels for a semi-arid fluvial system in central Arizona, USA. *Climate Research* 35:227-239. doi:10.3354/cr00727.

England, M.H., S. McGregor, P. Spence, G.A. Meehl, A. Timmermann, W. Cai, A.S. Gupta, M.J. McPhaden, A. Purich, A. Santoso. 2014. Recent intensification of wind-driven circulation in the Pacific and the ongoing warming hiatus. *Nature Climate Change* 4:222-227. doi:10.1038/NCLIMATE2106.

Fildes, R., N. Kourentzes. 2011. Validation and forecasting accuracy in models of climate change. *International Journal of Forecasting* 27:968-995. doi:10.1016/j.ijforecast.2011.03.008.

Fisher, J.C., R.H. Pry. 1971. A Simple Substitution Model of Technological Change. *Technological Forecasting and Social Change* 3:75-88.

Frigg, R., L.A. Smith, D.A. Stainforth. 2015. An assessment of the foundational assumptions in high-resolution climate projections: the case of UKCP09. *Synthese* 192:3979-4008. doi:10.1007/s11229-015-0739-8.

Fu, G., S.P. Charles, F.H.S. Chiew. 2007a. A two-parameter climate elasticity of streamflow index to assess climate change effects on annual streamflow. *Water Resources Research* 43:W11419. doi:10.1029/2007WR005890.

Fu, G., M.E. Barber, S. Chen. 2007b. Impacts of Climate Change on Regional Hydrological Regimes in the Spokane River Watershed. *Journal of Hydrologic Engineering* 12(5):452-461. doi:10.1061/(ASCE)1084-0699(2007)12:5(452).

Fyfe, J.C., N.P. Gillett. 2014. Recent observed and simulated warming. *Nature Climate Change* 4:150-151. doi:10.1038/nclimate2111.

Fyfe, J.C., N.P. Gillett, F.W. Zwiers. 2013. Overestimating global warming over the past 20 years. *Nature Climate Change* 3:767-769. doi:10.1038/nclimate1972.

Fyfe, J.C., G.A. Meehl, M.H. England, M.E. Mann, B.D. Santer, G.M. Flato, E. Hawkins, N.P. Gillett, S-P. Xie, Y. Kosaka, N.C. Stewart. 2016. Making sense of the early-2000s warming slowdown. *Nature Climate Change* 6:224-228.

Galloway, G.E. 2011. If Stationarity Is Dead, What Do We Do Now? *Journal of the American Water Resources Association* 47(3):563-570. doi:10.1111/j.1752-1688.2011.00550.x.

Gangopadhyay, S., T. Pruitt, L. Brekke, D. Raff. 2011. Hydrologic Projections for the Western United States. *EOS, Transactions, American Geophysical Union*, 92(48).

Gao, Y., J.A. Vano, C. Zhu, D.P. Lettenmaier. 2011. Evaluating climate change over the Colorado River basin using regional climate models. *Journal of Geophysical Research* 116:D13104. doi:10.1029/2010JD015278.

Garner, B.D., D.J. Bills. 2012. *Spatial and seasonal variability of base flow in the Verde Valley, central Arizona, 2007 and 2011*. U.S. Geological Survey Scientific Investigations Report 2012–5192.

Gober, P.A. 2013. Getting Outside the Water Box: The Need for New Approaches to Water Planning and Policy. *Water Resources Management* 27:955-957. doi:10.1007/s11269-012-0222-y.

Gober, P.A., C.W. Kirkwood, R. C. Balling, Jr., A. W. Ellis, S. Deitrick. 2010. Water Planning Under Climatic Uncertainty in Phoenix: Why We Need a New Paradigm. *Annals of the Association of American Geographers* 100(2):356-372. doi:10.1080/00045601003595420.

Gray, S.T., L.J. Graumlich, J.L. Betancourt, G.T. Pederson. 2004. A tree-ring based reconstruction of the Atlantic Multidecadal Oscillation since 1567 A.D. *Geophysical Research Letters* 31:L12205. doi:10.1029/2004GL019932.

Gumbel, E.J. 1958. *Statistics of Extremes*. Mineola NY: Dover Publications.

Gutzler, D., S. Keller, S. Rocha. 2012. Seasonal Diagnosis of Observed and Projected Drying Trends in Southwestern North America. *American Geophysical Union 2012 Fall Meeting, San Francisco CA*, paper GC52A-05.

Hansen, J.E. 1988. *The Greenhouse Effect: Impacts on Current Global Temperature and Regional Heat Waves*. Statement of James E. Hansen, NASA Goddard Institute for Space Studies, presented to United States Senate Committee on Energy and Natural Resources, 23 June 1988.

——. 2013. Minimizing Irreversible Impacts of Human-Made Climate Change. *American Geophysical Union 2013 Fall Meeting, San Francisco CA*, paper GC44A-06 (invited).

Hansen, J., I. Fung, A. Lacis, D. Rind, S. Lebedeff, R. Ruedy, G. Russell, P. Stone. 1988. Global Climate Changes as Forecast by GISS Three-Dimensional Model. *Journal of Geophysical Research* 93:9341-9364.

Hartmann, D.L. 1994. *Global Physical Climatology*. San Diego: Academic Press.

Held, I.M. 2013. The cause of the pause. *Nature* 501:318-319. doi:10.1038/501318a.

Hirschboeck K.K., D.M. Meko. 2005. "A Tree-Ring Based Hydroclimatic Assessment of Synchronous Extreme Streamflow Episodes in the Upper Colorado and Salt-Verde River Basins". Available at http://www.ltrr.arizona.edu/kkh/srp_final_report.htm.

——. 2008. "The Current Drought in Context: A Tree-Ring Based Evaluation of Water Supply Variability for the Salt-Verde River Basin". Available at http://www.ltrr.arizona.edu/kkh/srp2.htm.

Hoerling, M. 2014. A Climate Analyst Clarifies the Science Behind California's Water Woes. *The New York Times, Dot Earth, Climate Change*, 6 March 2014, communication from M. Hoerling to A. Revkin.

Hoerling, M., J. Eischeid. 2007. Past Peak Water in the Southwest. *Southwest Hydrology* 6(1):18-19,35.

Hoerling, M., X.W. Quan. 2012. Factors Driving Hadley Cell Variability. *American Geophysical Union 2012 Fall Meeting, San Francisco CA*, paper GC52A-08.

Hoerling, M., D.P. Lettenmaier, D. Cayan, B. Udall. 2009. Reconciling Projections of Colorado Streamflow. *Southwest Hydrology* 8(3):20-21,31.

Hu, A., G.A. Meehl, H. Teng, J. Arblaster, G. Branstator, J. Fasullo, K.E. Trenberth. 2013. Decadal Climate Variability and Prediction: Understanding the mid-1970s Climate Shift and the Early-2000s Hiatus. *American Geophysical Union 2013 Fall Meeting, San Francisco CA*, paper GC21F-02 (invited).

International Institute of Forecasters (IIF) at http://forecasters.org. "Forecasting Principles – Evidence-Based Forecasting". Available at www.forecastingprinciples.com.

IPCC. 2007. *Climate Change 2007. Synthesis Report. Contribution of Working Groups I, II and III to the Fourth Assessment Report of the Intergovernmental Panel on Climate Change*. Geneva Switzerland: IPCC.

IPCC. 2013. *Climate Change 2013: The Physical Science Basis. Contribution of Working Group I to the Fifth Assessment Report of the Intergovernmental Panel on Climate Change*. Stocker, T.F., D. Qin, G.-K. Plattner, M. Tignor, S.K. Allen, J. Boschung, A. Nauels, Y. Xia, V. Bex, and P.M. Midgley (Eds.). Cambridge, United Kingdom, and New York, NY, USA: Cambridge University Press.

Jeton, A.E., M.D. Dettinger, J.L. Smith. 1996. *Potential effects of climate change on streamflow, eastern and western slopes of the Sierra Nevada, California and Nevada*. United States Geological Survey (USGS) Water-Resources Investigations Report: 95-4260.

Jiang, J.H., H. Su, C. Zhai, L. Wu, K. Minschwaner, A.M. Molod, A.M. Tompkins. 2015. An Assessment of upper troposphere and lower stratosphere water vapor in MERRA, MERRA2, and ECMWF reanalyses using Aura MLS observations. *Journal of Geophysical Research: Atmospheres* 120:11468-11485. doi:10.1002/2015JD023752.

Katz, R.W. 2010. Statistics of extremes in climate change. *Climatic Change* 100:71-76.

Keeling, C.D., J.A. Adams Jr., C.A. Ekdahl Jr., P.R. Guenther. 1976. Atmospheric Carbon Dioxide Variations at the South Pole. *Tellus* 28:552-564. Available at http://scrippsco2.ucsd.edu/data/spo.html. Last accessed 15 January 2015.

Keenlyside, N.S., M. Latif, J. Jungclaus, L. Kornblueh, E. Roeckner. 2008. Advancing decadal-scale climate prediction in the North Atlantic sector. *Nature* 453:84-88. doi:10.1038/nature06921.

Kerr, R.A. 2000. A North Atlantic Climate Pacemaker for the Centuries. *Science* 288(5473):1984-1985. doi:10.1126/science.288.5473.1984.

Knight, J.R., R.J. Allan, C.K. Folland, M. Vellinga, M.E. Mann. 2005. A signature of persistent natural thermohaline circulation cycles in observed climate. *Geophysical Research Letters* 32:L20708. doi:10.1029/2005GL024233.

Knudsen, M.F., M-S. Seidenkrantz, B.H. Jacobsen, A. Kuijpers. 2011. Tracking the Atlantic Multidecadal Oscillation through the last 8000 years. *Nature Communications* 2:178. doi:10.1038/ncomms1186.

Knutti, R., J. Sedlacek. 2013. Robustness and uncertainties in the new CMIP5 climate model projections. *Nature Climate Change* 3:369-373. doi:10.1038/NCLIMATE1716.

Knutti, R., D. Masson, A. Gettleman. 2013. Climate model genealogy: Generation CMPI5 and how we got there. *Geophysical Research Letters* 40:1194-1199. doi:10.1002/grl.50256.

Knutti, R., C.Tebaldi. 2013. Uncertainties and Ensembles in Global Climate Models: Open Issues with Model Dependence, Performance, and Robustness. *American Geophysical Union 2013 Fall Meeting, San Francisco CA*, paper GC33E-04 (invited).

Kosaka, Y. 2014. Increasing wind sinks heat. *Nature Climate Change* 4:172-173. doi:10.1038/nclimate2138.

Kosaka, Y., S-P. Xie. 2013. Recent global-warming hiatus tied to equatorial Pacific surface cooling. *Nature* 501:403-407. doi:10.1038/nature12534.

Koutsoyiannis, D. 2011. Hurst-Kolmogorov Dynamics and Uncertainty. *Journal of the American Water Resources Association* 47(3):481-495. doi:10.1111/j.1752-1688.2011.00543.x.

Koutsoyiannis, D., A. Efstratiadis, N. Mamassis, A. Christofides. 2008. On the credibility of climate projections. *Hydrological Sciences Journal* 53(4):671-684. doi:10.1623/hysj.53.4.671.

Koutsoyiannis, D., A. Montanari, H.F. Lins, T.A. Cohn. 2009. Climate, hydrology and freshwater: towards an interactive incorporation of hydrological experience into climate research. *Hydrological Sciences Journal* 54(2). doi:10.1623/hysj.54.2.394.

Kundzewicz, Z.W., E.Z. Stakhiv. 2010. Are climate models "ready for prime time" in water resources management applications, or is more research needed? *Hydrological Sciences Journal* 55(7):1085-1089. doi:10.1080/02626667.2010.513211.

Kundzewicz, Z.W., L.J. Mata, N.W. Arnell, P. Doll. B. Jimenez, K. Miller, T. Oki, Z. Sen, I. Shiklomanov. 2008. The implications of projected climate change for freshwater resources and their management. *Hydrological Sciences Journal* 53(1):3-10. doi:10.1623/hysj.53.1.3.

Kundzewicz, Z.W., L.J. Mata, N.W. Arnell, P. Doll. B. Jimenez, K. Miller, T. Oki, Z. Sen. 2009. Water and climate projections. *Hydrological Sciences Journal* 54(2):406-415. doi:10.1623/hysj.54.2.406.

Kurtz, B.E. 2014. An Electrical Analogy Relating the Atlantic Multidecadal Oscillation to the Atlantic Meridional Overturning Circulation. *PLOS ONE* 9(6). doi:10.1371/journal.pone.0100306.

Lewis, N., J.A. Curry. 2015. The implications for climate sensitivity of AR5 forcing and heat uptake estimates. *Climate Dynamics* 45:1009-1023. doi:10.1007/s00382-014-2342-y.

Li, J., C. Sun, F-F. Jin. 2013. NAO implicated as a predictor of Northern Hemisphere mean temperature multidecadal variability. *Geophysical Research Letters* 40:5497-5502. doi:10.1002/2013GL057877.

Lins, H.F., T.A. Cohn. 2011. Stationarity: Wanted Dead or Alive? *Journal of the American Water Resources Association* 47(3):475-480. doi:10.1111/j.1752-1688.2011.00542.x.

Lovejoy, S. 2013. What is climate? *EOS, Transactions, American Geophysical Union,* 94(1):1-2. doi:10.1002/2013EO010001.

——. 2014. Scaling fluctuation analysis and statistical hypothesis testing of anthropogenic warming. *Climate Dynamics* 42(9-10):2339-2351. doi:10.1007/s00382-014-2128-2.

Mahlstein, I., R.W. Portmann, J.S. Daniel, S. Solomon, R. Knutti. 2012. Perceptible changes in regional precipitation in a future climate. *Geophysical Research Letters* 39:L05701. doi:10.1029/2011GL050738.

Makridakis, S., S.C. Wheelwright, R.J. Hyndman. 1998. *Forecasting Methods and Applications, 3rd Edition*. New York: John Wiley & Sons.

Matalas, N.C. 1990. *What Statistics Can Tell Us,* in *Climate Change and U.S. Water Resources* (139-149), edited by P.E. Waggoner. New York: John Wiley & Sons.

——. 2012. Comment on the Announced Death of Stationarity. *Journal of Water Resources Planning and Management* 138:311-312. doi:10.1061/(ASCE)WR.1943-5452.0000215.

Mazzarella, A., N. Scafetta. 2012. Evidences for a quasi 60-year North Atlantic Oscillation since 1700 and its meaning for global climate change. *Theoretical and Applied Climatology* 107:599-609. doi:10.1007/s00704-011-0499-4.

McCabe, G.J., D.M. Wolock. 2012. Joint variability of global sea-surface temperatures and runoff in the conterminous United States. *American Geophysical Union 2012 Fall Meeting, San Francisco CA*, paper GC52A-02.

Meehl, G.A., A. Hu, J.M. Arblaster, J. Fasullo, K.E. Trenberth. 2013. Externally Forced and Internally Generated Decadal Climate Variability Associated with the Interdecadal Pacific Oscillation. *Journal of Climate* 26:7298-7310. doi:10.1175/JCLI-D-12-00548.1.

Meehl, G.A., A. Hu, H. Teng. 2016. Initialized decadal prediction for transition to positive phase of the Interdecadal Pacific Oscillation. *Nature Communications* 7:11718. doi:10.1038/ncomms11718.

Mills, T.C. 2010. 'Skinning a cat': alternative models of representing temperature trends. An editorial comment. *Climatic Change* 101:415-426. doi:10.1007/s10584-010-9801-1.

Milly, P.C.D., K.A. Dunne, A.V. Vecchia. 2005. Global pattern of trends in streamflow and water availability in a changing climate. *Nature* 438(17):347-350. doi:10.1038/nature04312.

Milly, P.C.D., J. Betancourt, M. Falkenmark, R.M. Hirsch, Z.W. Kundzewicz, D.P. Lettenmaier, R.J. Stouffer. 2008. Stationarity Is Dead: Whither Water Management? *Science* 319:573-574. doi:10.1126/science.1151915.

Mishra, A.K., V.P. Singh. 2010. A review of drought concepts. *Journal of Hydrology* 391: 202-216. doi:10.1016/j.jhydrol.2010.07.012.

——. 2011. Drought modeling – A review. *Journal of Hydrology* 403:157-175. doi:10.1016/j.jhydrol.2011.03.049.

Morice, C.P., J.J. Kennedy, N.A. Rayner, P.D. Jones. 2012. Quantifying uncertainties in global and regional temperature change using an ensemble of observational estimates: The HadCRUT4 dataset. *Journal of Geophysical Research* 117:D08101. doi:10.1029/2011JD017187. Available at www.metoffice.gov.uk/hadobs/hadcrut4/. Last accessed 27 January 2016.

Murphy, B.S. 2015. "PyKrige 1.3.0. Kriging toolkit for Python supporting two- and three-dimensional ordinary and universal kriging. Author: Benjamin S. Murphy". Homepage: https://github.com/bsmurphy/PyKrige. Available at https://pypi.python.org/pypi/PyKrige.

Murphy, K.W., A.W. Ellis. 2014. An assessment of the stationarity of climate and stream flow in watersheds of the Colorado River Basin. *Journal of Hydrology* 509:454-473. doi:10.1016/j.jhydrol.2013.11.056.

Nelson, B.L. 1995. *Stochastic Modeling: Analysis and Simulation*. New York: McGraw-Hill Inc.

NIST. 2012. "NIST/SEMATECH e-Handbook of Statistical Methods, Section 1.3.5.10, Levene Test for Equality of Variances". Available at http://www.itl.nist.gov/div898/handbook.

Nowak, K., M. Hoerling, B. Rajagopalan, E. Zagona. 2012. Colorado River Basin Hydroclimatic Variability. *Journal of Climate* 25:4389-4403. doi:10.1175/JCLI-D-11-00406.1.

Otto, A., F.E.L. Otto, O. Boucher, J. Church, G. Hegerl, P.M. Forster, N.P. Gillett, J. Gregory, G.C. Johnson, R. Knutti, N. Lewis, U. Lohmann, J. Marotzke, G. Myhre, D. Shindell, B. Stevens, M.R. Allen. 2013. Energy budget constraints on climate response. *Nature Geoscience* 6(6):415-416. doi:10.1038/ngeo1836.

Paltridge, G., A. Arking, M. Pook. 2009. Trends in middle- and upper-level tropospheric humidity from NCEP reanalysis data. *Theoretical and Applied Climatology* 98:351-359. doi:10.1007/s00704-009-0117-x.

Percival, D.B., D.A. Rothrock. 2005. "Eyeballing" Trends in Climate Time Series: A Cautionary Note. *Journal of Climate* 18(6):886-891.

Phillips, D.H., Y. Reinink, T.E. Skarupa, C.E. Ester III, J.A. Skindlov. 2009. Water Resources Planning and Management at the Salt River Project, Arizona, U.S.A. *Irrigation and Drainage Systems* 23(2-3):109-124. doi:10.1007/s10795-009-9063-0.

Pielke, R.A., Jr. 2008. Climate predictions and observations. *Nature Geoscience* 1(4):206. doi:10.1038/ngeo157.

Pielke, R.A., Sr., R.L. Wilby. 2012. Regional Climate Downscaling – What's the Point? *EOS, Transactions, American Geophysical Union*, 93(5):52-53.

Privalsky, V., V. Yushkov. 2015. Validation of CMIP5 models for the contiguous United States. *Atmospheric Science Letters* 16:461-464. doi:10.1002/asl.582.

Ralph, F.M., P.J. Neiman, G.N. Kiladis, K. Weickmann, D.W. Reynolds. 2011. A Multiscale Observational Case Study of a Pacific Atmospheric River Exhibiting Tropical-Extratropical Connections and a Mesoscale Frontal Wave. *Monthly Weather Review* 139:1169-1189. doi:10.1175/2010MWR3596.1.

Reclamation. 2013. "Downscaled Climate and Hydrology Projections Website". Bulletin 2013-19. Available at http://gdo-dcp.ucllnl.org/downscaled_cmip_projections/.

Reisner, M. 1986. *Cadillac Desert – The American West and Its Disappearing Water*. New York: Penguin Books.

Risbey, J.S., D. Entekhabi. 1996. Observed Sacramento Basin streamflow response to precipitation and temperature changes and its relevance to climate impact studies. *Journal of Hydrology* 184:209-223.

Rogers, P. 2008. Coping with Global Warming and Climate Change. *Journal of Water Resources Planning and Management* 134(3):203-204. doi:10.1061/(ASCE)0733-9496.

Rogers, P.P., M.B. Fiering. 1990. *From Flow to Storage*, in *Climate Change and U.S. Water Resources* (207-221), edited by P.E. Waggoner. New York: John Wiley & Sons.

Salas, J.D., B. Rajagopalan, L. Saito, C. Brown. 2012. Special Section on Climate Change and Water Resources: Climate Nonstationarity and Water Resources Management. *Journal of Water Resources Planning and Management* 138:385-388. doi:10.1061/(ASCE)WR.1943-5452.0000279.

Salt River Project (SRP-a). "Dams and reservoirs managed by SRP". Available at http://www.srpnet.com/water/dams.

—— (SRP-b). "Watershed monitor". Available at http://www.watershedmonitor.com.

—— (SRP-c). *SRP 2013 Annual Report*.

Sankarasubramanian, A., R.M. Vogel. 2003. Hydroclimatology of the continental United States. *Geophysical Research Letters* 30(7):1363. doi:10.1029/2002GL015937.

Sankarasubramanian, A., R.M. Vogel, J.F. Limbrunner. 2001. Climate elasticity of streamflow in the United States. *Water Resources Research* 37(6):1771-1781.

Schaake, J.C. 1990. *From Climate to Flow*, in *Climate Change and U.S. Water Resources* (177-206), edited by P.E. Waggoner. New York: John Wiley & Sons.

Schlesinger, M.E., N. Ramankutty. 1994. An oscillation in the global climate system of period 65-70 years. *Nature* 367:723-726. doi:10.1038/367723a0.

——. 2000. Temperature oscillations in the North Atlantic. *Science* 288(5479):547-548. doi:10.1126/ science.289.5479.547b.

Schneider, S.H. 1992. *Introduction to Climate Modeling*, in *Climate System Modeling* (3-26), edited by K.E. Trenberth. Cambridge, United Kingdom: Cambridge University Press.

Seager, R., M. Ting, I. Held, Y. Kushnir, J. Lu, G. Vecchi, H-P. Huang, N. Harnik, A. Leetmaa, N-C. Lau, C. Li, J. Velez, N. Naik. 2007. Model Projections of an Imminent Transition to a More Arid Climate in Southwestern North America. *Science* 316:1181-1184. doi:10.1126/science.1139601.

Seager, R., G.A. Vecchi. 2010. Greenhouse warming and the 21st century hydroclimate of southwestern North America. *Proceedings of the National Academy of Sciences* 107(50):21277-21282. doi:10.1073/pnas.0910856107.

Shindell, D.T. 2014. Inhomogeneous forcing and transient climate sensitivity. *Nature Climate Change* 4:274-277. doi:10.1038/nclimate2136.

Shumway, R.H., D.S. Stoffer. 2010. *Time Series Analysis and Its Applications, 3rd Edition*. New York: Springer Science+Business Media.

Skeie, R.B., T. Berntsen, M. Aldrin, M. Holden, G. Myhre. 2014. A lower and more constrained estimate of climate sensitivity using updated observations and detailed radiative forcing time series. *Earth System Dynamics* 5:139-175. doi:10.5194/esd-5-139-2014.

Smith, K.L. 1986. *The Magnificent Experiment, Building the Salt River Reclamation Project 1890-1917*. Tucson: The University of Arizona Press.

Stakhiv, E.Z. 2011. Pragmatic Approaches for Water Management Under Climate Change Uncertainty. *Journal of the American Water Resources Association* 47(6):1183-1196. doi:10.1111/j.1752-1688.2011.00589.x.

Stephens, G.L., T. L'Ecuyer, R. Forbes, A. Gettleman, J-C. Golaz, A. Bodas-Salcedo, K. Suzuki, P. Gabriel, J. Haynes. 2010. Dreary state of precipitation in global models. *Journal of Geophysical Research* 115:D24211. doi:10.1029/2010JD014532.

Suckling, E.B., L.A. Smith. 2013. An Evaluation of Decadal Probability Forecasts from State-of-the-Art Climate Models. *Journal of Climate* 26:9334-9347. doi:10.1175/JCLI-D-12-00485.1.

Thomas, B.E. 2007. Climatic Fluctuations and Forecasting of Streamflow in the Lower Colorado River Basin. *Journal of the American Water Resources Association* 43(6):1550-1569. doi:10.1111/j.1752-1688.2007.00127.x.

Trenberth, K.E. 2010. More knowledge, less certainty. *Nature Climate Change* 4:20-21. doi:10.1038/climate.2010.06.

——. 2014. Challenges in Large-Scale Water Availability Changes. *American Geophysical Union 2014 Fall Meeting, San Francisco CA*, paper GC12B-02.

——. 2015. Has there been a hiatus? *Science* 349(6249):691-692. doi:10.1126/science.aac9225.

Trenberth, K.E., J. Fasullo. 2013. Earth's Energy Imbalance. *American Geophysical Union 2013 Fall Meeting, San Francisco CA*, paper GC44A-01.

Trenberth, K.E., J.T. Fasullo, G. Branstator, A.S. Phillips. 2014. Seasonal aspects of the recent pause in surface warming. *Nature Climate Change* 4:911-916. doi:10.1038/nclimate2341.

Tung, K-K., J. Zhou. 2013. Using data to attribute episodes of warming and cooling in instrumental records. *Proceedings of the National Academy of Sciences* 110(6):2058-2063. doi:10.1073/pnas.1212471110.

United States Bureau of Reclamation, Lower Colorado Region. 2012. *Colorado River Basin Water Supply & Demand Study*. Available at http://www.usbr.gov/lc/region/programs/crbstudy.html.

United States Geological Survey (USGS), National Water Information System (NWIS). Available at http://waterdata.usgs.gov/nwis. Last accessed 27 April 2016.

Vano, J.A., D.P. Lettenmaier. 2013. Two Ways to Quickly Evaluate Climate Change Impacts on Future Streamflow. *American Geophysical Union 2013 Fall Meeting, San Francisco CA*, poster GC41B-1003.

——. 2014. A sensitivity-based approach to evaluating future changes in Colorado River discharge. *Climatic Change* 122(4):621-634. doi;10.1007/s10584-013-1023-x.

Vano, J.A., T. Das, D.P. Lettenmaier. 2012. Hydrologic Sensitivities of Colorado River Runoff to Changes in Precipitation and Temperature. *Journal of Hydrometeorology* 13:932-949. doi:10.1175/JHM-D-11-069.1.

Vano, J.A., B. Udall, D.R. Cayan, J.T. Overpeck, L.D. Brekke, T. Das, H.C. Hartmann, H.G. Hidalgo, M. Hoerling, G.J. McCabe, K. Morino, R.S. Webb, K. Werner, D.P. Lettenmaier. 2014. Understanding Uncertainties in Future Colorado River Streamflow. *Bulletin of the American Meteorological Society* 95(1):59-78. doi:10.1175/BAMS-D-12-00228.1.

Watanabe, M., H. Shiogama, H. Tatebe, M. Hayashi, M. Ishii, M. Kimoto. 2014. Contribution of natural decadal variability to global warming acceleration and hiatus. *Nature Climate Change* 4:893-897. doi:10.1038/nclimate2355.

Water Utility Climate Alliance (WUCA). 2009. *Options for improving climate modeling to assist water utility planning for climate change*. Technical report of the WUCA. Available at http://www.wucaonline.org.

Wilby, R.L., S. Dessai. 2010. Robust adaptation to climate change. *Royal Meteorological Society – Weather* 65(7):180-185. doi:10.1002/wea.543.

Wilby, R.L., K. Miller, D.N. Yates, L. Kaatz. 2013. Use of Narrative Scenarios for Evaluating Drought Management Responses in the Upper Colorado River Basin. *American Geophysical Union 2013 Fall Meeting, San Francisco CA*, paper H34C-02 (invited).

World Meteorological Organization, Geneva Switzerland, 1966. *Climatic Change: Report of a working group of the Commission for Climatology*. Technical Note No.79. WMO – No.195, TP.100.

Wu, Z., N.E. Huang, J.M. Wallace, B.V. Smoliak, X. Chen. 2011. On the time-varying trend in global-mean surface temperature. *Climate Dynamics* 37(3-4):759-773. doi:10.1007/s00382-011-1128-8.

Wyatt, M.G., J.A. Curry. 2014. Role for Eurasian Arctic shelf sea ice in a secularly varying hemispheric climate signal during the 20th century. *Climate Dynamics* 42:2763-2782. doi:10.1007/s00382-013-1950-2.

Wyatt, M.G., S. Kravtsov, A.A. Tsonis. 2012. Atlantic Multidecadal Oscillation and Northern Hemisphere's climate variability. *Climate Dynamics* 38:929-949. doi:10.1007/s00382-011-1071-8.

Xie, S-P., Y. Kosaka. 2013. Current Hiatus of Global Warming Tied to Natural Variability of the Equatorial Pacific. *American Geophysical Union 2013 Fall Meeting, San Francisco CA*, poster GC41A-0996.

Yao, S-L., G. Huang, R-G. Wu, X. Qu. 2016. The global warming hiatus – a natural product of interactions of a secular warming trend and a multi-decadal oscillation. *Theoretical and Applied Climatology* 123:349-360. doi:10.1007/s00704-014-1358-x.

Zhang, R., T.L. Delworth, R. Sutton, D.L.R. Hodson, K.W. Dixon, I.M. Held, Y. Kushnir, J. Marshall, Y. Ming, R. Msadek, J. Robson, A.J. Rosati, M.F. Ting, G.A. Vecchi. 2013. Have Aerosols Caused the Observed Atlantic Multidecadal Variability? *Journal of the Atmospheric Sciences* 70(4):1135-1144. doi:10.1175/JAS-D-12-0331.1.

Zhen-Shan, L., S. Xian. 2007. Multi-scale analysis of global temperature changes and trend of a drop in temperature in the next 20 years. *Meteorology and Atmospheric Physics* 95:115-121. doi:10.1007/s00703-006-0199-2.

Zhou, J., K-K. Tung. 2013. Deducing Multidecadal Anthropogenic Global Warming Trends Using Multiple Regression Analysis. *Journal of the Atmospheric Sciences* 70(1):3-8. doi:10.1175/JAS-D-12-0208.1.

APPENDIX A

ABBREVIATIONS

ACF	Autocorrelation Function
AGU	American Geophysical Union
AGW	Anthropogenic Global Warming
AMO	Atlantic Multidecadal Oscillation
AMOC	Atlantic Meridional Overturning Circulation
AMS	American Meteorological Society
AR4, AR5	4^{th}, 5^{th} Assessment Report (of the IPCC)
CAP	Central Arizona Project
CMIP	Coupled Model Intercomparison Project
CO_2	Carbon Dioxide
CRB	Colorado River Basin
CRU	Climate Research Unit
CumProb	Cumulative Probability
ECR	Effective Climate Response
ENSO	El Niño Southern Oscillation
ET	Evapotranspiration
GCM	General Circulation Model, a.k.a. Global Climate Model
GHG	Greenhouse Gas
HK	Hurst-Kolmogorov
i.i.d.	independent and identically distributed
IPCC	Intergovernmental Panel on Climate Change
ISF	International Symposium on Forecasting
LCRB	Lower Colorado River Basin

LTDPM	Long-Term Drought Planning Model
LSHM	Land Surface Hydrology Model
ML	Miscellaneous Loss
NBS	Net Basin Supply (of water, NBS=RO-ML)
NOAA	National Oceanic and Atmospheric Administration
NWIS	National Water Information System
pdf (p.d.f.)	probability distribution (density) function
PDO	Pacific Decadal Oscillation
PE	Potential Evapotranspiration
PRISM	Parameter-elevation Regressions on Independent Slopes Model
RCM	Regional Climate Model
RCP	Representative Concentration Pathway
ResSim	Reservoir System Operations Simulation Model
RO	Runoff
SRP	Salt River Project
SST	Sea Surface Temperature
SWNA	Southwest North America
UCRB	Upper Colorado River Basin
USGS	United States Geological Survey
VIC	Variable Infiltration Capacity
WMO	World Meteorological Organization
WUCA	Water Utility Climate Alliance

APPENDIX B

WATERSHED MAPS

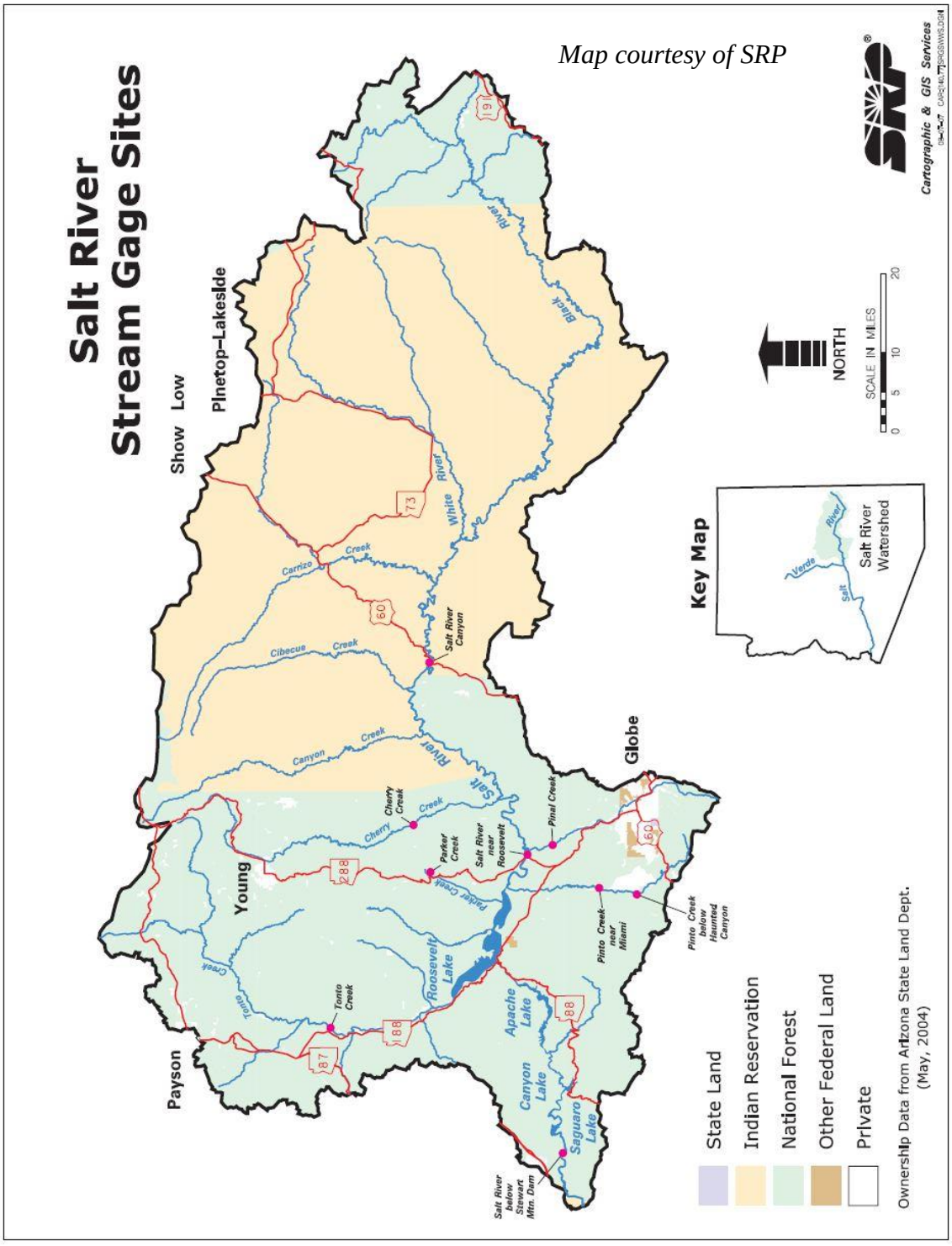

Figure B1. Map of Salt River Watershed.

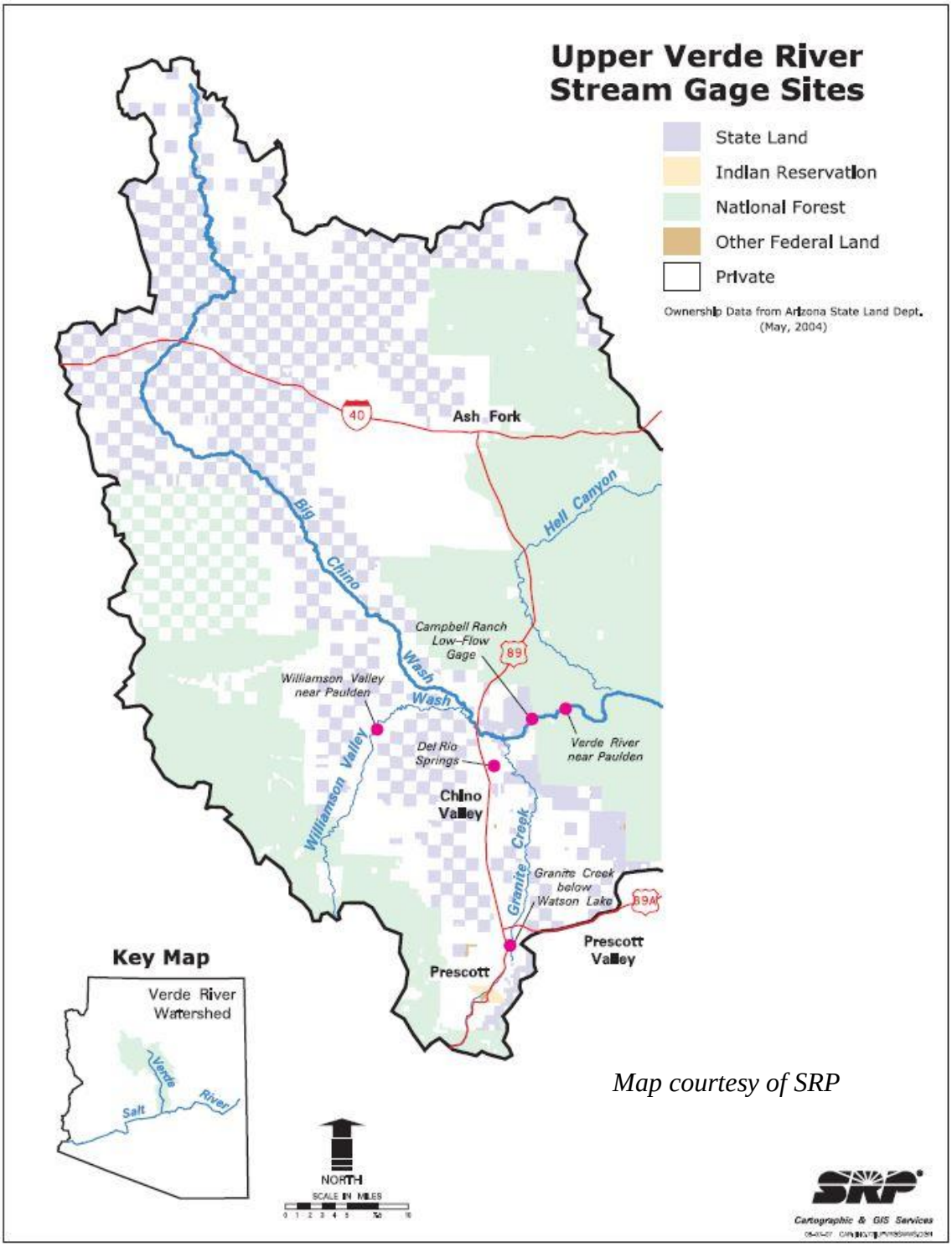

Map courtesy of SRP

Figure B2. Map of Upper Verde River Watershed.

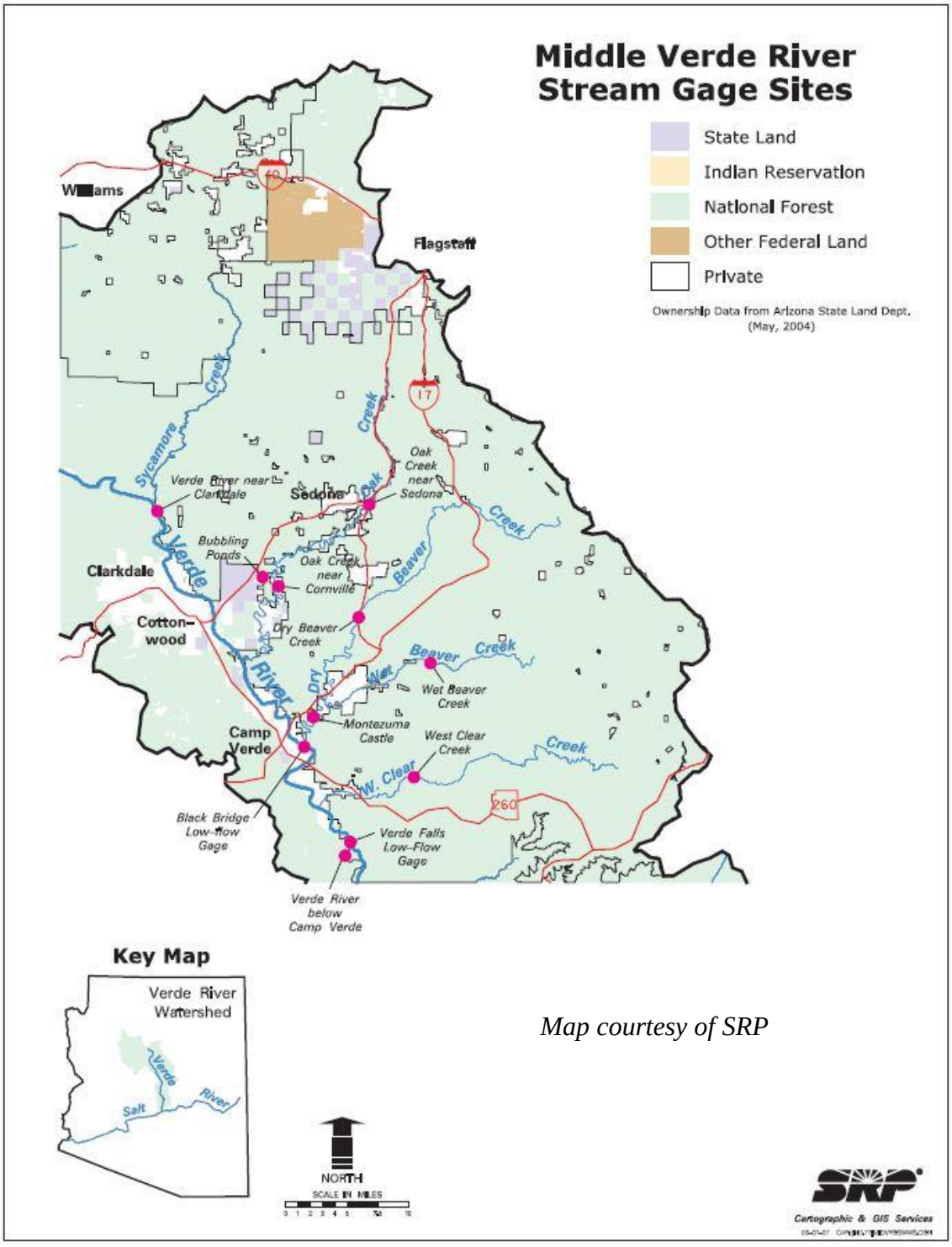

Map courtesy of SRP

Figure B3. Map of Middle Verde River Watershed.

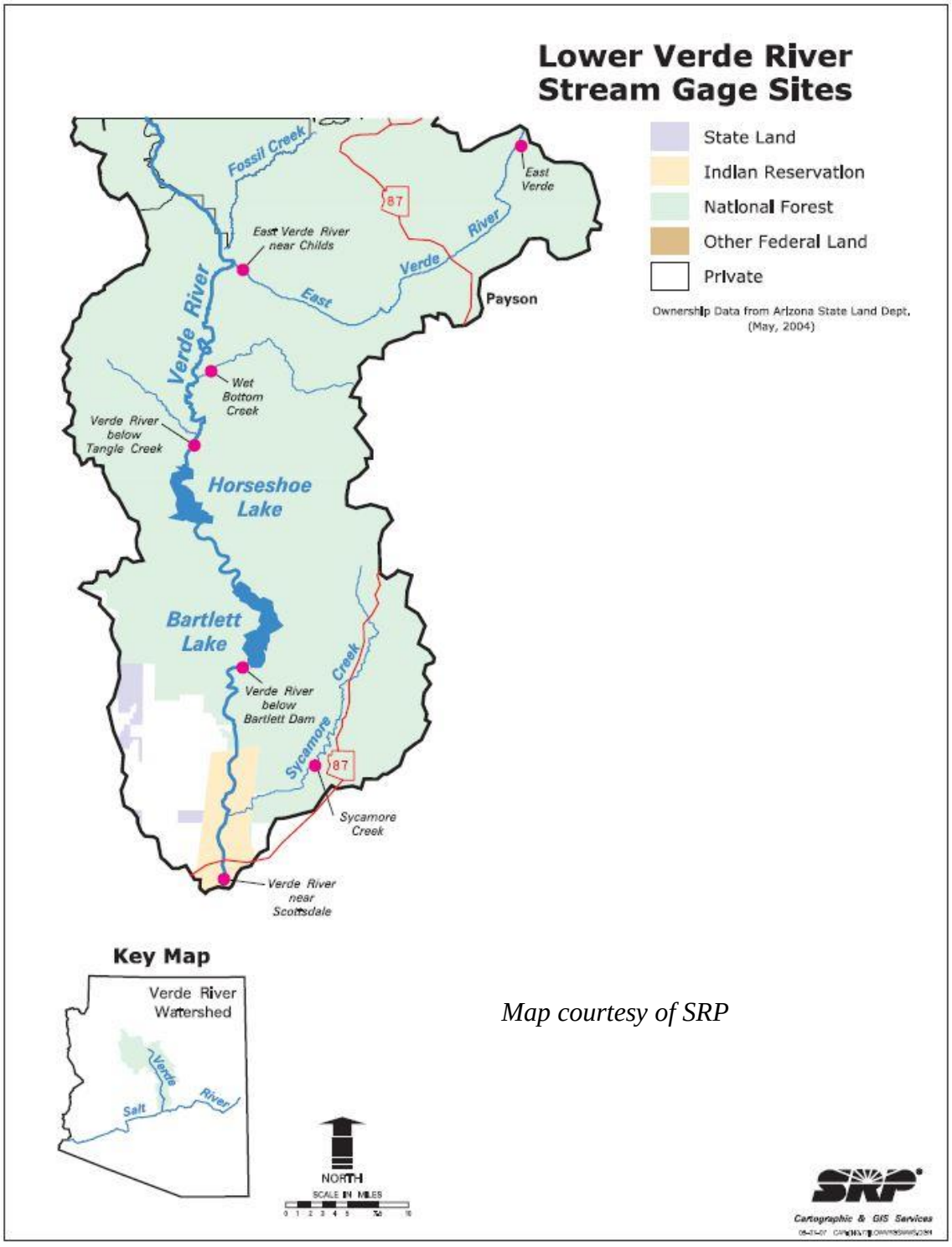

Map courtesy of SRP

Figure B4. Map of Lower Verde River Watershed.

APPENDIX C

STOCHASTIC SIMULATION PROCESS AND ALGORITHMS

RANDOM NUMBER GENERATION OF OUTCOMES - - OVERALL PROCESS

Some probability function terminology:

D(per pdf) = Discrete probability distribution, per a p.d.f. which defines a probability for each discrete value in a continuous range, with a defined maximum and minimum. Can be derived by best-fit to a historical data set.

N(mean, stddev) = Normal probability distribution having the defined mean and standard deviation. The mean will usually be zero in what follows below.

ABS[N(0, stddev)] = The Absolute Value of a random selection from a Normal probability distribution having Mean=0.

U(lo , hi) = Uniform probability distribution within the high and low values identified. A random number is usually generated from within the range of 0 to 1, but is modifiable by simple mathematical scaling to any desired range.

B(1, p) = Binomial probability distribution where the outcome is one of two possible values, one of which has probability, p. In what follows the outcome will be either 0 or 1, with equal probabilities, p=0.5.

E(lambda) = Exponential probability distribution, which is used to generate a Discrete p.d.f. The parameter, lambda, is the inverse of both the mean and the standard deviation, from which it is estimated.

Four series of SaltTonto and Verde in Winter and Summer are generated by:

I) Generate long (10,000) random values for Salt-Winter from Discrete pdf, Sw. Assign ID# per the sequence generated.

IIa) Generate long (10,000) paired values for Salt-Summer, Ss1, from correlation algorithms with Salt-Winter, Sw.

IIb) Generate long (10,000) random values for Salt-Summer, Ss2, from Discrete pdf, Ss.

III) Reconciliation process for the two series, Ss1 & Ss2:
- i) Sort the generated paired series from I (Sw) & IIa (Ss1) by Ss1, ascending, along with ID#.
- ii) Sort the generated series Ss2 from (IIb) by Ss2, ascending.
- iii) Substitute Ss2 values for Ss1 values, by position in sequence.
- iv) Sort paired Sw & Ss by ID#, ascending, returning series to original sequence.

IVa) Generate long (10,000) paired values for Verde-Winter, Vw1, from correlation algorithms with Salt-Winter, Sw.

IVb) Generate long (10,000) random values for Verde-Winter, Vw2, from Discrete pdf, Vw.

V) Reconciliation process for the two series, Vw1 & Vw2:
- i) Sort the generated paired series from I (Sw) & III (Ss) & IVa (Vw1) by Vw1, ascending, along with ID#.
- ii) Sort the generated series Vw2 from (IVb) by Vw2, ascending.
- iii) Substitute Vw2 values for Vw1 values, by position in sequence.
- iv) Sort paired Sw-Ss-Vw by ID#, ascending, returning series to original sequence.

VIa) Generate long (10,000) paired values for Verde-Summer, Vs1, from correlation algorithms with Salt-Summer, Ss.

VIb) Generate long (10,000) random values for Verde-Summer, Vs2, from Discrete pdf, Vs.

VII) Reconciliation process for the two series, Vs1 & Vs2:
- i) Sort the generated paired series from I (Sw) & III (Ss) & V (Vw) & VIa (Vs1) by Vs1, ascending, along with ID#.
- ii) Sort the generated series Vs2 from (VIb) by Vs2, ascending.
- iii) Substitute Vs2 values for Vs1 values, by position in sequence.
- iv) Sort paired Sw-Ss-Vw-Vs by ID#, ascending, returning series to original sequence.

VIII)
- i) Calculate all key statistics among resulting 4 series.
- ii) Examine correlations and modify where needed by correlation adjustment method (see NOTES),
- iii) Examine season-to-season correlations and introduce correlations where needed by resequencing process. esp: Salt Summer-to-Winter

RANDOM NUMBER GENERATION OF OUTCOMES - - WINTER SEASON RO-ML

Each pair of SaltTonto and Verde winter season outcomes is generated by:

I) Generate SaltTonto-Winter value from Sw = D(per pdf),
a random selection from the SaltTonto-Winter p.d.f., the details empirically defined elsewhere.
By definition of p.d.f. developed July 2015, Sw >=35,000 and <=2,995,000.

II) Generate Verde-Winter value, Vw1, correlated with the SaltTonto winter value, Sw, of step (I):

A) If SaltTonto value, Sw >= 900,000 then
- i) Calculate Vt = 0.55500*Sw + 66746
- ii) Generate value, Vr, from N(0, 186372)
  Vr = Vr - 10061
- iii) V = Vt + Vr
- iv) Is V >80000 ?
  - if yes, use V as the Verde value, Vw1
  - if no, re-run (iii) thru (v)

B) If SaltTonto value, Sw < 900,000 but >= 500,000 then
- i) Calculate Vt = 0.55500*Sw + 66746
- ii) Generate a value from B(1, 0.5)
- iii) If value from (ii) = 0 then
  StdDev = 0.1671*Sw + 4085
  Generate value, Vr, from ABS[N(0, StdDev)]
  Vr = -Vr - 10061
  If value from (ii) = 1 then
  Generate value, Vr, from ABS[N(0, 186372)]
  Vr = Vr - 10061
- iv) V = Vt + Vr
- v) Is V >80000 ?
  - if yes, use V as the Verde value, Vw1
  - if no, re-run (iii) thru (v)

C) If SaltTonto value, Sw < 500,000 then
- i) Calculate Vt = 0.55500*Sw + 66746
- ii) Generate a value from B(1, 0.5)
- iii) If value from (ii) = 0 and Sw<100,000 then
  StdDev = 0.2971*Sw - 8913
  If value from (ii) = 0 and Sw>=100,000 then
  StdDev = 0.1671*Sw + 4085
  Generate value, Vr, from ABS[N(0, StdDev)]
  Vr = -Vr - 10061
  If value from (ii) = 1 then
  StdDev = 0.3291*Sw + 16288
  Generate value, Vr, from ABS[N(0, StdDev)]
  Vr = Vr - 10061
- iv) V = Vt + Vr
- v) Is V >80000 ?
  - if yes, use V as the Verde value, Vw1
  - if no, re-run (iv) thru (vi)

III) Generate Verde-Winter value, Vw2, from D(per pdf),
a random selection from the Verde-Winter p.d.f., the details empirically defined elsewhere.
By definition of p.d.f. developed Oct'11, Vw >=85,000 and <=2,295,000.

IV) Reconcile dual Verde-Winter Vw1 & Vw2 series per process detailed elsewhere.

RANDOM NUMBER GENERATION OF OUTCOMES - - SUMMER SEASON RO-ML

Each pair of SaltTonto and Verde summer season outcomes is generated by:

I) Generate Salt-Summer value, = Ss1, correlated with a SaltWinter value, Sw, from WINTER step-I (previous sheet):

i) Calculate St = 0.11355*Sw + 89670
ii) Generate a value from B(1, 0.5)
iii) If value from (ii) = 0 then
Generate value, Sr, from ABS[N(0, 55343)]
Sr = -Sr - 16389
If value from (ii) = 1 then
Generate value, Sr, from D[E(1/75578)]
Sr = Sr - 16389
iv) S = St + Sr
v) Is S >10000 ?
- if yes, use S as the Salt-Summer value, Ss1
- if no, re-run (iii) thru (v)

II) Generate Salt-Summer value from Ss2 = D(per pdf),
a random selection from the SaltTonto-Summer p.d.f., the details empirically defined elsewhere.
By definition of p.d.f. developed July 2015, Ss >= 11,000 and <= 599,000.

III) Reconcile Salt-Summer Ss1 & Ss2 series per process detailed elsewhere.

IV) Generate Verde-Summer value, = Vs1, correlated with the Salt-Summer value, Ss, from step (III):

i) Calculate Vt = 0.16327*Ss + 40690
ii) Generate a value from B(1, 0.5)
iii) If value from (ii) = 0 then
Generate value, Vr, from ABS[N(0, 14109)]
Vr = -Vr - 2757
If value from (ii) = 1 then
Generate value, Vr, from Vr = D(per pdf) = E(1/16393)
Vr = Vr - 2757
iv) V = Vt + Vr
v) Is V >25000 ?
- if yes, use V as the Verde value, Vs1
- if no, re-run (iii) thru (v)

V) Generate Verde-Summer value, Vs2, from D(per pdf),
a random selection from the Verde-Summer p.d.f., the details empirically defined elsewhere.
By definition of p.d.f. developed July2015, Vs >=25,500 and <=149,500.

VI) Reconcile Verde-Summer Vs1 & Vs2 series per process detailed elsewhere.

NOTES:

1) **Parameter Estimates**

The slopes, intercepts, standard deviations, etc for the generating processes have been estimated based upon the historical data record. As additional years of evidence are added in the future, the parameters should be re-estimated.

2) **Correlation Adjustment Method**

After data series have been generated based upon the documented processes, correlations should be checked to examine how close they are to the targeted values seen in the historical record. Minor adjustments can be made by modification of the trend components in the generating algorithms -- the slope and intercepts in the St or Vt equations.

The mid-points (means) of the distribution fits should be held constant while slope and intercept are jointly adjusted, which modifies the resulting correlation amongst generated values.

APPENDIX D

HYDROLOGIC SENSITIVITY ALGORITHMS

Temperature Sensitivity, S_T

Watershed-Season	Range (units: acre-feet)	Temperature Sensitivity, S_T
Salt Winter	NBS: full range	0 %/^{o}C
Verde Winter	NBS ≤ 182,000	-3 %/^{o}C
	NBS > 182,000	0 %/^{o}C

So, for winter: $\Delta NBS = (1 - [1+ S_T]^{\Delta T}) NBS$

Salt Summer	RO = 0.87085 NBS + 35,082	
	RO < 74,000	-2 %/^{o}C
	74,000 ≤ RO < 112,000	0.28184 – 4.07895E-06 RO (%/^{o}C)
	112,000 ≤ RO ≤ 180,000	2.57353E-06 RO – 0.46324 (%/^{o}C)
	RO > 180,000	0 %/^{o}C

And, $\Delta ML / \Delta T_{res}$ = 10,000 (acre-feet/^{o}C), assessed at reservoirs

Verde Summer	RO = 0.77826 NBS + 16,524	
	RO < 37,000	-3 %/^{o}C
	37,000 ≤ RO < 48,300	0.313805 – 9.29204E-06 RO (%/^{o}C)
	48,300 ≤ RO ≤ 138,400	1.15050E-06 RO – 0.190794 (%/^{o}C)
	RO > 138,400	-3 %/^{o}C

And, $\Delta ML / \Delta T_{res}$ = 3405.43 – 1.16763E-02 NBS (acre-feet/^{o}C), assessed at reservoirs

So, for summer: $\Delta NBS = (1 - [1+ S_T]^{\Delta T}) RO + \Delta ML$

* Temperature sensitivities are applied multiplicatively to RO (as $[1+ S_T]^{\Delta T}$) and separately for RO & ML in summer due to watershed vs reservoir response differences.

Precipitation Elasticity, $\mathcal{E}_p$

$\delta = \Delta P/P$, and is assumed equally applied to reservoirs as to watersheds

	Estimated Baseflow, BF (acre-feet/season)
Salt Winter	74,000
Salt Summer	74,000
Verde Winter	83,000
Verde Summer	37,000

Watershed-Season	Range (units: acre-feet)	Precipitation Elasticity, $\mathcal{E}_p$
Salt Winter	NBS ≤ 570,000	
	RO′ = 0.96076 NBS + 27,171 - BF	
	NBS > 570,000	
	RO′ = 0.81126 NBS + 141,903 - BF	
	RO′ ≤ 30,656	1.0
	30,656 < RO′ ≤ 199,663	1.00623E-05 RO′ + 0.69153
	199,663 < RO′ ≤ 2,837,756	2.82930 – 6.44629E-07 RO′
	RO′ > 2,837,756	1.0
And,	NBS ≤ 400,000	ΔML = 0
	NBS > 400,000	ΔML = -0.1604092 (NBS + 899,646) δ (acre-feet)
Verde Winter	NBS ≤ 385,000	
	RO′ = 1.05444 NBS - 6385 - BF	
	NBS > 385,000	
	RO′ = 0.87798 NBS + 62,102 - BF	
	RO′ ≤ 7587	1.0
	7587 < RO′ ≤ 126,400	1.47652E-05 RO′ + 0.88797
	126,400 < RO′ ≤ 2,004,790	2.87256 – 9.34043E-07 RO′
	RO′ > 2,004,790	1.0

And,	NBS ≤ 200,000	ΔML = 0
	NBS > 200,000	ΔML = -0.1183025 (NBS + 600,793) δ (acre-feet)

Watershed-Season	Range (units: acre-feet)	Precipitation Elasticity, $\mathcal{E}_p$
Salt Summer	RO′ = 0.87085 NBS + 35,082 - BF	
	RO′ ≤ 1393	1.0
	1393 < RO′ ≤ 24,405	4.21542E-05 RO′ + 0.94126
	24,405 < RO′ ≤ 76,251	2.42662 – 1.87095E-05 RO′
	RO′ > 76,251	1.0
And,	NBS ≤ 165,000	ΔML = 0
	NBS > 165,000	ΔML = -0.52774 (NBS - 46651) δ (acre-feet)
Verde Summer	RO′ = 0.77826 NBS + 16,524 - BF	
	0 < RO′ ≤ 10,019	1.17074E-04 RO′ + 1.10385
	10,019 < RO′ ≤ 75,419	2.47248 – 1.95238E-05 RO′
	RO′ > 75,419	1.0
And,	NBS: full range	ΔML = -6.15223E-02 (NBS - 16030) δ (acre-feet)

So, $\Delta NBS = \delta \mathcal{E}_p RO' + \Delta ML$

APPENDIX E

WATERSHED-SEASON AND RESERVOIR-SEASON TEMPERATURE FORECASTS

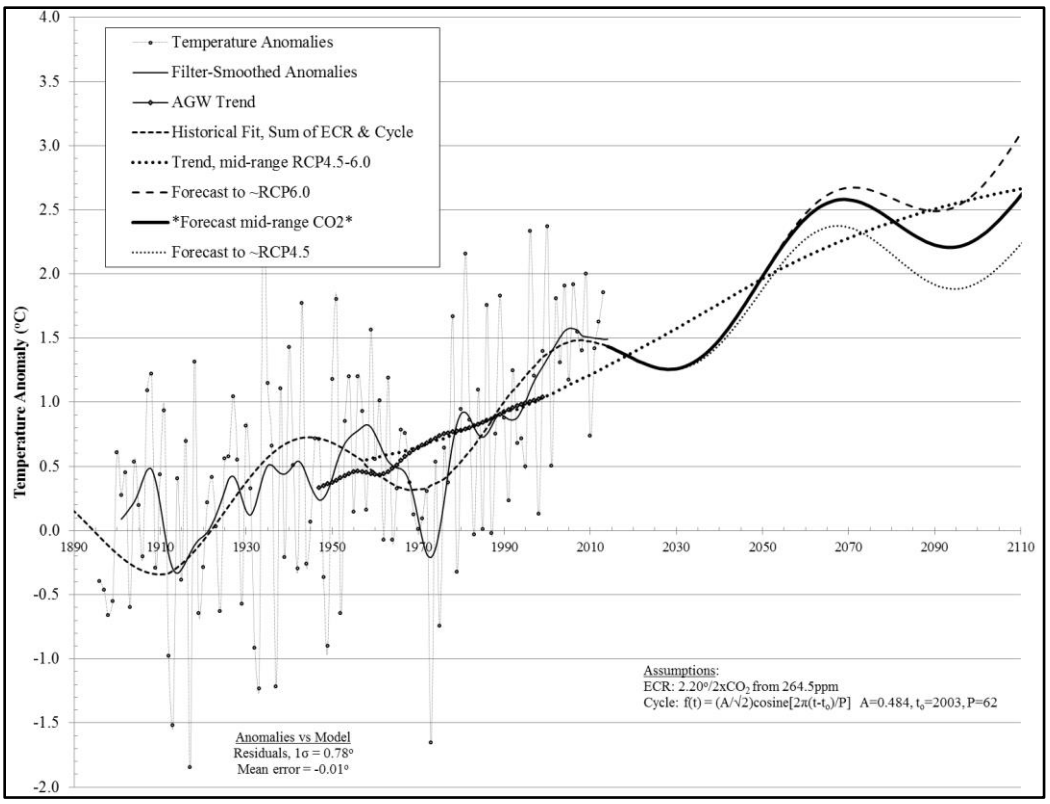

Figure E1. Temperature Change Forecast, Verde Watershed in Winter.

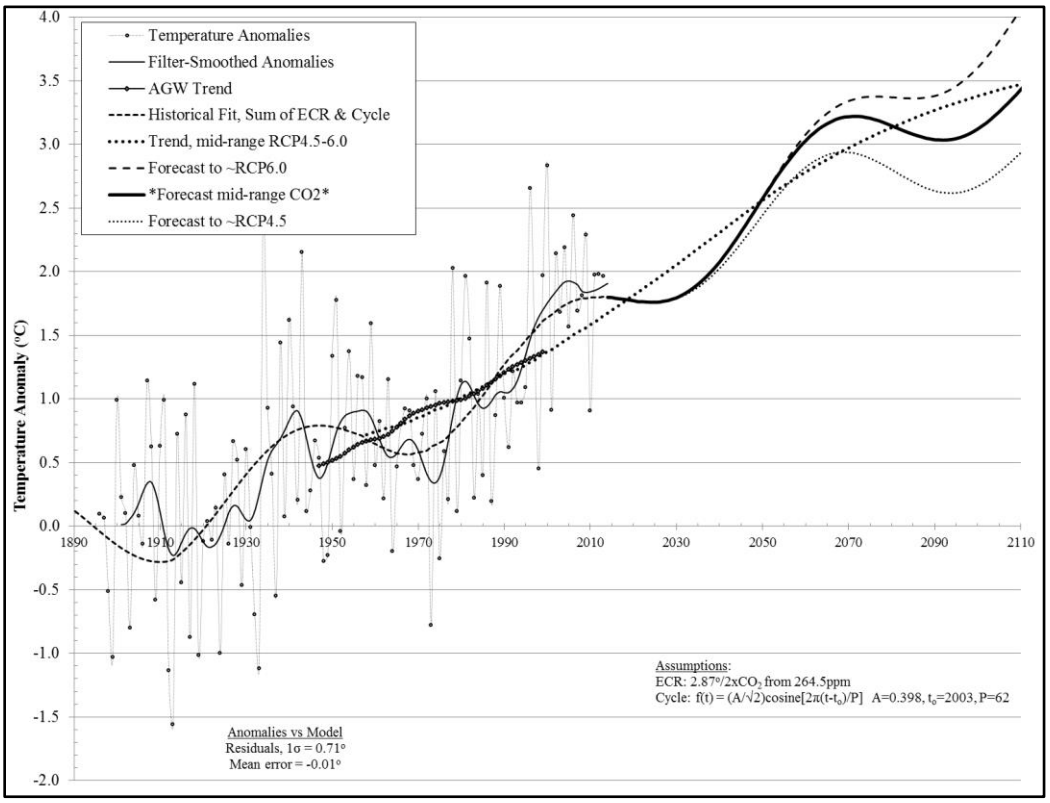

Figure E2. Temperature Change Forecast, Salt Watershed in Winter.

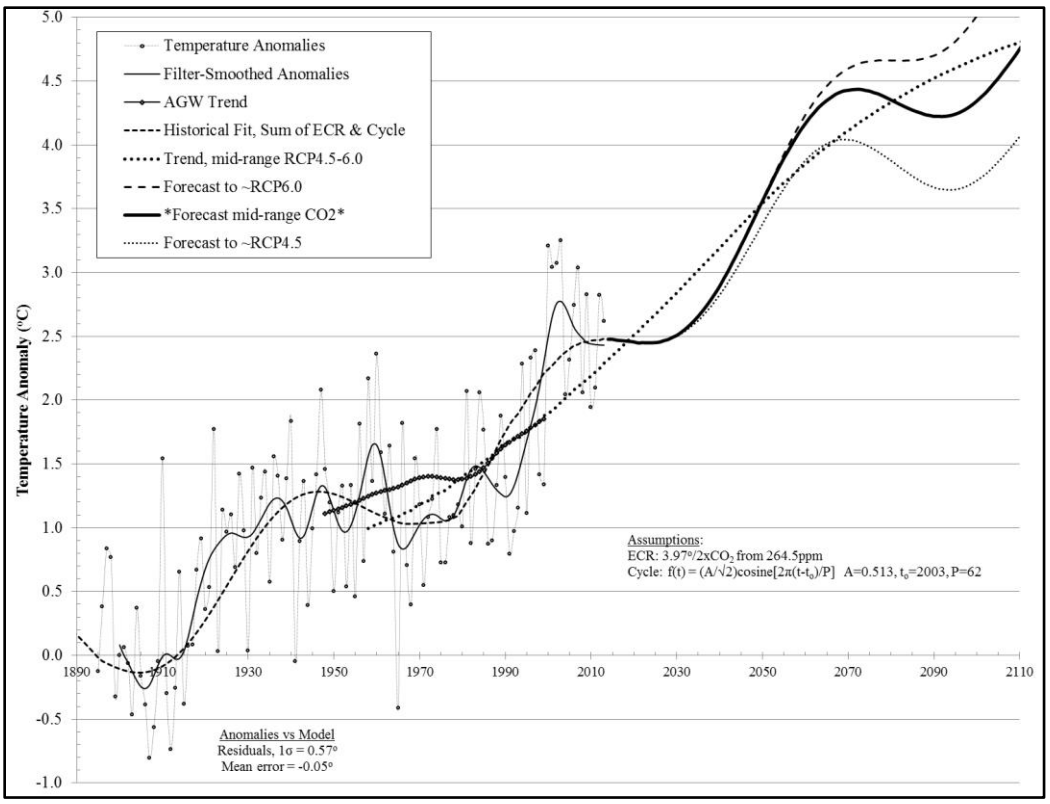

Figure E3. Temperature Change Forecast, Verde Watershed in Summer.

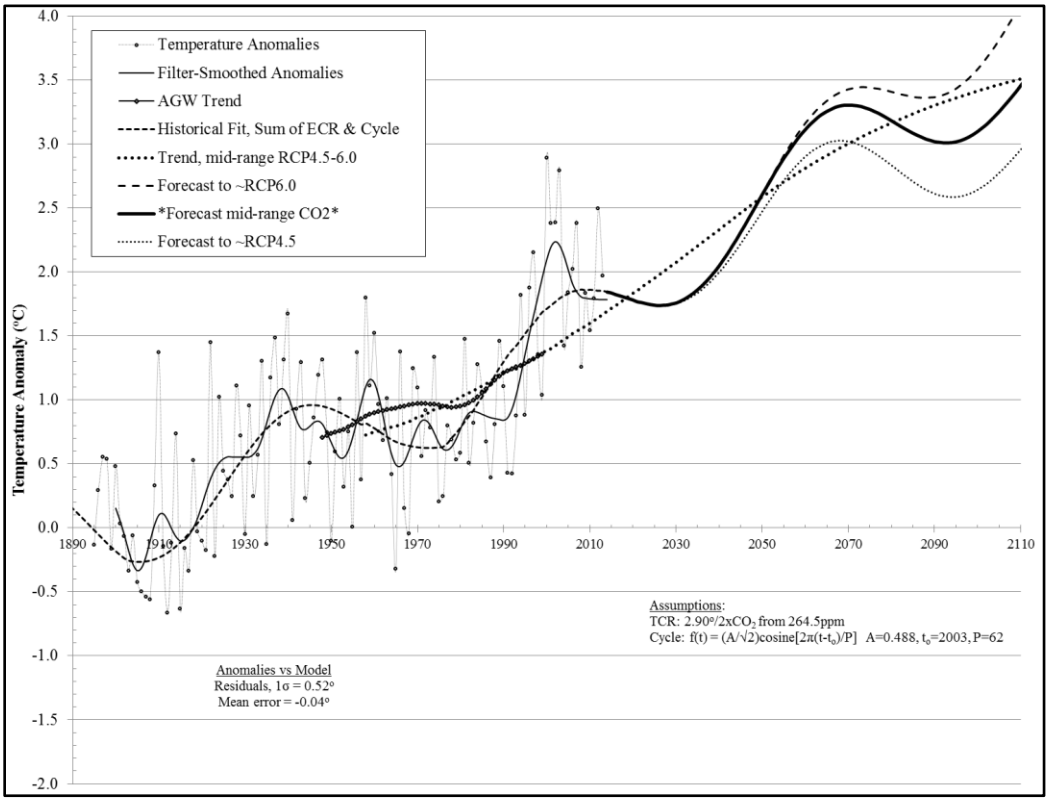

Figure E4. Temperature Change Forecast, Salt Watershed in Summer.

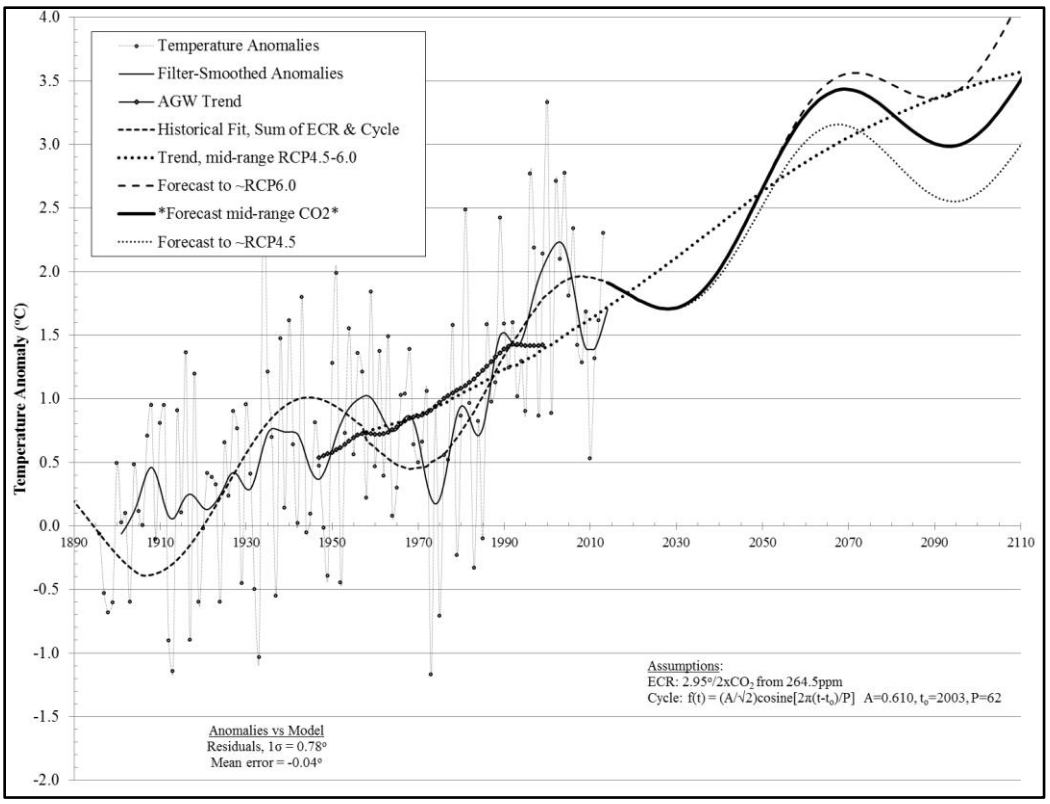

Figure E5. Temperature Change Forecast, Verde Reservoirs in Winter.

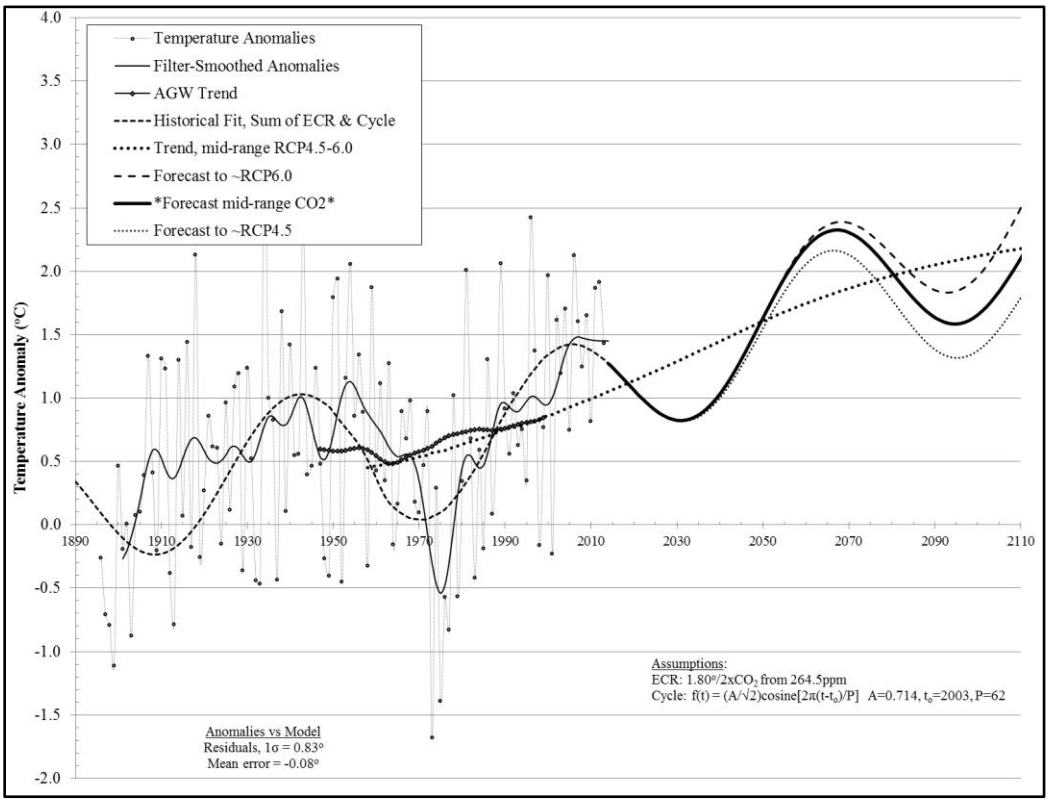

Figure E6. Temperature Change Forecast, Salt Reservoirs in Winter.

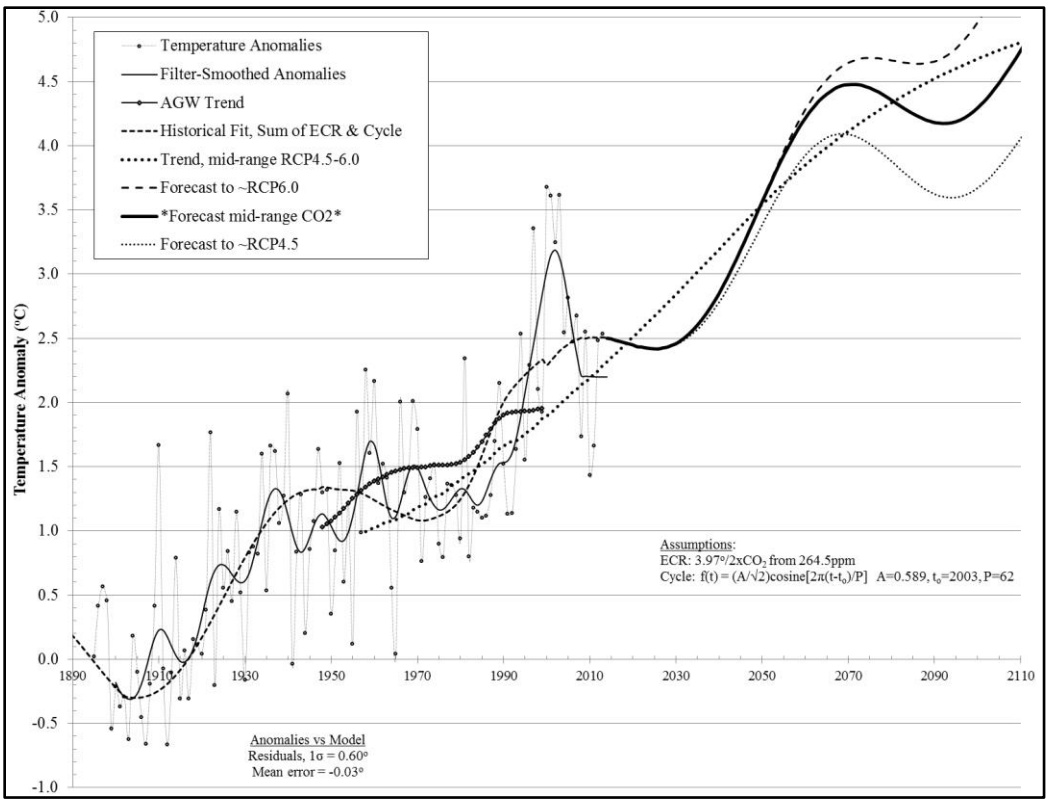

Figure E7. Temperature Change Forecast, Verde Reservoirs in Summer.

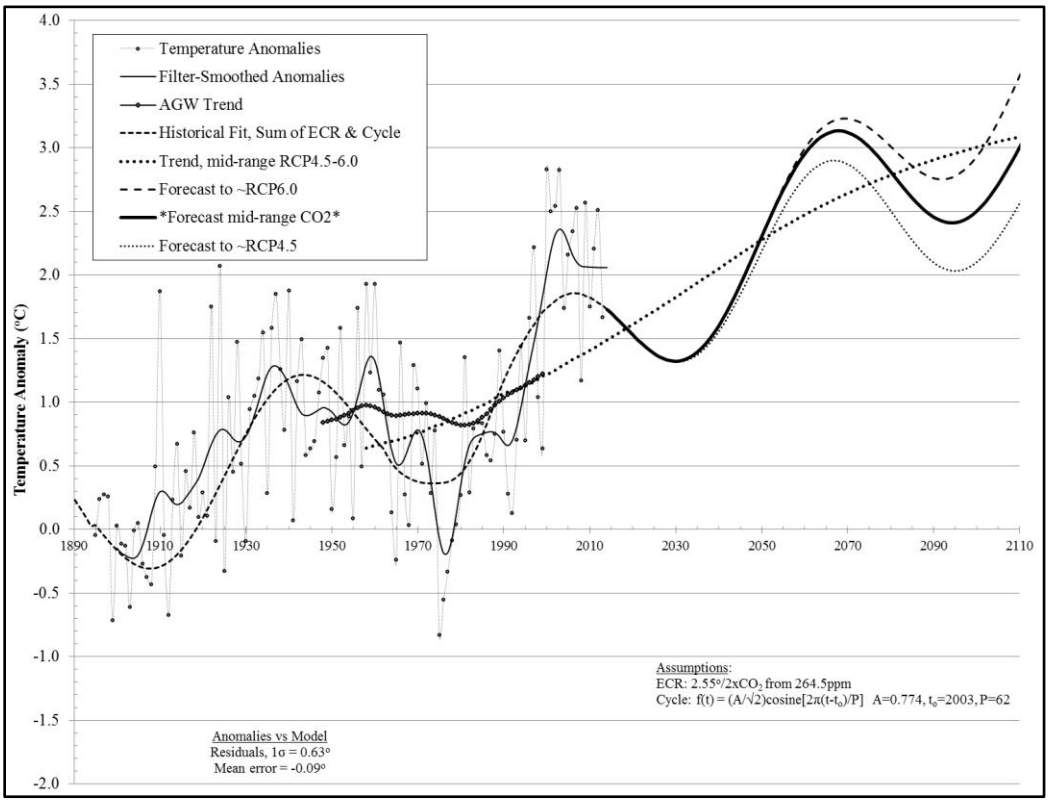

Figure E8. Temperature Change Forecast, Salt Reservoirs in Summer.

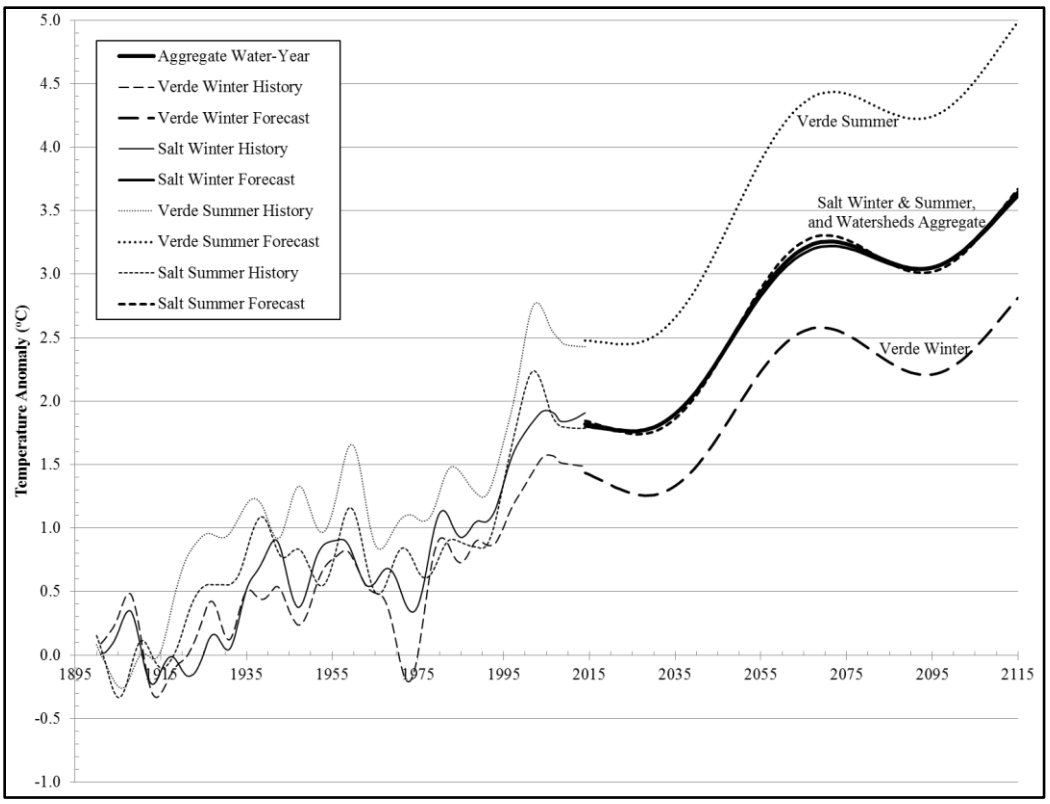

Figure E9. All Watershed-Season Temperature Change Forecasts.

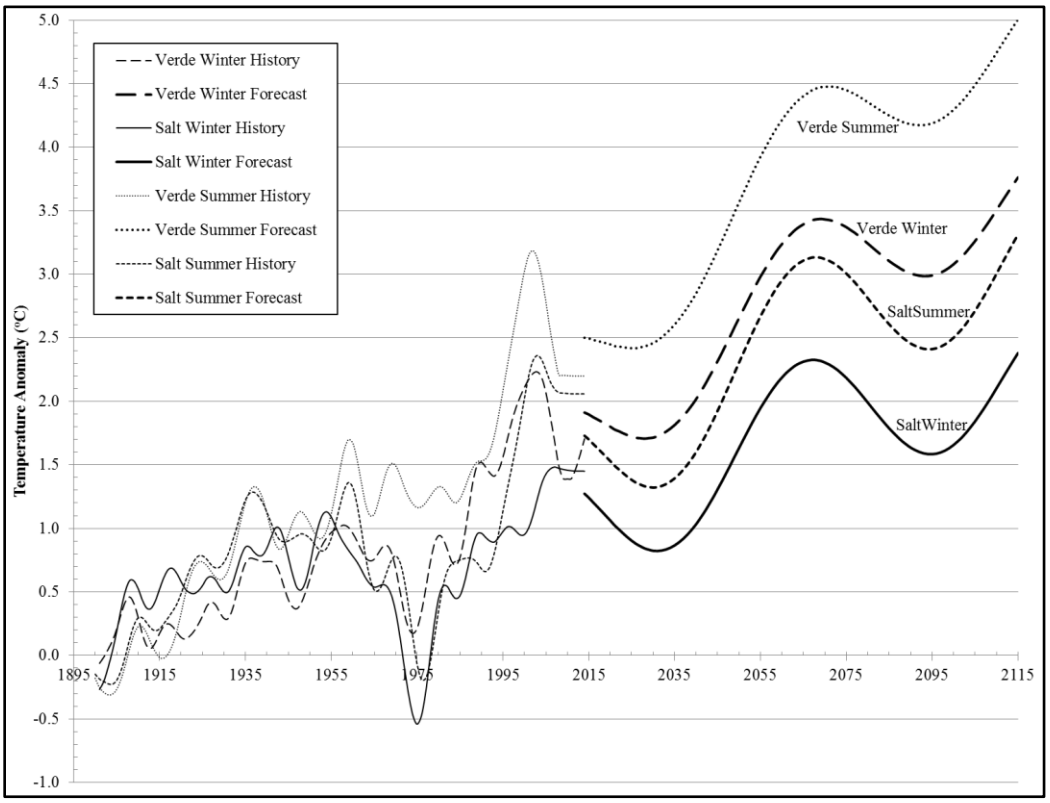

Figure E10. All Reservoir-Season Temperature Change Forecasts.

APPENDIX F

RESSIM MODEL DETAILS AND FLOW CHARTS

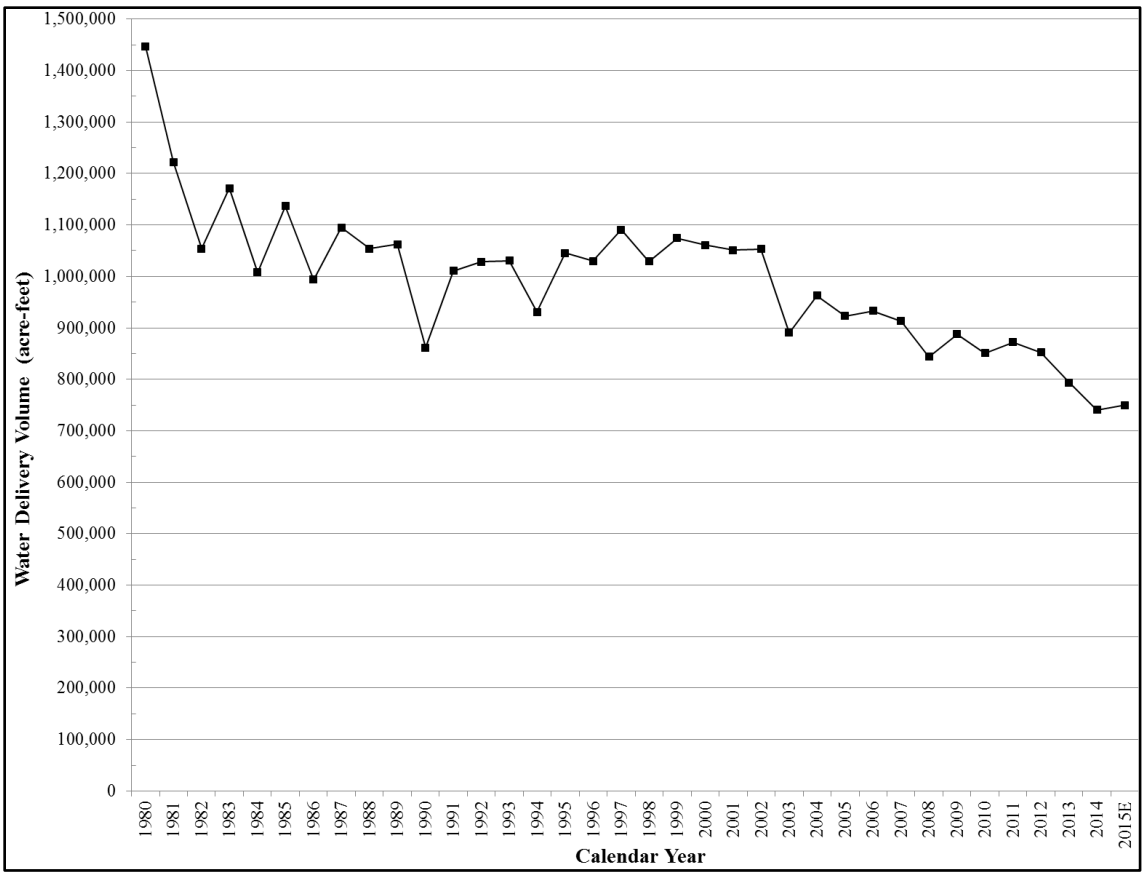

Figure F1. History of SRP Water Deliveries. The ResSim model was built per the 2003-2011 average delivery (900,000 acre-feet/year). (data courtesy of SRP)

Table F1. Standard Customer Water Demand Schedule for 900,000 acre-feet/year Annual Delivery (courtesy of SRP).

	Month	Demand		
Winter	Oct	78,000		
Winter	Nov	48,000		
Winter	Dec	38,000		
Winter	Jan	34,000		
Winter	Feb	39,000		
Winter	Mar	51,000	Winter Total	winter average
Winter	Apr	79,000	367,000	52,429 per month
Summer	May	103,000		
Summer	Jun	112,000		
Summer	Jul	116,000		
Summer	Aug	110,000	Summer Total	summer average
Summer	Sep	92,000	533,000	106,600 per month
Water-Year Total:		900,000 (acre-feet)	75,000	average per month

Table F2. Groundwater Pumping Algorithm, as a Function of Total Remaining Reservoir Storage.

Total Reservoirs Storage Level (acre-feet)	Annual Pumping Rate Algorithm	Winter Season	Summer Season
1,700,000 to 2,400,000	50,000	(212.25/365.25)	153/365.25
1,300,000 to 1,700,000	150,000-0.25*(S-1,300,000)	of annual	of annual
1,200,000 to 1,300,000	177,000-0.27*(S-1,200,000)	"	"
1,100,000 to 1,200,000	210,000-0.33*(S-1,100,000)	"	"
1,000,000 to 1,100,000	245,000-0.35*(S-1,000,000)	"	"
793,548 to 1,000,000	325,000-0.3875*(S-793,548)	"	"
0 to 793,548	325,000	"	"

Reservoirs Input-Output

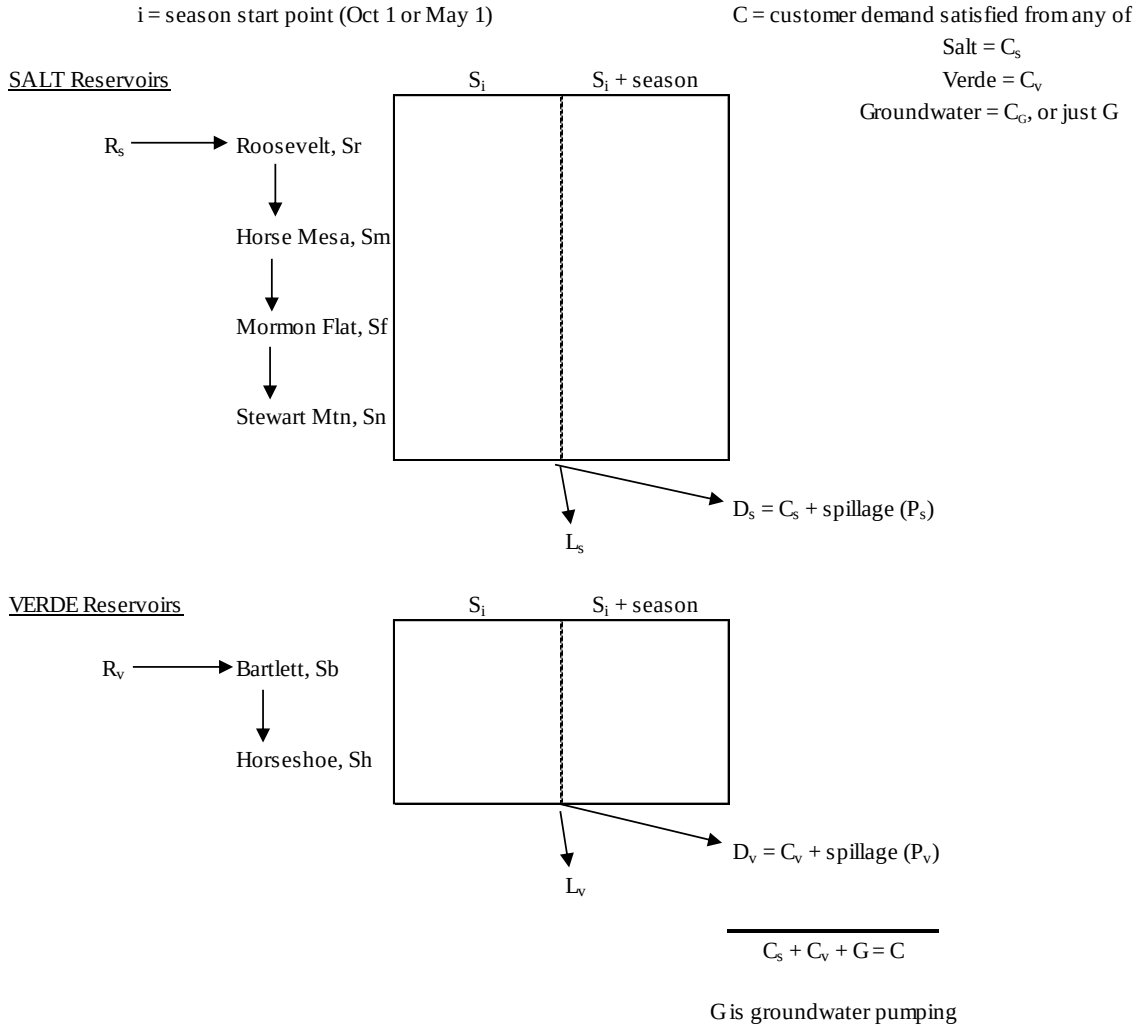

1) When SUM(S_i + season, all reservoirs) < 600,000 , Then C series is cut to 2/3rds.

2) When SUM(S_i + season, all reservoirs) < 50,000 , Then return message "Reservoirs Depleted" and [STOP] unless model is unabled for recovery.

Reservoir Status Change Algorithms

CAPACITIES

		% of Grand total
Roosevelt	1,653,043	71.46%
Horse Mesa (Apache Lake)	245,138	10.60%
Mormon Flat (Canyon Lake)	57,852	2.50%
Stewart Mtn (Saguaro Lake)	69,765	3.02%
Salt Sub-Total	**2,025,798**	**87.58%**
Bartlett	178,186	7.70%
Horseshoe	109,217	4.72%
Verde Sub-Total	**287,403**	**12.42%**

Key reservoir thresholds used in decision rules:

	100% is	95% is	75% is	40% is	15% is	5% is	55% is
Roosevelt	1,653,043		1,239,782		247,956	82,652	
Horse Mesa	245,138	232,881					
Mormon Flat	57,852	54,959					
Stewart Mtn	69,765	66,277					
Bartlett	178,186			71,274			98,002
Horseshoe	109,217						

GRAND TOTAL 2,313,201 All units in acre-feet of water

VERDE RESERVOIRS, general rules

Horseshoe is the first reservoir to be drawn down at beginning of summer season, completely if needed, starting by May1.
So, first summer season draw rule would make available all of Horseshoe, applied to first months of summer demand.
When it refills it does so proportionately with refill of Bartlett.

Bartlett is tapped in the summer season after Horseshoe is depleted.
It is drawn up and down for up to 60% of its capacity proportionately with Roosevelt (when Roosevelt in range of 75-100% of capacity).
When Bartlett is in range of 40-100% capacity, it is drawn down proportionately with Roosevelt, but not below the 40% level.
Further overall draw-downs are switched over to Roosevelt, with Bartlett held at 40%.
After Sept 30th, if not already at 40%, it is reduced at beginning of new water-year to 40% capacity in preparation for winter runoff.

SALT RESERVOIRS, general rules

Three smaller Salt reservoirs besides Roosevelt are typically left at ~95% of their capacity to facilitate backpumping.
So, if they're filled more than that, then the excess above 95% becomes available for the first release from Salt system.
Otherwise, they're left at 95% level and Roosevelt is drawn down to <15% of its capacity,
at which point all remaining storage (Bartlett & all Salt reservoirs) will be reduced proportionately.
Roosevelt is drawn down in 3 stages: 75-100% proportionately with Bartlett
15-75% as the major reservoir source
0-15% proportionately with all reservoirs (except Horseshoe, which would already be empty)
(SRP states that Roosevelt could, in principle, be drained to 18.000 acre-feet, which is 1.1%)
(SRP also indicates that as the system approaches depletion, the Salt reservoirs would be emptied in series,
from Roosevelt down to Stewart Mtn; not important for the model solutions)

JOINT SALT&VERDE RESERVOIR SYSTEM, general rules to address spillage situations

One side of the system should not spill while there is remaining capacity that could be filled in the other side.
Avoidance (or, reversal by our algorithm) of spillage only occurs if there is spillage on either the Salt or the Verde, but not on the other side of the system.
The amount of the spillage that can be avoided (reversed) is the lesser of:
(1) Pv or Ps (Pv or Ps > 0 indicates the reservoirs were full to overflowing on one side but not the other side of the system),
(2) what was released for customer demand on the non-spill side of the system during the course of the winter season, although the monthly winter demand schedule is such that only ~75% of this can be operationally managed (reversed),
or (3) open storage on the opposing set of reservoirs from where spillage occurs.
After the amount that can be reversed is calculated, it is applied to open reservoir storage and there is a recalculation of Cv, Cs, Ps or Pv, Ds, Dv.
Although there is the (very small) possibility of a Summer season with enough net runoff (R-L) to create spillage on one side of the system or the other,
from discussions with SRP it appears that they do not manage the system during summer with the expectation of gains sufficient for a spillage situation.
Therefore, the "Spill Check" algorithm is only applied to the Winter season and not the Summer season.

So, there are 4 General Operating Storage Ranges above the depleted condition - - -
(although in seasonal transitions these can vary somewhat)

1) Very High Levels (which is > ~95% total capacity utilization)
Horseshoe > 0
&/or 3 smaller Salt reservoirs > 95%
with Bartlett approaching 100%
with Roosevelt approaching 100%

2) Mid-High Range Level
Horseshoe @ 0
3 smaller Salt reservoirs @ 95%

			approx Draw-Proportions		or -
Bartlett in range of 40-100%	Bartlett = 0.60x178,186 =	106,912	0.206	= (Sb-40%level) / [(Sb-40%level) + (Sr-75%level)]
Roosevelt in range of 75-100%	Roosevelt = 0.25x1,653,043 =	413,261	0.794	= (Sr-75%level) / [(Sb-40%level) + (Sr-75%level)]

3) Mid-Low Range Level
Horseshoe @ 0
3 smaller Salt reservoirs @ 95%

	Draw-Proportions
Bartlett at 40%	
Roosevelt in range of 15-75%	1.000

4) Low-Range Level (which is < ~20% total capacity utilization)
Horseshoe @ 0

			approx Draw-Proportions		or -
Bartlett in range of 0-40%	Bartlett = 0.40x178,186 =	71,274	0.106		=Sb/(Sb+Sm+Sf+Sn+Sr)
HorseMesa in range of 0-95%	HorseMesa = 0.95x245,138 =	232,881	0.346		=Sm/(Sb+Sm+Sf+Sn+Sr)
MormonFlat in range of 0-95%	MormonFlat = 0.95x57,852 =	54,959	0.082		=Sf/(Sb+Sm+Sf+Sn+Sr)
StewartMtn in range of 0-95%	StewartMtn = 0.95x69,765 =	66,277	0.098		=Sn/(Sb+Sm+Sf+Sn+Sr)
Roosevelt in range of 0-15%	Roosevelt = 0.15x1,653,043 =	247,956	0.368		=Sr/(Sb+Sm+Sf+Sn+Sr)

To identify algorithms for filling in Reservoir System Status matrix - - -

First, regardless of the season, preliminary calculations and checks -

Algorithm for calculation of groundwater pumping, G, is defined on other page per S of Total System and Season (either W or S).

Es = Rs - Ls if Es positive then Salt has inflow excess (condition identifier: 1)
Es negative -- Salt has inflow deficit (condition identifier: 0), found to not happen in the historical record - an invalid condition
Ev = Rv - Lv if Ev positive then Verde has inflow excess (condition identifier: 1)
Ev negative -- Verde has inflow deficit (condition identifier: 0), found to not happen in the historical record - an invalid condition

* Check each reservoir system's runoff to assure that it exceeds misc losses and:
If Rs-Ls<0, message is returned:
"Invalid Salt Data, Misc Loss Exceeds Runoff"
If Rv-Lv<0, message is returned:
"Invalid Verde Data, Misc Loss Exceeds Runoff"

* Check Total System Storage and:
If S, Total System >600,000 then C,adjusted = C,demand
If S,TotalSystem >50,000 and <600,000 then C,adjusted =2/3rds of C,demand
and message is returned: "Customers on Allocation"
If S,TotalSystem <50,000 then message is returned "Reservoirs Depleted" and
if DepletedShutdownSwitch =1, then [STOP]
else, if DepletedShutdownSwitch = 0, then
RecoveryModeSwitch=1 until S,TotalSystem >600,000 and S,SaltSystem >450,000

DepletedShutdownSwitch (DSS) is a user-defined option for either: 1 = terminate program if reservoirs reach depleted criteria
or: 0 = continue to run program if reservoirs reach depleted criteria, allowing recovery/replenishment

RecoveryModeSwitch (RMS) is a criteria-induced condition triggered by the program for either: 0 = program runs in normal mode
or: 1 = program ceases to allow reservoir releases,
so that system replenishes to operable conditions before returning to normal mode

Second, identify total net flow condition to know which set of algorithms to use.

TS = Rs + Rv - Ls - Lv - (Cadj - G) if TS positive then Total System has a net flow excess (condition identifier: 1),
and there is a net storage gain for the system.
if TS negative then Total System has a net flow deficit (condition identifier: 0),
and there is a net storage loss for the system.

Season = Winter

Ev \ Es	1	0
1	W 1	ZZ
0	ZZ	XX

TS: 1

Ev \ Es	1	0
1	W 0	ZZ
0	ZZ	ZZ

TS: 0

Season = Summer

Ev \ Es	1	0
1	S 1	ZZ
0	ZZ	XX

TS: 1

Ev \ Es	1	0
1	S 0	ZZ
0	ZZ	ZZ

TS: 0

XX cases don't exist because
Es&Ev<0 and finite C requires that TS<0

Es and Ev have been shown to always be positive,
so **ZZ** cases don't exist in actuality (see graph below)

Assessment of Reservoir In-Flows Net of Misc Losses (R-L)

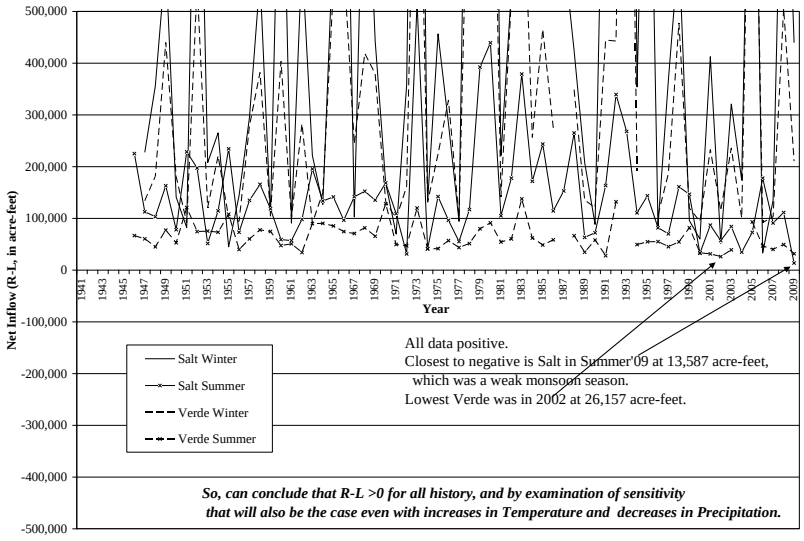

So, there are just 2 possible flow conditions for the Winter season (W1 & W0), and 2 possible flow conditions for the Summer season (S1 & S0).
Storage change algorithms are defined below per the flow conditions and status of the reservoirs.

NOTE: *Simulation model needs to track cumulative increments in each variable, as is clear by the rules below.*

W 1 **SEQUENCE OF RULES FOR - WINTER and TS: 1** *TS is positive, so total reservoir system storage will increase.*

Assumption -- Bartlett must release any water in excess of 40% of its capacity at the beginning of the Winter Season to prepare for winter inflows on the Verde, whether or not they come.

Rules for Verde --

a) If Bartlett above 40% of its capacity (71,274), it releases down to 40% level, with the water applied to Cv.
Cv = Bartlett40%release + Cvextra

b) Calculate Cvextra and Cs according to Ev & Es values; that is, proportional to the net inflows that the watersheds deliver.
Cvextra = Ev/(Es+Ev) x (Cadj - G - Bartlett40%release)
and
Cs = Es/(Es+Ev) x (Cadj - G - Bartlett40%release)

c) Calculate Verde storage change subsequent to Bartlett release from: (Rv - Lv - Cvextra).

This storage change is applied to Horseshoe and Bartlett in proportion to their open volume capacities, with Bartlett often having 60% open since it just dumped to the 40% level, but Horseshoe could be at any level (altho often very low).

d) Account for the water changes, check against total Bartlett & Horseshoe capacities, and if end up with excess water -- spill it as Pv.

Then, Cv = Bartlett40%release + Cvextra and change of Storages according to calc'ns in (c).
and Dv = Cv + Pv

Rules for Salt --

Calculate Es - Cs (= Rs - Ls - Cs) and distribute it in the order of - -

e) Bring 3 small Salt reservoirs up to 95% capacity, in order of (1) Stewart Mtn, (2) Mormon Flat, (3) Horse Mesa

f) Once the 3 small reservoirs are at 95%, fill Roosevelt to 100%.

g) If still have water, fill 3 small reservoirs to 100%.

h) If still have excess water, spill it as Ps.

Then, change of Storages according to above calc'ns.
and Ds = Cs + Ps

Spill Check -- If Pv & Ps =0, skip spill adjustment and proceed to final calculations for the season (D, S, etc).
If Pv>0 & Ps>0, skip spill adjustment and proceed to final calculations for the season (D, S, etc).
If Ps>0 and Pv =0, then -
Calculate amount of spillage to be reversed, which is the minimum of :
1) Ps
2) Cv - Bartlett40%release (40%release would've happened before action could be taken on potential spillage)
if Cv-B40 meets the minimum criteria, then reverse only 75% of it
or 3) BartlettCapacity - Sb + HorseshoeCapacity - Sh (remaining open storage in Verde reservoirs)
Fill Verde reservoirs with amount reversed in the order of (1) Bartlett, (2) Horseshoe; which can result in new Sb & Sh.

Recalculate:		
	Cv = Cv - AmtReversed	Sv = Sb + Sh
	Cs = Cs + AmtReversed	Ss = same, no change
	Ps = Ps - AmtReversed	Dv = Cv + Pv(which=0)
		Ds = Cs + Ps

If Pv>0 and Ps =0, then -
Calculate amount of spillage to be reversed, which is the minimum of :
1) Pv
2) Cs
if Cs meets the minimum criteria, then reverse only 75% of it
or 3) StewartMtnCapacity - Sn + MormonFlatCapacity - Sf + HorseMesaCapacity - Sm + RooseveltCapacity - Sr
(remaining open storage in Salt reservoirs)
Fill Salt reservoirs with amount reversed in the order of (1) Roosevelt, (2) StewartMtn, (3) MormonFlat, (4) HorseMesa; which can result in new Sn, Sf, Sm, Sr.

Recalculate:		
	Cs = Cs - AmtReversed	Ss = Sn + Sf + Sm + Sr
	Cv = Cv + AmtReversed	Sv = same, no change
	Pv = Pv - AmtReversed	Dv = Cv + Pv
		Ds = Cs + Ps(which=0)

D (total reservoirs discharge, Dv + Ds) must never be < (Cadj - G)
In other words, have to release water from Salt & Verde reservoirs to satisfy customer demand allocation not satisfied by groundwater.
This is a validity check after the season's calculations are completed.

W 0 **SEQUENCE OF RULES FOR - WINTER and TS: 0**

TS is negative so total reservoir system storage will decrease.
(but in a particular circumstance, due to Bartlett Oct 1st draw-down,
reservoirs refill after that draw-down)

Assumption -- Bartlett must release any water in excess of 40% of its capacity at the beginning of the Winter Season to prepare for winter inflows on the Verde, whether or not they come.

Rules --

a) If Bartlett above 40% of its capacity (71,274), it releases down to 40% level, with the water applied to Cv.
Cv = Bartlett40%release + Cvextra

b) Test for (Cadj - G - Bartlett40%release) > (Es + Ev)

i) If yes, then apply all Es to Cs and apply all Ev to Cvextra, and continue with (c) below.

ii) If no, then return message: "Bartlett fall release allows winter reservoir refills" , and then apply a portion of Es to Cs & a portion of Ev to Cvextra, according to:
portion to Cs: Es/(Es+Ev) x (Cadj - G - Bartlett40%release)
and
portion to Cvextra: Ev/(Es+Ev) x (Cadj - G - Bartlett40%release)

And, any surplus Ev is applied to Horseshoe and Barlett in proportion to their open volume capacities.
Check against total Bartlett & Horseshoe capacities, and if exceed them, spill excess water as Pv.

And, any surplus Es is distributed in the order of -
1) Bring 3 small Salt reservoirs up to 95% capacity, in order of (1) Stewart Mtn, (2) Mormon Flat, (3) Horse Mesa
2) Once the 3 small reservoirs are at 95%, fill Roosevelt to 100%.
3) If still have water, fill 3 small reservoirs to 100%.
4) If there is any further excess water, spill it as Ps.

Spill Check --
If Pv & Ps =0, skip spill adjustment and proceed to final calculations for the season (D, S, etc).
If Pv>0 & Ps>0, skip spill adjustment and proceed to final calculations for the season (D, S, etc).
If Ps>0 and Pv =0, then -
Calculate amount of spillage to be reversed, which is the minimum of :
1) Ps
2) Cv - Bartlett40%release (40%release would've happened before action could be taken on potential spillage)
if Cv-B40 meets the minimum criteria, then reverse only 75% of it
or 3) BartlettCapacity - Sb + HorseshoeCapacity - Sh (remaining open storage in Verde reservoirs)
Fill Verde reservoirs with amount reversed in the order of (1) Bartlett, (2) Horseshoe; which can result in new Sb & Sh.

Recalculate:	Cv = Cv - AmtReversed	Sv = Sb + Sh
	Cs = Cs + AmtReversed	Ss = same, no change
	Ps = Ps - AmtReversed	Dv = Cv + Pv(which=0)
		Ds = Cs + Ps

If Pv>0 and Ps =0, then -
Calculate amount of spillage to be reversed, which is the minimum of :
1) Pv
2) Cs
if Cs meets the minimum criteria, then reverse only 75% of it
or 3) StewartMtnCapacity - Sn + MormonFlatCapacity - Sf + HorseMesaCapacity - Sm + RooseveltCapacity - Sr
(remaining open storage in Salt reservoirs)
Fill Salt reservoirs with amount reversed in the order of (1) Roosevelt, (2) StewartMtn, (3) MormonFlat, (4) HorseMesa; which can result in new Sn, Sf, Sm, Sr.

Recalculate:	Cs = Cs - AmtReversed	Ss = Sn + Sf + Sm + Sr
	Cv = Cv + AmtReversed	Sv = same, no change
	Pv = Pv - AmtReversed	Dv = Cv + Pv
		Ds = Cs + Ps(which=0)

Skip step (c).

c) Allocate from reservoirs for the remaining demand, to Cs & Cvextra, in the order of -
1) Horseshoe, taking as much as needed down to its zero level. allocate to Cvextra)
2) If any of the 3 small Salt reservoirs are at >95%, take them each down to 95%
in the order of (1) Horse Mesa, (2) Mormon Flat, (3) Stewart Mtn. (allocate to Cs)
3) Test for Roosevelt >5% capacity
i) If yes, then draw from Roosevelt until the needs are filled or it's at 5%. (allocate to Cs)
ii) If no, or still need to draw more water after Roosevelt has been reduced to 5%,
then use the Low Range proportions:

Bartlett	= Sb/(Sb+Sm+Sf+Sn+Sr)	(allocate to Cvextra)
HorseMesa	= Sm/(Sb+Sm+Sf+Sn+Sr)	(allocate to Cs)
MormonFlat	= Sf/(Sb+Sm+Sf+Sn+Sr)	(allocate to Cs)
StewartMtn	= Sn/(Sb+Sm+Sf+Sn+Sr)	(allocate to Cs)
Roosevelt	= Sr/(Sb+Sm+Sf+Sn+Sr)	(allocate to Cs)

The reservoirs approach zero together by this calculation.

If reservoirs are all reduced to zero (or below),
then [STOP] and message is returned "Reservoirs Depleted"

Then, change of Storages according to above calc'ns.
and Ds = Cs + Ps , and Dv = Cv + Pv = Bartlett40%release + Cvextra + Pv

D (total reservoirs discharge) must never be < C,adjusted less G
In other words, have to release water from Salt & Verde reservoirs to satisfy customer demand allocation not satisfied by groundwater.
This is a validity check after the season's calculations are completed.

S 1 **SEQUENCE OF RULES FOR - SUMMER and TS:1** *TS is positive, so total reservoir system storage will increase.*

a) Calculate Cv and Cs according to Ev & Es values; that is, proportional to the net inflows that the watersheds delivered.
Cv = Ev/(Es+Ev) x (Cadj - G)
and
Cs = Es/(Es+Ev) x (Cadj - G)

Rules for Verde --

b) Calculate Verde storage change from net inflow less customer release: Ev - Cv = Rv - Lv - Cv
This storage change is applied to Horseshoe and Bartlett in proportion to their open volume capacities at the start of summer.

c) Account for the water changes and check against total Bartlett & Horseshoe capacities,
and if end up with excess water -- spill it as Pv.

Then, change of Storages according to calc'ns in (c).
and Dv = Cv + Pv

Rules for Salt -- Calculate Es - Cs (= Rs - Ls - Cs) and distribute it in the order of - -

d) Bring 3 small Salt reservoirs up to 95% capacity, in order of (1) Stewart Mtn, (2) Mormon Flat, (3) Horse Mesa

e) Once the 3 small reservoirs are at 95%, fill Roosevelt to 100%.

f) If still have water, fill 3 small reservoirs to 100%.

g) If still have excess water, spill it as Ps.

Then, change of Storages according to above calc'ns.
and Ds = Cs + Ps

D (total reservoirs discharge) must never be < C,adjusted less G
In other words, have to release water from Salt & Verde reservoirs to satisfy customer demand allocation not satisfied by groundwater.
This is a validity check after the season's calculations are completed.

S 0 **SEQUENCE OF RULES FOR - SUMMER and TS:0** *TS is negative so total reservoir system storage will decrease.*

Demand, Cadj - G = Cs + Cv
Rules -- Allocate from inflows and reservoirs to Cs and Cv in the following order, stopping when demand is filled:

a) Apply all Es to Cs, and apply all Ev to Cv.

b) From Horseshoe, take as much as needed down to its zero level. (allocate to Cv)

c) If any of the 3 small Salt reservoirs are at >95%, take them down to 95%
in the order of (1) Horse Mesa, (2) Mormon Flat, (3) Stewart Mtn. (allocate to Cs)

d) Test for Bartlett >40% capacity and Test for Roosevelt >75% capacity

i) If no (Bartlett) & no (Roosevelt), go to next step.

ii) If no (Bartlett) & yes (Roosevelt) -
draw from Roosevelt, but only until it is reduced to 75% of its capacity (allocate to Cs)

iii) If yes (Bartlett) & no (Roosevelt) -
draw from Bartlett until it is reduced to 40% of its capacity (allocate to Cv)

iv) If yes (Bartlett) & yes (Roosevelt) -
draw per the Mid-High Range proportions:
Bartlett = (Sb-40%level) / [(Sb-40%level) + (Sr-75%level)] (allocate to Cv)
Roosevelt = (Sr-75%level) / [(Sb-40%level) + (Sr-75%level)] (allocate to Cs)
maximum Bartlett draw of (storage level - 40%capacity)
maximum Roosevelt draw of (storage level - 75%capacity)

e) Test for Roosevelt >5% capacity

i) If yes, then draw from Roosevelt until the needs are filled or it's at 5%. (allocate to Cs)

ii) If no, or still need to draw more water after Roosevelt has been reduced to 5%,
then use the Low Range proportions:
Bartlett = Sb/(Sb+Sm+Sf+Sn+Sr) (allocate to Cv)
HorseMesa = Sm/(Sb+Sm+Sf+Sn+Sr) (allocate to Cs)
MormonFlat = Sf/(Sb+Sm+Sf+Sn+Sr) (allocate to Cs)
StewartMtn = Sn/(Sb+Sm+Sf+Sn+Sr) (allocate to Cs)
Roosevelt = Sr/(Sb+Sm+Sf+Sn+Sr) (allocate to Cs)
The reservoirs approach zero together by this calculation.

If reservoirs are all reduced to zero (or below),
then [STOP] and message is returned "Reservoirs Depleted"

Then, change of Storages according to above calc'ns.
and Ds = Cs and Dv = Cv

D (total reservoirs discharge) must never be < C,adjusted less G
In other words, have to release water from Salt & Verde reservoirs to satisfy customer demand allocation not satisfied by groundwater.
This is a validity check after the season's calculations are completed.

ResSim Model FlowCharts

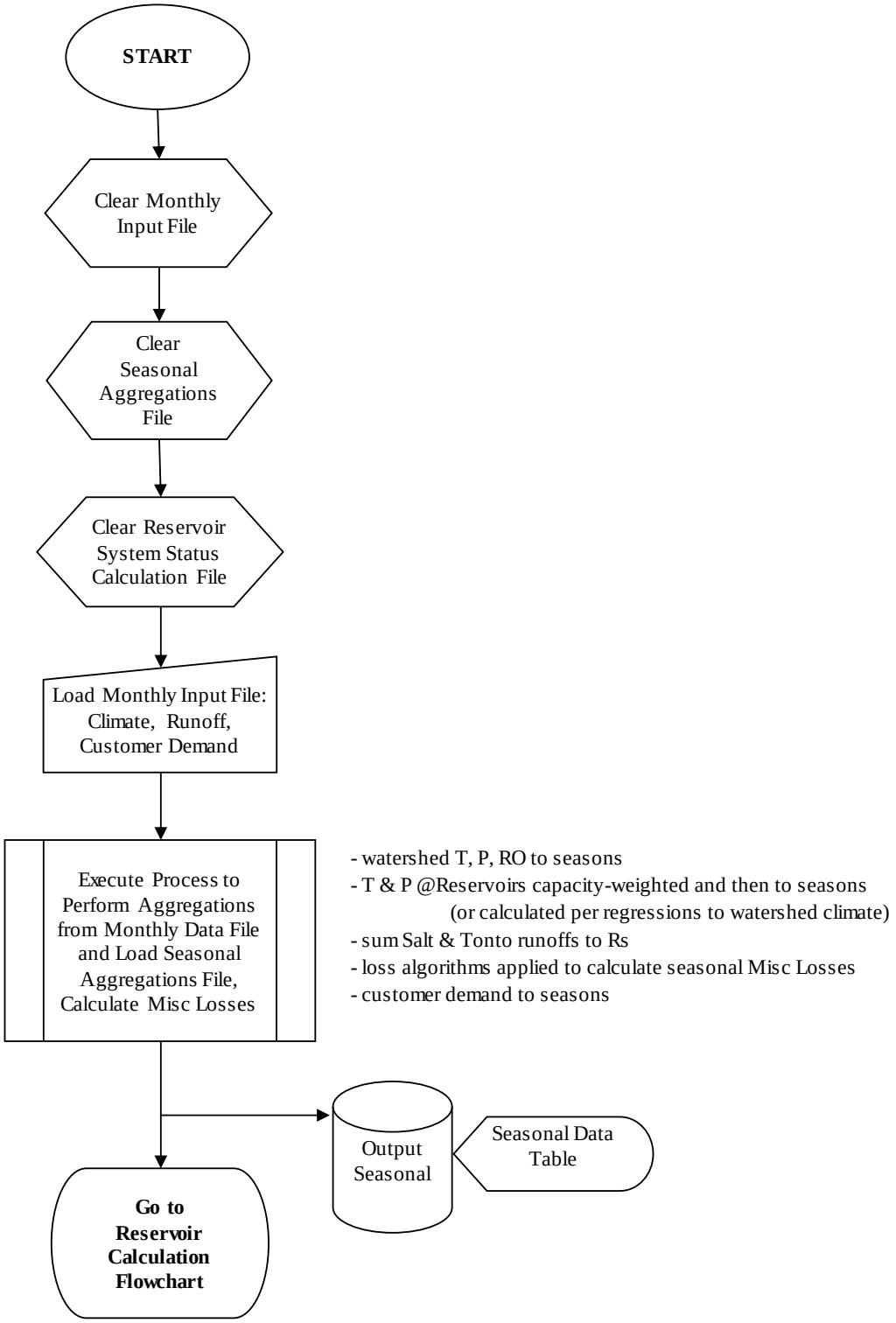

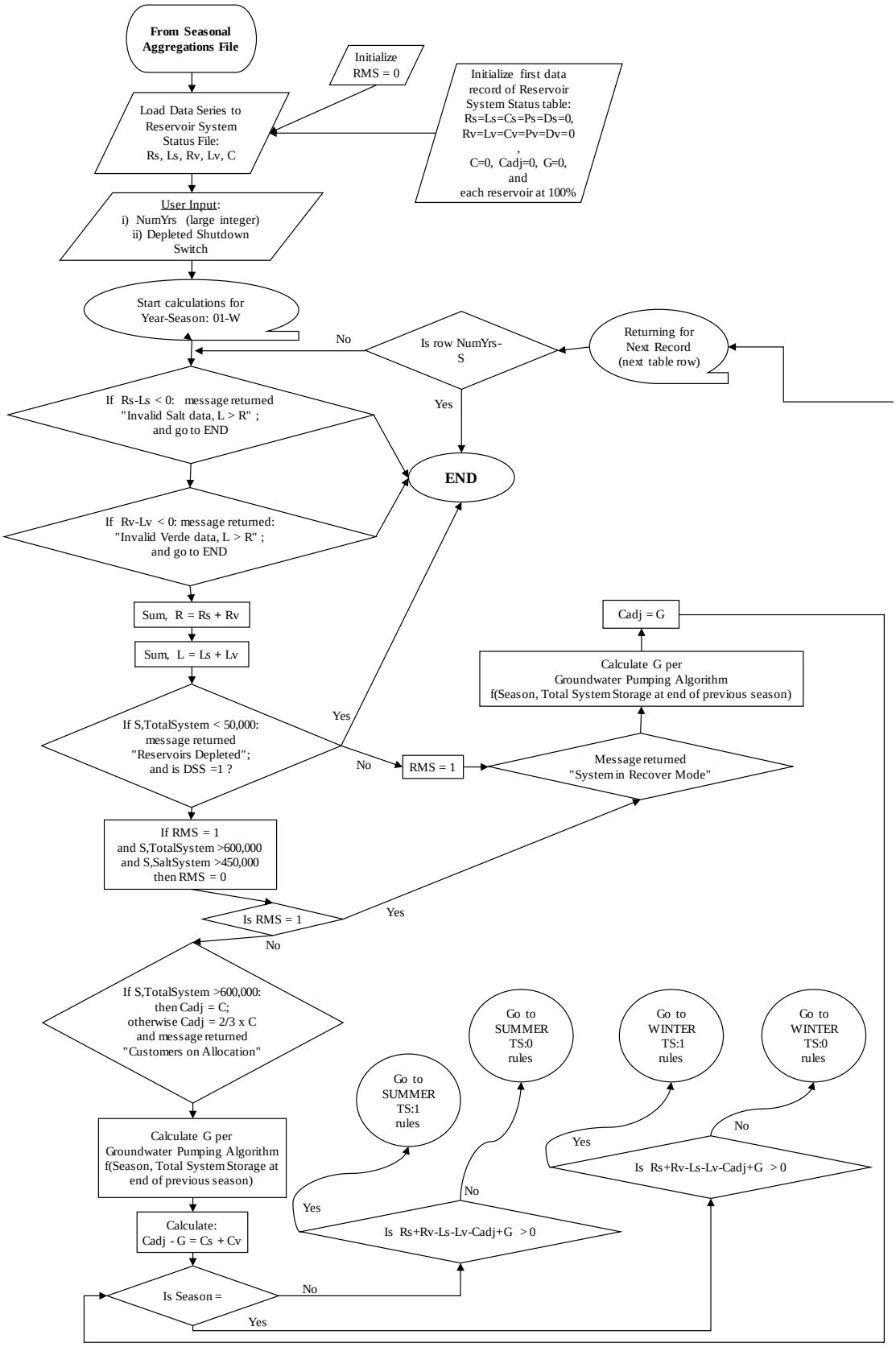
From Seasonal Aggregations File
Initialize RMS = 0
Initialize first data record of Reservoir System Status table: Rs=Ls=Cs=Ps=Ds=0, Rv=Lv=Cv=Pv=Dv=0, C=0, Cadj=0, G=0, and each reservoir at 100%
Load Data Series to Reservoir System Status File: Rs, Ls, Rv, Lv, C
User Input: i) NumYrs (large integer) ii) Depleted Shutdown Switch
Start calculations for Year-Season: 01-W
Is row NumYrs-S
No
Yes
Returning for Next Record (next table row)
If Rs-Ls < 0: message returned "Invalid Salt data, L > R" ; and go to END
END
If Rv-Lv < 0: message returned: "Invalid Verde data, L > R" ; and go to END
Sum, R = Rs + Rv
Sum, L = Ls + Lv
If S,TotalSystem < 50,000: message returned "Reservoirs Depleted"; and is DSS =1 ?
Yes
No
RMS = 1
Message returned "System in Recover Mode"
Calculate G per Groundwater Pumping Algorithm f(Season, Total System Storage at end of previous season)
Cadj = G
If RMS = 1 and S,TotalSystem >600,000 and S,SaltSystem >450,000 then RMS = 0
Is RMS = 1
Yes
No
If S,TotalSystem >600,000: then Cadj = C; otherwise Cadj = 2/3 x C and message returned "Customers on Allocation"
Calculate G per Groundwater Pumping Algorithm f(Season, Total System Storage at end of previous season)
Calculate: Cadj - G = Cs + Cv
Is Season =
No
Yes
Is Rs+Rv-Ls-Lv-Cadj+G > 0
Yes
No
Go to SUMMER TS:1 rules
Go to SUMMER TS:0 rules
Is Rs+Rv-Ls-Lv-Cadj+G > 0
Yes
No
Go to WINTER TS:1 rules
Go to WINTER TS:0 rules

Starts with reservoir levels from end of the last season.
Reservoirs are being incrementally increased or drained as step through the flowchart.
Cs and Cv are also being progressively added to in sequential steps.

to next page

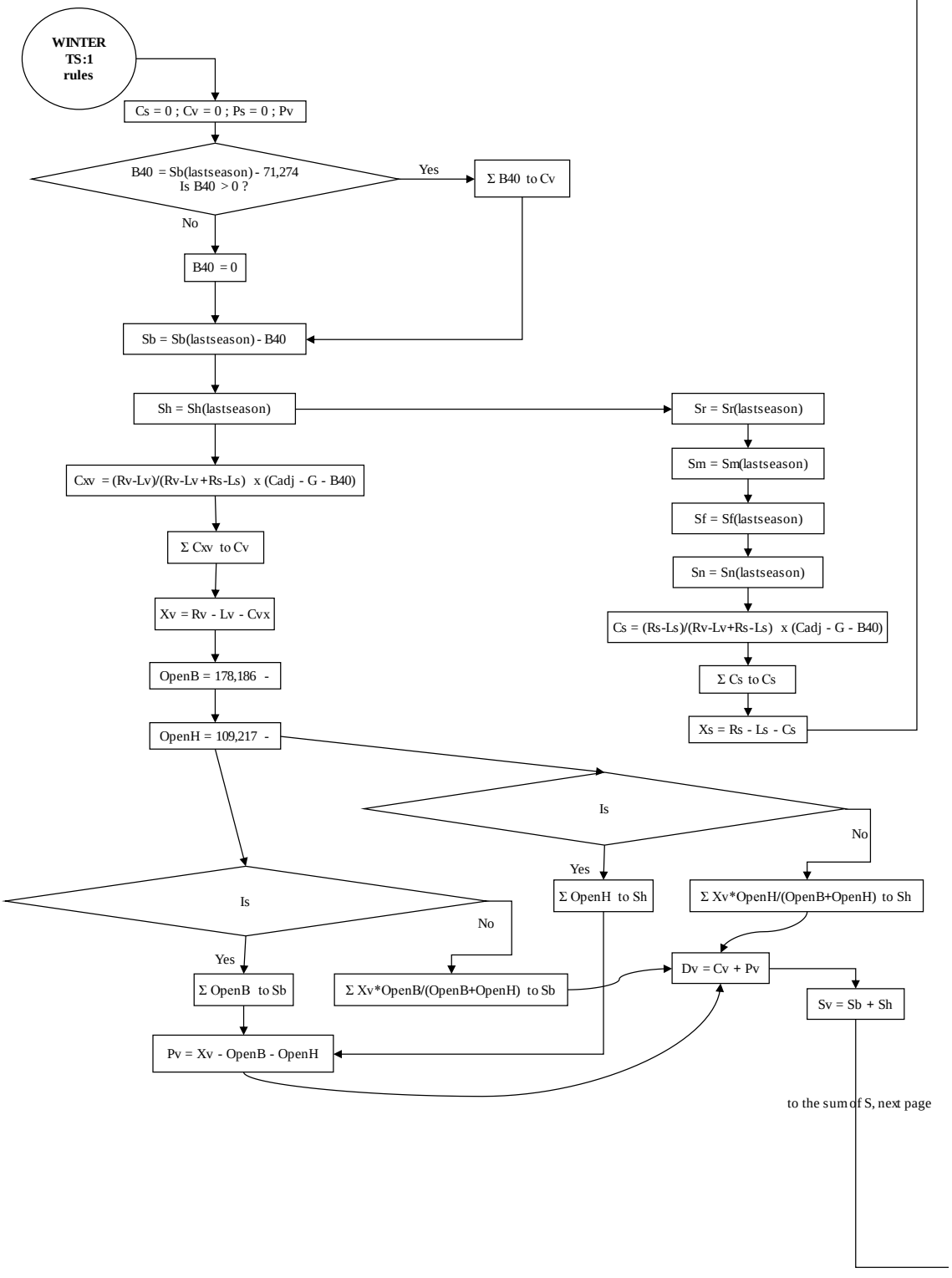

to the sum of S, next page

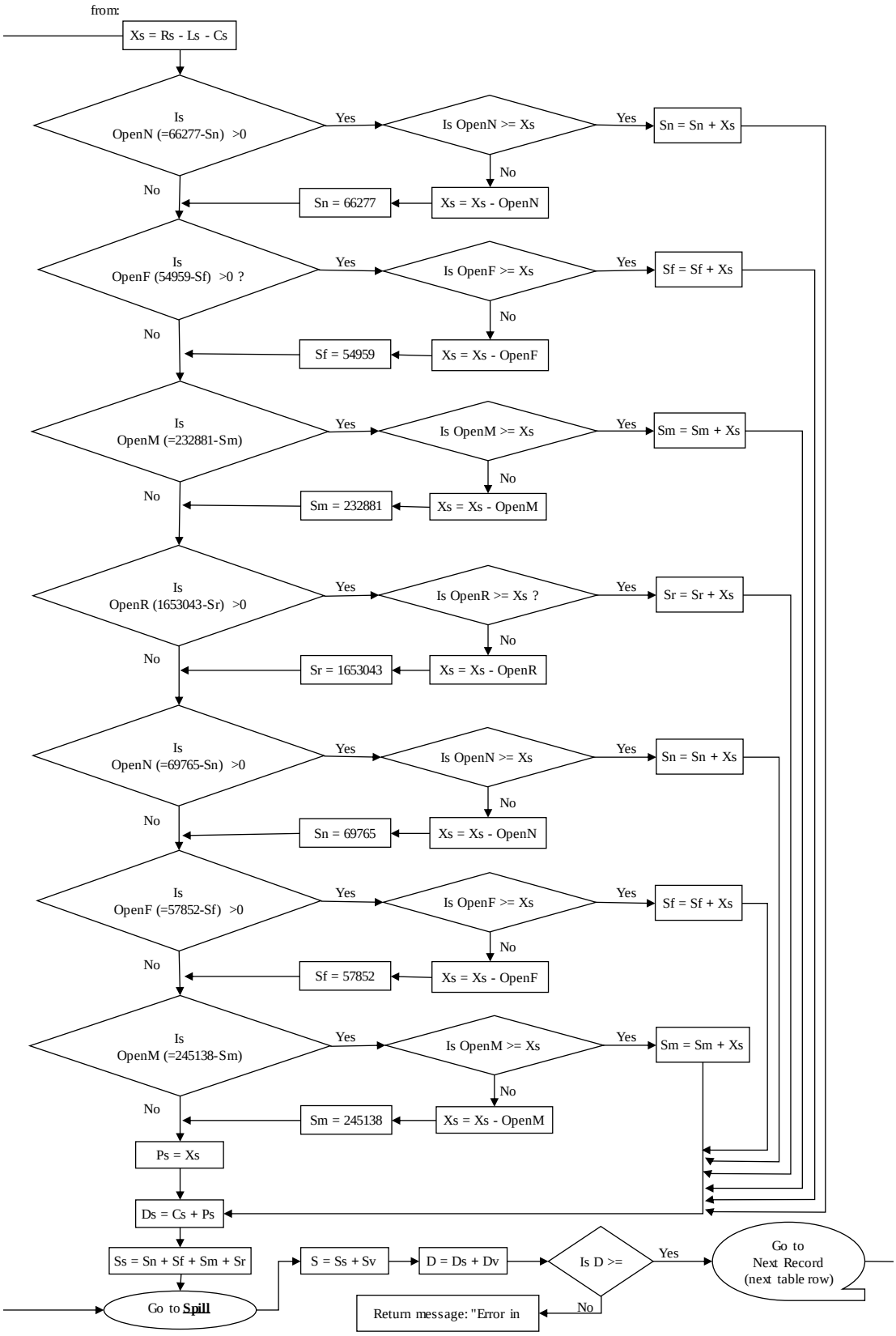
from:
Xs = Rs - Ls - Cs
Is OpenN (=66277-Sn) >0
Yes
Is OpenN >= Xs
Yes
Sn = Sn + Xs
No
Xs = Xs - OpenN
Sn = 66277
No
Is OpenF (54959-Sf) >0 ?
Yes
Is OpenF >= Xs
Yes
Sf = Sf + Xs
No
Xs = Xs - OpenF
Sf = 54959
No
Is OpenM (=232881-Sm)
Yes
Is OpenM >= Xs
Yes
Sm = Sm + Xs
No
Xs = Xs - OpenM
Sm = 232881
No
Is OpenR (1653043-Sr) >0
Yes
Is OpenR >= Xs ?
Yes
Sr = Sr + Xs
No
Xs = Xs - OpenR
Sr = 1653043
No
Is OpenN (=69765-Sn) >0
Yes
Is OpenN >= Xs
Yes
Sn = Sn + Xs
No
Xs = Xs - OpenN
Sn = 69765
No
Is OpenF (=57852-Sf) >0
Yes
Is OpenF >= Xs
Yes
Sf = Sf + Xs
No
Xs = Xs - OpenF
Sf = 57852
No
Is OpenM (=245138-Sm)
Yes
Is OpenM >= Xs
Yes
Sm = Sm + Xs
No
Xs = Xs - OpenM
Sm = 245138
No
Ps = Xs
Ds = Cs + Ps
Ss = Sn + Sf + Sm + Sr
Go to Spill
S = Ss + Sv
D = Ds + Dv
Is D >=
Yes
Go to Next Record (next table row)
No
Return message: "Error in

Starts with reservoir levels from end of the last season.
Reservoirs are being incrementally increased or drained as step through the flowchart.
Cs and Cv are also being progressively added to in sequential steps.

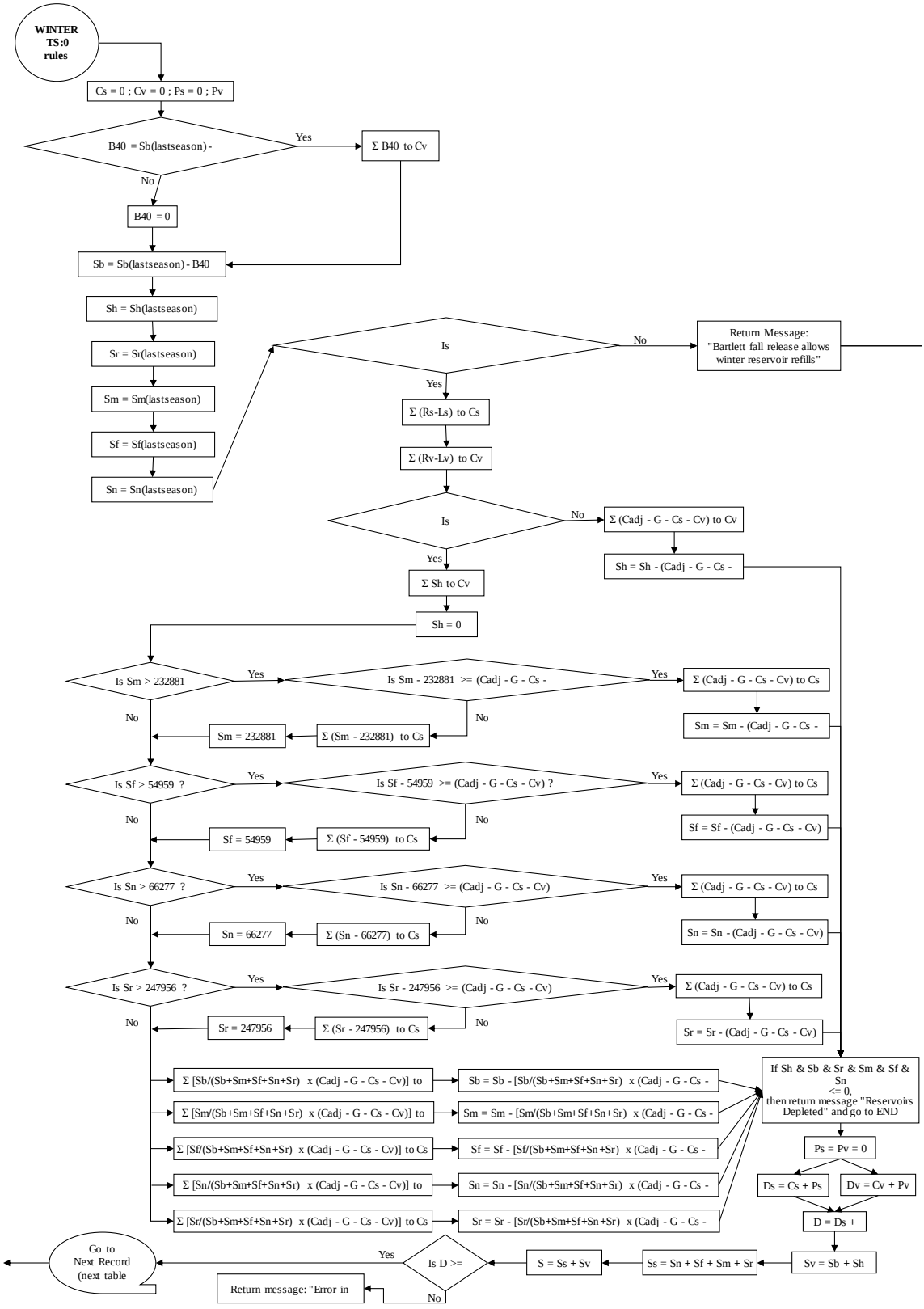

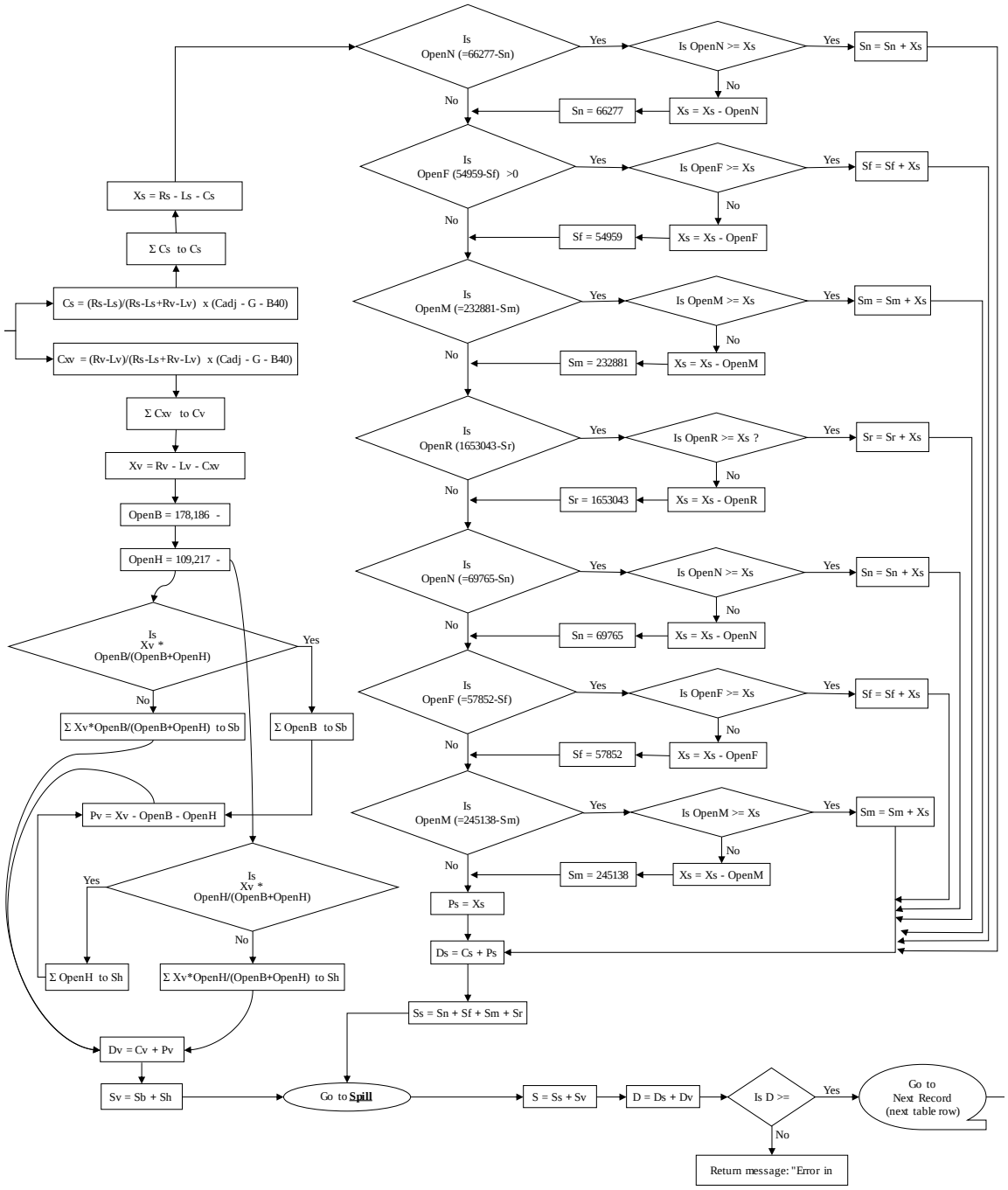
Is OpenN (=66277-Sn)
Yes
Is OpenN >= Xs
Yes
Sn = Sn + Xs
No
No
Sn = 66277
Xs = Xs - OpenN
Is OpenF (54959-Sf) >0
Yes
Is OpenF >= Xs
Yes
Sf = Sf + Xs
No
No
Sf = 54959
Xs = Xs - OpenF
Is OpenM (=232881-Sm)
Yes
Is OpenM >= Xs
Yes
Sm = Sm + Xs
No
No
Sm = 232881
Xs = Xs - OpenM
Is OpenR (1653043-Sr)
Yes
Is OpenR >= Xs ?
Yes
Sr = Sr + Xs
No
No
Sr = 1653043
Xs = Xs - OpenR
Is OpenN (=69765-Sn)
Yes
Is OpenN >= Xs
Yes
Sn = Sn + Xs
No
No
Sn = 69765
Xs = Xs - OpenN
Is OpenF (=57852-Sf)
Yes
Is OpenF >= Xs
Yes
Sf = Sf + Xs
No
No
Sf = 57852
Xs = Xs - OpenF
Is OpenM (=245138-Sm)
Yes
Is OpenM >= Xs
Yes
Sm = Sm + Xs
No
No
Sm = 245138
Xs = Xs - OpenM
Ps = Xs
Ds = Cs + Ps
Ss = Sn + Sf + Sm + Sr
Xs = Rs - Ls - Cs
Σ Cs to Cs
Cs = (Rs-Ls)/(Rs-Ls+Rv-Lv) x (Cadj - G - B40)
Cxv = (Rv-Lv)/(Rs-Ls+Rv-Lv) x (Cadj - G - B40)
Σ Cxv to Cv
Xv = Rv - Lv - Cxv
OpenB = 178,186 -
OpenH = 109,217 -
Is Xv * OpenB/(OpenB+OpenH)
Yes
No
Σ Xv*OpenB/(OpenB+OpenH) to Sb
Σ OpenB to Sb
Pv = Xv - OpenB - OpenH
Is Xv * OpenH/(OpenB+OpenH)
Yes
No
Σ OpenH to Sh
Σ Xv*OpenH/(OpenB+OpenH) to Sh
Dv = Cv + Pv
Sv = Sb + Sh
Go to Spill
S = Ss + Sv
D = Ds + Dv
Is D >=
Yes
Go to Next Record (next table row)
No
Return message: "Error in

Starts with reservoir levels from end of the last season.
Reservoirs are being incrementally increased or drained as step through the flowchart.
Cs and Cv are also being progressively added to in sequential steps.

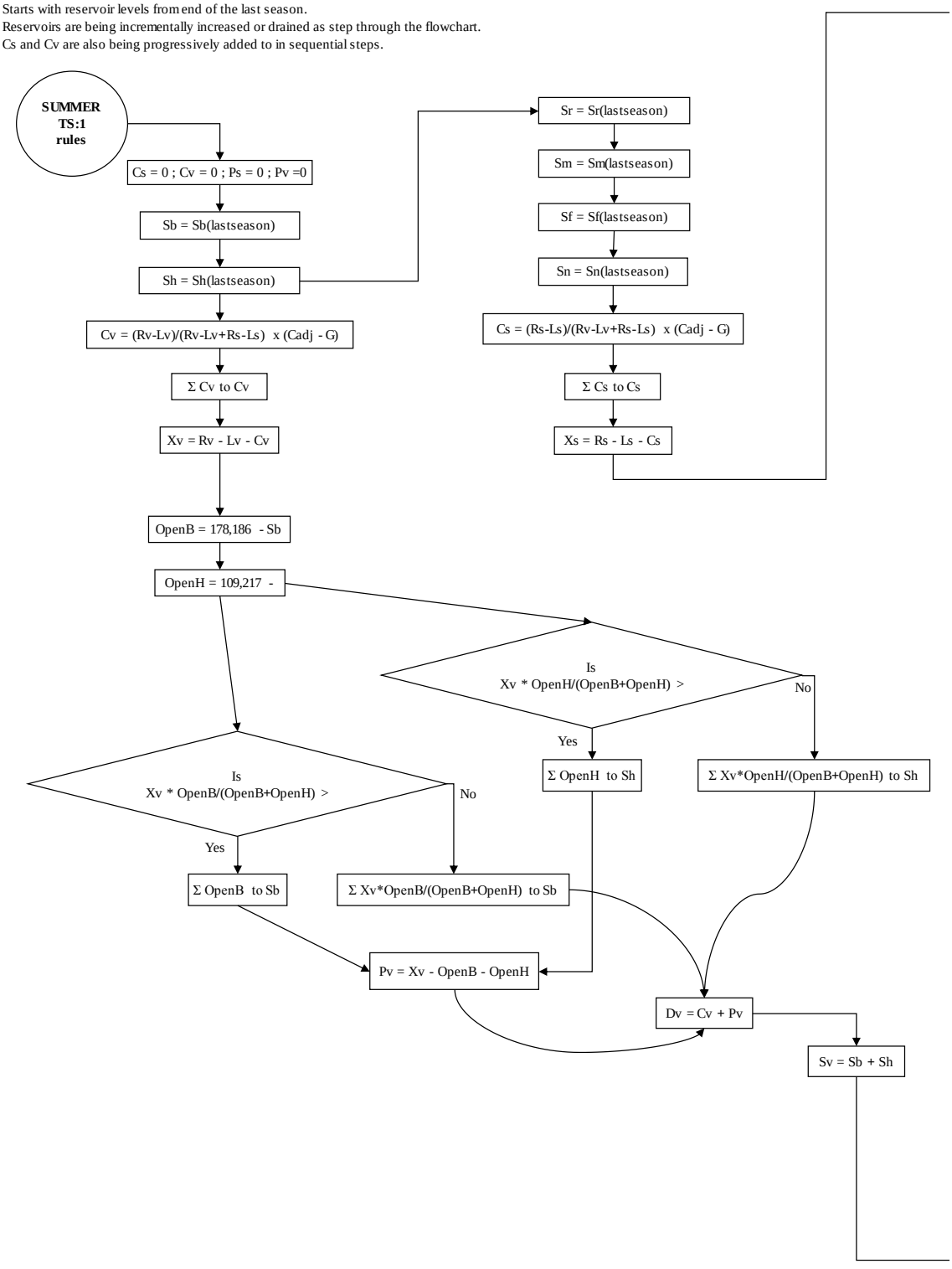

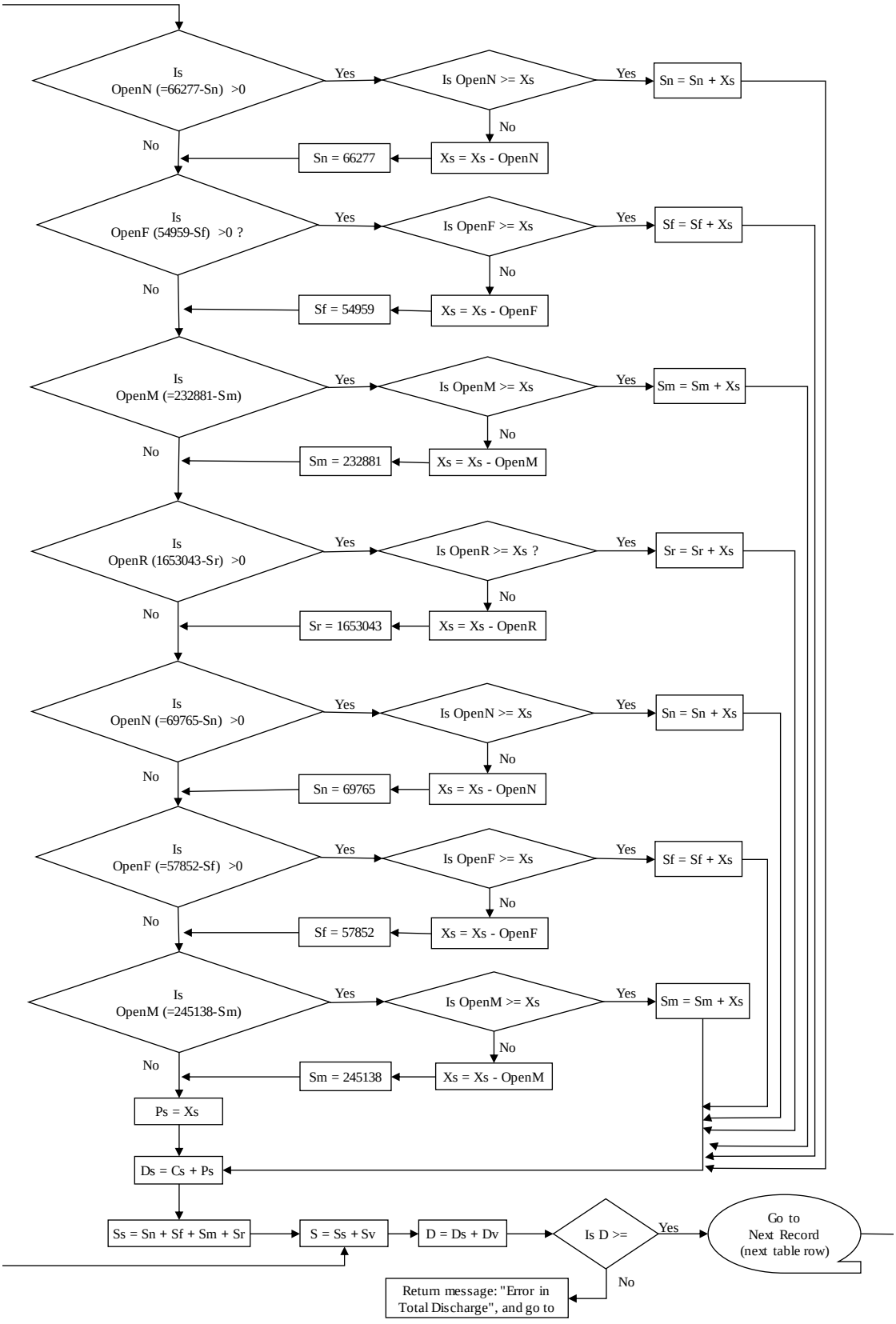
Is
OpenN (=66277-Sn) >0
Yes
Is OpenN >= Xs
Yes
Sn = Sn + Xs
No
Xs = Xs - OpenN
Sn = 66277
No
Is
OpenF (54959-Sf) >0 ?
Yes
Is OpenF >= Xs
Yes
Sf = Sf + Xs
No
Xs = Xs - OpenF
Sf = 54959
No
Is
OpenM (=232881-Sm)
Yes
Is OpenM >= Xs
Yes
Sm = Sm + Xs
No
Xs = Xs - OpenM
Sm = 232881
No
Is
OpenR (1653043-Sr) >0
Yes
Is OpenR >= Xs ?
Yes
Sr = Sr + Xs
No
Xs = Xs - OpenR
Sr = 1653043
No
Is
OpenN (=69765-Sn) >0
Yes
Is OpenN >= Xs
Yes
Sn = Sn + Xs
No
Xs = Xs - OpenN
Sn = 69765
No
Is
OpenF (=57852-Sf) >0
Yes
Is OpenF >= Xs
Yes
Sf = Sf + Xs
No
Xs = Xs - OpenF
Sf = 57852
No
Is
OpenM (=245138-Sm)
Yes
Is OpenM >= Xs
Yes
Sm = Sm + Xs
No
Xs = Xs - OpenM
Sm = 245138
No
Ps = Xs
Ds = Cs + Ps
Ss = Sn + Sf + Sm + Sr
S = Ss + Sv
D = Ds + Dv
Is D >=
Yes
Go to
Next Record
(next table row)
No
Return message: "Error in
Total Discharge", and go to

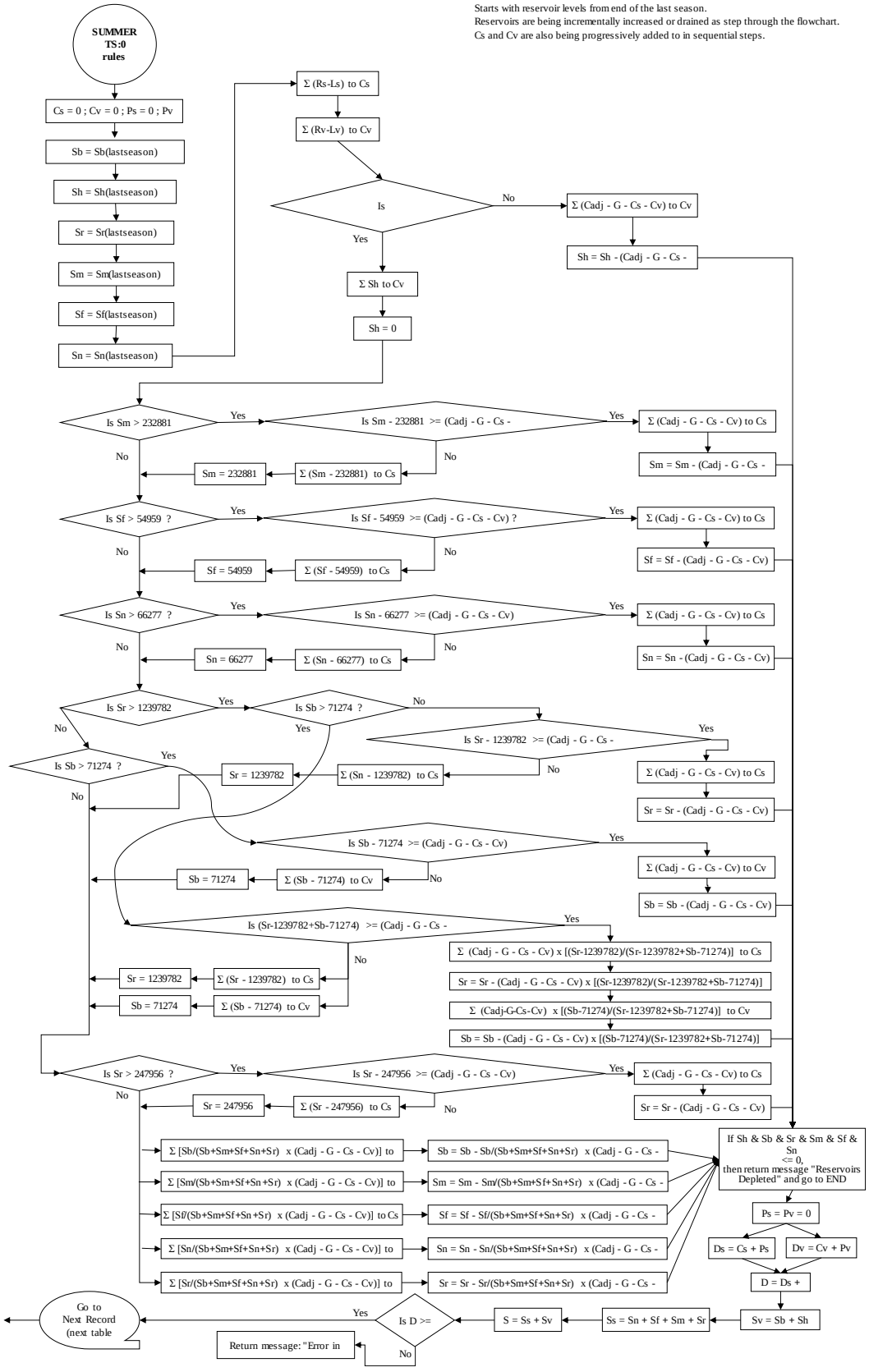
Starts with reservoir levels from end of the last season.
Reservoirs are being incrementally increased or drained as step through the flowchart.
Cs and Cv are also being progressively added to in sequential steps.
SUMMER
TS:0
rules
Cs = 0 ; Cv = 0 ; Ps = 0 ; Pv
Sb = Sb(lastseason)
Sh = Sh(lastseason)
Sr = Sr(lastseason)
Sm = Sm(lastseason)
Sf = Sf(lastseason)
Sn = Sn(lastseason)
Σ (Rs-Ls) to Cs
Σ (Rv-Lv) to Cv
Is
No
Yes
Σ (Cadj - G - Cs - Cv) to Cv
Sh = Sh - (Cadj - G - Cs -
Σ Sh to Cv
Sh = 0
Is Sm > 232881
Yes
Is Sm - 232881 >= (Cadj - G - Cs -
Yes
Σ (Cadj - G - Cs - Cv) to Cs
Sm = Sm - (Cadj - G - Cs -
No
Sm = 232881
Σ (Sm - 232881) to Cs
Is Sf > 54959 ?
Is Sf - 54959 >= (Cadj - G - Cs - Cv) ?
Σ (Cadj - G - Cs - Cv) to Cs
Sf = Sf - (Cadj - G - Cs - Cv)
Sf = 54959
Σ (Sf - 54959) to Cs
Is Sn > 66277 ?
Is Sn - 66277 >= (Cadj - G - Cs - Cv)
Σ (Cadj - G - Cs - Cv) to Cs
Sn = Sn - (Cadj - G - Cs - Cv)
Sn = 66277
Σ (Sn - 66277) to Cs
Is Sr > 1239782
Is Sb > 71274 ?
Is Sr - 1239782 >= (Cadj - G - Cs -
Σ (Cadj - G - Cs - Cv) to Cs
Sr = Sr - (Cadj - G - Cs - Cv)
Sr = 1239782
Σ (Sn - 1239782) to Cs
Is Sb - 71274 >= (Cadj - G - Cs - Cv)
Σ (Cadj - G - Cs - Cv) to Cv
Sb = Sb - (Cadj - G - Cs - Cv)
Sb = 71274
Σ (Sb - 71274) to Cv
Is (Sr-1239782+Sb-71274) >= (Cadj - G - Cs -
Σ (Cadj - G - Cs - Cv) x [(Sr-1239782)/(Sr-1239782+Sb-71274)] to Cs
Sr = Sr - (Cadj - G - Cs - Cv) x [(Sr-1239782)/(Sr-1239782+Sb-71274)]
Σ (Cadj-G-Cs-Cv) x [(Sb-71274)/(Sr-1239782+Sb-71274)] to Cv
Sb = Sb - (Cadj - G - Cs - Cv) x [(Sb-71274)/(Sr-1239782+Sb-71274)]
Sr = 1239782
Σ (Sr - 1239782) to Cs
Sb = 71274
Σ (Sb - 71274) to Cv
Is Sr > 247956 ?
Is Sr - 247956 >= (Cadj - G - Cs - Cv)
Σ (Cadj - G - Cs - Cv) to Cs
Sr = Sr - (Cadj - G - Cs - Cv)
Sr = 247956
Σ (Sr - 247956) to Cs
Σ [Sb/(Sb+Sm+Sf+Sn+Sr) x (Cadj - G - Cs - Cv)] to
Sb = Sb - Sb/(Sb+Sm+Sf+Sn+Sr) x (Cadj - G - Cs -
Σ [Sm/(Sb+Sm+Sf+Sn+Sr) x (Cadj - G - Cs - Cv)] to
Sm = Sm - Sm/(Sb+Sm+Sf+Sn+Sr) x (Cadj - G - Cs -
Σ [Sf/(Sb+Sm+Sf+Sn+Sr) x (Cadj - G - Cs - Cv)] to Cs
Sf = Sf - Sf/(Sb+Sm+Sf+Sn+Sr) x (Cadj - G - Cs -
Σ [Sn/(Sb+Sm+Sf+Sn+Sr) x (Cadj - G - Cs - Cv)] to
Sn = Sn - Sn/(Sb+Sm+Sf+Sn+Sr) x (Cadj - G - Cs -
Σ [Sr/(Sb+Sm+Sf+Sn+Sr) x (Cadj - G - Cs - Cv)] to
Sr = Sr - Sr/(Sb+Sm+Sf+Sn+Sr) x (Cadj - G - Cs -
If Sh & Sb & Sr & Sm & Sf & Sn
<= 0,
then return message "Reservoirs Depleted" and go to END
Ps = Pv = 0
Ds = Cs + Ps
Dv = Cv + Pv
D = Ds +
Sv = Sb + Sh
Ss = Sn + Sf + Sm + Sr
S = Ss + Sv
Is D >=
Return message: "Error in
Go to
Next Record
(next table

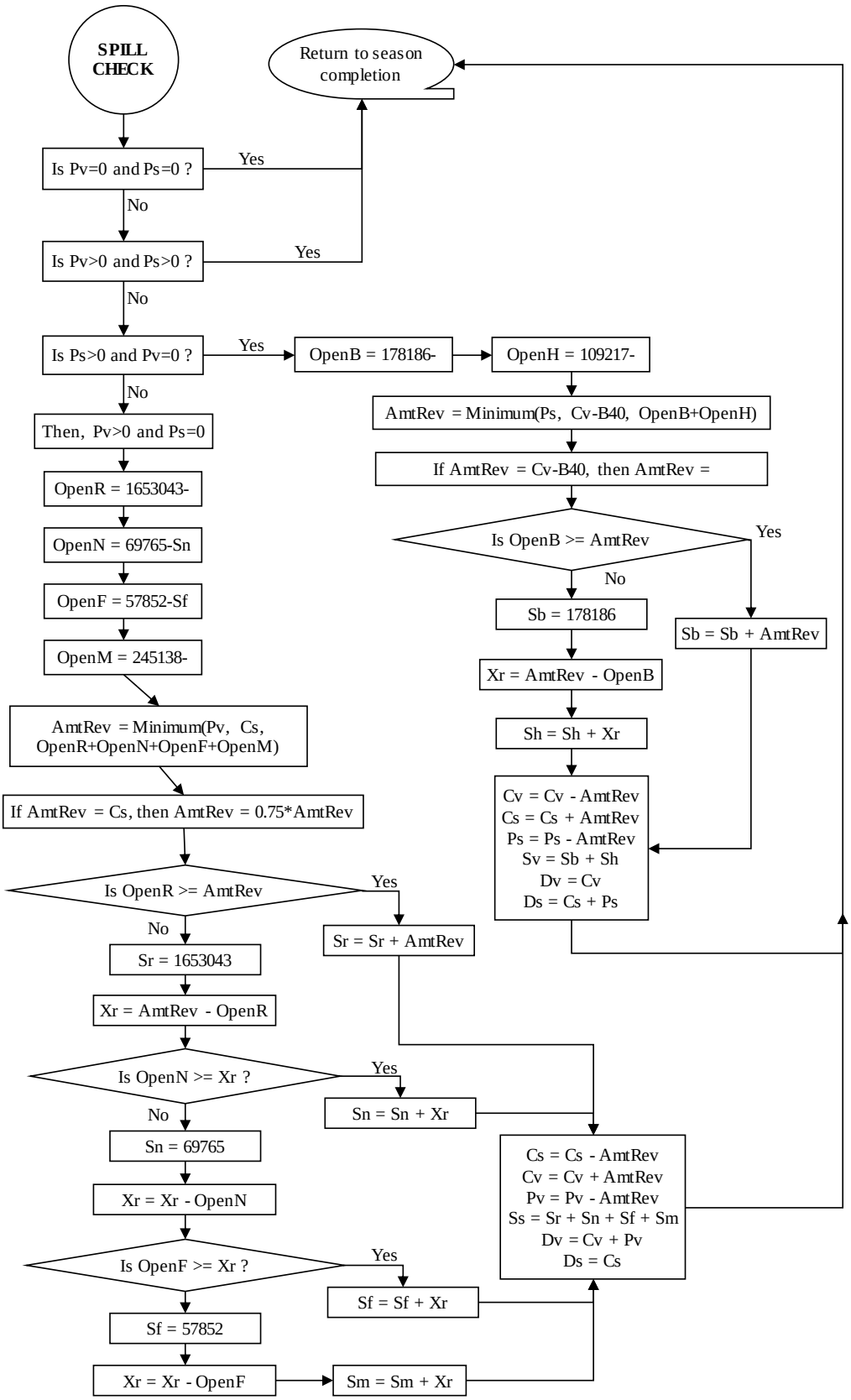
SPILL CHECK
Return to season completion
Is Pv=0 and Ps=0 ?
Yes
No
Is Pv>0 and Ps>0 ?
Yes
No
Is Ps>0 and Pv=0 ?
Yes
OpenB = 178186-
OpenH = 109217-
AmtRev = Minimum(Ps, Cv-B40, OpenB+OpenH)
If AmtRev = Cv-B40, then AmtRev =
Is OpenB >= AmtRev
Yes
No
Sb = 178186
Sb = Sb + AmtRev
Xr = AmtRev - OpenB
Sh = Sh + Xr
Cv = Cv - AmtRev
Cs = Cs + AmtRev
Ps = Ps - AmtRev
Sv = Sb + Sh
Dv = Cv
Ds = Cs + Ps
No
Then, Pv>0 and Ps=0
OpenR = 1653043-
OpenN = 69765-Sn
OpenF = 57852-Sf
OpenM = 245138-
AmtRev = Minimum(Pv, Cs, OpenR+OpenN+OpenF+OpenM)
If AmtRev = Cs, then AmtRev = 0.75*AmtRev
Is OpenR >= AmtRev
Yes
Sr = Sr + AmtRev
No
Sr = 1653043
Xr = AmtRev - OpenR
Is OpenN >= Xr ?
Yes
Sn = Sn + Xr
No
Sn = 69765
Xr = Xr - OpenN
Is OpenF >= Xr ?
Yes
Sf = Sf + Xr
Sf = 57852
Xr = Xr - OpenF
Sm = Sm + Xr
Cs = Cs - AmtRev
Cv = Cv + AmtRev
Pv = Pv - AmtRev
Ss = Sr + Sn + Sf + Sm
Dv = Cv + Pv
Ds = Cs

APPENDIX G

HYPOTHESIS TEST STATISTICS, CLIMATE CHANGE IMPACTS

Table G1. Hypothesis Tests Statistics for Temperature Change Impact to Net Basin Supply.

	Annual Net Basin Supply (acre-feet)		
	Current System	Most Likely Forecast	IPCC AR5 Projection
10th percentile	341,500	296,100	245,125
25th percentile	486,500	442,061	393,984
95% Confidence Interval, Median - Lo	844,500	803,967	761,166
Median	849,500	809,140	766,429
95% Confidence Interval, Median - Hi	855,500	813,844	772,086
95% Confidence Interval, Mean - Lo	1,158,580	1,118,752	1,076,653
Mean	1,164,010	1,124,206	1,082,138
95% Confidence Interval, Mean - Hi	1,169,441	1,129,660	1,087,622
75th percentile	1,488,500	1,451,382	1,412,391
90th percentile	2,416,500	2,386,068	2,352,526
Std Dev	959,751	963,907	969,368
95% Confidence Interval, StdDev - Hi	963,607	967,779	973,262
95% Confidence Interval, StdDev - Lo	955,927	960,066	965,505
Std Dev of Mean	2,771	2,783	2,798

The changes in NBS distribution parameters between temperature projections are all statistically significant to >95% confidence, as the number of simulated years is very large (120,000).

Table G2. Hypothesis Tests for Difference in Number of Droughts for Climate Change Forecasts.

Drought Duration (years):	≥3	≥4	≥5	≥6	≥7	≥8	≥9	≥10	≥11	≥12	≥13	≥14	≥15	≥16
Most Likely Forecast vs Current System														
calculated t-statistic:	6.287	6.140	5.116	4.051	3.098	2.687	1.686	1.930	1.923	1.558	1.131	1.254	0.484	0.000
p-value:	<0.5%	<0.5%	<0.5%	<0.5%	<0.5%	<1%		<5%	<5%					
IPCC AR5 vs Current System														
calculated t-statistic:	13.068	13.359	10.545	8.299	6.573	5.669	4.176	4.235	3.309	2.926	2.200	2.000	1.483	1.076
p-value:	<0.5%	<0.5%	<0.5%	<0.5%	<0.5%	<0.5%	<0.5%	<0.5%	<0.5%	<0.5%	<2.5%	<5%		
IPCC AR5 vs Most Likely Forecast														
calculated t-statistic:	6.593	6.889	5.802	4.352	3.490	3.064	2.591	2.286	1.664	1.655	1.165	0.886	1.067	1.076
p-value:	<0.5%	<0.5%	<0.5%	<0.5%	<0.5%	<0.5%	<1%	<2.5%						

each sequence is a 10,000-year simulation — values in matrices are number of drought events

CURRENT SYSTEM	≥3	≥4	≥5	≥6	≥7	≥8	≥9	≥10	≥11	≥12	≥13	≥14	≥15	≥16
Sequence A	624	308	155	80	39	18	11	5	2	1	1	0	0	0
Sequence B	659	335	182	100	64	37	25	12	6	2	1	1	1	1
Sequence C	643	310	148	68	34	17	10	4	0	0	0	0	0	0
Sequence D	627	305	138	74	37	18	13	10	5	4	3	1	0	0
Sequence E	646	320	166	86	43	26	11	4	1	1	1	0	0	0
Sequence F	583	304	154	62	33	14	7	2	1	1	1	0	0	0
Sequence G	653	318	161	86	43	22	10	6	4	1	0	0	0	0
Sequence H	652	314	146	67	26	9	4	3	3	0	0	0	0	0
Sequence I	630	294	146	74	34	17	8	3	2	1	0	0	0	0
Sequence J	634	343	182	76	39	17	8	5	5	0	0	0	0	0
Sequence K	614	299	151	77	37	17	12	7	3	1	1	1	0	0
Sequence L	625	322	170	88	33	19	7	3	2	1	1	1	1	0
Mean:	632.5	314.3	158.3	78.2	38.5	19.3	10.5	5.3	2.8	1.1	0.8	0.3	0.2	0.1
StdDev:	20.79	14.32	14.24	10.57	9.31	6.90	5.21	3.03	1.85	1.08	0.87	0.49	0.39	0.29
StdDev of Mean:	6.002	4.133	4.110	3.052	2.687	1.993	1.505	0.873	0.534	0.313	0.250	0.142	0.112	0.083

MOST LIKELY FORECAST	≥3	≥4	≥5	≥6	≥7	≥8	≥9	≥10	≥11	≥12	≥13	≥14	≥15	≥16
Sequence A	671	337	192	97	47	26	14	7	5	3	1	0	0	0
Sequence B	711	378	208	118	70	41	26	15	8	3	2	1	1	1
Sequence C	698	353	182	89	45	24	13	5	0	0	0	0	0	0
Sequence D	682	353	174	92	51	25	16	11	5	4	3	1	0	0
Sequence E	690	356	185	95	53	30	12	5	2	1	1	0	0	0
Sequence F	640	338	177	75	44	20	13	6	4	1	1	0	0	0
Sequence G	703	351	184	107	58	31	16	10	5	2	0	0	0	0
Sequence H	712	353	172	83	34	16	6	4	4	2	2	2	1	0
Sequence I	689	333	178	94	45	26	12	7	4	2	1	1	0	0
Sequence J	689	388	214	99	53	24	10	6	6	0	0	0	0	0
Sequence K	667	341	184	101	54	24	15	9	5	3	2	2	0	0
Sequence L	674	351	189	105	46	31	14	8	4	1	1	1	1	0
Mean:	685.5	352.7	186.6	96.3	50.0	26.5	13.9	7.8	4.3	1.8	1.2	0.7	0.3	0.1
StdDev:	20.51	16.21	12.86	11.28	8.87	6.30	4.70	3.11	1.97	1.27	0.94	0.78	0.45	0.29
StdDev of Mean:	5.921	4.680	3.712	3.257	2.561	1.820	1.357	0.897	0.569	0.366	0.271	0.225	0.131	0.083

IPCC AR5 PROJECTION	≥3	≥4	≥5	≥6	≥7	≥8	≥9	≥10	≥11	≥12	≥13	≥14	≥15	≥16
Sequence A	715	378	216	114	59	35	22	13	9	5	2	0	0	0
Sequence B	757	425	239	141	79	47	28	15	7	3	1	0	0	0
Sequence C	734	404	220	117	61	33	18	8	1	0	0	0	0	0
Sequence D	735	391	201	106	60	31	22	16	10	7	4	1	0	0
Sequence E	752	410	221	118	64	39	16	8	3	1	1	1	1	1
Sequence F	709	388	204	99	58	31	18	8	5	2	2	0	0	0
Sequence G	757	411	223	131	69	37	21	11	7	4	2	2	1	1
Sequence H	772	397	200	100	45	23	10	5	4	2	2	2	1	0
Sequence I	744	387	209	111	55	32	15	11	6	3	1	1	0	0
Sequence J	738	426	242	125	70	30	17	11	9	2	0	0	0	0
Sequence K	717	377	217	120	65	33	20	12	5	4	3	3	1	0
Sequence L	734	391	219	127	63	39	18	10	5	2	2	2	2	1
Mean:	738.7	398.8	217.6	117.4	62.3	34.2	18.8	10.7	5.9	2.9	1.7	1.0	0.5	0.3
StdDev:	18.97	16.56	13.31	12.52	8.44	5.95	4.43	3.14	2.64	1.88	1.15	1.04	0.67	0.45
StdDev of Mean:	5.475	4.780	3.842	3.613	2.435	1.718	1.280	0.907	0.763	0.543	0.333	0.302	0.195	0.131

Table G3. Hypothesis Tests for Temperature Change Impact to Drought Intensity & Depth.

	DROUGHT INTENSITY								
Duration (years):	3	4	5	6	7	8	9	10	≥11
Current System									
Maximum	833,167	812,000	752,700	710,833	687,929	657,625	651,167	636,100	640,864
Mean	506,713	505,266	510,288	507,350	511,481	505,612	504,799	502,697	505,907
Median	503,833	505,250	511,300	506,833	512,357	506,250	508,000	491,300	509,860
Minimum	241,167	279,750	314,300	337,833	343,929	375,375	387,500	414,400	381,577
Std Deviation	96,841	87,778	73,793	65,876	64,079	62,241	69,589	55,190	50,817
count	3,818	1,873	961	476	231	105	62	30	34
StdDev of Mean	1,567	2,028	2,380	3,019	4,216	6,074	8,838	10,076	8,715
Most Likely Forecast									
Maximum	816,597	806,016	757,778	731,489	706,873	699,851	611,953	626,396	590,017
Mean	478,316	476,771	481,354	477,209	482,011	486,990	478,696	471,868	468,694
Median	474,435	475,704	481,037	477,567	480,080	487,721	483,246	459,105	468,237
Minimum	206,688	241,361	275,084	295,334	304,531	331,122	342,202	368,382	332,036
Std Deviation	103,597	93,158	78,795	69,555	67,839	69,968	70,189	59,150	50,237
count	3,994	1,993	1,084	555	282	151	74	41	52
StdDev of Mean	1,639	2,087	2,393	2,952	4,040	5,694	8,159	9,238	6,967
test statistic, Mean, vs Current System	12.521	9.792	8.572	7.137	5.047	2.237	2.170	2.255	3.335
IPCC AR5 Projection									
Maximum	818,310	768,416	710,690	690,210	648,142	682,447	656,248	580,323	608,208
Mean	447,539	446,523	448,140	444,816	450,971	449,996	446,735	444,705	440,362
Median	442,612	443,825	445,804	448,258	446,863	448,023	451,863	436,812	436,483
Minimum	165,594	192,450	225,717	248,449	259,695	281,496	292,084	317,461	278,166
Std Deviation	111,435	100,584	84,221	75,162	70,636	73,306	75,428	65,976	60,563
count	4,079	2,174	1,202	661	338	185	97	57	72
StdDev of Mean	1,745	2,157	2,429	2,923	3,842	5,390	7,659	8,739	7,137
test statistic, Mean, vs Most Likely Forecast	12.856	10.078	9.740	7.796	5.568	4.719	2.856	2.136	2.841

	DROUGHT DEPTH								
Duration (years):	3	4	5	6	7	8	9	10	≥11
Current System									
Maximum	805,500	741,500	669,500	602,500	524,500	491,500	404,500	363,500	361,500
Mean	363,772	335,827	320,288	306,941	302,223	285,948	283,597	273,367	274,353
Median	345,500	321,500	307,500	293,500	298,500	279,500	275,000	266,500	275,500
Minimum	167,500	164,500	175,500	168,500	176,500	175,500	176,500	201,500	188,500
Std Deviation	99,654	88,532	74,222	65,993	63,630	56,955	51,448	43,215	44,496
count	3,818	1,873	961	476	231	105	62	30	34
StdDev of Mean	1,613	2,046	2,394	3,025	4,187	5,558	6,534	7,890	7,631
Most Likely Forecast									
Maximum	800,068	758,201	670,847	587,091	474,202	457,320	363,013	360,654	315,726
Mean	325,788	297,704	282,958	266,728	262,288	254,304	245,142	233,588	233,452
Median	304,221	278,043	266,494	251,805	249,608	243,417	234,482	222,206	225,232
Minimum	140,689	137,055	146,698	142,532	151,287	142,846	167,524	171,781	152,327
Std Deviation	103,672	89,249	75,311	64,606	59,264	58,822	47,157	41,489	41,080
count	3,994	1,993	1,084	555	282	151	74	41	52
StdDev of Mean	1,640	1,999	2,287	2,742	3,529	4,787	5,482	6,479	5,697
test statistic, Mean, vs Current System	16.512	13.328	11.273	9.849	7.293	4.314	4.509	3.896	4.295
IPCC AR5 Projection									
Maximum	786,423	704,255	631,287	554,333	489,146	419,272	351,480	363,378	360,373
Mean	283,878	255,646	237,164	221,745	219,032	202,957	201,622	194,574	191,171
Median	257,134	232,899	219,449	207,016	206,297	191,359	189,933	174,195	179,470
Minimum	105,855	103,863	114,731	109,480	119,183	107,190	137,741	134,024	120,788
Std Deviation	109,421	91,068	74,704	63,757	60,754	54,234	41,201	52,227	41,423
count	4,079	2,174	1,202	661	338	185	97	57	72
StdDev of Mean	1,713	1,953	2,155	2,480	3,305	3,987	4,183	6,918	4,882
test statistic, Mean, vs Most Likely Forecast	17.669	15.048	14.573	12.166	8.947	8.242	6.311	4.116	5.636

Differences of means between temperature projections are all statistically significant.

Table G4. Hypothesis Tests for Temperature Change Impact to Reduced Water Allocation Occurrences and Time On Allocation.

	Current System		Most Likely Forecast		IPCC AR5 Projection	
	mean % of time on allocation	mean # occurrences per century	mean % of time on allocation	mean # occurrences per century	mean % of time on allocation	mean # occurrences per century
Sequence-A	1.98%	0.72	3.61%	1.24	6.33%	2.14
Sequence-B	2.35%	0.76	4.33%	1.45	7.09%	2.24
Sequence-C	1.53%	0.62	3.25%	1.29	6.08%	2.29
Sequence-D	1.83%	0.62	3.51%	1.19	6.34%	2.08
Sequence-E	1.60%	0.60	3.39%	1.31	6.27%	2.30
Sequence-F	1.74%	0.66	3.44%	1.26	6.22%	2.19
Sequence-G	1.94%	0.77	3.89%	1.41	6.97%	2.42
Sequence-H	1.27%	0.53	3.14%	1.26	5.75%	2.17
Sequence-I	1.81%	0.59	3.10%	1.06	5.87%	2.00
Sequence-J	1.54%	0.63	3.17%	1.24	5.95%	2.25
Sequence-K	1.55%	0.65	3.40%	1.24	6.43%	2.23
Sequence-L	1.80%	0.69	3.95%	1.41	7.24%	2.40
Overall Mean	1.74%	0.65	3.51%	1.28	6.38%	2.23
Std Dev	0.28%	0.07	0.38%	0.11	0.48%	0.12
+1.96 StdDev:	2.29%	0.79	4.25%	1.49		
-1.96 StdDev:			2.78%	1.07	5.43%	1.99
			confidence intervals do not overlap, cases are statistically different			